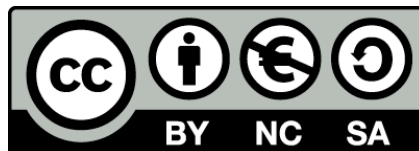




UNIVERSITAT<sub>DE</sub>  
BARCELONA

## Atomic force microscopy to elucidate lipid membranes enhanced by engineered liposomes

Adrià Botet Carreras



Aquesta tesi doctoral està subjecta a la llicència **Reconeixement- NoComercial – Compartir Igual 4.0. Espanya de Creative Commons.**

Esta tesis doctoral está sujeta a la licencia **Reconocimiento - NoComercial – Compartir Igual 4.0. España de Creative Commons.**

This doctoral thesis is licensed under the **Creative Commons Attribution-NonCommercial-ShareAlike 4.0. Spain License.**

Doctoral Thesis

Atomic force microscopy to elucidate  
lipid membranes enhanced by  
engineered liposomes.

Adrià Botet Carreras



UNIVERSITAT DE  
BARCELONA

---

Facultat de Farmàcia  
i Ciències de l'Alimentació



# Atomic force microscopy to elucidate lipid membranes enhanced by engineered liposomes

Doctoral Program in Nanoscience

Author:

Adrià Botet Carreras

Directors:

Òscar Domènech Cabrera

Jordi Borrell Hernández

Tutor:

Jordi Borrell Hernández

Department of Pharmacy and Pharmaceutical Technology  
and Physical Chemistry, Faculty of Pharmacy and Food  
Sciences



UNIVERSITAT DE  
BARCELONA





## Abstract

The research in this thesis aimed to study and generate an engineered formulation that can fuse with cell membranes and carry drugs or other compounds into cells. HeLa cells were chosen as the target cells and prior to their use, a model membrane mimicking the lipid membrane of HeLa cells was developed.

Starting from the basic components and using a bottom-up approach, different phospholipids were studied and compared to identify the construction blocks of liposomes and assess the effects of cholesterol on these phospholipids. After selecting the desired composition, a membrane model mimicking the HeLa cell membrane was developed to test its fusion with the engineered liposomes and to understand the fusion process before starting *in vitro* assays with living HeLa cells. In the *in vitro* assays, the engineered liposomes were able to fuse with the cell membrane as well as carry and liberate a model drug (methotrexate) into the cells, demonstrating that the engineered liposomes can work efficiently as nanocarriers.

Across the entire thesis, one technique was constantly used, atomic force microscopy (AFM). This technique enables the study of the smallest samples, such as lipid monolayers, as well as larger samples, like HeLa cells. AFM can also be used to obtain the physicochemical properties of samples using the force spectroscopy mode, allowing the analysis of samples and providing insight into the nanomechanics of the samples studied.

Several techniques were used in this thesis, including the application of a Langmuir-Blodgett trough to study the physicochemical properties of lipids, fluorescence resonance energy transfer (FRET) to determine the fusion of the engineered liposomes, visualization techniques like AFM and confocal microscopy, as well as viability assays to test the toxicity of the engineered liposomes to HeLa cells.

Finally, we demonstrated the ability of the engineered liposomes to fuse with cells, acting as nanocarriers based on their physicochemical properties. The ability of the membrane model to mimic the HeLa cell lipid membrane was also validated.

## Resum

Aquesta tesi té com a objectiu l'estudi i el disseny d'una formulació capaç de fusionar i transportar fàrmacs o altres molècules a les cèl·lules. Per a l'estudi, les cèl·lules objectiu seleccionades han estat cèl·lules HeLa i abans del seu ús, s'ha desenvolupat un model de membrana que imita la membrana lipídica de les cèl·lules HeLa.

Partint dels components bàsics, des d'un punt de vista del desenvolupament "bottom-up", s'han estudiat i comparat diferents fosfolípids per trobar els blocs de construcció adequats per als liposomes, també s'han estudiat els efectes del colesterol sobre aquests fosfolípids. Després de seleccionar la composició desitjada, s'ha desenvolupat una formulació que imita en composició la membrana cel·lular de les cèl·lules HeLa per provar la fusió dels liposomes dissenyats i per intentar entendre el procés de fusió abans d'iniciar els assajos *in vitro* amb cèl·lules HeLa. Pel que fa als assajos *in vitro*, els liposomes han demostrat ser capaços de fusionar-se a la membrana, així com transportar i alliberar un fàrmac model (metotrexat) a les cèl·lules, demostrant que els liposomes dissenyats en aquesta tesi són capaços de funcionar de manera eficient com a "nanocarriers".

Al llarg d'aquesta tesi, una tècnica ha estat constantment present, la microscòpia de força atòmica (AFM), ja que ofereix la possibilitat de realitzar estudis des de les mostres més petites, com l'estudi de monocapes lipídiques, fins a mostres més grans com les cèl·lules HeLa. Aquesta tècnica també permet fer observacions fisicoquímiques de qualsevol d'aquestes mostres mitjançant el mode d'espectroscòpia de força que permet sondejar les mostres i obtenir informació sobre la nanomecànica de les mostres estudiades.

Amb aquesta finalitat s'han utilitzat diverses tècniques, tant les que han ajudat a estudiar les propietats fisicoquímiques dels lípids, com el de Langmuir-Blodgett, com altres per determinar els efectes de fusió dels liposomes com la transferència d'energia per ressonància fluorescent (FRET) o tècniques de visualització com l'AFM o microscòpia confocal i fins i tot tècniques de viabilitat per provar la viabilitat de la formulació a les cèl·lules HeLa.

Finalment, hem desenvolupat i demostrat les capacitats dels liposomes per fusionar-se amb les cèl·lules, podent, en funció de les seves propietats fisicoquímiques, actuar com a "nanocarriers". El model de membrana que imita les cèl·lules HeLa s'ha validat corroborant la capacitat per imitar la membrana lipídica de les cèl·lules HeLa reals.



## Publications from the thesis work

The results of the present doctoral thesis entitled “Atomic force microscopy to elucidate lipid membranes enhanced by engineered liposomes” have been presented in four original peer-reviewed articles and in one manuscript submitted to *Nanomedicine: Nanotechnology, Biology and Medicine*. Adrià Botet Carreras, as a PhD student, participated in the conception, planning, experimental work, data analysis, and manuscript writing for all the articles. The impact factor of each journal is described below.

[1] **A. Botet-Carreras**, M.T. Montero, Ò. Domènech, J.H. Borrell, Effect of cholesterol on monolayer structure of different acyl chained phospholipids, *Colloids Surfaces B Biointerfaces*. 174 (2019) 374–383. DOI: 10.1016/j.colsurfb.2018.11.040

Impact Factor (2019): 4.389 Q1 in BIOPHYSICS -- SCIE

[2] M.L. Vázquez-González, **A. Botet-Carreras**, Ò. Domènech, M. Teresa Montero, J.H. Borrell, Planar lipid bilayers formed from thermodynamically-optimized liposomes as new featured carriers for drug delivery systems through human skin, *Int. J. Pharm.* 563 (2019) 1–8. DOI: 10.1016/j.ijpharm.2019.03.052

Impact Factor (2019): 4.845 Q1 in PHARMACOLOGY & PHARMACY -- SCIE

[3] **A. Botet-Carreras**, M.T. Montero, J. Sot, Ò. Domènech, J.H. Borrell, Characterization of monolayers and liposomes that mimic lipid composition of HeLa cells, *Colloids Surfaces B Biointerfaces*. 196 (2020) 111288. DOI: 10.1016/j.colsurfb.2020.111288

Impact Factor (2020): 5.268 Q1 in BIOPHYSICS -- SCIE

[4] **A. Botet-Carreras**, M.T. Montero, J. Sot, Ò. Domènech, J.H. Borrell, Engineering and development of model lipid membranes mimicking the HeLa cell membrane, *Colloids Surfaces A Physicochem. Eng. Asp.* 630 (2021) 127663. DOI: 10.1016/j.colsurfa.2021.127663

Impact Factor (2020): 4.539 Q2 in CHEMISTRY, PHYSICAL – SCIE

[5] **A. Botet-Carreras**, M. Bosch Marimón, R. Millan-Solsonad, E. Aubets, C. J. Ciudad, V. Noé, M. T. Montero, Ò. Domènech, and J.H. Borrell, On the uptake of cationic liposomes by HeLa cells: from changes in elasticity to internalization, *Nanomedicine: Nanotechnology, Biology and Medicine*. Submitted

Impact Factor (2020): 6.458 Q1 in MEDICINE, RESEARCH & EXPERIMENTAL

Dr. Jordi Borrell Hernández and Dr. Òscar Domènech.

We certify that the above-mentioned information is true.

## Content

Chapter 1. Introduction .....	1
Chapter 2. Objective of the thesis .....	29
Chapter 3. Results: Bottom-up .....	31
Effect of cholesterol on monolayer structure of different acyl chained phospholipids. .	31
Techniques introduced .....	31
Langmuir isotherms and Langmuir-Blodgett monolayer deposition .....	31
Atomic force microscopy .....	33
Summary .....	39
Highlights .....	44
Chapter 4. Results: A side quest .....	55
Planar lipid bilayers formed from thermodynamically-optimized liposomes as new featured carriers for drug delivery systems through human skin .....	55
Techniques introduced .....	55
Sample preparation .....	55
Sample characterization .....	57
Spectrofluorometry .....	59
Liposomal encapsulation efficiency .....	61
High performance liquid chromatography .....	61
Ultraviolet and visible spectrometry .....	62
Summary .....	63
Highlights .....	66



Chapter 5. Results: The model .....	75
Characterization of monolayers and liposomes that mimic lipid composition of HeLa cells. .....	75
Techniques introduced .....	75
Langmuir-Blodgett trough.....	75
BAM.....	76
Summary.....	77
Highlights .....	81
Chapter 6. Results: Testing.....	91
Engineering and development of model lipid membranes mimicking the HeLa cell membrane.....	91
Techniques introduced .....	91
Spectrofluorometry.....	91
AFM .....	99
Summary.....	100
Highlights .....	103
Chapter 7. Results: The cell .....	119
On the uptake of cationic liposomes by HeLa cells: from changes in elasticity to internalization.....	119
Techniques introduced .....	119
Flow cytometry.....	119
Confocal microscopy .....	120
Viability assays .....	121
Phospholipid quantification with the Marshall dye.....	121

Summary .....	123
Highlights .....	126
Chapter 8. Discussion .....	155
Detailed discussion .....	155
General discussion .....	174
Chapter 9. Conclusions and perspectives.....	177
Conclusions .....	177
Perspectives .....	179
Chapter 10. References .....	181
Appendix.....	203
List of publications .....	203
Conference participations and other events .....	205
Contributions to scientific events.....	207
Acknowledgments .....	209
Symbols and acronyms.....	211



## Chapter 1. Introduction

Cell membranes are crucial structures that maintain the integrity of living organisms, providing a barrier that compartmentalizes cell contents. These membranes are composed of different building blocks including different types of lipids and proteins, which are responsible for transport through cell membranes, thereby maintaining the homeostasis of the organism. Interestingly, in the origins of cellular life on earth, it has been hypothesized that the first membranes were simply a compartmentalization of primitive surfactant molecules forming self-assembled closed vesicles [1].

Protein membranes are the target of many drugs and metabolites. Furthermore, membranes are involved in essential biological processes such as mitosis and meiosis, as well as in the fusion between cells, which is the focus of this thesis. Since the concealment of water molecules and the maintenance of integrity are mediated by different structures such as the outer cell membrane and the membranes of many different organelles like endosomes, ribosomes, nuclei, the Golgi apparatus and mitochondria, membranes are extremely complex and heterogeneous structures that are far from being fully understood.

Cell membranes can be stripped down to a single common element. All of them have a phospholipid bilayer. Depending on their function and the organelle or tissue to which they belong, the lipid composition of this bilayer can vary. A variety of proteins and some carbohydrates linked to certain proteins can also be found in membranes, providing great specialization for different tasks. Cell membranes can show even more complexity through interactions with cytoskeletal structures.

One of the main factors used to differentiate between life forms is the presence or absence of a single sterol (particularly cholesterol) that resides within the amphipathic phospholipid bilayer. Notably, cholesterol affects the important physicochemical properties of membranes such as the phase and microviscosity. The presence or absence of cholesterol is used to discriminate between eukaryotic and prokaryotic cells, respectively. Prokaryotic

cells include bacteria, while eukaryotic cells include human cells and those of pluricellular organisms.

Since cell membranes are crucial for living, it is not a surprise that their compositions and properties have been widely scrutinized with a large battery of techniques and approaches. However, some aspects are still unknown, even with new emerging techniques and the knowledge obtained in recent decades.

Nowadays, to understand the general properties of membranes, we have to turn our attention to the 1972 seminal publication of Singer and Nicholson [2] that proposed a new general model for understanding the structure and function of cell membranes. The model, called the **fluid mosaic model**, stated that cell membranes are not static, but a dynamic structure where proteins are embedded within the lipid bilayer, with both types of molecules undergoing diffusion in the plane. Not long after this model was proposed, it was observed that cell membranes could be separated between detergent-resistant and detergent-labile fractions, indicating that there were different regions in the biological membranes [3]. These observations led to the further evolution of the model and the concept of **rafts** [4]. This concept has been controversial, since some in the scientific community do not believe in the existence of these rafts *in vivo* and consider them an artefact. However, it has been proposed that membranes have a two-dimensional liquid-like nature with a defined diffusion in the two dimensions, the rafts being a stable lipid-protein structure involved in signal transduction.

Some observations made with biomimetic membrane models have indicated that there are preferential interactions between different types of lipids, engaging in a collective behavior that produces large-scale microdomains. These interactions not only occur between lipids, but also between some proteins that require a certain type of lipid to operate in the membrane where they are inserted [5–9]. Finally, with all the evidence gathered, the following definition was adopted in 2006: *Membrane rafts are small (10–200 nm), heterogeneous, highly dynamic, sterol- and sphingolipid-enriched domains that compartmentalize cellular processes. Small rafts can sometimes be stabilized to form larger*

*platforms through protein-protein and protein-lipid interactions* [10]. This definition was developed by listing all the terms used to describe lipid rafts up to that moment. One important aspect to consider from this description is the fact that it assumes the existence of microdomains in cell membranes, but not in model membranes, since it is believed that models are governed by different properties given their simplicity.

After extensive work on rafts using biophysical techniques, it would be interesting to consider that the domains present on both sides of the lipid bilayer are coupled across the bilayer to form the functional platforms mentioned before [11]. Indeed, Nicholson himself proposed a reviewed version of his fluid model membrane based on new discoveries on membrane properties [12]. Based on current information, the general idea of what a plasma membrane looks like is shown in Figure 1.

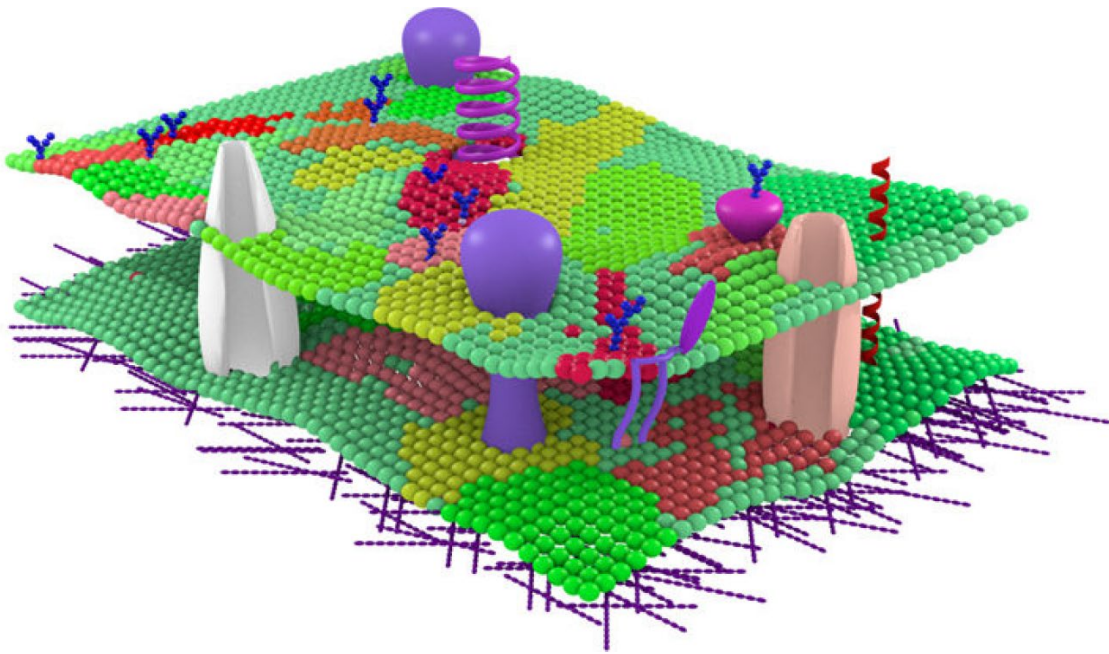


*Figure 1. Lateral representation of the heterogeneity of a plasma membrane, including rafts and several other entities such as glycoproteins, cholesterol and transmembrane proteins* [13].

The principal component of a cell membrane is the amphipathic phospholipid molecule composed of a hydrophilic region or a polar head and a hydrophobic region also called the

nonpolar tails. The polar region presents an  $\text{NH}_3$  group and is connected to the nonpolar region by a glycerol backbone, which is connected to the tails by ester bonds. The nonpolar region is composed of two hydrocarbon tails presenting different lengths (depending on the number of carbon atoms they have) and different shapes since they can present several unsaturations that can bend the tails (Figure 2).

The degree of unsaturation and the length of the chains influence the physical properties of cell membranes [14,15]. In addition, the polar head shows variations, with phosphatidylcholine (PC) and phosphatidylethanolamine (PE) being the most abundant headgroups in biological membranes [16].

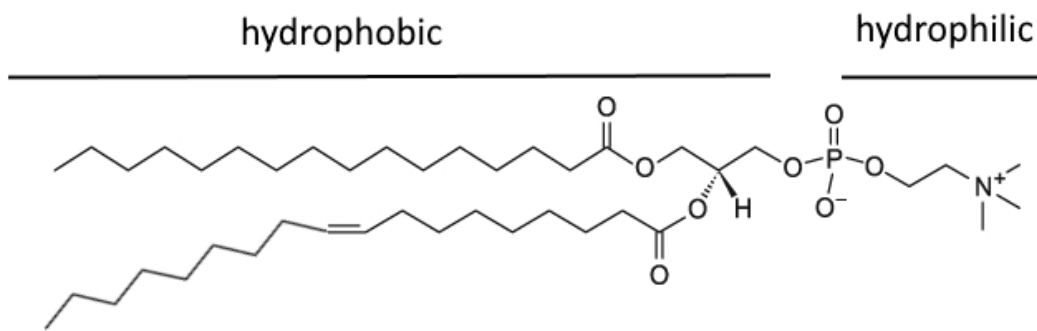


Figure 2. 1-palmitoyl-2-oleoyl-glycero-3-phosphocholine (POPC) phospholipid and the hydrophobic and hydrophilic regions.

All these possible variations provide a wide range of properties to these molecules that directly affect the properties and specific function of the cell. Moreover, the presence of cholesterol in eukaryotic cells dramatically increases the range of properties since the sterol regulates membrane fluidity, avoiding sudden changes provoked by external factors and allowing the cell to adapt to changes in temperature [17].

Membranes have certain dynamic properties, not only caused by the proportion of saturated and unsaturated lipids, but also by other factors such as [18,19]:

- The rotation of the carbon links in the hydrocarbon tails.

- The flexibility of the chains through the presence of double bonds, which can produce kinks in the shape of the chain.
- Rotational diffusion, which makes the molecules rotate on a fixed axis or an already moving axis.
- Lateral diffusion, which is a translational movement along the surface of the bilayer that allows molecules to move in all possible directions depending on the rigidity of the membrane.
- Fluctuations such as wavelike movements of the membrane that are commonly found in the proximities of the phase transitions of the lipids.
- Transmembrane diffusion, also known as a flip-flop event, which is the translocation movement of one of the molecules from one side of the lipid bilayer to the other side.

Structurally speaking, the presence of the polar and nonpolar regions is responsible for creating the membrane itself. Since cells are formed in a water environment, the nonpolar hydrophobic tails reorient themselves, creating the lipid bilayer, which has a thickness of approximately 5 nm. A theory on the hydrophobic effect [20] that gives a thermodynamic rationale to this fact was proposed by Israelachvili [21].

To obtain a lipid bilayer, certain conditions need to be met: temperature, pressure, ionic strength, pH and the phospholipid structure, which is probably the most important factor [22,23]. Thus, phospholipids can be found in different phases, ranging from a non-organized one to a compact self-organized phase.



In the study of model membranes [24], which will be addressed later in this Introduction, it is common to observe these different phases that are primarily affected by temperature and the water content (thermotropic and lyotropic effect, respectively) [25]. From a biological perspective, the most important ones are:

- Lamellar gel-like ( $L_{\beta}$ ) phase: the phospholipids are tightly packed and ordered, presenting limited freedom of movement because the acyl chain tails are fully extended and are more rigid and straight.
- Lamellar liquid-crystalline ( $L_{\alpha}$ ) phase: the phospholipids have a more thermal motion than in the  $L_{\beta}$  phase. Since the acyl chain tails are not rigid, the phospholipids are loosely packed and have rotational freedom.

An important concept that links  $L_{\beta}$  to  $L_{\alpha}$  is the transition temperature ( $T_m$ ), which is the specific temperature required to induce the transition from  $L_{\beta}$  to  $L_{\alpha}$ .

- Non-lamellar phases appear after the temperature keeps increasing, forming non-bilayer structures that can be hexagonal or cubic. These intermediate structures are involved in the events occurring during fusion [26].

As amphiphilic lipids can form monolayers at the air-liquid interface and present different surface states depending on their lateral compactness, different forms of interactions occur between the components [27].

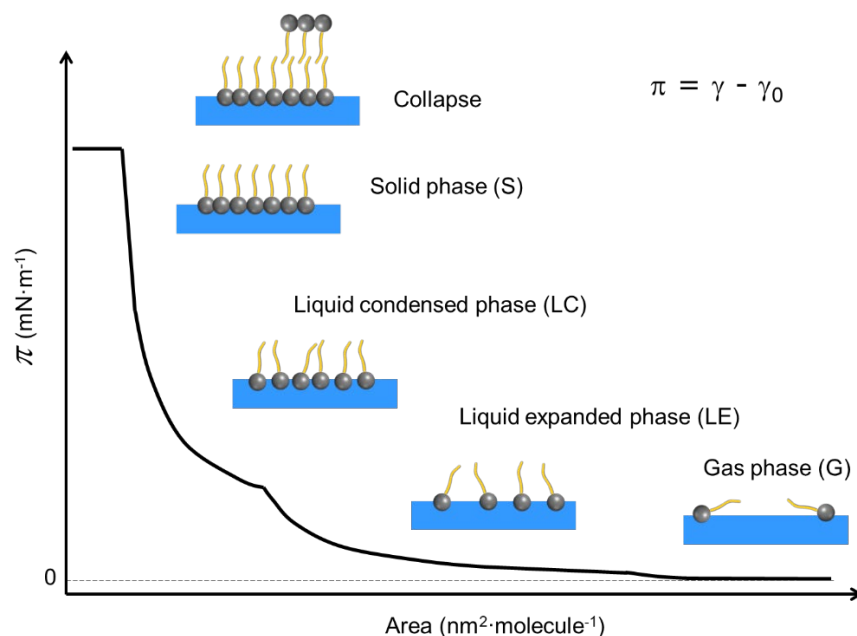


Figure 3. A Langmuir isotherm plot of surface pressure against area per molecule for an example showing the gas (G) phase, liquid expanded (LE) phase, liquid condensed (LC) phase, solid (S) phase and the collapse of the monolayer.

Figure 3 schematically depicts the Langmuir isotherm for a hypothetical system. For a high area per molecule, the monolayers are assimilated into a **gaseous (G)** phase. In this two-dimensional space, the values of surface pressure ( $\pi$ ) are zero or nearly zero, indicating that the molecules are far apart from one another and are not interacting much and not affecting the determination of the surface tension of the subphase.

Under lateral compression of the monolayer, the molecules become closer and, consequently, the area per molecule decreases as  $\pi$  increases. The interactions and compression restrict the freedom in movement, causing the molecules to start shifting to find a new position at the interface and entering a **liquid expanded (LE)** phase. In this phase, the behavior of the lipids is similar to that of liquid in three dimensions, thus making it similar to lipids in the  $L_\alpha$  phase. Direct correlation between the LE (in 2D) and  $L_\alpha$  (3D) phases remains a matter of theoretical considerations.

If the compression keeps increasing,  $\pi$  values continue to rise and the molecules become more tightly packed. At a certain point, the isotherm profile reaches the next stage, which is more restrictive in the two-dimensional plane. This new state makes the monolayer behave like a solid-like sheet and it is called the **liquid condensed (LC)** phase. Reaching this phase theoretically implies that the molecules are perfectly compacted and oriented perpendicularly to the interface, occupying a very small area per molecule. Moreover, any further compression implies a large increase in the  $\pi$  values.

At higher surface pressure values, the LC phase is transformed into the **solid (S)** phase without discontinuously changing the density. This phase is reached right before the **collapse** of the monolayer, where the area per molecule and  $\pi$  reach a critical value and the molecules break the monolayer structure, escaping downwards into the bulk liquid or upwards to form multilayers.

Membrane proteins are scattered in lipid bilayers, granting many functions to cells. These proteins interact with the membrane in different ways, but what all of them have in common is that they have specific amino acids exposed on their surfaces that allow them to be incorporated into or bind to the membranes. Consequently, there are two major groups of membrane proteins: peripheral and integral proteins [28].

One of the current models for membrane organization and dynamics has been postulated by Brown [29], who introduced the **flexible surface model** of the membrane, giving crucial relevance to the intrinsic lipid curvature [30] in the adaptation to the protein surface. This property should be considered in the fusion processes occurring between cells and drug carriers such as liposomes.

Peripheral proteins have a specific sequence of amino acids that allow them to either interact with the headgroup of the phospholipids or bind to integral membrane proteins. This occurs in the specific binding of cytochrome c to the inner mitochondrial membrane [31] and for some cytoskeletal membrane proteins in the inner membrane surface of erythrocytes that create a cytoplasmic network involving spectrin [32].

Integral proteins differ from peripheral proteins as a large proportion of this type of protein is embedded into the structure of the lipid bilayer. These proteins,  $\alpha$ -helices or  $\beta$ -barrels or mixtures of both structures, present large hydrophobic surfaces that can be integrated into the hydrophobic core of the lipid membrane. Integral proteins can be further subdivided into two groups: transmembrane proteins, which fully span the lipid membrane and are exposed on both sides (such as sodium channels and secondary transporters), and anchored proteins, which are only exposed on one side of the membrane (like the membrane-bound form of acetylcholinesterase).

Within the context of this thesis, we aimed to obtain a lipid-based drug carrier that can fuse with lipid membrane models as well as with living cells. Therefore, we had to consider the properties or possible roles of all the building blocks: lipids and proteins.

Membrane proteins are very relevant due to their involvement in many cellular processes like transport, energy production, information and stimulus processing, growth and cell division. Thus, membrane proteins can be subdivided into many groups including enzymes, membrane receptors and energy transducers. The transmembrane proteins in the subgroup involved with the transport of ions, metabolites and/or drugs across membranes can be classified into three types [33]:

- **Ion channels and pores:** These provide an access way for ions, which are small, charged and polar molecules. These molecules can cross the membrane barrier using this pathway by diffusion due to the concentration gradients occurring between the two sides of the membrane.
- **Passive and secondary active transporters:** Like the group mentioned above, these transmembrane proteins use gradients to allow molecules to pass from one side to the other side of the barrier. However, in this case, the molecules are usually larger. Transport becomes more specialized since the molecules can bind to one of many specific sites. Passive transporters can be: (i) uniporters if they carry one molecule/ion at a time; (ii) symporters if they carry two molecules/ions in the same

direction; and (iii) antiporters if they carry two molecules/ions but in opposite directions. Most of these transporters couple the transport to the electrochemical transmembrane potential, as explained by the chemiosmotic theory [34].

- **Primary active transporters:** These are like the passive transporters, including the uniporter, symporter and antiporter classes, but they need a source of energy (ATP) for transport. To operate properly, these proteins need to change their conformation following specific cycles. This means that their relationship with the surrounding phospholipids is highly important since this lipid-protein interaction can be essential in the correct functioning of the proteins, regulating or modulating them as well as disabling or shifting the transport activity [35–37].

The complexity of the lipid-protein interplay demonstrates that lipids do not simply provide a matrix in which the proteins are embedded, but they also participate actively in the regulation of protein processes, even their localization. These interactions are highly specific and could be considered a fingerprint for each protein in the membrane [38,39].

To understand the interactions between lipids and proteins, it is worth mentioning here the three different regions where lipids can surround a protein.

1. **Bulk lipids:** These lipids are far away from a protein and do not directly interact with it. They form a stable membrane, separating the cytosol from the cytoplasm. Therefore, we can expect non-specific interactions with the protein since they are far away from the protein.
2. **Annular lipids:** As their name implies, these lipids are set around a protein like a dynamic ring, establishing a boundary around it. They interact more with a protein than bulk lipids. Their motion is restricted [40] compared to that of bulk lipids, but they can exchange with them at a fast rate, indicating a weak affinity between the

lipids and the protein [41]. Annular lipids seem to associate with the protein through van der Waals forces. In general, annular lipids are able to adapt the protein surface, integrating it in a cooperative way [42].

3. **Non-annular lipids for integral proteins:** These lipids often reside within membrane protein complexes where there are the binding sites for hydrophobic molecules. Hence, they are distinct from annular lipids and are found buried inside the proteins. They are usually found in  $\alpha$ -helices or at protein-protein interfaces [43]. These locations are not simply a space into which a lipid fits. The absence or malfunction of these lipids can be completely devastating for protein function. Non-annular lipids are not exclusively phospholipids. They can be sterols like cholesterol found in nicotinic acetylcholine receptors (AChR) [44–46].

As we have already described, the hydrophobic surface of the proteins is heterogeneous and surrounded by the transient annular lipids. The interactions between lipids and the surfaces of the proteins are greater and much more complex than can be described here. However, some of the most important aspects are key in understanding the general behavior of the lipids around a protein, such as:

- **The phospholipid phase:** As expected, membrane proteins show preference for lipids in the liquid (fluid) crystalline phase over lipids in the gel (rigid) phase. If lipids need to modify their structure all around a protein to seal it into the membrane, it will always be easier for the lipids to be in a more fluid phase than a rigid one. In addition, a fluid membrane will facilitate the fitting of the lipids around the protein, making it easier for the van der Waals contacts to occur. In a lipid bilayer, where lipids can occur in different phase states, lipids close to proteins should preferentially be in a liquid-crystalline phase. Several experiments using freeze-fracture electron microscopy, fluorescence studies or infrared techniques have shown a perfect partitioning of the lipids in a membrane into domains in the  $L_{\alpha}$  phase [47–49].

- **The headgroup structure:** In general, for bulk and annular lipids, there are little selectivity effects on the headgroup. Only some small selectivity effects are observed for anionic phospholipids, which decrease if the protein increases the ionic strength, as observed with ion channels ( $\text{Na}^+$ , $\text{K}^+$ -ATPase), showing an important electrostatic component to the interactions, but not an exclusive one [40]. The binding of the headgroup in non-annular lipid sites shows more selectivity. A classic example is the binding of the cardiolipin lipid to specific sites in cytochrome c oxidase [50].
- **The chain length and hydrophobic mismatch:** An important factor to consider is the thickness of the hydrophobic region of the lipid bilayer. The thickness of the hydrophobic region of the protein should match the thickness of the hydrophobic region of the bilayer, but this is not so simple. It is obvious that the thickness of the hydrophobic region varies among different transmembrane proteins, resulting in what is called hydrophobic mismatch. In this situation, the hydrophobic mismatch between the hydrophobic regions of the protein and the lipid bilayer can be compensated by: (i) the adjustment of the thickness of the lipid bilayer around a protein by using lipids with shorter or longer hydrocarbon chains to match the thickness of the hydrophobic region of the protein (Figure 4), but this would increase the energy costs associated with the cell changing the thickness of the bilayer; (ii) the aggregation of proteins, exposing a smaller area of their surface to the lipid bilayer; and (iii) the distortion of a transmembrane  $\alpha$ -helix to provide better matching, possibly by the rotation of the  $\text{C}\alpha$ - $\text{C}\beta$  bond to link the sidechain to the polypeptide backbone [51], but this is not exempt from possible conformational restraints, which is the reason why it is not always possible.

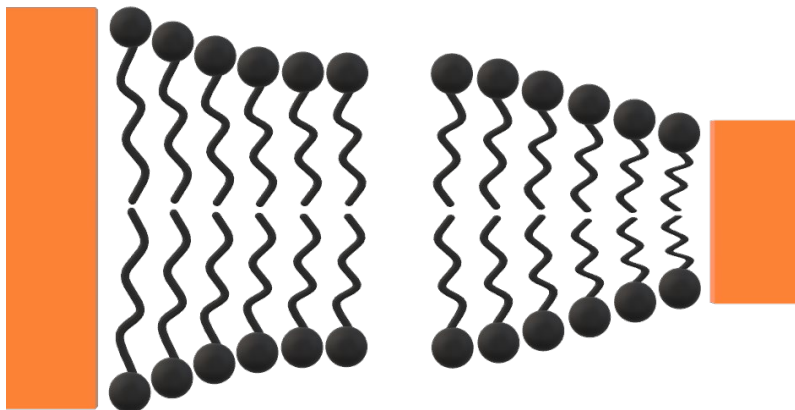


Figure 4. Hydrophobic mismatch with lipid molecules shaping the membrane around a protein expanding or contracting to adjust to the thickness of the hydrophobic region of the transmembrane protein.

If the energy costs to incorporate a protein into a membrane are too high, the protein can be excluded from the bilayer [52], with high amounts of hydrophobic mismatches leading to the formation of non-lamellar lipid phases [53]. In any case, there is an energy cost associated with any change in the thickness of a lipid bilayer to adjust to a membrane protein. This illustrates the importance of the annular region of the lipids around a protein [49,54–56].

Most of the current knowledge on membrane structure and function comes from studies of *in vitro* models. Typically, *in vitro* assays are performed with microorganisms, biological molecules or cells (single cell, tissue or organ) outside their normal biological context. Cell culture, which is a technique based on the extraction of cells from an organism, allows us to place cells in a fluid medium where they can be maintained and grown. In the development of any new pharmacological treatment, the regular steps after the discovery and characterization of a new molecule, system or technique involve performing tests *in vitro*, followed by assays in animals (*in vivo*) and finally in humans.

In the present study, we worked *in vitro* using the HeLa cell line. HeLa cells have an interesting background as a model and have revolutionized science both in the ethical and practical sense [57].



HeLa cells come from Henrietta Lacks (Figure 5), a 31-year-old African-American woman who died in 1951 from an aggressive case of cervical cancer [58]. Her cancerous cells were observed to reproduce quite fast compared to other cell cultures, doubling their number in only 24 hours. Furthermore, these cells are immortal. One of the mutations in these cancerous cells causes the telomeres at the end of each chromosome to be restored each time the cell divides, preventing cellular senescence. This means that HeLa cells are immortal. Unless there is an external factor, they can keep dividing forever. HeLa cells became the first immortal human cells to be ever grown in a laboratory.



*Figure 5. Henrietta Lacks [58].*

With the importance of a cell line like the HeLa one, it is not surprising that samples of these cells have been sent across the world to different laboratories for use in a wide range of studies. HeLa cells were critical for many biomedical breakthroughs from the past half century, becoming the standard laboratory cell culture. Nowadays, we can probably find frozen or active HeLa cells in any research institute on the planet.

All of this would have been great except for the simple fact that the family of Henrietta Lacks was unaware of the use of her cells since there was never any consent for it in anything other than her cancer diagnosis.

The issue was finally settled through the courts several years ago, with the family of Henrietta Lacks compensated. Nevertheless, this raised concerns in bioethics since it is important to inform and obtain consent for any activities involving human cells or tissues.

Another interesting fact that reminds us how strong HeLa cells are and how fast they can divide is the contamination by these cells of other cell cultures around the world. This is probably due to poor laboratory practices or through air droplets carrying HeLa cells to other cultures in the laboratories. This could lead to contamination of an existing cell line, with the HeLa cells eventually outgrowing the other cell line it invaded [59].

The complexity of cell lines, based on the need to maintain and grow them as well as the resources and time that these require, has motivated the development of simpler model systems that allow faster testing and give more physicochemical and functional information, since they eliminate possible interferences that can be later seen and studied in *in vitro* assays.

Over the last few years, many models and approaches have emerged, providing different information and allowing the scientific community to perform several different experiments [60]. Some of these, as will be discussed in the Results, are of great relevance for this work.

Supported lipid bilayers (SLBs) are membrane models where lipids form a bilayer on a solid substrate, such as a plate of the mica muscovite in our case, which are adequate for studies with atomic force microscopy (AFM).

SLBs are usually produced by two methods: by a Langmuir-Blodgett transfer or by the rupture and deposition of bilayer vesicles onto mica. Vesicles can also be used as membrane models themselves, with varying numbers of layers and diameter. Small unilamellar vesicles (SUVs) are the smallest ones measuring tens of nanometers, while giant unilamellar vesicles (GUVs) have a diameter ranging from one to ten microns [61]. Regarding the number of layers, multilamellar vesicles (MLVs) have a series of concentric bilayers, while unilamellar vesicles (LUVs) are composed of a single bilayer. GUVs tend to become MLVs given their large diameter, while SUVs tend to form LUVs since they are too small to form more than one layer.

In addition, it is possible to obtain membranes from natural sources like cells. This usually consists of breaking down a cell to obtain the membranes after a series of purifications or simply attaching cells to a functionalized surface to break them down, leaving the membrane attached to the surface [62,63].

Another type of membrane model can be obtained by tethering cells to solid supports with a different range of strategies like DNA hybridization [64–66] or biotin-streptavidin binding [67–69].

Another strategy is the formation of nanodiscs, which consist of a circular area of a lipid bilayer surrounded by a membrane scaffold protein. The idea is to have a jail of proteins around the lipids because in this case, the technique has been developed to isolate and display integral membrane proteins [70,71].

Finally, it is important to mention that computational modeling is on the rise, enabling us to predict many factors and modeling all the possible interactions that can be designed [72–75].

Once we know all the possible tools that we can use to perform our studies, we can decide on the type of approach and techniques to apply. Based on the background of our laboratory, we looked at the tools associated with the microscale and nanoscale levels.

Most people understand nanotechnology as something futuristic where tiny sophisticated bots crawl inside our bodies to fix something. The reality is a bit far from this idea. Nanotechnology in our era has not reached this level of science fiction yet. What we do mostly in the biomedical field is to develop biocompatible therapeutic agents or materials comprising different systems, each with characteristics that make them more suitable for certain treatments compared to others.

There are two different approaches for developing nanotechnology devices with pharmaceutical purposes (presently called nanoparticles because of their size). The first approach is the production of nanoparticles in a **top-down** style in which materials are

made and transformed into the desired structure by decreasing their size through printing, carving or machining. The second is called the **bottom-up** approach and involves the construction of organic and inorganic structures atom by atom and molecule by molecule. The first approach is like carving a sculpture from a block of stone, while the second is like making the same sculpture by connecting small blocks until the desired structure is formed.

Nanoparticles can be used for two main purposes (from the point of view of human therapeutics). One is for use as a drug delivery system, where nanoparticles are the vehicle that delivers a certain drug to a specific target. The other is when the nanoparticles are themselves the therapeutic agent. Although not common, nanoparticles can perform both roles at the same time. Furthermore, engineered nanoparticles can also be used for diagnostic and theranostic purposes.

Nanoparticles must have certain characteristics such as stability, low toxicity, optimal properties for drug transport and release if needed, and a long half-life in the bloodstream or specific target organ. These properties can vary depending on the ultimate purpose of the formulation.

There are different types of nanoparticles with their own characteristics. The most common are:

- **Carbon-based nanoparticles:** Fullerenes and carbon nanotubes are formed from carbon making a porous structure and display high strength and electrical conductivity [76].
- **Metal nanoparticles:** These are made from metal precursors usually used for their optic and electrical properties. Some examples are gold nanoparticles as photothermic agents used in the fight against tumors [77], superparamagnetic nanoparticles that are attracted to a magnetic field but retain no residual magnetism when the magnetic field has been removed, and iron oxide nanoparticles with diameters ranging from 5 to 100 nm [78]. Nano-projectiles are another type of metal nanoparticles. These small particles are several hundred nanometers in diameter

and fabricated using nano-engineering techniques. They are composed of a core material (usually silica) and a coating (usually gold), and are shot at high speed to help them penetrate into their target cells [79].

- **Ceramic nanoparticles:** These are inorganic nonmetallic solids usually used in catalysis. They are made by heating and successive cooling. These nanoparticles have a wide range of possible applications as they can be highly porous or dense and amorphous or polycrystalline [80].
- **Semiconductor nanoparticles:** Semiconductor materials possess properties that are between those of metals and nonmetals. Therefore, they are used in various applications like water splitting for the production of renewable hydrogen [81] or quantum dots (nanocrystals), which, depending on their size, can emit light in the entire visible spectrum [82].
- **Polymeric nanoparticles:** These nanoparticles represent a large group ranging from organic to metallic compounds and are usually presented as nanospheres, nanoparticles or nanocapsules. Some examples are metal-organic frameworks (MOFs) [83], which are crystalline coordination polymers built from the ion covalent association of inorganic units (atoms, clusters and layers, among others) with organic linkers bearing several complexant groups (carboxylates, imidazolates and phosphonates, among others) [84,85]. Nanoshells (core-shell) contain a spherical core of a particular compound (e.g., a therapeutic agent) surrounded by another material that thickens the sphere by a few nanometers [86].
- **Lipid-based nanoparticles:** These are characteristically spherical and can be mainly subdivided into two types: solid/liquid lipid nanoparticles, with a solid/liquid core of lipid that provides a matrix containing lipophilic molecules [87], and **liposomes**, which are composed of a spherical lipid bilayer surrounding an aqueous core.

Liposomes are used extensively in the pharmaceutical and cosmetic fields for their ability to get inside cells once their releasing role has been completed. Liposomes were the first nanoparticles used as a delivery system and many commercial formulations currently exist on the market such as those used for the delivery of doxorubicin and vincristine [88].

There are several techniques to obtain different types of nanoparticles. It is important to differentiate between formulation and characterization.

For formulation, as we have mentioned before, it is important to know whether we are using the top-down or bottom-up approach. Moreover, we need to consider the physicochemical properties of the nanoparticles we want to obtain because the techniques to produce these are many and sometimes specific. A simple reflux reaction, sonication or even microwave irradiation of formulations can affect the properties of the components, therefore showing the importance of controlling elementary laboratory parameters.

In this study, we focused our efforts on the bottom-up procedure to formulate liposomes since we wanted to make them fusogenic.

To formulate liposomes, we need to consider their lipid nature and size. In addition, it is important to consider the other components of the formulation, for example, the incorporation of proteins or the encapsulation of sensitive molecules such as RNA. Another important factor to consider is the electrical charge of the liposomes, as this could affect the encapsulation of charged molecules and their stability, impeding flocculation and precipitation before the desired target is reached.

The most important parameter that should be considered first is the rigidity of the lipid bilayer of liposomes, namely, microviscosity. Since a phospholipid bilayer can present  $L_{\alpha}$  or  $L_{\beta}$  phases, its  $T_m$  has to be surpassed to obtain liposomes.

The nature of fusogenic liposomes will depend on the precise selection of the lipids. Phospholipids and cholesterol can be obtained from different sources. For example,

phospholipids can be extracted from natural sources such as eggs or soybean or they can be synthesized ex-novo or modified through semi-synthesis [89]. Moreover, commercial phospholipids and cholesterol are available that are of a high quality.

The most used phospholipid headgroups in the production of liposomes are phosphatidylcholine (PCs), phosphatidylethanolamine (PEs) and phosphatidylserine (PSs). Cholesterol and other lipids or enhancers [90] can be also used.

There are several methods that can be used to prepare liposomes [91]. We can sort them into four main groups, with the last one containing the scale-up techniques mostly used in industrial formulations:

1. Mechanical methods:

- a. **Thin film method:** This is the simplest procedure and one of the oldest [92]. It consists of forming liposomes by hydrating a lipid film previously deposited onto a glass wall and shaking it at temperatures above its  $T_m$ . This method produces a heterogeneously sized population of MLVs with diameters over 1  $\mu\text{m}$ .
- b. **Ultrasonication method:** Sonicating an aqueous solution of formed liposomes in an ultrasonic bath or with a probe usually produces SUVs of around 15 to 25 nm in diameter [93].

2. Methods based on solvent replacement:

- a. **Reverse-phase evaporation:** In this method, a lipid mixture in an organic solvent is supplemented with an aqueous phase to evaporate the organic phase in a rotatory evaporator. A group of lipid droplets are created that

slowly adjust to the aqueous space, creating large macromolecular vesicles known as reverse-phase evaporation vesicles (REV) [94].

- b. Vaporization method (ether or ethanol):** In this case, a mixture of lipids in an organic solvent is directly and slowly injected into a warm aqueous solution to produce microsomal unilamellar vesicles with a regular size distribution [95]. The difference between using ethanol or ether is the immiscibility of ether, which makes it easier to totally remove it from the liposomal product since the warmed aqueous phase is above the boiling point of ether.
- c. Detergent-dialysis method:** Lipids solubilized with detergent form micelles that are placed in a dialysis membrane to remove the detergent, resulting in homogeneous unilamellar vesicles [96].

3. Methods based on the fusion of preformed vesicles or size transformation:

- a. Freeze-thaw extrusion method:** After generating liposomes by other methods, such as the thin film method, they are vortexed until the entire film is suspended, forming MLVs. The preparation is then frozen, thawed in warm water and vortexed again. After several cycles, the sample is extruded [97]. This method was brought to our laboratory in 1986, where an extruder prototype has been used ever since.
- b. Dehydration-rehydration method:** Previously formed SUVs, like those produced with the ultrasonication method, are mixed with the component to be encapsulated and dried all together. After rehydration, they form large heterogeneous vesicles [98].



Sometimes, once liposomes are obtained using any of the methods mentioned above, it is necessary to resize them to a desired diameter. For the sizing of liposomes, the usual method is a sequential extrusion through polycarbonate membranes presenting the desired pore size. Usually, the liposomes obtained will be larger than the nominal membrane pore size due to the elasticity of the bilayer membranes when passing through the filter. For example, for a pore size of 100 nm, it is usual to obtain liposomes of around 120 nm. Another option is to use gel chromatography. However, such a technique usually leads to a loss of material and is reserved for removing non-encapsulated components from the liposome. Finally, another common process is sonication with a titanium probe that produces small unilamellar vesicles of around tens of nanometers (50-80 nm) in diameter. This specific method has some disadvantages since the preparation can warm up, degrading some components. Moreover, the titanium probe releases metal particles, among other non-controlled disadvantages. These problems can be avoided with the use of a sonication bath. However, the reproducibility of the method may be compromised since there are too many varying parameters with the use of a sonication bath. Otherwise, sonication can be helpful in reducing the multilamellarity of liposomes when they are kept frozen for convenience.

4. Scaling up methods for industrial production:

- a. **Heating method:** This method uses glycerol, which is water soluble and physiologically acceptable. It is based on the heating of the components in the presence of glycerol at temperatures up to 120 °C and does not require the removal of the glycerol at the end of the process. Adequate stirring and the temperature allow the formation of stable liposomes. Furthermore, the employment of this temperature abolishes the need for any post-sterilization procedure [91].

- b. Spray-drying method:** This process is already used in the pharmaceutical industry to prepare fine granulate. It is considered a fast procedure to produce liposomes, where the mixture is sprayed into a Venturi tube that dries it, leading to the formation of liposomes [99].
  
- c. Freeze-drying method:** This method produces sterile and pyrogen-free submicron liposomes and forms a homogeneous dispersion of lipids. The lipids and water-soluble carrier materials are dissolved in tert-butyl alcohol/water cosolvent systems to form a clear isotropic monophasic solution. The solution is sterilized by filtration and placed in freeze-drying vials to lyophilize the solution. After the addition of water, liposomes are spontaneously formed [100].
  
- d. Modified ethanol injection methods:** This is based on the method described before with some variations.

  - i. Crossflow injection method:** As the name indicates, this method uses a continuous crossflow where two tubes welded together at 90° have an injection hole at their connection point. A lipid mixture is injected while a buffer flow goes through the tubes [101].
  
  - ii. Microfluidic channel method:** This method uses a microfluidic hydrodynamic focusing platform (MHF) where liposomes are formed by injecting the lipid phase and the water phase into a microchannel. Their size is mainly controlled by changing the flow rate [102].

- iii. **Membrane contactor method:** In this production method, an organic phase containing lipids is pressed through a membrane with a specific pore size, while an aqueous phase flows tangentially to the membrane surface at the other side, sweeping away the liposomes formed within the membrane [103].

These techniques allow the leap from batch production, common in research, to potential large-scale continuous production. There are many methods that can be used to produce liposomes and we have to decide which method depending on what we want to achieve.

The first parameter usually characterized in a nanoparticle in general or in a liposome in particular is size. The most common method used across many laboratories is the dynamic light scattering (DLS) technique, which provides the hydrodynamic size distribution profile of small particles in suspension or a solution of a sample.

Another common parameter to assess is the zeta potential ( $\zeta$ -potential). Usually measured by the same DLS instrument,  $\zeta$ -potential indicates the surface potential in the slipping plane surface of the liposomes. This is relevant for two main reasons. One of them is that a neutral charge could imply aggregation of the liposomes in suspension, leading them to flocculate. The other reason is more relevant to our final goal. If liposomes have the same charge as the target membrane, they will repel one another and they will have a lower chance of physically entering the target. However, if liposomes have the opposite charge to that of the target, they will be electrostatically attracted and have a higher chance of interacting.

The characterization information of samples is the same for any type of nanoparticles: size, the number of loaded molecules, and the technique used. The techniques will vary slightly between different types of nanoparticles, while several diverse techniques can be performed in the same type of nanoparticle and produce similar results. As can be seen in Table 1 adapted from [104], each parameter can be assessed by several techniques and depending on some characteristics of the nanoparticles, some of these techniques are more likely to be used than others.

Table 1. Parameters and their most common techniques to characterize them [104].

ENTITY CHARACTERIZED	CHARACTERIZATION TECHNIQUES SUITABLE
SIZE (STRUCTURAL PROPERTIES)	TEM, XRD, DLS, NTA, SAXS, HRTEM, SEM, AFM, EXAFS, FMR, DCS, ICP-MS, UV-Vis, MALDI, NMR, TRPS, EPLS, magnetic susceptibility
SHAPE	TEM, HRTEM, AFM, EPLS, FMR, 3D-tomography
ELEMENTAL-CHEMICAL COMPOSITION	XRD, XPS, ICP-MS, ICP-OES, SEM-EDX, NMR, MFM, LEIS
CRYSTAL STRUCTURE	XRD, EXAFS, HRTEM, electron diffraction, STEM
SIZE DISTRIBUTION	DCS, DLS, SAXS, NTA, ICP-MS, FMR, superparamagnetic relaxometry, DTA, TRPS, SEM
CHEMICAL STATE–OXIDATION STATE	XAS, EELS, XPS, Mössbauer spectroscopy
GROWTH KINETICS	SAXS, NMR, TEM, cryo-TEM, liquid-TEM
LIGAND	XPS, FTIR, NMR, SIMS, FMR, TGA, SANS
BINDING/COMPOSITION/DENSITY/ARRANGEMENT/ MASS, SURFACE COMPOSITION	
SURFACE AREA, SPECIFIC SURFACE AREA	BET, liquid NMR
SURFACE CHARGE	Zeta potential, EPM
CONCENTRATION	ICP-MS, UV-Vis, RMM-MEMS, PTA, DCS, TRPS
AGGLOMERATION STATE	Zeta potential, DLS, DCS, UV-Vis, SEM, cryo-TEM, TEM
DENSITY	DCS, RMM-MEMS
SINGLE PARTICLE PROPERTIES	Sp-ICP-MS, MFM, HRTEM, liquid TEM
3D VISUALIZATION	3D-tomography, AFM, SEM
DISPERSION OF NP IN MATRICES/SUPPORTS	SEM, AFM, TEM
STRUCTURAL DEFECTS	HRTEM, EBSD
DETECTION OF NPS	TEM, SEM, STEM, EBSD, magnetic susceptibility
OPTICAL PROPERTIES	UV-Vis-NIR, PL, EELS-STEM
MAGNETIC PROPERTIES	SQUID, VSM, Mössbauer spectroscopy, MFM, FMR, XMCD, magnetic susceptibility

With nanoparticles, particularly liposomes, we can apply them to treat different types of diseases by using them as nanocarriers to deliver drugs or other agents like proteins inside cells or to insert them into the membrane itself to treat a specific illness. The interaction with and internalization of liposomes may occur in many ways: endocytosis, capture by filopodia (if present), adsorption and or fusion. We focused on the latter two processes in this thesis by integrating several techniques.

There are many diseases associated with defects in the cell membrane, with most of them caused by the malfunction or absence of specific proteins. Many of these diseases are inherited and are, therefore, difficult to treat. Some examples of protein malfunction or absence are due to mutations in the DNA.

Hereditary elliptocytosis is a disorder in which erythrocytes have an abnormal shape (Figure 6) and is common in countries where malaria is endemic. Curiously, this disease is known to give certain resistance against malaria. At the same time, these erythrocytes tend to break down easily, resulting in severe anemia. The deformation is due to mutations and a consequent lack of 4.1R, spectrin and actin proteins, which, even if present, are not in their correct conformation to function properly [105].

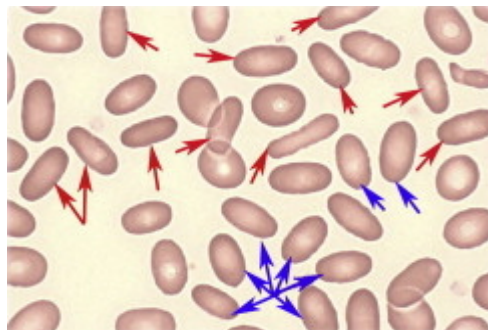


*Figure 6. Hereditary elliptocytosis with the classical form (red arrows) and the more ovalocytic red blood cells (blue arrows) [106].*

Cystic fibrosis is a common autosomal recessive disorder that affects the lungs and digestive system. It is characterized by the body producing thick mucus that can obstruct the pancreas and clog the lungs, leading to infections and respiratory failure. It is caused by a mutation in the cystic fibrosis transmembrane conductance regulator (CFTR) gene [107].

The malfunction of this transmembrane protein makes the cell unable to transport chloride ions to the cell surface to produce salt, where it is needed to attract water to make the regular mucus fluid [108].

Bartter syndrome, a kidney disease, is characterized by an imbalance in multiple molecules including sodium and potassium ions. There are different types of Bartter syndrome and each one is due to a defect in a specific protein. These proteins are the SLC12A1 Na-K-2CL symporter, the ROMK/KCNJ1 K<sup>+</sup> channel, the CLCNKB Cl<sup>-</sup> channel, the BSND Cl<sup>-</sup> channel accessory subunit, the CaSR calcium-sensing receptor and the SLC12A3 Na-Cl symporter. All these possible defects can produce neonatal symptoms like polyhydramnios, which is an increase in fluid in the amniotic sac. Typically, individuals with this disorder fail to grow as expected, but they gain weight, as they should by age ratios. As it is a renal disorder, there is a depletion of ions, leading to dehydration, constipation, polyuria, hypercalciuria and, subsequently, nephrocalcinosis that can lead to kidney failure, osteopenia that weakens the bones, and hypokalemia that weakens muscles and produces fatigue and cramps [109,110].

Some diseases are not strictly hereditary, but are acquired. A classic example associated with the malfunction or depletion of macromolecule receptors is type II diabetes. In this case, the insulin receptor stops functioning, leading to insulin overproduction by the pancreas to maintain glucose cell uptake and, subsequently, insulin resistance. After some time, this leads to the exhaustion of the pancreas and, thus, diabetes [111–113].

From an overall perspective, a better understanding of why these proteins are not functioning well would allow the development of useful palliative drugs.

A good way of finding a novel technique to set the foundation for new treatments using liposomes would be to use a bottom-up approach to select appropriate components and test them first on model membranes before jumping to *in vitro* assays involving living cells. If the *in vitro* assays are successful, the next step would be to perform *in vivo* assays in different animal models and assess pharmacokinetics and biodistribution before undertaking assays in humans. The development of new treatments usually takes a decade

**Chapter 1. Introduction**

if everything goes as predicted and the treatment is approved for use in humans by the relevant authorities. Due to this long journey, this work aimed to reach the *in vitro* stage as a halfway mark in the full development of an approved treatment.

## Chapter 2. Objective of the thesis

The main objective of this thesis was to develop engineered liposomes (a lipid composition showing fusogenic potential with cells) as nanocarriers, using a bottom-up structural approach by measuring the physicochemical properties of the phospholipid components of the liposomes. The liposomes had to be non-toxic and capable of fusing with the selected immortal HeLa cell line.

To achieve this objective, some specific objectives were defined:

1. The selection of an appropriate phospholipid candidate to develop the engineered liposomes and the assessment of its physicochemical interaction with cholesterol, which confers fusogenic properties.
2. The development of model membranes reproducing the physicochemical properties of the lipid membrane of HeLa cells to study fusion events prior to *in vitro* assays.
3. The investigation of the fusion process of the engineered liposomes with membrane models mimicking the HeLa cell membrane to elucidate the capabilities of the membranes developed.





## Chapter 3. Results: Bottom-up

Effect of cholesterol on monolayer structure of different acyl chained phospholipids.

**A. Botet-Carreras**, M. T. Montero, Ò. Domènech, and J. H. Borrell

*Colloids and Surfaces B Biointerfaces*, vol. 174, pp. 374–383, Feb. 2019

DOI: 10.1016/j.colsurfb.2018.11.040

### Techniques introduced

Langmuir isotherms and Langmuir-Blodgett monolayer deposition

Usually, the first step in the study of a cell membrane *ex vivo*, especially if we intend to study a completely artificial one, is to exploit the half-membrane model provided by lipid monolayers at the air-water interface. Compression isotherms are traditionally used to analyze physicochemical properties, particularly interactions, between the basic lipid building blocks of a membrane, one of which is cholesterol. This enables us to observe lipids and lateral phase separation, and correlate this with the interactions between themselves or with other components of the monolayer.

To perform these measurements, a Langmuir-Blodgett trough was used. This device consists of a reservoir, a surface pressure sensor and mobile barriers (one or two), as can be seen in Figure 7.



Figure 7. A Langmuir-Blodgett trough with an extractor. Any part that could be in contact with the buffer or the lipid monolayer: the reservoir, the barriers and the tweezers made of Teflon®.

This configuration allows the self-assembly of amphiphilic molecules into lipid monolayers at the air-water interface, where the instrument detects the surface pressure ( $\pi$ ) and the surface molecular area ( $A$ ). With these two parameters, we can analyze the behavior of the components in a monolayer while compressing or expanding it. Moving the barriers and altering the surface pressure of the monolayers can be used to stabilize them at specific surface pressures like  $30 \text{ mN m}^{-1}$ , which is accepted to be equivalent to the lateral surface pressure of a closed biological bilayer [114–116].

Once the monolayer becomes stable, it can be extracted with a stepper motor that attaches a solid substrate like a mica plate. Since mica muscovite plates are atomically flat, the deposition of molecules onto the mica surface leads to the formation of a monolayer in a single deposition or a bilayer if a double extraction of the monolayer (rising/dipping) is performed.

Isotherms are unique for each molecule and can be considered a fingerprint for each lipid or lipid mixture, yielding information on the organization and packing of lipid molecules in a monolayer [27]. As we decrease the surface area enclosing the molecules at the air-water interface, the surface pressure ( $\pi$ ) increases, as follows:

$$\pi = \gamma_0 - \gamma$$

where  $\gamma$  and  $\gamma_0$  are the surface tensions of the liquid in the presence and absence of the surface active agent present at the interface, respectively. This implies that the information provided by  $\pi$  is related to the lateral compactness of the amphiphilic molecules being analyzed. In addition, as mentioned already in Figure 3 of the Introduction, the  $\pi$  vs.  $A$  isotherm diagram shows different regions depending on the organization of the molecules at the interface.

Besides the information related to the organization of phospholipids upon compression, the isotherms also allow the calculation of several thermodynamic parameters such as the isotherm compressibility modulus ( $C_s$ ) or the Gibbs excess energy ( $G^E$ ) in mixed isotherms, as discussed later in this chapter.

### *Surface potential*

Another study that can be performed in monolayers is the measurement of their surface potential as their molecular area is reduced.

For this purpose, an electrical sensor replaces the surface pressure sensor of the Langmuir-Blodgett trough. This sensor has two parts, a metallic plate that stays beneath the monolayer connected directly to the detector, which is directly above it, millimeters above the surface of the liquid where the monolayer is formed. The detector has a vibrating capacitor, which does not have to be in contact with or disrupt the sample in any way. This setup measures the potential difference between the areas above and beneath the film, depending on the surface pressure or molecular area of the monolayer.

### *Atomic force microscopy*

Atomic force microscopy (AFM) is a high-resolution near-field microscopy technique that emerged in the 1980s. This technique belongs to the family of scanning probe microscopes

(SPMs), which were developed after the invention of scanning tunneling microscopy back in 1983 [117]. All these microscopes are non-optical. Instead, they are based on sensing near-field physical interactions between two elements, a probe and the sample, placed extremely close together or directly touching one another. In the case of AFM, we used a probe that is a sharp tip attached to a cantilever, with a laser beam reflected on the surface of the cantilever before striking a sensitive photodiode. Changes in the laser position inside the photodiode indicate the smallest changes in the cantilever position scanning the sample topography, thereby sensing extremely low interaction forces.

As can be seen in Figure 8, the sample is placed on a piezoelectric scanner that controls the lateral and vertical relative position of the AFM probe at the surface of the sample. The scanner moves in a raster pattern, creating a feedback loop that controls the vertical extension of the scanner in order to maintain a near-constant AFM cantilever deflection value, i.e., a constant interaction force. Finally, the AFM software combines all the single scanned lines into a three-dimensional image of the surface.

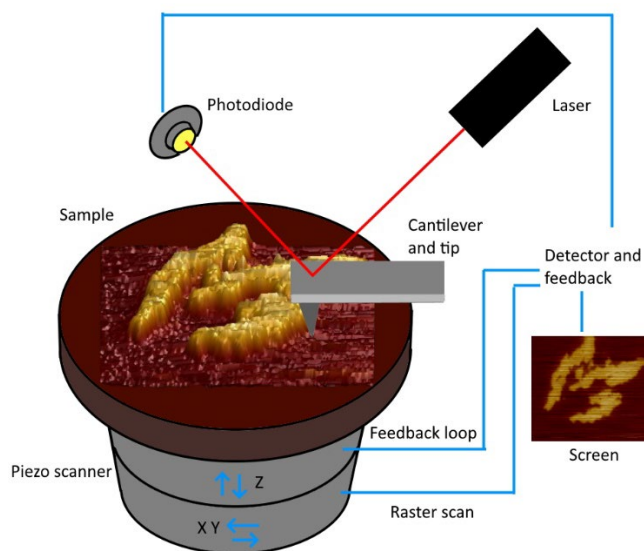


*Figure 8. The principal elements of an AFM instrument, with a laser beam reflecting on the surface of a cantilever before detection by a photodiode.*

Depending on the nature of the sample, the tip used as a probe can vary from the classic sharp V-shaped ones made of silicon nitride (that were used in this work to study Langmuir-

Blodgett monolayers and SLBs) to rounded ones where the tip is a small polystyrene ball. These rounded tips are used in studies on living cells or special functionalized ones.

Besides being nondestructive, AFM measurements can be performed in air, liquid or ultra-tight vacuum depending on the specifications of the samples.

In addition to some custom modified AFM instruments, there are mainly two basic operation modes to obtain an image: the **static** or **contact mode** and the **dynamic mode** that is subdivided into **tapping®** or **intermittent-contact mode** and **non-contact mode**, depending on the interactions between the tip and the sample.

It is important to recall here that the interactions between the tip and the sample do not start when they make contact. Right before making contact, when the tip approaches the sample, the cantilever deflects at the appearance of short-range forces acting between the two surfaces. These can be either attractive or repulsive. These forces depend on the nature of the interaction (e.g., friction forces, capillary forces, electrostatic forces, van der Waals forces, and chemical forces) [118]. In addition, due to this and the feedback loop generated between the tip-cantilever-laser-receptor pathway and the piezo scanner, the non-contact mode becomes possible.

In the **contact mode**, the tip is constantly in contact with the sample, whilst the cantilever scans the surface. The feedback system ensures a constant cantilever deflection and, consequently, a constant interaction force.

In the **intermittent-contact mode**, the cantilever is oscillated by a piezoelectric actuator at its resonance frequency (or very close to it). The probe is then lowered into the sample surface so that the tip slightly touches the surface at the maximum amplitude of the oscillation and the oscillation amplitude is dampened. The feedback loop maintains a constant oscillation amplitude and, hence, a constant interaction force.

In the **non-contact mode**, the cantilever oscillates like in the **intermittent-contact mode**, but at a smaller amplitude, keeping the tip at a distance away from the surface, but in the region of attractive interaction forces. Therefore, images are obtained without the sample

being touched at all. The disadvantage of this mode is that it is challenging to maintain the tip in the region of attractive forces during scanning.

Choosing the mode usually depends on the nature of the sample and on different aspects like softness, possible lateral forces, sticky surfaces or the delicateness of the sample.

#### *AFM force spectroscopy (AFM-FS)*

Besides the topographic modes where the AFM probe is used to scan a sample surface, the AFM probe can be used to interact with a sample in the effective touching mode. For instance, the AFM tip can be used to gain insight into the nanomechanical characteristics of a sample at a sub-nanonewton resolution, known as the force spectroscopy (FS) mode [119]. In this mode, we can control and manage the tip to approach the sample surface in the Z axis, while the cantilever deflection is monitored as a function of the vertical displacement of the scanner. As can be seen in Figure 9, where a model **force curve** is displayed, the tip first approaches the sample (blue line) before the **jump to contact** event, where the same forces observed with the topographic modes occur, making the cantilever deflect and touch the surface of the sample. Once the tip is in contact, the decrease in the distance between the sample and the tip increases the cantilever deflection until it reaches a maximum value, at which point the sample cannot sustain the pressure exerted by the probe and the tip penetrates the sample. If the distance between the sample and the tip continues to decrease, the deflection of the cantilever increases due to the pressure exerted on the substrate. When the AFM probe presses the substrate, the curve reverses and the distance between the tip and the sample increases (red line) until the tip is liberated from the sample, recovering the initial values of deflection. The data from the cantilever-deflection versus scanner-displacement curves, which can be transformed into different data such as force-distance curves or stiffness data using appropriate models, can be useful in obtaining the physicochemical parameters of samples [120,121].

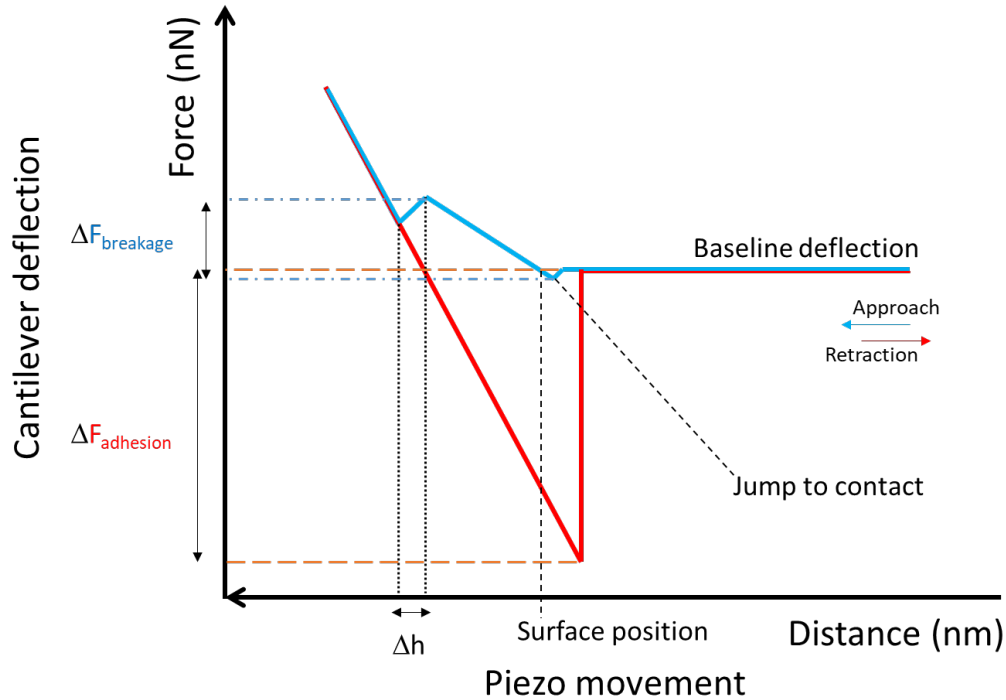


Figure 9. Example of a force curve depicting the first jump to contact event followed by a break (blue line) and retraction (red line) with the adhesion forces.

AFM force curves can provide information on various mechanical properties of a sample, including **adhesion**, which allows us to study the stickiness of a sample. It focuses on the last part of the retraction process and can reveal quantitative adhesive differences between samples, as can be seen in the monolayer investigations presented in this dissertation.

**Rupture** forces and **stiffness (Young's modulus)** are directly related to the approaching part of the curve and give information on how hard the surface is. In some cases, if the surface can be ruptured, the height of that membrane can be measured by the rupture created in the approaching curve. **The indentation depth** basically indicates how much the tip has penetrated the sample at a given loading force.

Whilst a single force curve can give information on the sample studied, it is necessary to obtain many of them to have enough accurate and meaningful statistical data. To do this, there is a specific mode, the **force volume** mode, which allows us to obtain many force curves easily. Thus, force images, pixel by pixel, can be created from the curves collected.



**Chapter 3. Results: Bottom-up**

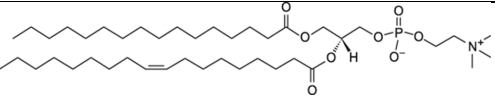
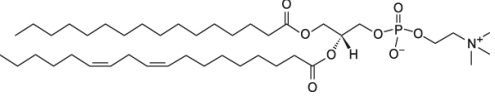
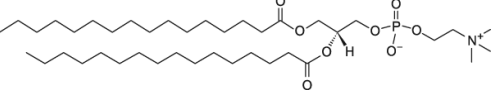
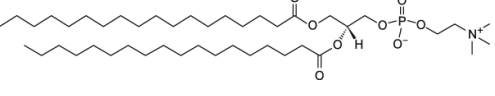
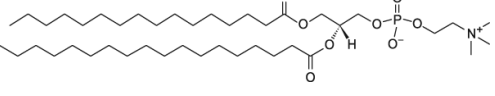
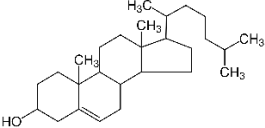
This mode extracts and displays the force curves in a grid shape for a specific area under study. For example, a force map of a  $1\ \mu\text{m}^2$  area using a  $32 \times 32$  grid will give 1024 individual force curves, providing substantial statistical data. Furthermore, if the selected region contains different domains with different properties, a force map can be created to visualize the differences between the areas, as will be later shown in Chapter 5.

## Summary

To accomplish the objectives of this thesis, we had to decide on using the bottom-up or top-down approach. As discussed in the Introduction, the bottom-up approach was the most convenient given the possibilities of controlling the physicochemical properties during development. We decided to start by obtaining an appropriate lipid composition for the engineered liposomes.

Knowing that eukaryotic cells have cholesterol (CHOL) and focusing on the fact that we wanted the liposomes to be as biomimetic as possible, we selected the phospholipids based on their different lengths and degree of unsaturation:

Table 2. Phospholipid candidates and cholesterol.

Molecule	Acronym	Name
	POPC	1-palmitoyl-2-oleoyl-sn-glycerol-3-phosphatidylcholine
	PLPC	1-palmitoyl-2-linoleyl-sn-glycerol-3-phosphatidylcholine
	DPPC	1,2-palmitoyl-sn-glycerol-3-phosphatidylcholine
	DSPC	1,2-distearoyl-sn-glycerol-3-phosphatidylcholine
	PSPC	1-palmitoyl-2-stearoyl-sn-glycerol-3-phosphatidylcholine
	CHOL	Cholesterol

All these phospholipids have the same polar heads, phosphatidylcholine (PC). We used PCs since we can find them in all eukaryotic cells. Moreover, at the molar ratio, they are one of

the most abundant phospholipids. Even if we used the same headgroup, their tails, the hydrophobic part of the phospholipids, are quite different, as can be seen in Table 2. The differences in length and saturation are enough to confer different physicochemical properties. A classic example would be the melting transition temperature that is characteristic for each phospholipid [122].

Beyond the different nature of the phospholipids studied, we had to contemplate the effect of adding CHOL to the system under study. CHOL is not only an important molecule as it can be found in eukaryotic cells, but it can also alter the physicochemical properties of the lipids with which it is associated. The integration of CHOL into the membranes has two main effects: (i) it modifies the enthalpy of the melting transitions of the phospholipids [123] and (ii) it broadens the temperature range encompassing the main transition, being able to abolish the transition from  $L_{\beta}$  to  $L_{\alpha}$  if the amount of CHOL is high enough. The CHOL concentration necessary to abolish this transition depends on the phospholipid. Thus, it is of interest to obtain a better understanding of how phospholipids interact with CHOL.

The CHOL molar concentration needed to abolish the enthalpy transition when mixing with the selected phospholipids was determined previously by members of our group [124]: PLPC:CHOL (0.93:0.07 mol/mol), POPC:CHOL (0.85:0.15, mol/mol), PSPC:CHOL, (0.70:0.30, mol/mol), DPPC:CHOL (0.70:0.30, mol/mol) and DSPC:CHOL (0.70:0.30, mol/mol).

To analyze the thermodynamic properties of pure phospholipids and their mixtures with CHOL, we used Langmuir isotherms. We started by performing monolayer experiments with the Langmuir-Blodgett trough at 24 °C using pure CHOL, the 5 pure phospholipids, and their mixtures with CHOL at the selected molar ratios.

As expected, each phospholipid isotherm had different features. As the compression progressed, we observed different phases or different surface pressure collapse values, as well as different  $\pi$ -molecular area profiles. For instance, the presence of CHOL in the mixed monolayers provoked a shift of the isotherms towards smaller molecular areas due to the condensing effect of CHOL.

More precisely, the changes were slightly different for each phospholipid. POPC and PLPC collapsed at  $48.0 \pm 0.1 \text{ mN m}^{-1}$  and  $46.2 \pm 0.3 \text{ mN m}^{-1}$ , respectively, while their mixtures with CHOL, besides showing a condensation effect, showed collapse surface pressure values close to those of the pure phospholipids. This behavior could be reasonably attributed to the low proportion of CHOL in both mixtures. While pure DSPC showed a subtle transition at  $57.2 \pm 0.4 \text{ mN m}^{-1}$ , it collapsed at  $65.3 \pm 0.5 \text{ mN m}^{-1}$ . Its mixture with CHOL showed a collapse surface pressure value of  $54.0 \pm 0.3 \text{ mN m}^{-1}$ , which was between the collapse surface pressure values of pure DSPC and pure CHOL. Pure PSPC collapsed at  $64.0 \pm 0.1 \text{ mN m}^{-1}$  and its mixture with CHOL collapsed at  $53.6 \pm 0.3 \text{ mN m}^{-1}$ . PSPC was the only phospholipid that revealed a transition in its mixture with CHOL. We observed also a subtle transition in the mixed monolayer at a surface pressure of  $44 \text{ mN m}^{-1}$ , close to the collapse surface pressure value of pure CHOL. Finally, pure DPPC showed the characteristic transition from the liquid expanded (LE) to the liquid condensed (LC) phase and collapsed at around  $55.0 \pm 0.1 \text{ mN m}^{-1}$ . Its mixture with CHOL collapsed at  $54.3 \pm 0.6 \text{ mN m}^{-1}$  and the transition vanished.

The data from the isotherms were used to perform some calculations such as the compression modulus, more precisely the inverse of the compression modulus ( $C_s^{-1}$ ), which showed that CHOL increased the packing density when mixed with saturated phospholipids, but not when mixed with unsaturated phospholipids. We focused on the  $C_s^{-1}$  values at  $30 \text{ mN m}^{-1}$  since this is the lateral surface pressure in a monolayer that is accepted to be equivalent to the lateral surface pressure in bilayers [114].

The isotherm data were also used to obtain the Gibbs excess energy, from which, considering the mixture as a gas in two dimensions, we obtained the Gibbs energy of the mixing output. The negative values of  $\Delta_{\text{mix}}G$  observed for all the mixed monolayers studied indicated attractive interactions between the two components in all the binary systems, showing that the mixture of PSPC:CHOL was the most stable.

As a complementary study to the Langmuir isotherms, we studied the surface potential of the samples, more precisely the variation in the overall vertical component of the dipole

moment ( $\mu_{\perp}$ ), a complex parameter that includes contributions from the dipole moment of the polar headgroup, the hydrocarbon chain and the surface water molecules (Figure 10).

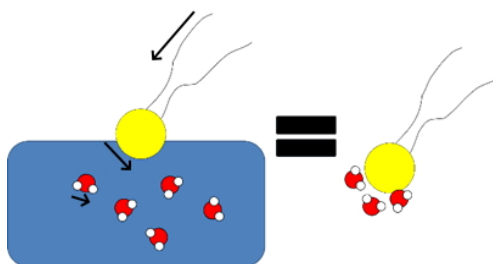


Figure 10. Vertical component of the dipole moment, showing the contributions of the hydrocarbon chain, the polar head group and the water molecules.

We observed that the  $\mu_{\perp}$  values for all the monolayers studied decreased as  $\pi$  increased. This behavior has been reported before [125–129] and has been attributed to the strength of the depolarized molecular interactions in the monolayers as compression progresses. We observed that the addition of CHOL to the pure phospholipids changed the behavior of the monolayer depending on whether the phospholipids were saturated or unsaturated. For the mixtures of CHOL with POPC and PLPC (one and two unsaturations, respectively), we noted that the  $\mu_{\perp}$  values were higher than those of the corresponding pure phospholipid, that is, a vertical orientation of the acyl chains was induced with respect to the normal of the monolayer. By contrast, the mixtures of CHOL with DPPC, DSPC and PSPC (without unsaturations) presented lower values of  $\mu_{\perp}$  than the corresponding pure phospholipids, thereby preventing their acyl chains adopting the all-*trans* configuration and leading to a tilt towards the surface of the monolayer.

With all these data, we proceeded to deposit the monolayers onto a mica plate for further examination with AFM, creating Langmuir-Blodgett monolayer depositions (also known as Langmuir-Blodgett; LB) at 30 mN m<sup>-1</sup>.

The AFM topographic images of all the pure phospholipid LBs showed flat and featureless surfaces except for some occasional defects. However, all the LBs of the phospholipid and CHOL mixtures showed the presence of domains. These domains were different in shape depending on the phospholipid involved. However, in general, their surface covering area (in percentage) was always lower than the nominal CHOL molar concentration. This

indicated the mixing of CHOL up to a certain concentration with the corresponding phospholipid, with the observed domains being laterally segregated domains enriched with CHOL. While a direct correlation could not be made, all the data collected before were consistent with the size and height of the domains, which seemed to be related to the thermodynamic stability of the monolayer and the verticality of the molecules at the interface. Curiously, the height of the domains, from higher to lower, matched with the  $\Delta_{\text{mix}}G$  values of the mixtures from less stable to more stable.

With the techniques available, it was not possible to determine the exact composition of the lipid domains observed by AFM, but we were able to obtain measurements of the physical properties of the different monolayers using AFM in the FS mode.

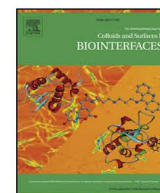
Focusing on adhesion forces ( $F_{\text{adh}}$ ), the differences between the base area (lower regions) and domains (taller regions) were clearly observable. As described before with the other techniques, monolayers containing unsaturated phospholipids demonstrated the opposite behavior to that of monolayers containing saturated phospholipids. The adhesion forces showed higher values for the lipid domains than the base area. More interestingly, comparing the adhesion forces obtained from the base areas of the mixtures of CHOL and a pure phospholipid, we found that their  $F_{\text{adh}}$  values were not the same. This clearly indicated that CHOL was not only present in the domains, but also in the base area, probably at lower concentrations. For the base areas in the mixtures of pure phospholipids without CHOL, we obtained the same values of  $F_{\text{adh}}$  that we had for the pure phospholipid LBs.

With all this information, we were able to select a suitable phospholipid to build engineered liposomes and to continue with the rest of the research plan of this thesis. Considering that phospholipids in a natural extract usually present one saturated hydrocarbon chain and one hydrocarbon chain with one unsaturation, the most suitable candidate was POPC. Its mixing behavior with CHOL showed good stability, presenting the second lowest absolute  $\Delta_{\text{mix}}G$  values. The selection of lipid mixtures presenting negative  $\Delta_{\text{mix}}G$  values might be considered slightly contradictory if we take into account that we wanted fusogenic properties, i.e., disrupts the layer. However, we needed a CHOL-phospholipid mixture that was stable

enough for liposome formation and with a low absolute  $\Delta_{\text{mix}}G$  value in order to facilitate *in vivo* fusion with the target membrane.

## Highlights

- We evaluated several phospholipid candidates for use in the development of engineered liposomes with biomimetic membranes.
- Variations in the length and/or degree of unsaturation of the phospholipid tails produced large physicochemical differences.
- Saturated PCs were more condensed in the presence of cholesterol than unsaturated ones.
- Saturated phospholipids showed a stronger interaction with cholesterol.
- Using AFM-FS, we demonstrated that the two types of domains appearing in the mixed monolayers were not of pure CHOL or pure PCs.
- The mixture of POPC and CHOL seemed to be the most appropriate for use in the development of lipid membranes.



## Effect of cholesterol on monolayer structure of different acyl chained phospholipids

Adrià Botet-Carreras<sup>a,b</sup>, M. Teresa Montero<sup>a,b</sup>, Òscar Domènech<sup>a,b</sup>, Jordi H. Borrell<sup>a,b,\*</sup>

<sup>a</sup> Secció de Físicoquímica, Facultat de Farmàcia i Ciències de l'Alimentació, Spain

<sup>b</sup> Institute of Nanoscience and Nanotechnology (IN<sup>2</sup>UB), Universitat de Barcelona (UB), 08028, Barcelona, Catalonia, Spain

### ARTICLE INFO

#### Keywords:

Phospholipids  
Cholesterol  
Langmuir-Blodgett  
Surface potential  
AFM  
Adhesion forces

### ABSTRACT

In this work we have investigated the effect of cholesterol (CHOL) in phospholipid monolayers on a series of phosphatidylcholines differing in acyl chain composition. We have used the CHOL proportion that abolishes the gel ( $L_{\beta}$ )-to-liquid-crystalline ( $L_{\beta}$ ) transition in bilayers in order to investigate the mixing properties and laterally-segregated domains formed by specific phospholipid-CHOL ratios at the air-water interface. The binary monolayers were formed by mixing CHOL with 1,2-palmitoyl-*sn*-glycero-3-phosphatidylcholine (DPPC); 1,2-distearoyl-*sn*-glycero-3-phosphatidylcholine (DSPC); 1-palmitoyl-2-stearoyl-*sn*-glycero-3-phosphatidylcholine (PSPC); 1-palmitoyl-2-oleoyl-*sn*-glycero-3-phosphatidylcholine (POPC) and 1-palmitoyl-2-linoleyl-*sn*-glycero-3-phosphatidylcholine (PLPC), respectively. From surface pressure-area ( $\pi$ - $A$ ) isotherms the isothermal compression modulus were calculated, and the mixing properties of the monolayers obtained by performing a basic surface thermodynamic analysis. From the excess Gibbs energy, the interaction parameter and the activity coefficients were also calculated. The study of the monolayers was complemented by determining the molecular dipole moment normal to the plane of the monolayer. The existence of laterally segregated domains was assessed by atomic force microscopy (AFM) of Langmuir-Blodgett films (LBs) extracted at 30 mNm<sup>-1</sup>. To get insight into the nature and composition of the observed domains force spectroscopy (FS) based on AFM was applied to the LBs.

### 1. Introduction

The primary function of cell membranes is compartmentalization. That is, they act as physical boundaries for the necessary separation between their respective inner media and their external surroundings. Cell membranes provide protection, shape, and regulate the interactions between cells and their environment. Crucial tasks whose natural substrate is the membrane include transport mechanisms, energy generation, signalling processes and cell differentiation, among many others. The physical and chemical properties of biological membranes are of great importance to understand membrane functions, since it is known that their physiological activities occur under a complex combination of forces that depend on their chemical composition and physicochemical properties of their components. For these reasons, membrane structure, composition and function have been and will be extensively investigated over the years.

Plasma membranes, regardless of their source, are constituted of two fundamental building blocks: lipids and proteins. There are three major kinds of membrane lipids found in eukaryote and bacteria:

phospholipids, glycolipids and cholesterol (CHOL) [1]. The extreme complexity of membrane organization [2] it remains intriguing the extensive variety of phospholipids found in the membranes [3,4]. The interaction between phospholipids and CHOL has been extensively investigated using a variety of biophysical techniques [5–7], including differential scanning calorimetry (DSC) [8,9]. Phospholipids in aqueous environment are thermotropic and undergo a transition between the gel ( $L_{\beta}$ ) and the liquid-crystalline ( $L_{\alpha}$ ) phases. The  $L_{\beta}$  to  $L_{\alpha}$  phase transition is of endothermic nature and shows a transition temperature ( $T_m$ ) which is characteristic for each phospholipid or mixture of lipids. The integration of CHOL into bilayers of phospholipids generally has two effects on the endotherm: (i) a decrease in the enthalpy of the transition; and (ii) a broadening of the transition. Interestingly, abolition of the transition occurs at a different percentage of CHOL depending on the specific phospholipid investigated [10]. Without entering into details of the molecular interactions between the steroid and phospholipids, CHOL has the role of “buffering” the physicochemical properties of the whole membrane. Thus, above  $T_m$ , CHOL increases bilayer rigidity by ordering the  $L_{\alpha}$  phase, and below  $T_m$ , CHOL increases bilayer fluidity.

\* Corresponding author at: Secció de Físicoquímica, Facultat de Farmàcia i Ciències de l'Alimentació, Av. Joan XXIII s.n., 08028, Barcelona, Spain.

E-mail address: [jordiborrell@ub.edu](mailto:jordiborrell@ub.edu) (J.H. Borrell).

<https://doi.org/10.1016/j.colsurfb.2018.11.040>

Received 4 June 2018; Received in revised form 1 November 2018; Accepted 19 November 2018

Available online 19 November 2018

0927-7765/ © 2018 Elsevier B.V. All rights reserved.



The interaction between lipid components of membranes has been extensively investigated by means of monolayers [11–14]. A lipid monolayer represents half of a membrane, and is a very well-defined planar system that is well-suited for studying intermolecular interactions between membrane lipids and lipid-protein interactions. At the air-water interface, a lipid monolayer presents different phases depending on the lateral surface pressure ( $\pi$ ) applied. At low  $\pi$ , the molecular area occupied by a monolayer is large and it is said to be in gaseous phase. By increasing  $\pi$ , the molecular density increases from a liquid-expanded (LE) to a more ordered liquid-condensed (LC) phase. There is general agreement on equivalences: (i) between the LE phase in monolayers and the  $L_a$  phase in bilayers; and (ii) on the  $\pi = 30\text{--}35\text{ mN m}^{-1}$  [15] of a monolayer and the actual pressure of a bilayer. In general, CHOL interacts with phospholipids in monolayers by condensing its packaging, reducing acyl chain motion in lipids above their LE to LC transition, allowing increased motion, and reducing the order in acyl chains of phospholipids at temperatures below their respective phase transitions.

Another important observation is the formation of laterally separated lipid domains occurring in pure phospholipids when they undergo a phase transition, and for mixtures of CHOL and phospholipids [7]. The existence of such domains was earlier investigated by epifluorescence of monolayers doped with fluorescent phospholipids [16]. As expected, domain formation under stressing conditions, i.e. changes of temperature or surface pressure, result in changes in the viscosity of the monolayers and, therefore in their nanomechanical properties. The emergence of surface probe microscopies such as atomic force microscopy (AFM) and AFM in force spectroscopy (FS) mode introduces the possibility of extracting nanomechanical magnitudes from force curve measurements [17,18].

While most naturally occurring phospholipids found in membranes are heteroacid phosphatidylcholines, with a saturated acyl chain in the *sn*-1 position and unsaturated acyl chain in the *sn*-2 position [19]; homoacid phosphatidylcholines, with both *sn*-1 and *sn*-2 positions formed by saturated acyl chains, can be found in specialized membrane systems such as lung surfactant [20]. Taking into account the enormous variety of membrane lipid composition [19], in this study we have investigated the interaction of CHOL with homoacid and heteroacid phospholipids. Specifically, we selected two saturated homoacid phospholipids: 1,2-palmitoyl-*sn*-glycero-3-phosphatidylcholine (DPPC) and 1,2-distearoyl-*sn*-glycero-3-phosphatidylcholine (DSPC); one heteroacid saturated phospholipid: 1-palmitoyl-2-stearoyl *sn*-glycero-3-phosphatidylcholine (PSPC); and two heteroacid phospholipids with the *sn*-2 acyl chain with one and two unsaturations, 1-palmitoyl-2-oleoyl-*sn*-glycero-3-phosphatidylcholine (POPC) and 1-palmitoyl-2-linoleyl-*sn*-glycero-3-phosphatidylcholine (PLPC), respectively. We took the proportion of CHOL required to abolish the  $L_\beta$  to  $L_a$  transition from an earlier paper [10], and investigated the mixing properties at the interface when these specific CHOL-phospholipid ratios were used. In order to know the electrical behaviour at the air-water interface measurements of the molecular dipole moment of the monolayers were made [11]. In addition to the surface studies complementary characterization of Langmuir-Blodgett films transferred at  $30\text{ mN m}^{-1}$  were made employing AFM and AFM-FS. The aim of this study was to provide information on variations in behaviour of laterally segregated domains formed at saturation concentration of CHOL.

## 2. Experimental section

### 2.1. Materials

DPPC, DSPC, PLPC, POPC, PSPC and CHOL were purchased from Avanti Polar Lipids (Alabaster, USA). All the other chemicals were acquired from Sigma-Aldrich (St. Louis, USA) and used as received. Lipids were dissolved in a chloroform/methanol (3:1, v/v) solution to obtain a final concentration of 1 mg/ml. These solutions were used to obtain the

mixtures of PLPC:CHOL (0.93/0.07 mol/mol), POPC:CHOL (0.85/0.15, mol/mol), PSPC:CHOL, (0.70/0.30, mol/mol), DPPC:CHOL (0.70/0.30, mol/mol) and DSPC:CHOL (0.70/0.30, mol/mol).

### 2.2. Monolayer experiments

Monolayers were prepared in a 312 DMC Langmuir-Blodgett trough (NIMA Technology Ltd. Coventry, England) with a total area of  $300\text{ cm}^2$ . The trough was placed onto a vibration-isolated table (Newport, Irvine, CA, USA) enclosed in an environmental chamber. The resolution of surface pressure measurement was  $0.1\text{ mN m}^{-1}$  and the barriers' velocity was fixed at a  $20\text{ cm}^2\text{ min}^{-1}$ . Surface potential experiments were carried out using a surface potential sensor with a resolution of 1 mV. The entire system was maintained at  $24.0 \pm 0.20^\circ\text{C}$  with a water circulating bath. The trough was filled with buffer solution (10 mM Tris, 150 mM NaCl, pH 7.40), thereafter aliquots of lipid were spread carefully onto the surface with a microsyringe. A period of 15 min was required to allow the solvent to evaporate before the experiment was started. No less than three identical replicas were achieved for each isotherm analysed.

The Langmuir-Blodgett monolayer deposition was performed on square mica surfaces (Ted Pella, Redding, CDN) used as substrates for the AFM experiments, at  $30\text{ mN m}^{-1}$ , which is considered a biologically relevant surface pressure, and with a dip speed of  $1\text{ mm min}^{-1}$ . Prior to observation of the surface, mica squares were attached to steel discs with double-sided tape.

### 2.3. Elasticity of the monolayer

To evaluate the lateral packing of the monolayer the compression modulus values at a defined composition ( $G_s^{-1}$ ) [21,22] were calculated according to

$$C_s^{-1} = -A \left( \frac{\partial \pi}{\partial A} \right)_{T,n} \quad (1)$$

The derivative of the experimental data was computed by fitting a straight line to a window of area width of  $0.2\text{ nm}^2\text{ molecule}^{-1}$  around any given surface pressure value, so that experimental noise was filtered out.

### 2.4. Thermodynamic analysis

The interaction between two components in a mixed monolayer, at a constant surface pressure  $\pi$  and temperature, can be evaluated by calculating the excess Gibbs energy ( $G^E$ ), which is given by

$$G^E = \int_0^\pi [A_{12} - (\chi_1 A_1 + \chi_2 A_2)] d\pi \quad (2)$$

where  $\chi_1$ ,  $A_1$  and  $\chi_2$ ,  $A_2$  are the molar fractions and the area per molecule of the pure component 1 and 2, respectively, and  $A_{12}$  is the area per molecule of the mixed monolayer. Positive  $G^E$  values indicate repulsion between the components in the monolayer, while negative  $G^E$  values indicate attraction between them. Zero  $G^E$  values could be interpreted as ideal behaviour of the mixture or as complete segregation of the components. For a quantitative comparison between monolayers with different compositions, it is more suitable to obtain the Gibbs energy of mixing,  $\Delta_{\text{mix}}G$ , expressed as

$$\Delta_{\text{mix}}G = G^E + RT(\chi_1 \ln \chi_1 + \chi_2 \ln \chi_2) \quad (3)$$

where  $\chi_i$  are the molar fractions of each component in the mixed monolayer, and  $R$  and  $T$  are the universal gas constant and temperature, respectively. Whilst  $\Delta_{\text{mix}}G > 0$  indicate instability of the monolayer, negative values indicate stability.

Furthermore the regular solution theory (RST) can be applied to obtain the interaction parameter ( $\xi$ ) [23,24] which is expressed as



$$\xi = \frac{G^E}{RT\chi_1\chi_2} \quad (4)$$

in which  $R$  and  $T$ , are the universal gas constant and temperature, respectively. Then, knowing  $\xi$  we can obtain the activity coefficient ( $\gamma$ ) of the two components of the bilayer by using the following equations

$$\ln \gamma_1 = \xi (1 - \chi_1)^2 \quad (5)$$

and

$$\ln \gamma_2 = \xi (1 - \chi_2)^2 \quad (6)$$

### 2.5. Surface potential measurements

Lipids and phospholipids are usually molecules with a non-zero value of dipolar moment, meaning that the interaction of these dipoles with an external electric field leads to their reorientation in the direction of the field that is applied. The average component of the molecular dipole moment normal to the plane of the monolayer ( $\mu_{\perp}$ ) was calculated according to the Helmholtz equation:

$$\mu_{\perp} = \Delta V A \epsilon_0 \epsilon_r \quad (7)$$

where  $A$  is the average molecular area,  $\Delta V$  is the experimentally determined surface potential, and  $\epsilon_0$  and  $\epsilon$  are permittivities of the vacuum and the monolayer, respectively. Usually,  $\epsilon$  is taken as 1, but some authors [25] have determined that for a DPPC bilayer this value is 3.2. Therefore, we took a value of 1.6 as representative for a lipid monolayer.

### 2.6. AFM imaging and force spectroscopy

AFM images and force spectroscopy measurements were performed with a Nanoscope IV from Digital Instruments (Santa Barbara, CA) equipped with a 15  $\mu\text{m}$  piezoelectric scanner. Similarly to preceding works [26] images and force curves were acquired using V-shaped silicon nitride cantilevers (OMCL TR400PSA, Olympus, Japan) with a nominal spring constant of 80 pN  $\text{nm}^{-1}$ , in air and in Tapping<sup>®</sup> mode. During the experiments, the force applied to the samples was kept as low as possible to minimize monolayer damage. All the images were processed using Digital Instrument software.

For the force spectroscopy experiments, individual spring constants ( $k_c$ ) were calibrated using the equipartition theorem, after having correctly determined the photodetector optical sensitivity (V/nm) by measuring it at high voltages. Applied forces  $F$  are given by  $F = k_c \times \Delta$ , where  $\Delta$  stands for the cantilever deflection. The surface deformation is given as penetration ( $\delta$ ), evaluated as  $\delta = z - \Delta$ , where  $z$  represents the piezo-scanner displacement. Hundreds of force versus tip-sample distance curves were acquired to obtain enough relevant data. Temperature was controlled and constantly monitored during the experiments, so that the system was always thermally equilibrated at 24 °C.

## 3. Results and discussion

There are still many questions that remain to be answered regarding phospholipid-CHOL interactions within membranes. The heart of the problem lies in the extreme variety and different proportions of naturally occurring phospholipids and CHOL present in the membranes [19]. In this study, we selected two heteroacid unsaturated phospholipids (POPC and PLPC) with one and two double bonds in the *sn*-2 acyl chain respectively; two homoacid saturated phospholipids (DPPC and DSPC) differing in two methylene groups in length; and one heteroacid saturated phospholipid (PSPC), for which information on the amount of CHOL required to abolish the  $L_{\beta}$  to  $L_{\alpha}$  transition in bilayers is available from earlier published DSC data [10].

The surface pressure-area ( $\pi$ - $A$ ) isotherms recorded at

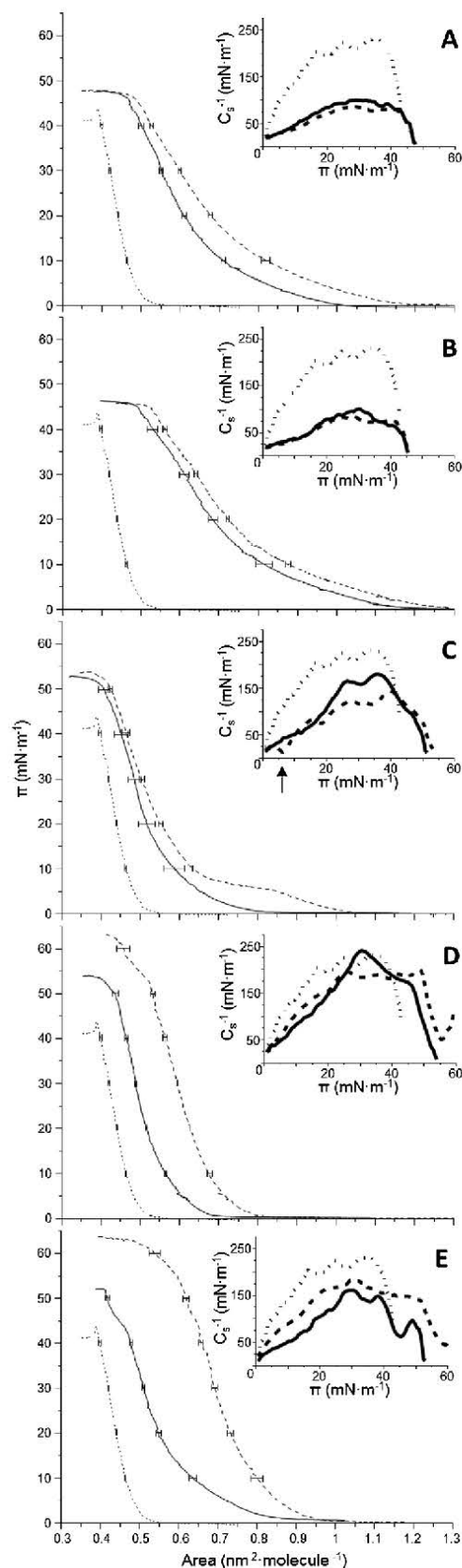


**Fig. 1.** The surface pressure ( $\pi$ ) area isotherms and compression modulus ( $C_s^{-1}$ ) (inset) for pure CHOL (dotted line), pure phospholipid (dashed line) and their mixture (continuous line). The mixtures were: POPC:CHOL (0.85:0.15, mol/mol) (A); PLPC:CHOL (0.93:0.07, mol/mol) (B); DPPC:CHOL (0.70:0.30, mol/mol) (C); DSPC:CHOL (0.70:0.30, mol/mol) (D); and PSPC:CHOL (0.70:0.30, mol/mol) (E).



$24.0 \pm 0.2^\circ\text{C}$  for pure phospholipids, pure CHOL and the various binary mixtures investigated in this study are shown in Fig. 1. The features of the CHOL isotherm were typical: it was in a condensed-like state until it collapsed at  $\pi_c = 44.1 \pm 0.5 \text{ mN m}^{-1}$  [27]. This isotherm is included in all Fig. 1 for better comparison.

As expected, each phospholipid isotherm had particular features: LC, LE or the coexistence of both phases and surface collapse pressure ( $\pi_c$ ). As can be seen, the features of the pure lipid isotherms are similar to others published elsewhere: for POPC and PLPC [28], for POPC and DSPC [12], and for PSPC [29,30]. For DPPC extensive literature showing the features of the corresponding compression isotherm is also available [31,32,23], and references thereafter, which coincide with the general behaviour observed in the present work and shown here as a proof of concept.

The  $\pi$ - $A$  isotherms of pure POPC and pure PLPC are shown in Fig. 1A and B, respectively. The features of both monolayers were in agreement with isotherms in the expanded state, until collapse occurred at  $48.0 \pm 0.1 \text{ mN m}^{-1}$  for POPC and  $46.2 \pm 0.3 \text{ mN m}^{-1}$  for PLPC. The binary systems POPC:CHOL (0.85:0.15, mol/mol) and PLPC:CHOL (0.93:0.07, mol/mol) isotherms shifted, as expected, to lower molecular areas with respect to each pure phospholipid isotherm in proportion to the amount of CHOL present. The  $\pi_c$  observed in both unsaturated binary systems closely coincided with that of the pure phospholipid, which is reasonable taking into account the low proportion of CHOL present. In turn, the  $\pi$ - $A$  isotherm of pure DSPC (Fig. 1D) was the most condensed of the other pure phospholipid monolayers presented in this study. Features of this isotherm are the subtle transition observed at  $57.2 \pm 0.4 \text{ mN m}^{-1}$  and the  $\pi_c$  that appeared at  $65.3 \pm 0.5 \text{ mN m}^{-1}$ . The binary system DSPC:CHOL (0.70:0.30, mol/mol) underwent also the shift toward lower molecular areas by comparison with the  $\pi$ - $A$  isotherms of pure DSPC. There was no higher-pressure transition equivalent to the one seen for DSPC, possibly because the monolayer of the mixture collapse at  $54.0 \pm 0.3 \text{ mN m}^{-1}$ . The compression isotherm of pure DPPC (Fig. 1C) showed the well-known liquid-expanded (LE) to liquid-condensed (LC) phase transition with a typical plateau between  $5.3 \pm 0.2 \text{ mN m}^{-1}$  and  $8.6 \pm 0.2 \text{ mN m}^{-1}$  and  $\pi_c = 55.0 \pm 0.1 \text{ mN m}^{-1}$ . In the case of the DPPC:CHOL (0.70:0.30, mol/mol) monolayer, apart from the expected shift to lower molecular areas, the plateau region was not observed and  $\pi_c$  was reached at  $54.3 \pm 0.6 \text{ mN m}^{-1}$ . Pure PSPC (Fig. 1E) underwent a monotonic surface pressure increase under progressive compression toward lower molecular areas, reaching  $\pi_c$  at  $64.0 \pm 0.1 \text{ mN m}^{-1}$ . The PSPC:CHOL (0.70:0.30, mol/mol) monolayer shifted to lower molecular areas than pure PSPC with a  $\pi_c$  at  $53.6 \pm 0.3 \text{ mN m}^{-1}$ . Interestingly, the mixed isotherm revealed the existence of a subtle transition at  $44 \text{ mN m}^{-1}$  that coincided with the surface pressure collapse of pure CHOL.

In any event, the interaction of CHOL with the phospholipids that were investigated occurs in monolayers with different degrees of packing has been discussed elsewhere [9]. The common trend, however, was a shift to lower molecular areas in the presence of CHOL. This effect has been exhaustively studied for the case of DPPC from the late 1960s [33] to the present [14]; for the case of DSPC [13] and also for acyl unsaturated species such as POPC and PLPC [28]. However, whilst we have selected the particular molar proportion of CHOL that abolishes the  $L_\beta$  to  $L_\alpha$  transition in bilayers, the observed shift appears in proportion to the amount of CHOL present in the binary system.

At the temperature of the experiments,  $24.0 \pm 0.2^\circ\text{C}$ , the changes in compressibility modulus (Eq. 1) with the surface pressure are shown in the insets of Fig. 1. The compression modulus were calculated at  $30 \text{ mN m}^{-1}$  and  $24.0 \pm 0.2^\circ\text{C}$ . As mentioned above this lateral pressure in monolayers is accepted as the equivalent lateral pressure in a bilayer [15]. Thus, whilst POPC and PLPC are in the LE phase, DPPC, DSPC and PSPC are in the LC state. Notably, when kept below the corresponding critical temperature [34] and surface pressure, phospholipid monolayers may undergo several phase transitions. The maximal values of  $C_s^{-1}$  were observed for pure CHOL, which proves the

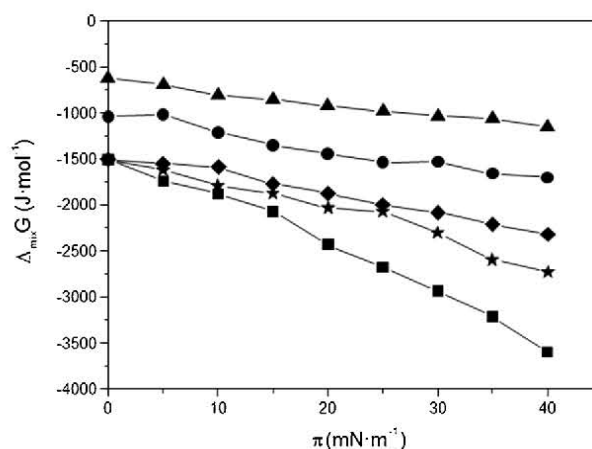


Fig. 2. The variation of Gibbs energy of mixing as a function of surface pressure for: PLPC:CHOL (0.93:0.07, mol/mol) (▲), POPC:CHOL (0.85:0.15, mol/mol) (●), DPPC:CHOL (0.70:0.30, mol/mol) (◆), DSPC:CHOL (0.70:0.30, mol/mol) (\*) and PSPC:CHOL (0.70:0.30, mol/mol) (■).

condensed-like state of this monolayer. For POPC (Fig. 1A) and PLPC (Fig. 1B),  $C_s^{-1}$  values at  $30 \text{ mN m}^{-1}$  were below  $100 \text{ mN m}^{-1}$ , typical of LE phases. In the DPPC monolayer (Fig. 1C), the characteristic minimum of  $C_s^{-1}$  (see black arrow in Fig. 1C) reflected the LE-LC transition of this monolayer. At  $30 \text{ mN m}^{-1}$ , DSPC and PSPC monolayers (Fig. 1D and E) showed  $C_s^{-1}$  values above  $100 \text{ mN m}^{-1}$ , which are typical of the LC state [21]. The incorporation of CHOL into the saturated phospholipids at the given proportions of interest induced an increase in the  $C_s^{-1}$  values respect to the values of the pure phospholipid except for the PSPC:CHOL mixture (Fig. 1E). This reflected the increase in packing density undergone by the film. On the contrary the addition of CHOL to unsaturated phospholipids did not modify  $C_s^{-1}$  values at the molar fraction used.

From isotherm data of phospholipid-CHOL mixtures, we can perform a basic surface thermodynamic analysis. On the basis of isotherm data points and using Eq. 3, we can use  $\Delta_{\text{mix}}G$  values for the mixtures to estimate the mixing behaviour and the stability of the monolayers. The negative values of  $\Delta_{\text{mix}}G$  observed for all the mixed monolayers studied (Fig. 2) indicate stability of all binary systems investigated. Notice that phase separation could be predicted only if several proportions PC:CHOL are studied [35]. Interestingly, the mixture of CHOL with the heteroacids POPC and PLPC showed the lowest absolute values of  $\Delta_{\text{mix}}G$ . For instance, at a surface pressure of  $30 \text{ mN m}^{-1}$ , the  $\Delta_{\text{mix}}G^{\text{POPC}}$  value was  $-1535 \text{ J mol}^{-1}$  and the  $\Delta_{\text{mix}}G^{\text{PLPC}}$  value was  $-1034 \text{ J mol}^{-1}$ . For the saturated phospholipids, the binary systems with CHOL followed an order of stability as follows: DPPC < DSPC < PSPC. Actually, the mixture of CHOL with DPPC, DSPC and PSPC, showed quite similar  $\Delta_{\text{mix}}G$  values below  $10 \text{ mN m}^{-1}$ . At high surface pressures, i.e.  $30 \text{ mN m}^{-1}$ , monolayers became more stable ( $\Delta_{\text{mix}}G$  values are more negative) and the mixture of CHOL with PSPC was the most stable. Caution should be taken with data in Fig. 2 because the direct comparison of  $\Delta_{\text{mix}}G$  values is only possible between mixtures having the same proportion of CHOL, in our case between the mixtures with saturated phospholipids. However, data for the mixtures of CHOL with unsaturated phospholipids are also shown in Fig. 2. Notice that we are comparing mixing behaviour at such a CHOL concentration that abolishes the  $L_\beta$  to  $L_\alpha$  phase transition in bilayers.

Supplementary data result from the calculation of  $\xi$  and  $\gamma$  by using Eqs. 4, 5 and 6, respectively. Notice that these three equations depend on the value of  $G^E$  (Eq. 2) and that the more negative values of  $G^E$ , the more stable the monolayers are [13]. As can be seen in Table 1, all values of  $G^E$  and  $\xi$  were negative, indicating attractive interactions between the two components of the system. According to  $\xi$  the cohesive forces are higher for the PSPC:CHOL and PLPC:CHOL systems than for



**Table 1**

Excess Gibbs energy, interaction parameter and activity coefficients of PC and Chol.

System	$G^E$ (J mol <sup>-1</sup> )	$\xi$	$\gamma_{PC}$	$\gamma_{CHOL}$
POPC:CHOL	-491.01	-1.56	0.97	0.32
PLPC:CHOL	-439.53	-2.54	0.99	0.11
DPPC:CHOL	-289.51	-0.56	0.95	0.76
DSPC:CHOL	-793.04	-1.53	0.87	0.47
PSPC:CHOL	-1429.81	-2.75	0.78	0.26

DPPC:CHOL, DSPC:CHOL and POPC:CHOL systems. On one hand the activity coefficient values in Table 1 show always smaller values of  $\gamma_{CHOL}$  than for  $\gamma_{PCs}$ . On the other hand values of  $\gamma_{CHOL}$  were higher (less deviation from the ideal mixing) for systems formed with homoacid phospholipids than for the ones formed with the heteroacid phospholipids. The only reference available in our knowledge comes from the work of Kodama et al., [23] that provided values of  $\gamma$  for DPPC and CHOL of 0.81 and 0.33 at 30 mN m<sup>-1</sup>, respectively. At the same surface pressure our calculations were 0.95 and 0.77 for the same system. These differences might arise from the different composition of the subphases used.

For completeness, the lateral organization of the molecules in the monolayer was investigated by determining the vertical component of the dipole moment, calculated according to Eq. 7. The variations of  $\mu_{\perp}$  as a function of the surface pressure for the monolayers of interest are shown in Fig. 3. We observed a decrease in  $\mu_{\perp}$  values as the surface pressure increased. Observation of the pure CHOL curve (dotted line in Fig. 3) revealed that it presented the lowest  $\mu_{\perp}$  values, in comparison with the pure phospholipid and mixtures with CHOL. There were two general trends: (i) addition of CHOL to phospholipids resulted in a monotonic decrease as the surface pressure increased; and (ii) when CHOL was mixed with unsaturated species (POPC, PLPC), the absolute values of  $\mu_{\perp}$  were higher than those of the pure phospholipids (Fig. 3A and B); and when mixed with the saturated phospholipids (DPPC, DSPC and PSPC), CHOL provoked a decrease of  $\mu_{\perp}$ , in comparison with the pure phospholipids (Fig. 3C–E).

The decrease of  $\mu_{\perp}$  as  $\pi$  increases has been reported previously [36–40] and is attributed to strengthening of the depolarized molecular interactions in the monolayers as compression progresses. Although all phospholipids under investigation share the same headgroup, theoretical calculations [41] suggest that the interactions at this level with the water surface molecules may be different between saturated and unsaturated species. This fact was already contemplated by the three-layer model that suggested the existence of three independent contributions to  $\mu_{\perp}$ : one from the hydrophilic head group, a second one from the hydrophobic tails and the third one from the underlying water subphase [21,22]. Furthermore, the variations in  $\mu_{\perp}$  in the presence of CHOL would be caused mainly by differences in the respective acyl chains of the phospholipids with the rigid steroid nucleus.

These results can be tentatively interpreted using the umbrella model [42,43] that suggests a preferential interaction of CHOL molecules with the hydrophobic tails of the phospholipids leaving the hydroxyl group nearby to the phospholipid headgroup. As discussed elsewhere [44] this suggests that CHOL modifies preferably the  $\mu_{\perp}$  component associated with the verticality of the tails. When the monolayers are in the LE phase, as it is the case of POPC and PLPC, the molecule of CHOL associates with the phospholipids in such a way that induce an increase of the  $\mu_{\perp}$  value. These values could be correlated with a more vertical orientation of the acyl chains with respect to the normal orientation of the monolayer without decreasing the molecular area of the components, as suggested by the compressibility modulus, insets in Fig. 1A and B, where  $C_s^{-1}$  values of the mixed monolayer are close to the pure phospholipid monolayers. Conversely, the interaction of CHOL into LC monolayers such as DPPC, DSPC and PSPC would prevent their acyl chains from adopting the all-trans configuration

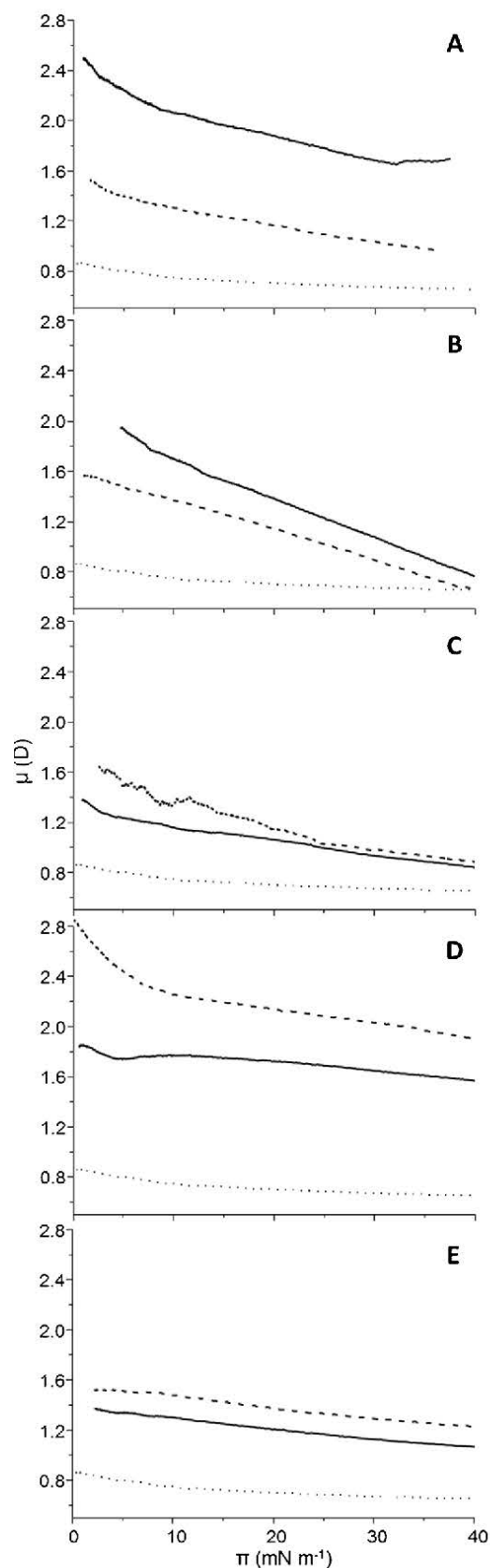


**Fig. 3.** Vertical component of the dipole moment ( $\mu_{\perp}$ ) as a function of the surface pressure for pure CHOL (dotted line), pure phospholipid (dashed line) and their mixture (continuous line). The mixtures were: POPC:CHOL (0.85:0.15, mol/mol) (A); PLPC:CHOL (0.93:0.07, mol/mol) (B); DPPC:CHOL (0.70:0.30, mol/mol) (C); DSPC:CHOL (0.70:0.30, mol/mol) (D); and PSPC:CHOL (0.70:0.30, mol/mol) (E).

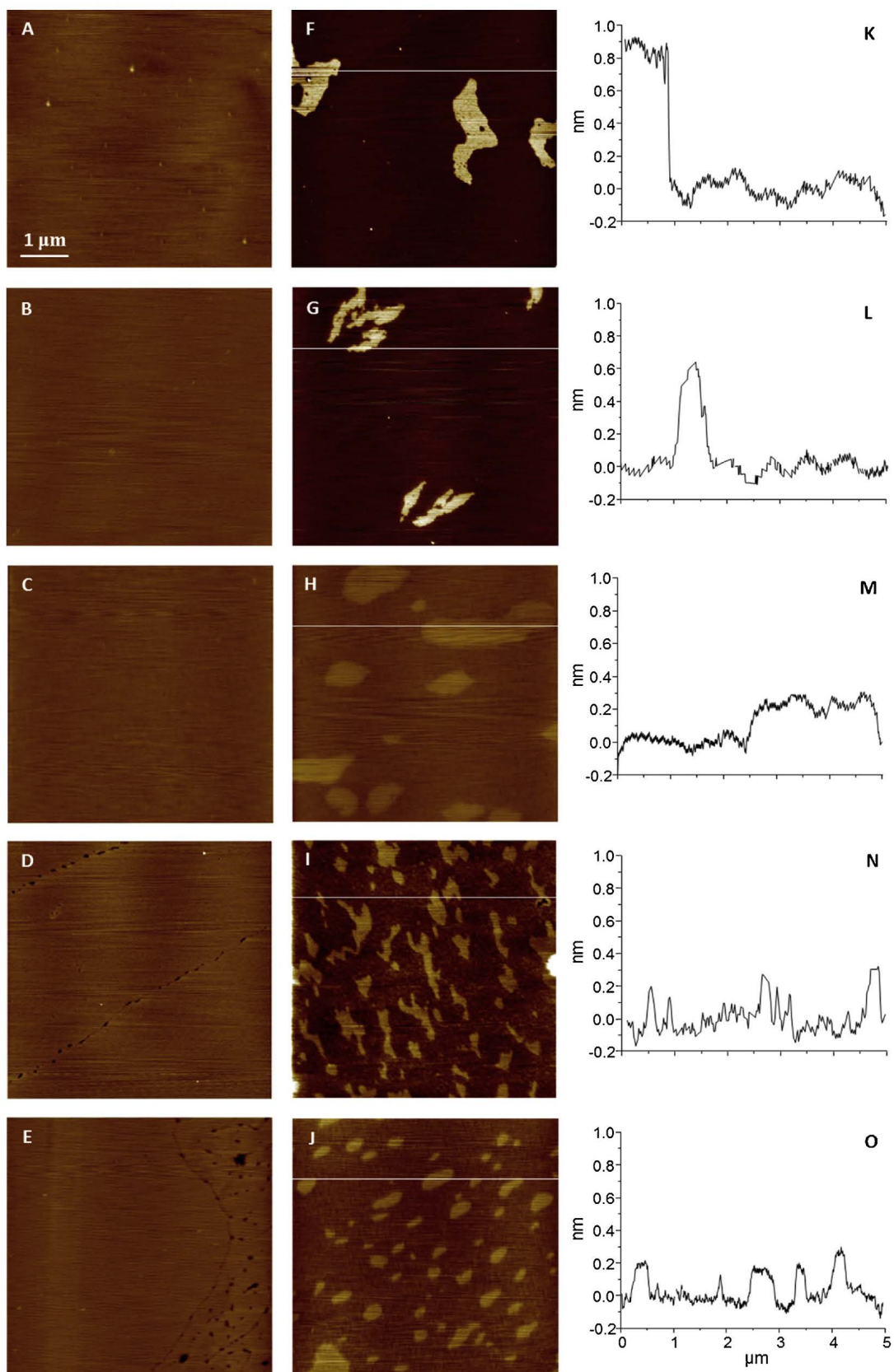


**Fig. 4.** AFM topographic images of POPC (A), PLPC (B), DPPC (C): DSPC (D) and PSCP (E), POPC:CHOL (0.85:0.15, mol/mol) (F), PLPC:CHOL (0.93:0.07, mol/mol) (G), DPPC:CHOL (0.70:0.30, mol/mol) (H), DSPC:CHOL (0.70:0.30, mol/mol) (I) and PSCP:CHOL (0.70:0.30, mol/mol) (J) LBs. Line profile analysis of images F to J (K to O).



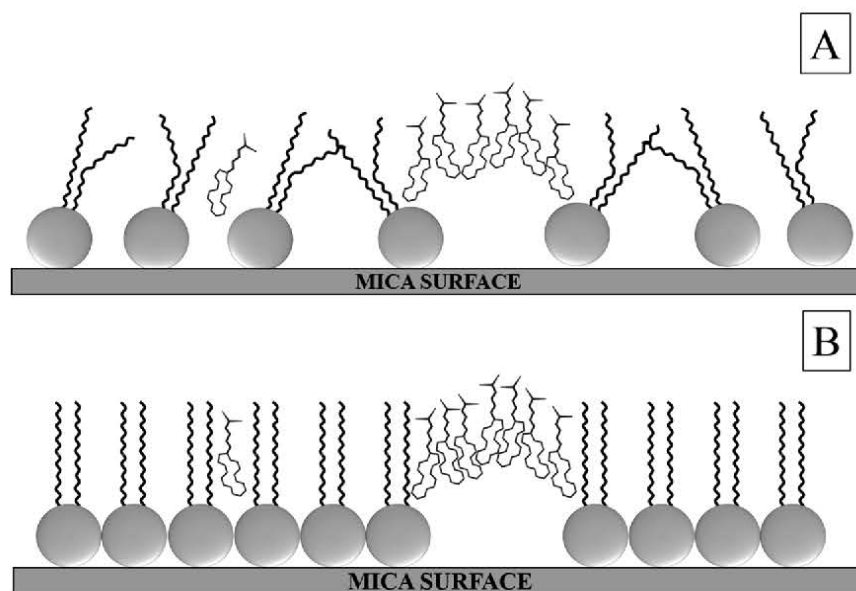


Fig. 5. Cartoon representation of the possible organization of CHOL with unsaturated (A) and saturated (B) phospholipids in the LB film.

leading to tilt in the monolayer chains.

AFM was used to image topography of monolayers at nanoscale level. The monolayers were transferred onto mica substrates at the surface pressure of  $30 \text{ mN m}^{-1}$ . While LBs of pure phospholipids show flat and featureless surfaces (Fig. 4A–E), occasionally with some defects (black spots in the images in Fig. 4D and E) [24], all images of mixed phospholipid-CHOL LBs show the presence of two distinct domains (Fig. 4F–J). The features for the LBs of DPPC:CHOL (0.7:0.3, mol/mol) are highly similar to those reported in previous work [45] where LBs of a similar DPPC:CHOL ratio (0.75:0.25, mol/mol), were transferred at  $15 \text{ mN m}^{-1}$  using water as a subphase. Therefore, as suggested elsewhere [46] the bright (higher) domains that we observe might be attributed to CHOL enriched domains (see cartoon in Fig. 5). It should be noted that studies performed with monolayers of DPPC:CHOL at very low percentages of the steroid (as low as 5%) [6] have reported the existence of nanodomains formed by pure CHOL molecules dispersed in a DPPC matrix. The authors of that previous work suggested a limit of solubility of 5% CHOL in phospholipid monolayers. Therefore, we conclude that the amounts of CHOL required to abolish the  $L_{\beta}$  to  $L_{\alpha}$  transition (all largely above of 5%) led to the formation of micrometer segregated domains highly enriched in the sterol such as those we have observed in Fig. 4F–J. That is, above a solubility limit for each phospholipid species, higher amounts of CHOL would result in laterally separated (and higher) domains that are enriched in CHOL. Meanwhile, the domains observed in the LBs formed with unsaturated phospholipids plus CHOL are fewer in number and larger in size (Fig. 4F and 4G) than the domains corresponding to saturated species (Fig. 4H–J). These characteristics seem to be influenced by the thermodynamic characteristics of the monolayers, based on  $\Delta_{\text{mix}}G$  (Fig. 2) and  $\xi$  (Table 1) but the nuances of the relationships are fully discernible from the information at hand. The smallest domains are observed in the PSpC:CHOL monolayer which shows the highest decreases of  $\Delta_{\text{mix}}G$ , the most stable binary system according to Fig. 2 data.

The size of the domains seems to be related to the concentration of CHOL and with the saturated or unsaturated nature phospholipid, the thermodynamic stability of the monolayer, and the verticality of the molecules at the interface. Moreover, the step height differences between the upper (brighter) and lower (darker) domains for the monolayers in the LE phase (POPC:CHOL and PLPC:CHOL) were higher than for the monolayers in the LC phase (DPPC:CHOL, DSPC:CHOL and PSpC:CHOL) (Fig. 4K–O). A direct correlation cannot be ascertained, however, with the data available.

The double collapse of the isotherm of DSPC (Fig. 1D) and the variation in collapse pressures between PSpC and DSPC and their corresponding binary mixtures with CHOL, might suggest that the smaller bright regions observed by AFM for these mixtures could be due also to the segregation of enriched CHOL domains. This tendency of the molecules to interact preferentially with molecules of the same kind is in agreement with the observation of phase separation shown by Brewster angle microscopy (BAM) of PSpC:CHOL monolayers [12]. This effect might be a phenomenon shared with DPPC and DSPC. Conversely, the interaction between CHOL and POPC or PLPC, with hydrogen bonding and van der Waals attractions, act as stabilizing forces and might result in larger domains, probably composed of high concentration levels of CHOL and the corresponding unsaturated phospholipid (Fig. 4F and G). To the best of our knowledge, the only comparable prior observations of these kinds of domains were obtained using epifluorescence microscopy of POPC:CHOL monolayers [16] and BAM images obtained for DOPC:CHOL monolayers [12].

Our results are in agreement with the common assumption that the effect of CHOL on unsaturated phospholipids is weaker than the effect exerted on saturated phospholipids [12,14]. However, the size, shape and chemical composition of the laterally segregated domains are different, as is the amount of CHOL required to abolish the  $L_{\beta}$  to  $L_{\alpha}$  transition in bilayers [10]. This can be inferred from many surface imaging techniques, including BAM and AFM [47].

Furthermore, these domains, which were brighter in the images, were slightly rougher than the lower domains. As can be seen in Table 2, the nominal percentage of CHOL does not coincide with the area displayed by the higher domains observed by AFM. It should be noted, however, that percentages are not directly comparable because the mean molecular areas of pure components are strongly different in the monolayer than in the transferred LB. The line profile analysis

Table 2

Area covered (%) by the high domains in the images 4F–4J and nominal concentration of CHOL ( $\chi_{\text{chol}}$ ) in the systems.

System	AFM image (%)	$\chi_{\text{chol}}$ (%)
POPC:CHOL	7	15
PLPC:CHOL	4.3	7
DPPC:CHOL	17.9	30
DSPC:CHOL	24.4	30
PSpC:CHOL	16.5	30

through the lines traced in Fig. 4F–4J are shown in Fig. 4K–O. The step height differences ( $n = 50$ ) between the top domains (bright) and the lower domains were established in  $0.92 \pm 0.09$  and  $0.64 \pm 0.07$  nm for POPC (Fig. 4K) and PLPC (Fig. 4L) respectively; and  $0.2 \pm 0.04$  for DPPC (Fig. 4M),  $0.30 \pm 0.05$  nm, for DSPC (Fig. 4N) and  $0.20 \pm 0.03$  for PSPC (Fig. 4O).

Although phospholipids used in this study are quite similar in length, the addition of CHOL seems to induce the formation of domains of quite different thickness depending on the physical state of the phospholipids. When CHOL is in high proportions in a mixed monolayer, it segregates into enriched CHOL domains (Fig. 5). These domains are quite rigid and when they are in a LC monolayer (Fig. 5B), as the case of DSPC, DPPC or PSPC the topographic profile shown by the AFM in Tapping<sup>®</sup> mode reflects the step height differences due to the lateral organization. On the contrary, when CHOL is segregated in a LE matrix (Fig. 5A) it is possible that the AFM tip could slightly push down the unsaturated lipids (less rigid) but not the CHOL regions altering the measure of the step height between domains.

The available techniques do not provide direct information about the composition of the domains. However, we can obtain a measure of the physical properties of these domains by using AFM in FS mode. There are basically two nanomechanical properties that we can extract applying FS on supported lipid bilayers and LBs: (i) the so-called breakthrough or indentation force, or force that the monolayer can withstand before breaking; and (ii) the adhesion force [18]. The poor statistics of the indentation forces obtained for monolayers has been discussed elsewhere [48], and for this reason we have focused our efforts on obtaining  $F_{adh}$  values that became useful for discrimination of phase-separated lipid domains [49] and lipid-protein segregated domains [50] as observed by AFM. First of all, in order to get reference values, we measured the  $F_{adh}$  of pure phospholipid monolayers (Fig. 6). The mean values obtained by Gaussian fitting of the data in the histograms reveals lower values of  $F_{adh}$  for the unsaturated than for the saturated phospholipids. Thus, whilst the lowest mean  $F_{adh}$  value was obtained for pure POPC (29.74 nN) (Fig. 6A), the highest was obtained for pure PSPC (92.34 nN) (Fig. 6E). This behaviour seems apparently correlated with the lower verticality of unsaturated species in comparison to that of the saturated ones as deduced from the  $C_s^{-1}$  values (Fig. 1). The histograms for the different domains observed in the mixed monolayers were also studied (Fig. 7). The mean  $F_{adh}$  values for POPC:CHOL and PLPC:CHOL (Fig. 7A and B) showed lower  $F_{adh}$  values for the background domains (black bars) than the higher domains (white bars). Conversely, the mean  $F_{adh}$  value of DPPC:CHOL, DSPC:CHOL and PSPC:CHOL monolayers were lower for the higher domains than for the lower domain (Fig. 7C–E). In addition, it is worth noting that  $F_{adh}$  values in the DPPC:CHOL and DSPC:CHOL monolayers did not discriminate very well between domains, both in LC state while conversely, for POPC:CHOL, PLPC:CHOL and PSPC:CHOL the difference between  $F_{adh}$  mean values of the domains were clearly differentiated although PSPC:CHOL is in LC state

These results could be interpreted to indicate that the domains are not formed by pure CHOL or phospholipids. Conversely, the domains could contain both molecules: with one domain rich in CHOL (upper domain) and the other rich in phospholipid (lower domain). We can conclude that the qualitative behaviour varies between the binary mixtures of CHOL with saturated and unsaturated phospholipids. This principle, however, might not apply to the DPPC:CHOL system for which the average  $F_{adh}$  values of the brighter domains are higher than for the rest of the monolayer. It is worth mentioning that the surface thermodynamic analysis of the DPPC:CHOL monolayers reveal the existence of attractive interactions that are mid-way between the unsaturated and other saturated phospholipids and  $\mu_{\perp}$  showed very low modification of the DPPC curve when 30% of CHOL is present in the monolayer.

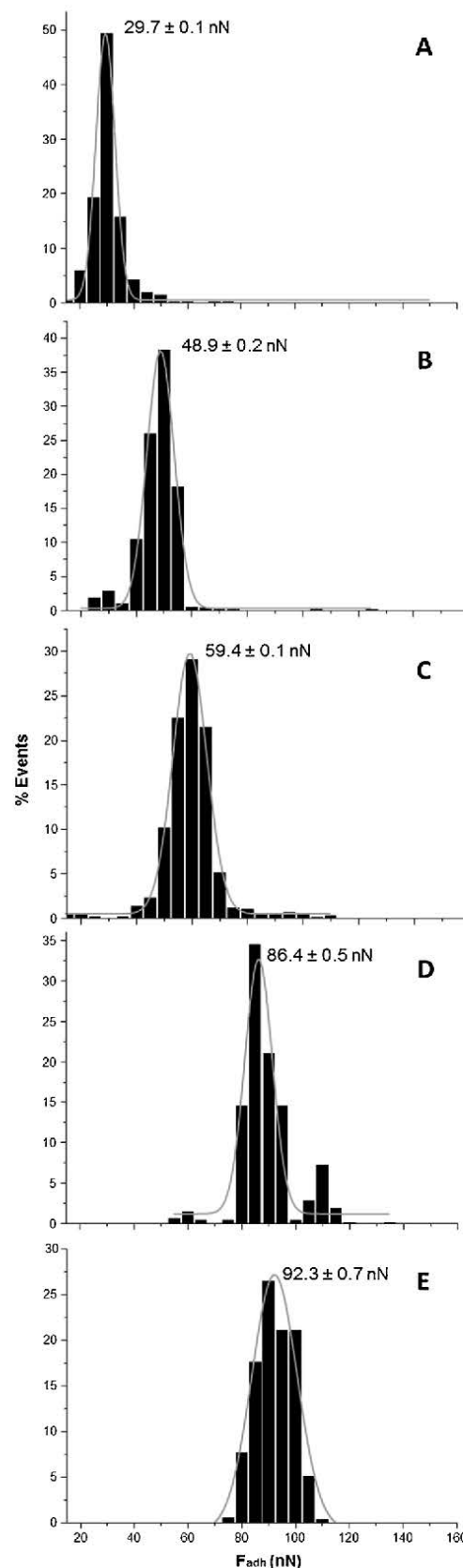


**Fig. 6.** Histograms for the  $F_{adh}$  values of pure POPC (A), PLPC (B), DPPC (C), DSPC (D) and PSPC (E). Values represent the mean  $F_{adh}$  value  $\pm$  the standard deviation obtained after fitting the data shown in the histogram to a Gaussian distribution.



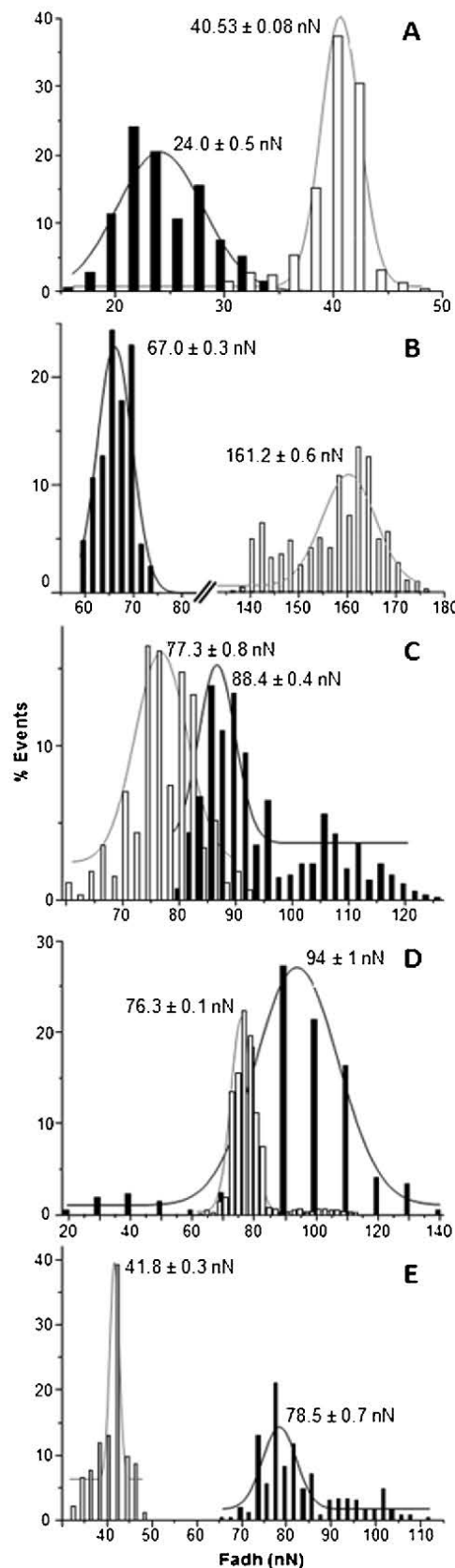


**Fig. 7.** Histograms for the  $F_{adh}$  values of the background (black columns) and higher domains (white columns) of the AFM images in Fig. 4. POPC:CHOL (0.85:0.15, mol/mol) (A), PLPC:CHOL (0.93:0.07, mol/mol) (B), DPPC:CHOL (0.70:0.30, mol/mol) (C), DSPC:CHOL (0.70:0.30, mol/mol) (D) and PSPC:CHOL (0.70:0.30, mol/mol) (E). Values represent the mean  $F_{adh}$  value  $\pm$  the standard deviation obtained after fitting the data shown in the histogram to a Gaussian distribution.

#### 4. Conclusions

One of the conclusions of the present study is that mixed monolayers of saturated PCs, are more condensed than the monolayers containing unsaturated PCs. Also, in agreement with multiple references, and although the proportions of CHOL are different, the interactions between the two components is stronger for the monolayers that contain saturated phospholipids in comparison with the unsaturated ones. The differentiated behaviour between the mixtures of CHOL with unsaturated and saturated phospholipids, is repeated when the vertical component of the dipole moment of the molecules is determined. Going further, the topography of the LBs transferred demonstrate the existence of two types of laterally segregated domains. Applying AFM in its force spectroscopy mode, we demonstrate that neither of these two domains is composed of pure CHOL or pure PCs.

#### Acknowledgements

The author would like to thank Dr. Kevin M.W. Keough for constructive criticism of the manuscript and to Dr. Christopher Evans for correcting the English. This study was carried out with the support of Grant no. TEC2016-79156-P from the Spanish Government's Ministry of Economy and Competitiveness. A.B-C has been sponsored through the 214SGR 1442 action of the Catalan Government (Generalitat de Catalunya).

#### References

- [1] G.W. van Meer, G. Voelker, E.R. Feigenson, Membrane lipids: where they are and how they behave, *Nat. Rev. Mol. Cell Biol.* 9 (2009) 112–124.
- [2] H.I. Ingo, M.N. Melo, F.J. Van Erden, C.A. Lopez, T.A. Wassenaar, X. Periole, A.H. De Vries, D.P. Tieleman, S.J. Marrink, *J. Am. Chem. Soc.* 136 (2014) 14554–14559 Lipid Organization of the Plasma Membrane.
- [3] W. Dowhan, Molecular basis form membrane phospholipid diversity: why are there so many lipids? *Annu. Rev. Biochem.* 16 (1996) 199–232.
- [4] G. van Meer, D.R. Voelker, G.W. Feigenson, Membrane lipids: where they are and how they behave, *Nat. Rev. Mol. Cell Biol.* 9 (2008) 112–124.
- [5] M.D. Houslay, K.K. Stanley, *Dynamics of Biological Membranes*, John & Wiley Sons, Chichester, 1982.
- [6] K. Kim, S.Q. Choi, Z. a Zell, T.M. Squires, J. a Zasadzinski, Effect of cholesterol nanodomains on monolayer morphology and dynamics, *Proc. Natl. Acad. Sci. U. S. A.* 110 (2013) E3054–60.
- [7] G.W. Feigenson, Phase diagrams and lipid domains in multicomponent lipid bilayer mixtures, *Biochim. Biophys. Acta Biomembr.* 1788 (2009) 47–52.
- [8] K.M.W. Keough, P.J. Davis, K. Morris, L.A. Manson (Eds.), *Membrane Fluidity* (Chapter 2), Plenum Publishing Corporation, New York, 1984.
- [9] P.J. Davis, K.M.W. Keough, Differential scanning calorimetric studies of aqueous dispersions of mixtures of cholesterol with some Mixed-Acid and Single-Acid, *Biochemistry* (1983) 5334–6340.
- [10] J. Hernandez-Borrell, K.M.W. Keough, Heteroacid phosphatidylcholines with different amounts of unsaturation respond differently to cholesterol, *Biochim. Biophys. Acta* 1153 (1993) 277–282.
- [11] H.M. Möhwald, R. Lipowsky, E. Sackman (Eds.), *Handbook of Biological Physics*, Vol. 1 Elsevier, Amsterdam, 1995.
- [12] P. Wydro, S. Knapczyk, M. Lapczyńska, Variations in the condensing effect of cholesterol on saturated versus unsaturated phosphatidylcholines at low and high sterol concentration, *Langmuir* 27 (2011) 5433–5444.
- [13] D.-L. Patrycja, K. Hąc-Wydro, Interactions between phosphatidylcholines and cholesterol in monolayers at the air/water interface, *Colloid Surf. B: Biointerfaces* 37 (2004) 21–25.
- [14] M. Jurak, Thermodynamic aspects of cholesterol effect on properties of phospholipid monolayers: langmuir and langmuir-blodgett monolayer study, *J. Phys. Chem. B* 117 (2013) 3496–3502.
- [15] D. Marsh, Lateral pressure in membranes, *Biochim. Biophys. Acta – Rev. Biomembr.* 1286 (1996) 183–223.
- [16] L.A. Worthman, K. Nag, P.J. Davis, K.M. Keough, Cholesterol in condensed and fluid phosphatidylcholine monolayers studied by epifluorescence microscopy, *Biophys. J.* 72 (1997) 2569–2580.
- [17] S. Garcia-Manyes, F. Sanz, Nanomechanics of lipid bilayers by force spectroscopy with AFM: a perspective, *Biochim. Biophys. Acta Biomembr.* 1798 (2010) 741–749.
- [18] L. Picas, P.E. Milhiet, J. Hernández-Borrell, Atomic force microscopy: a versatile tool to probe the physical and chemical properties of supported membranes at the nanoscale, *Chem. Phys. Lipids* 165 (2012) 845–860.
- [19] T. Harayama, H. Riezman, Understanding the diversity of membrane lipid composition, *Nat. Publ. Gr.* 19 (2018) 281–296.
- [20] J. Pérez-Gil, Structure of pulmonary surfactant membranes and films: the role of proteins and lipid – protein interactions, *Biochim. Biophys. Acta* 1778 (2008)



- 1676–1695.
- [21] J.T. Davies, E.K. Rideal, *Interfacial Phenomena*, 1st. ed., Academic Press Inc., New York, 1963.
- [22] M.C. Petty, *Langmuir-Blodgett Films: an Introduction*, Cambridge Univ. Press, Cambridge, 1996.
- [23] M. Kodama, O. Shibata, S. Nakamura, S. Lee, G. Sugihara, A monolayer study on three binary mixed systems of dipalmitoyl phosphatidyl choline with cholesterol, cholesterol and stigmasterol, *Colloid Surf. B: Biointerfaces* 33 (2004) 211–226.
- [24] G. Xu, C. Hao, L. Zhang, R. Sun, Investigation of surface behavior of DPPC and curcumin in langmuir monolayers at the air-water interface, *Scanning* (2017) 1–12 2017 Article ID 6582019.
- [25] G. Gramse, A. Dols-Perez, M.A. Edwards, L. Fumagalli, G. Gomila, Nanoscale measurement of the dielectric constant of supported lipid bilayers in aqueous solutions with electrostatic force microscopy, *Biophys. J.* 104 (2013) 1257–1262.
- [26] G. Oncins, G. Oncins, L. Picas, L. Picas, J. Hernandez-Borrell, S. Garcia-Manyes, F. Sanz, Thermal response of Langmuir-Blodgett films of dipalmitoylphosphatidylcholine studied by atomic force microscopy and force spectroscopy, *Biophys. J.* 93 (2007) 2713–2725.
- [27] K. Gong, S.S. Feng, M.L. Go, P.H. Soew, Effects of the pH on the stability and compressibility of DPPC/CHOL monolayers at the air-water interface, *Colloid. Surf. A: Physicochem. Eng. Aspects* 207 (2002) 113–125.
- [28] J.M. Smaby, M.M. Momsen, H.L. Brockman, R.E. Brown, Phosphatidylcholine acyl unsaturation modulates the decrease in interfacial elasticity induced by cholesterol, *Biophys. J.* 73 (1997) 1492–1505.
- [29] S. Ali, J.M. Smaby, M.M. Momsen, H.L. Brockman, R.E. Brown, Acyl chain-length asymmetry alters the interfacial elastic interactions of phosphatidylcholines, *Biophys. J.* 74 (1998) 338–348.
- [30] O. Bouffloux, A. Berquand, M. Eeman, M. Paquot, Y.F. Dufrière, R. Brasseur, M. Deleu, Molecular organization of surfactin-phospholipid monolayers: effect of phospholipid chain length and polar head, *Biochim. Biophys. Acta Biomembr.* 1768 (2007) 1758–1768.
- [31] T.H. Chou, C.H. Chang, Thermodynamic behavior and relaxation processes of mixed DPPC/cholesterol monolayers at the air/water interface, *Colloid Surf. B: Biointerfaces* 17 (2000) 71–79.
- [32] K. Kim, C. Kim, Y. Byun, Preparation of dipalmitoylphosphatidylcholine/cholesterol Langmuir-Blodgett monolayer that suppresses protein adsorption, *Langmuir* 17 (2001) 5066–5070.
- [33] M.C. Phillips, D. Chapman, Monolayer characteristics of saturated 1,2,-diacyl phosphatidylcholines (lecithins) and phosphatidylethanolamines at the air-water interface, *Biochim. Biophys. Acta* 163 (1968) 301–313.
- [34] J.H. Borrell, Ò. Domènech, Critical temperature of 1-Palmitoyl-2-oleoyl-sn-glycero-3-phosphoethanolamine monolayers and its possible biological relevance, *J. Phys. Chem. B* 121 (2017) 6882–6889.
- [35] R.A. Alberty, R.J. Silbey, *Physical Chemistry*, 1st. ed., John Wiley & Sons, Inc, New York, 1992.
- [36] F. He, Y. Lin, R. Li, G. Tang, D. Wu, Effects of lipid chain length on the surface properties of alkylaminomethyl rutin and of its mixture with model lecithin membrane, *Colloid Surf. B: Biointerfaces* 87 (2011) 164–172.
- [37] T. Hiranita, S. Nakamura, M. Kawachi, H.M. Courrier, T.F. Vandamme, M.P. Krafft, O. Shibata, Miscibility behavior of dipalmitoylphosphatidylcholine with a single-chain partially fluorinated amphiphile in Langmuir monolayers, *J. Colloid Interface Sci.* 265 (2003) 83–92.
- [38] H. Nakahara, S. Nakamura, K. Nakamura, M. Inagaki, M. Aso, R. Higuchi, O. Shibata, Cerebroside Langmuir monolayers originated from the echinoderms: I. Binary systems of cerebroside and phospholipids, *Colloid Surf. B: Biointerfaces* 42 (2005) 157–174.
- [39] K. Hoda, H. Nakahara, S. Nakamura, S. Nagadome, G. Sugihara, N. Yoshino, O. Shibata, Langmuir monolayer properties of the fluorinated-hydrogenated hybrid amphiphiles with dipalmitoylphosphatidylcholine (DPPC), *Colloid Surf. B: Biointerfaces* 47 (2006) 165–175.
- [40] Y. Ikeda, M. Inagaki, K. Yamada, T. Miyamoto, R. Higuchi, O. Shibata, Langmuir monolayers of cerebroside with different head groups originated from sea cucumber: binary systems with dipalmitoylphosphatidylcholine (DPPC), *Colloid Surf. B: Biointerfaces* (2009) 272–283.
- [41] G.F. Fausto Martelli, Hsin-Yu Ko, Carles Calero Borrallo, Structural properties of water confined by phospholipid membranes, *Front. Phys.* 13 (2018) 136801.
- [42] J. Huang, G.W. Feigenson, A microscopic interaction model of maximum solubility of cholesterol in lipid bilayers, *Biophys. J.* 76 (1999) 2142–2157.
- [43] P.R. Adhyapak, S.V. Panchal, A. Venkata, R. Murthy, Cholesterol induced asymmetry in DOPC bilayers probed by AFM force spectroscopy, *Biochim. Biophys. Acta Biomembr.* 1860 (2018) 953–959.
- [44] T. Starke-Peterkovic, N. Turner, M.F. Vitha, M.P. Waller, D.E. Hibbs, R.J. Clarke, Cholesterol effect on the dipole potential of lipid membranes, *Biophys. J.* 90 (2006) 4060–4070.
- [45] C. Yuan, L.J. Johnston, Phase evolution in cholesterol/DPPC monolayers: atomic force microscopy and near field scanning optical microscopy studies, *J. Microsc.* 205 (2002) 136–146.
- [46] L. Zhao, S.S. Feng, Effects of cholesterol component on molecular interactions between paclitaxel and phospholipid within the lipid monolayer at the air-water interface, *J. Colloid Interface Sci.* 300 (2006) 314–326.
- [47] Ó. Domènech, J. Ignés-Mullol, M. Teresa Montero, J. Hernandez-Borrell, Unveiling a complex phase transition in monolayers of a phospholipid from the annular region of transmembrane proteins, *J. Phys. Chem. B* 111 (2007) 10946–10951.
- [48] S. Garcia-Manyes, O. Domènech, F. Sanz, M.T. Montero, J. Hernandez-Borrell, Atomic force microscopy and force spectroscopy study of Langmuir-Blodgett films formed by heteroacid phospholipids of biological interest, *Biochim. Biophys. Acta* 1768 (2007) 1190–1198.
- [49] C.E.H. Berger, K.O. van der Werf, R.P.H. Kooyman, B.G. de Groot, J. Greve, Functional group imaging by adhesion AFM applied to lipid monolayers, *Langmuir* 11 (1995) 4188–4192.
- [50] C. Suárez-Germà, Ó. Domènech, M.T. Montero, J. Hernández-Borrell, Effect of lactose permease presence on the structure and nanomechanics of two-component supported lipid bilayers, *Biochim. Biophys. Acta Biomembr.* 1838 (2014) 842–852.

## Chapter 4. Results: A side quest

Planar lipid bilayers formed from thermodynamically-optimized liposomes as new featured carriers for drug delivery systems through human skin

M.L. Vázquez-González, **A. Botet-Carreras**, Ò. Domènech, M. Teresa Montero, J.H. Borrell

*International Journal of Pharmaceutics*, vol. 563, pp. 1–8, May. 2019

DOI: 10.1016/j.ijpharm.2019.03.052

### Techniques introduced

#### Sample preparation

##### *Extrusion*

Liposomes, particularly those made for this research, were prepared using the thin film method followed by extrusion. More specifically, the different components of the formulations were mixed in their stock solutions of chloroform:methanol (2:1, v/v) in a glass balloon flask, before being dried in a rotatory evaporator at room temperature and protected from the light. This process yielded a thin film adhering to the glass surface, which was afterwards exposed to a vacuum to remove any traces of the solvents.

At this point, after the addition of the buffer, we started subjecting the mixture to temperatures over its  $T_m$  and vortexed it before cooling it in an ice bath. Going over and under the  $T_m$  for five consecutive cycles, we created multilamellar liposomes in suspension. These were extruded using a syringe coupled to an extruder, like the one shown in Figure 11, where a polycarbonate filter was used to obtain the desired liposome diameter.

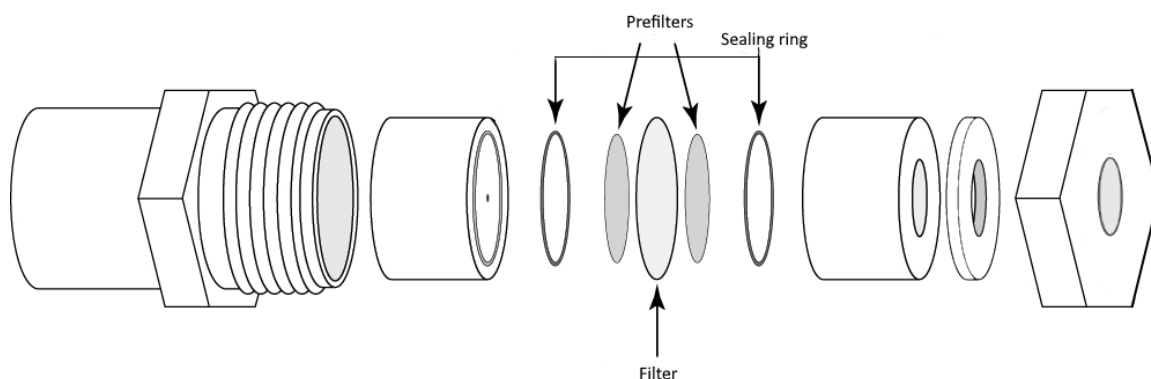


Figure 11. Syringe extruder, designed to extrude small volume formulations of between 0.5 and 1 ml. Two syringes are connected to the sides, allowing the user to push the volume from side to side in the extruder.

As the preparation went through the extruder at least eleven times, liposomes with diameters from 100 nm to 130 nm were obtained when passing through a 100-nm filter due to the intrinsic elasticity of the liposomes. This device was used to produce small batches of liposomes (0.5-1 ml). To produce larger amounts, we used a larger nitrogen-powered extruder, like the one shown in Figure 12, providing a great way to test the scalability of the formulation.

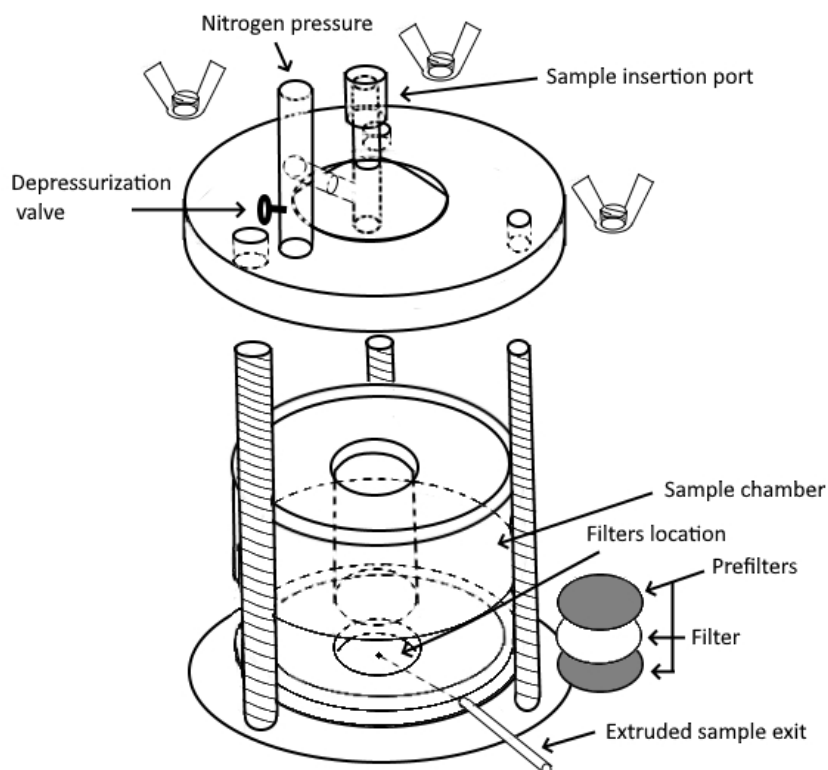


Figure 12. Nitrogen powered extruder, designed to extrude larger volumes of formulations, allowing scalability assays.

## Sample characterization

### *Nanosizer*

When preparing any liposome formulation, several analytical techniques can be performed. There are two classic techniques that are commonly used to characterize the size and charges of liposomes: the DLS technique to assess size and the analysis of the  $\zeta$ -potential to measure charge.

The DLS technique can determine the size distribution of each sample due to the scattered light of the laser beam. This well-established technique is typically used in the submicron region and is based on the Brownian motion of dispersed particles. When particles are dispersed in a liquid, they move randomly in all directions. The idea behind Brownian motion is that particles are constantly colliding with the solvent molecules, causing a certain amount of energy to be transferred that induces particle movement. Since the energy transfer is more or less constant, smaller particles are affected more, resulting in them moving at higher speeds than large particles [130].

The relationship between particle size and its movement is given by the Stokes-Einstein equation:

$$D = \frac{k_B T}{6\pi\eta R_H}$$

where  $D$  is the diffusion coefficient,  $k_B$  the Boltzmann constant,  $T$  the temperature,  $\eta$  the viscosity and  $R_H$  the hydrodynamic radius.

This equation considers that the movement of the particles is solely based on Brownian motion. This means that if there is sedimentation in the sample, there will be no random particle movement, thereby producing inaccurate results.

As shown in Figure 13, the basic setup for DLS measurements consists of a single-frequency laser directed at a sample. If the sample contains particles, the laser gets scattered in all directions. This scattered light is then detected at a certain angle over time.

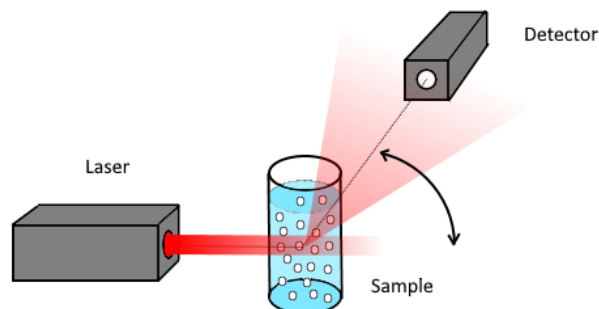


*Figure 13. Basic DLS measurement system. The sample is placed in a cuvette and the scattered light can be detected at different angles.*

As well as the size of the particles, another related important parameter is the polydispersity index (PDI), which indicates the broadness of the particle size distribution. A value below 0.1 reflects a good distribution and indicates that all the measured particles have a similar size.

As mentioned above, another important technique used for sample characterization is the measurement of the  $\zeta$ -potential to assess particle charge.  $\zeta$ -potential measurements have become important for characterizing surface functionality and the stability of dispersed particles in solution. This provides information on the effective surface charge of the sample. The  $\zeta$ -potential or electrokinetic potential is established at the surface of any material when it is exposed to a liquid medium and is typically given in millivolt units. In this work,  $\zeta$ -potential was important for two reasons: (i) any liposomes produced must bear a positive or negative potential, enough to give stability to avoid aggregation through electrostatic repulsions; and (ii) the membranes should have a similar surface charge or at least the same voltage sign as a living cell membrane in order to mimic it. As we expected a primary electrostatic interaction between the cells and the engineered liposomes, we needed to ensure that the vesicles had the opposite charge to that of the outer lipid monolayer of the cell membrane.

## Spectrofluorometry

Spectrofluorometric techniques are based on fluorescence from a sample or a probe added to it. Any fluorescent molecule can emit radiation when excited at a certain wavelength, emitting radiation with a longer wavelength.

Therefore, usually, in addition to the wavelength selectors and occasionally polarizers, the alignment between the source of excitation and the detector is not linear like it is in a conventional spectrophotometer, as we want to avoid the radiation from the source, which will be otherwise added to the emitted light. For this reason, there is usually a 90° source-detector configuration, as shown in Figure 14.

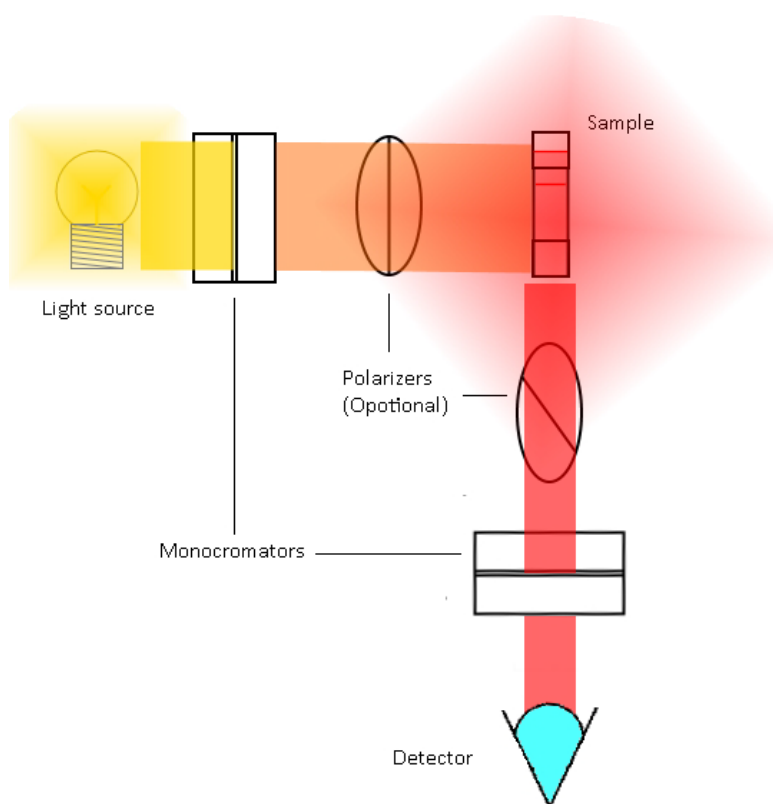


Figure 14. Basic spectrofluorometer setup. The light travels across the monochromator allowing the selection of the desired wavelength to excite the sample. The consequent emission light from the sample travels to the detector, crossing another monochromator, that filters out undesirable light like the excitation one.



### Laurdan

Laurdan is a fluorescent probe that can be used to distinguish differences in phospholipid orders due to changes in membrane fluidity. Laurdan is a polarity-sensitive probe that monitors dipolar relaxation and tends to be located at the glycerol backbone of the bilayer, with the lauric acid tail anchored in the phospholipid acyl chain region.

This probe was incubated with the liposomes under study at a lipid:probe ratio of 300:1. After the incubation, the Laurdan-liposome fluorescence was measured at different wavelengths and different temperatures. The generalized polarization ( $GP_{ex}$ ) was calculated as follows:

$$GP_{ex} = \frac{I_{440} - I_{490}}{I_{440} + I_{490}}$$

where  $I_{440}$  and  $I_{490}$  are the fluorescence intensities at emission wavelengths 440 nm (gel phase,  $L_{\beta}$ ) and 490 nm (liquid-crystalline phase,  $L_{\alpha}$ ), respectively. In general, high  $GP_{ex}$  values indicate the presence of a gel phase ( $L_{\beta}$ ), while low  $GP_{ex}$  values show the presence of a liquid-crystalline phase ( $L_{\alpha}$ ).

By examining the values of  $GP_{ex}$  at different temperatures, we can obtain information on the gel-to-fluid phase transition temperature ( $T_m$ ) as well as the slope of the curve, which indicates the cooperativity of the process.  $GP_{ex}$  values, as a function of temperature, were fitted to a Boltzmann-like equation:

$$GP_{ex} = GP_{ex}^2 + \frac{GP_{ex}^1 - GP_{ex}^2}{1 + \exp\left\{\frac{T_m - T}{m}\right\}}$$

where  $GP_{ex}^1$  and  $GP_{ex}^2$  are the maximum and minimum values of  $GP_{ex}$ , respectively, and  $m$  the slope of the curve.

$GP_{ex}$  values can be evaluated as a function of the excitation wavelength. On the plots of  $GP_{ex}$  at different excitation wavelengths, positive slopes are interpreted because of the presence

of domains of different compositions in different ordered phases in the lipid bilayer, while negative slopes imply transition towards a more fluid phase.

### Liposomal encapsulation efficiency

The encapsulation efficiency (*EE*) is a simple but useful way of quantifying the amount of drug or molecules encapsulated in a liposome sample. We can quantify this amount by high-performance liquid chromatography (HPLC), spectrophotometry or other quantitative techniques, applying the following equation:

$$EE = \frac{m_T - m'}{m_T} \times 100$$

where  $m_T$  and  $m$  are the total and non-entrapped amount of the drug in the samples, respectively.

### High performance liquid chromatography

HPLC separates the components of a sample using a chromatographic technique. The sample is passed through a column that is packed with different components designed to slow down the analytes by their molecular weight, charge or other physicochemical attributes. Depending on the retention time of the analytes in the column, they exit the system at different times.

HPLC is a classic method that has evolved in power. It uses high-performance pumps to provide high pressure and a stable flow, which, compared to the classic method, accelerates the process. In addition, the columns are specially designed to hold high pressures and the overall setup is coupled to a detector, allowing very accurate and high-resolution analyses.



## Ultraviolet and visible spectrometry

Spectrophotometers are based on the absorption of the visible and ultraviolet regions of the spectrum. The sample placed in a cuvette (cell) absorbs some of the incident radiation and the remainder is transmitted to the detector (see Figure 15).

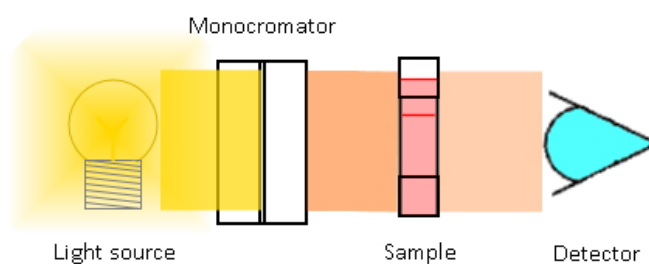


Figure 15. Basic spectrophotometer setup. The light travels across the monochromator, allowing the selection of the desired wavelength to go through the sample, which will be partly absorbed by the sample on its way to the detector.

The qualitative applications of absorption spectrometry depend on the fact that a given molecule absorbs radiation only in specific regions of the spectrum. A plot of the absorbance versus wavelength (absorption spectrum) serves as a fingerprint to identify the molecule.

Absorption of radiation by molecules at specific wavelengths is frequently used for quantitative analysis owing to the direct relationship between absorbance and concentration.

## Summary

The main objective of this work was to investigate how liposomes formed with the main components of the stratum corneum (SC) matrix, using the best thermodynamically optimized molar composition, behaved on the human skin surface when used as drug delivery systems. To achieve this, we engineered liposomes using phosphatidylcholine (PC), ceramides (CER) and CHOL.

To determine the most adequate composition of the liposomes, we performed a surface thermodynamic analysis of the lipid monolayers spread at the water-air interface. To find out the most stable composition of a ternary system, we calculated the Gibbs excess energy of different mixtures. Firstly, we investigated the PC:CHOL binary system, for which we obtained the most stable composition. Using this information, we optimized the molar proportion of CER for the PC:CHOL mixture, analyzing the stability of the mixtures.

From the isotherm analysis, we observed the condensing effect of CHOL on the PC monolayers, shifting them to lower molecular areas depending on the proportion of CHOL present in the system. This effect was in concordance with the findings of the previous chapter of this thesis. According to the  $C_s^{-1}$  values, the monolayers were in the LE phase, except for the pure CHOL monolayer.

Analyzing the activity coefficient of the components in the monolayers, we were able to find a common pattern. PC molecules behaved quite ideally below CHOL molar fractions of 0.8, while CHOL molecules behaved non-ideally at low CHOL molar fractions. Basically, we found a window of ideal behavior for both components at any surface pressure. This could be because the CHOL molecules may be laterally segregated in the monolayer at high CHOL molar fractions, but show good mixing in the PC matrix at low CHOL molar fractions.

The Gibbs energy of the mixtures showed a maximum stability for the PC:CHOL (0.6:0.4 mol/mol) system at surface pressures higher than  $20 \text{ mN m}^{-1}$ , with these data relevant since a surface pressure of  $30 \text{ mN m}^{-1}$  is considered to be equivalent to the lateral surface pressure of a bilayer.

After obtaining the most stable mixture of PC:CHOL, we followed up by adding increasing proportions of CER. The CER molecules behaved ideally at the highest CER molar fraction, suggesting that the molecules can be segregated and form CER-enriched regions in the monolayers. However, the most stable monolayer was obtained with 40% CER.

Therefore, we established that the most stable ternary monolayer of PC:CHOL:CER had a molar proportion of 0.36:0.24:0.4, mol/mol/mol.

We used this composition to prepare the liposomes, either empty or encapsulating ibuprofen or hyaluronic acid. These were evaluated in the presence or absence of a skin penetration enhancer like Tween 80. The drugs induced slight changes in the morphology of the liposomes, but all the liposomes had a diameter size ranging from 108 to 134 nm and had negative  $\zeta$ -potential values.

Liposome fluidity was a core property to study since it was expected to play a role in the spread of liposomes. Here, we took advantage of the dipole relaxation of laurdan, which tends to be located at the glycerol backbone of the bilayer, with the lauric acid tail anchored in the phospholipid acyl chain region.

After studying the changes in the fluorescence intensity of the probe as a function of the excitation wavelength at temperatures ranging from 5 °C to 55 °C, we observed a negative value of the slopes generated, implying that there was no phase separation in the mixture and a transition to a more fluid phase. High  $GP_{ex}$  values indicate the existence of the gel ( $L_{\beta}$ ) phase, while low  $GP_{ex}$  values show the existence of the liquid-crystalline ( $L_{\alpha}$ ) phase.

The melting transition temperature ( $T_m$ ) was evaluated by plotting  $GP_{ex}$  values at 340 nm as a function of temperature, using the modified Boltzmann equation. We observed that the transition of  $L_{\beta}$  to  $L_{\alpha}$  occurred at 5.46 °C. This means that if applied to the skin, liposomes will be in the  $L_{\alpha}$  phase at room temperature, which could be beneficial for the spread and possible fusion of the liposomes with the SC.

Using AFM, we evaluated the effect of the liposomes on human skin. Human skin presents multiple furrows and terraces, with a roughness value of 22 nm and furrow depths ranging from 50 to 300 nm.

After the application of the liposomes, we observed that the surface of the skin became smoother, showing a roughness value of 8.2 nm, probably because planar structures were formed on the surface. The spreading process and final fusion seemed to be favored by the low transition temperature of the lipid mixture.

After the addition of the skin penetration enhancer (Tween 80), the liposomes transformed into planar structures. Importantly, the properties of the drug incorporated into the liposomes played an important role in the process. For instance, the different results obtained with the presence of ibuprofen could be mostly because it tends (in a defined proportion) to be coencapsulated within the bilayer instead of in the aqueous inner volume of the liposome. This affects the spreading properties of the liposomes on the SC. In addition, the incorporation of hyaluronic acid, which was encapsulated inside the liposome in the aqueous region, seemed to modify the mechanism of deposition. In this case, liposomes transformed easily into planar structures when hyaluronic acid was incorporated.

Thus, liposomes transformed into planar structures more effectively with the incorporation of hyaluronic acid than with the incorporation of ibuprofen. This could be mainly due to the place where the molecules are incorporated into the vesicles. The encapsulated drugs were also able to influence the effect of the skin penetration enhancer as a facilitator of the fusion process.

## Highlights

- We observed the deposition and spread of liposomes in suspension on human skin, demonstrating the potential of the formulation to release drugs in transdermal applications.
- The presence of CER and CHOL in the composition of liposomes influenced their spread on human skin.
- Liposomes mimicking the SC lipid matrix and loaded with drugs formed higher and rougher structures on human skin than PC liposomes.
- We analyzed the thermodynamic behavior of lipid monolayers to evaluate the optimal composition mimicking the human SC.
- The ternary PC:CHOL:CER mixture showed the lowest Gibbs energy, suggesting that it would be the most suitable formulation for preparing drug carriers for topical administration.
- Laurdan fluorescence demonstrated non-phase-separated liposomes at room temperature.
- AFM showed the different behavior of the drugs incorporated into the liposomes: hyaluronic acid improved liposome spread and transformation into planar structures on human skin more than ibuprofen.
- The incorporation of a skin penetration enhancer modified the permeation of the molecule through the SC, but did not dramatically enhance the spread of the liposomes on human skin.
- The engineered liposomes tended to form flat layers covering the human skin surface.



## Planar lipid bilayers formed from thermodynamically-optimized liposomes as new featured carriers for drug delivery systems through human skin

Martha L. Vázquez-González, Adrià Botet-Carreras, Òscar Domènech, M. Teresa Montero, Jordi H. Borrell\*

Department of Pharmacy, Pharmaceutical Technology and Physical Chemistry, Faculty of Pharmacy and Food Sciences and Institute of Nanoscience and Nanotechnology (IN<sup>2</sup>UB), University of Barcelona (UB), 08028 Barcelona, Catalonia, Spain



### ARTICLE INFO

#### Keywords:

Surface thermodynamic analysis  
Liposomes  
Skin  
Drug delivery  
Stratum Corneum  
Atomic force microscopy

### ABSTRACT

The fundamental objective pursued in this work is to investigate how liposomes formed with a thermodynamically optimized molar composition formed by the main components of the *stratum corneum* matrix behave on the human skin surface when used as drug delivery systems. To this purpose we engineered liposomes using phosphatidylcholines, ceramides and cholesterol. The specific molar ratio of the three components was established after studying the mixing properties of the lipid monolayers of the lipid components formed at the air–water interface. Liposomes loaded and unloaded with ibuprofen and hyaluronic acid were characterized by quasi-elastic light scattering and fluorescence polarization. Optimized liposomes, with and without drugs, were applied onto human skin and the structures formed evaluated using atomic force microscopy. Since penetration enhancers improve the permeation of the drugs encapsulated, we also examined the effects of Tween® 80 on the physical properties of the liposomes and on their extensibility over skin.

In the present work we were able to observe the deposition and extension of liposomes in suspension onto human skin demonstrating the potential of liposomes without a secondary vehicle for releasing drugs in transdermal applications.

### 1. Introduction

The use of liposomes for transdermal drug delivery (TDD) has been extensively studied due to the high efficacy reached by these systems and all the advantages that the use of this route of administration represents (Elsayed et al., 2007). Meanwhile, liposomes supplemented with penetration enhancers (PEs) have been developed in order to improve extending them over the skin, which is the first step in achieving systemic effects (Vázquez-González et al., 2014). The *stratum corneum* (SC) is the outermost layer of skin, and it is considered the main barrier protecting against harmful agents. The SC is in fact constituted of dead cells embedded in a complex lipid matrix formed after the metabolization of the so-called lamellar-bodies by enzymes. Specifically, glucosylceramides and sphingomyelin are converted into ceramides (CER) while phospholipids are degraded to free fatty acids and glycerol. The principal components of this lipid matrix are: ceramides, cholesterol (CHOL) and free fatty acids (Bouwstra and Ponc, 2006) in equimolar proportion. The topical application of formulations with one or two of these main components results in an abnormal appearing lamellar bodies and also in a delay in the repair of the permeability

barrier (Man et al., 1996). This indicates that the composition of the formulations for drug-delivery is of crucial relevance. Pursuing this objective, liposomes formed using the lipid components of the SC have been studied, in order to promote fusion of the vesicles with the skin (Abraham and Downing, 1989; Gaur et al., 2013; Tokudome et al., 2009).

To prepare a liposome formulation that mimics the SC accurately, it is important to know as much as possible about the mixture of the components that will form the lipid bilayer. Although the equimolar composition of the three components is experimentally observed, when drugs are incorporated to a liposomes formulation, the most rationale option seems to select the more thermodynamically stable formulation of the three main components of the SC. One way to establish the thermodynamic properties of a lipid system is to study lipid monolayers formed at the air–water interface. From the corresponding compression isotherms, it is easy to obtain quantitative information on the miscibility of the components studied, and on the interactions that occur between the different molecules of interest. Specifically, here we studied the binary phosphatidylcholine (PC) and CHOL system, in order to determine the proportions that present greatest stability. Having

\* Corresponding author at: Av. Joan XXIII s.n., 08028 Barcelona, Spain.  
E-mail address: [jordiborrell@ub.edu](mailto:jordiborrell@ub.edu) (J.H. Borrell).



established that, we then studied the same properties for the ternary system PC:CHOL:CER. With this information, we produced liposomes using these three components at the composition that presents the highest stability. Since free fatty acids do not form liposomes but micelles in solution, we used PC as a first approximation for the liposome formulation mimicking the SC matrix. Although phospholipids are not present in the SC matrix they are one of the components of the lamellar-bodies, therefore PC could be degraded later by enzymes present in the SC.

To evaluate the behaviour of the optimized liposomes as drug delivery systems with the human skin surface, both empty liposomes and liposomes loaded with ibuprofen (IBP) or hyaluronic acid (HA) were applied to the skin surface and observed by atomic force microscopy (AFM). Similarly, and using the same technique, the influence of a specific PE (Tween 80®) on the process of deposition on the skin was studied.

## 2. Experimental section

### 2.1. Materials

L- $\alpha$  Phosphatidylcholine (egg yolk, 99% purity), ceramide (CER) (bovine spinal cord  $\geq 98\%$ ), ibuprofen (IBP), polyoxyethylene sorbitan mono oleate (Tween® 80), HEPES sodium salt and sodium hydroxide salt were purchased from Sigma Chemical Co. (St. Louis, MO, USA). Cholesterol (CHOL) (ovine wool  $> 98\%$ ) was purchased from Avanti Polar Lipid Inc. (Alabaster, AL, USA). Methanol, chloroform and monophosphate potassium were purchased from Panreac (Barcelona, Spain). Hyaluronic acid (sodium hyaluronate: HA) from *Streptococcus equi* was purchased from Fagron Iberica (Barcelona, Spain) with a MW of 1.0–1.4 MDa. Human skin was obtained from plastic surgery (Hospital de Barcelona, SCIAS, Barcelona, Spain).

The experimental protocol was approved by the Bioethics Committee of the Barcelona-SCIAS Hospital (Spain) and study participants gave their written informed consent.

### 2.2. Monolayer experiments

Monolayers were prepared in a 312 DMC Langmuir-Blodgett trough (NIMA Technology Ltd. Coventry, UK) with a total area of 300 cm<sup>2</sup>. The trough was placed on a vibration-isolated table (Newport, Irvine, CA, USA) enclosed in an environmental chamber. The resolution of surface pressure measurements was 0.1 mN m<sup>-1</sup> and the barrier velocity was fixed at 20 cm<sup>2</sup> min<sup>-1</sup>. The entire system was maintained at 24 °C using a water circulating bath. The trough was filled with buffer solution (KH<sub>2</sub>PO<sub>4</sub> 0.2 M, pH 7.40). The corresponding aliquots of lipid were spread carefully, drop by drop, onto the surface of the solution with a microsyringe. A period of 15 min was required to allow the solvent to evaporate before the experiment was started. No less than three identical replicas were performed for each isotherm analysed.

### 2.3. Elasticity of the monolayer

To evaluate the lateral packing of the monolayer, we used the inverse of the isothermal compressibility of the monolayer or elastic area compressibility modulus ( $C_s^{-1}$ ), calculated as:

$$C_s^{-1} = -A \left( \frac{\partial \pi}{\partial A} \right)_{T,n} \quad (1)$$

The derivative of the experimental data was computed by fitting a straight line to a window with a width of 0.2 nm<sup>2</sup> molec<sup>-1</sup> around any given surface pressure value, so that experimental noise was filtered out.

### 2.4. Thermodynamic analysis

The interaction between two components in a mixed monolayer, at a constant surface pressure,  $\pi$ , and temperature can be evaluated by calculating the excess Gibbs energy ( $G^E$ ), which is given by:

$$G^E = \int_0^\pi [A_{12} - (\chi_1 A_1 + \chi_2 A_2)] d\pi \quad (2)$$

where  $\chi_1 A_1$  and  $\chi_2 A_2$  are the molar fractions and the area per molecule of the pure components 1 and 2, respectively; and  $A_{12}$  is the area per molecule of the mixed monolayer. Positive  $G^E$  values indicate instability within the monolayer, while negative  $G^E$  values indicate stability of the mixture. Zero  $G^E$  values can be interpreted as ideal behaviour of the mixture or as complete segregation of the components. Furthermore, the regular solution theory (RST) can be applied to obtain the interaction parameter ( $\xi$ ) (Kodama et al., 2004; Xu et al., 2017) which is expressed as:

$$\xi = \frac{G^E}{RT\chi_1\chi_2} \quad (3)$$

in which  $R$  and  $T$  are the gas constant and temperature respectively. Then, knowing  $\xi$ , we can obtain the activity coefficient ( $\gamma_i$ ) of the components of the monolayer using the following equation:

$$\gamma_i = e^{\xi A_i (1-\chi_i)^2} \quad (4)$$

For a quantitative comparison between monolayers with different compositions, it is more suitable to obtain the Gibbs energy of mixing,  $\Delta_{mix}G$ , expressed as:

$$\Delta_{mix}G = G^E + RT \left( \sum \chi_i \hat{A}_i \ln(a_i) \right) \quad (5)$$

where  $\chi_i$  and  $a_i$  are the molar fractions and the activity of each component in the mixed monolayer; and  $R$  and  $T$  are the universal gas constant and temperature, respectively. Moreover, the activity of each component can be calculated as:

$$a_i = \gamma_i \hat{A}_i \chi_i \quad (6)$$

### 2.5. Liposome preparation and characterization

#### 2.5.1. Unloaded liposomes

Liposomes were prepared according to methods published elsewhere (Picas et al., 2010; Suarez-Germà et al., 2012). Briefly, a chloroform-methanol (2:1 vol/vol) solution containing the appropriate amounts of each component was placed in a balloon and dried in a rotary evaporator at room temperature, protected from light. The resulting thin film was kept under a high vacuum overnight to remove any traces of organic solvent. Multilamellar liposomes were obtained by redispersion of the thin film in Hepes buffer solution (20 mM Hepes-HCl, 150 mM NaCl), pH 7.4. The liposomes were extruded through an Avanti® Mini-extruder (Avanti Polar Lipids Inc., Alabaster, AL, USA), using polycarbonate membranes with a pore size of 100 nm. Lipid concentration was measured by a colorimetric assay (Steward, 1980). This formulation was used as blank liposomes and named F1.

#### 2.5.2. Liposomes with IBP

Liposomes loaded with IBP (F2) were prepared as described in Section 2.5.1 were IBP molecule was incorporated simultaneously with the lipids in the chloroform-methanol solution before evaporation of the solvent. The final concentration of IBP in liposomes was assessed by HPLC (HP 1100, Chemstrations, Agilent Technologies, USA) after precipitation of liposomes at 150,000  $\times g$  and subsequent disruption of precipitated vesicles with 50% isopropanol. Samples were injected on a C18 reverse-phase column (C18, Kromasil 100 C18  $\mu m$  25  $\times$  0.46) and detected at 221 nm. Eluent was a mixture of acetonitrile:acidified water (9:1, v/v) at a flow rate of 1.5 cm<sup>3</sup> min<sup>-1</sup>. Standard calibration curve



(0.78–100  $\mu\text{g cm}^{-3}$ ) was used to measure the IBP content in the samples studied. IBP-lipid ratio was typically between 0.28 and 0.37 (mol/mol).

### 2.5.3. Liposomes with HA

Liposomes loaded with HA (F3) were prepared as described in Section 2.5.1 where HA molecule was incorporated simultaneously with the Hepes buffer solution to form multilamellar vesicles. The final concentration of non-encapsulated HA was assessed by HPLC (HP 1100, Chemstrations, Agilent Technologies, USA) after separation of liposomes by Ultracel 10 centrifugal filter devices (Amicon®, Millipore, MA, USA) at 4000  $\times g$ . Supernatants were injected on a C18 reverse-phase column (C18, Kromasil 100 C18  $\mu\text{m}$  25  $\times$  0.46) and detected at 195 nm. Eluent was a mixture of water:acetonitrile (98:2, v/v) at a flow rate of 0.5  $\text{cm}^3 \text{min}^{-1}$ . Standard calibration curve (25–750  $\mu\text{g cm}^{-3}$ ) was used to measure the HA content in the samples studied. HA-lipid ratio was typically between 0.26 and 0.56 (mol/mol).

### 2.5.4. Liposome formulations supplemented with penetration enhancers (PE)

A PE was added to the formulations to ensure partial destabilization of the lipid bilayer, thereby enhancing its transformation into planar lipid structures when deposited on the skin surface (Vázquez-González et al., 2014). Briefly, different concentrations of PE (1%–10% v/v) were added to the different formulations of liposomes and based on the average particle size and polydispersity (PDI) values (data not shown) the final formulations were prepared by adding 7% of Tween® 80 extemporaneously (added to the liposome suspensions after extrusion and at the same moment of application onto the skin) to each studied liposome suspension. Formulations F2 and F3, when supplemented with Tween® 80, were then named F4 and F5, respectively.

### 2.5.5. Encapsulation efficiency

The encapsulation efficiency (EE) was calculated using:

$$EE = \frac{m_T - m'}{m_T} \times 100 \quad (7)$$

where  $m_T$  and  $m'$  are the total and the non-entrapped amount of drug in the samples, respectively.

### 2.6. Particle size and $\zeta$ potential

The mean particle size and PDI values of the liposomes were measured by dynamic light scattering. Electrophoretic mobility, to assess the effective surface electrical charge, was determined with a Zetasizer Nano ZS90 (Malvern Instruments, Malvern, UK). To obtain accurate values, the liposomal suspensions were diluted 50-fold with Hepes buffer solution before measuring; the values presented are the average of three different experiments.

### 2.7. Fluorescence measurements

We monitored the bilayer fluidity-dependent fluorescence spectral shift of laurdan taking advantage on the dipolar relaxation phenomenon. Determinations were carried out using an SLM-Aminco 8100 spectrofluorimeter equipped with a jacketed cuvette holder. The temperature was controlled ( $\pm 0.2$  °C) using a circulating bath (Thermo Scientific Haake, USA). The excitation and emission slits were 4 and 4 nm, and 8 and 8 nm, respectively. The lipid concentration in the liposome suspension was adjusted to 250  $\mu\text{M}$ , and laurdan was added to give a lipid/probe ratio of 300. Generalized polarization ( $GP_{\text{ex}}$ ) for the emission spectra was calculated according to:

$$GP_{\text{ex}} = \frac{I_{440} - I_{490}}{I_{440} + I_{490}} \quad (8)$$

where  $I_{440}$  and  $I_{490}$  are the fluorescence intensities at emission wavelengths of 440 nm (gel phase,  $L_{\beta}$ ) and 490 nm (liquid crystalline phase,

$L_{\alpha}$ ), respectively. Then,  $GP_{\text{ex}}$  values as a function of temperature were fitted to a Boltzmann-like equation:

$$GP_{\text{ex}} = GP_{\text{ex}}^2 + \frac{GP_{\text{ex}}^1 - GP_{\text{ex}}^2}{1 + \exp\left\{\frac{T_m - T}{m}\right\}} \quad (9)$$

where  $GP_{\text{ex}}^1$  and  $GP_{\text{ex}}^2$  are the maximum and minimum values of  $GP_{\text{ex}}$ , respectively,  $T$  is the temperature,  $T_m$  is the  $L_{\beta}$ -to- $L_{\alpha}$  phase transition temperature of the composition studied and  $m$  is the slope of the graph that represents phase transition, this is a parameter that provides information on the cooperativity of the transition process. The  $GP_{\text{ex}}$  values also depend on the  $\lambda_{\text{ex}}$ . In lipid mixtures and at constant temperature, a positive slope of  $GP_{\text{ex}}$  versus  $\lambda_{\text{ex}}$  indicates coexistence of domains with different compositions.

### 2.8. Human skin preparation

Human skin was prepared at previous reported (Vázquez-González et al., 2015). Briefly human skin was frozen to  $-20$  °C and cut with a dermatome (Model GA 630, Aesculap, Tuttlingen, Germany) to 400  $\mu\text{m}$  thick pieces, starting from the SC. Transepidermal water loss (TEWL) was measured with a Tewlmeter TM210 (Courage & Khazaka, Koln, Germany) obtaining TEWL values below 10  $\text{g m}^{-2} \text{h}^{-1}$  verifying the human skin integrity. The experimental protocol was approved by the Bioethics Committee of the Barcelona-SCIAS Hospital (Spain) and study participants gave their written informed consent.

### 2.9. Atomic force microscopy

Atomic force microscopy was performed with a Multimode AFM controlled by Nanoscope V electronics (Bruker AXS Corporation, Santa Barbara, CA, USA). Silicon AFM tips with a nominal spring constant of 42  $\text{nN nm}^{-1}$  were used. The spring constant of each cantilever was determined using the thermal noise method (Picas et al., 2010) and the values matched satisfactorily those supplied by the manufacturer. The instrument was equipped with an “E” scanner (10  $\mu\text{m}$ ).

Human skin was defrosted at room temperature and immediately glued onto a steel disc with glue. Afterwards, the skin was cleaned with ethanol. The formulations were applied to the skin and incubated at 37 °C for 30 min. After this period, the surface was rinsed gently with buffer and water, and subsequently dried with nitrogen. Each sample was directly mounted on top of the AFM scanner and imaged. Images were acquired in air and in contact mode, at 0° scan angle, with a scan rate of 3 Hz. The environment was maintained at 24 °C and 60% humidity. All the images were processed using Nano Scope Analysis Software (Bruker AXS Corporation, Madison, WI, USA).

### 2.10. Statistical analysis

AFM height and width values were expressed as means  $\pm$  SD while roughness value is expressed only as the mean value because the roughness value is by itself a measure of the error associated to the height of the structure studied.

## 3. Results and discussion

Our primary objective was to form liposomes with the main components of the SC, CHOL, CER and free fatty acids. However, to ensure liposome formation, performance and stability (free fatty acids tend to form micelles in solution) free fatty acids were replaced by L- $\alpha$  Phosphatidylcholine (PC). Notice that, although phospholipids are not present in the SC matrix they are precursor of the free fatty acids that result by degradation from the so-called lamellar bodies. Furthermore, it is possible that the PC molecules that could permeate through the SC could be degraded by the same enzymes without mainly altering the SC lipid composition. In regard to the lipid bilayer composition for the



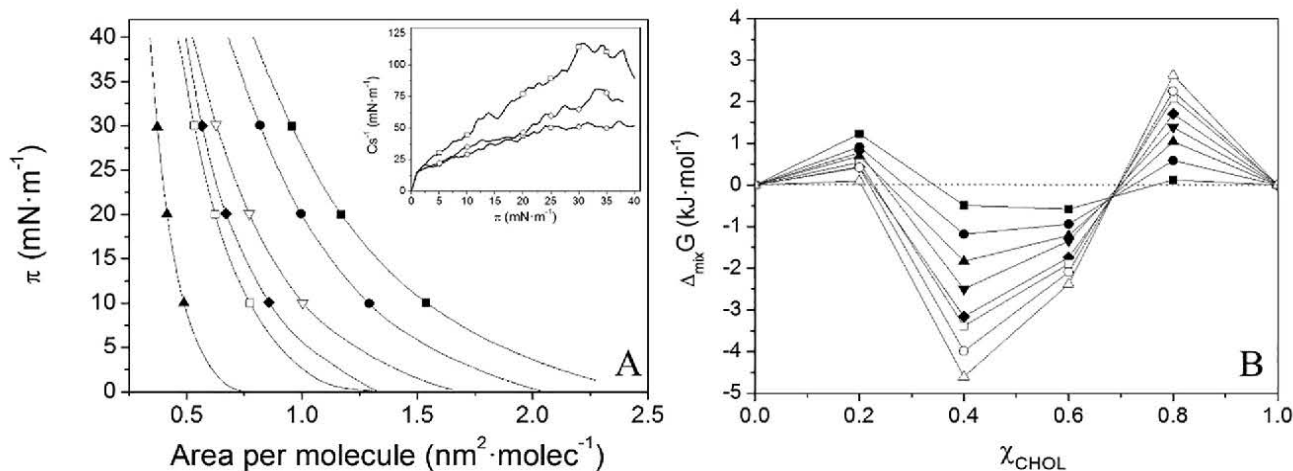


**Fig. 1.** Isotherms of the PC:CHOL mixtures (A) (■)  $\chi_{\text{CHOL}} = 0$ , (●)  $\chi_{\text{CHOL}} = 0.20$ , (▽)  $\chi_{\text{CHOL}} = 0.40$ , (◆)  $\chi_{\text{CHOL}} = 0.60$ , (□)  $\chi_{\text{CHOL}} = 0.80$ , (▲)  $\chi_{\text{CHOL}} = 1$  and corresponding compressibility modulus in the inset; Gibbs energy of mixing of the binary PC:CHOL system (B) (■)  $\pi = 5$ , (●)  $\pi = 10$ , (▲)  $\pi = 15$ , (▽)  $\pi = 20$ , (◆)  $\pi = 25$ , (□)  $\pi = 30$ , (○)  $\pi = 35$  and (Δ)  $\pi = 40$  mN m<sup>-1</sup>.

liposomes engineered CER nature is also a matter of discussion. Thus, although up to 16 different types of CER are known, CER[NP] and CER[NH] are the more abundant in the SC matrix (rKindt et al., 2012). In the present work, and as a first approximation, we used commercial CER from cerebrosides without focusing our research on its particular molecular structure which is out of the scope of the present investigation.

To optimize the molar ratio of the three components chosen to mimic de SC matrix (PC, CHOL and CER) we exploited lipid monolayers that are formed at the air–water interface, to find, via calculation of the Gibbs energy excess of mixing, the most stable composition of the PC:CHOL:CER ternary system. As we were dealing with a ternary composition system, we first studied the PC:CHOL binary system and from our results, we obtained the composition of PC:CHOL most stable, then we added CERs to studied the PC:CHOL:CER ternary system.

The compression isotherms of PC, CHOL and their mixtures are shown in Fig. 1A. There, the well-known compression exerted by CHOL on PC monolayers can be clearly observed as zones shifted to lower molecular areas, which are proportional to the proportion of CHOL present in the system. According to the  $C_s^{-1}$  values established by Davies and Rideal (Davies and Rideal, 1963), the monolayers are in the liquid expanded (LE) phase, except for CHOL, (see inset in Fig. 1A).

From the isotherms, we can evaluate how ideal the mixing is by analysing the activity coefficients of each component of the monolayer. Table 1 shows the values of  $\gamma_i$  calculated using Eqs. (2)–(4). PC molecules behave quite ideally (values that are nearly 1) below CHOL molar fractions of 0.8, at all the surface pressures studied; while CHOL molecules behave non-ideally at low CHOL molar fractions. This can be understood if we take into account that at high CHOL molar fractions,

**Table 1**  
Activity coefficients for PC and CHOL for the different monolayers studied.

$\pi$ (mN m <sup>-1</sup> )	$\chi_{\text{CHOL}}$							
	0.2		0.4		0.6		0.8	
	$\gamma_{\text{PC}}$	$\gamma_{\text{CHOL}}$	$\gamma_{\text{PC}}$	$\gamma_{\text{CHOL}}$	$\gamma_{\text{PC}}$	$\gamma_{\text{CHOL}}$	$\gamma_{\text{PC}}$	$\gamma_{\text{CHOL}}$
5	1.13	7.32	1.17	1.43	1.39	1.16	3.70	1.09
10	1.11	5.69	1.07	1.16	1.25	1.10	6.61	1.13
15	1.10	4.78	0.98	0.95	1.15	1.06	11.20	1.16
20	1.11	5.08	0.89	0.78	1.10	1.04	16.35	1.19
25	1.09	3.86	0.82	0.64	0.98	0.99	22.76	1.22
30	1.09	4.23	0.79	0.59	0.93	0.97	32.67	1.24
35	1.09	3.81	0.73	0.49	0.88	0.94	39.25	1.26
40	1.07	2.94	0.67	0.41	0.81	0.91	48.32	1.27

the CHOL molecules may be segregated in the monolayer. In that situation, few PC molecules would be present and they could not disrupt the homogeneity of the CHOL-enriched region. Conversely, at low CHOL molar fractions, the CHOL molecules may be dissolved in the PC matrix, thereby increasing the phospholipid–lipid interaction before its segregation at higher CHOL molar fractions.

With data in Table 1, we can evaluate the activity values of the components in the monolayer; i.e., the Gibbs energy of mixing, using Eq. (5). Fig. 1B depicts the variation of the Gibbs energy of mixing as a function of the CHOL molar fraction at different surface pressures. As can be seen in the graph, maximum stability is achieved with the PC:CHOL (0.6:0.4, mol/mol) system at surface pressures higher than 20 mN m<sup>-1</sup>. These data are relevant, since a surface pressure of the monolayer of 30 mN m<sup>-1</sup> is considered equivalent to that of the bilayer with the same composition (Marsh, 1996).

With the same objective, that is, to determine the most stable ternary composition, we obtained the PC:CHOL (0.6:0.4, mol/mol) isotherms, and then we added increasing proportions of CER. These isotherms are shown in Fig. 2A. In this case, the ternary monolayer is quite complex; especially as two of the three components are not phospholipids. At surface pressures above 10–15 mN m<sup>-1</sup>, the isotherms display the same behaviour as in Fig. 1A: the higher the molar fraction of CER, the lower the area per molecule of the isotherm. Below these surface pressures, compaction of some of the components is possible, making the interpretation of the lift off of each isotherm difficult. In any case, from the inset in Fig. 2A, it is possible to observe that the monolayers are in the LE phase, except for the pure CER monolayer.

As in the case of PC and CHOL, we can also evaluate the ideal behaviour of each component in the monolayer by calculating their activity coefficients. Table 2 shows the activity coefficients for PC:CHOL and CER at different surface pressures. In this case, as expected due to the complex nature of a ternary monolayer, the CER molecules behave ideally at the highest CER molar fraction, suggesting that these molecules can be segregated and form CER-enriched regions in the monolayers.

The stability of the ternary mixture was evaluated and values of the Gibbs energy of mixing as a function of the CER molar fraction are plotted in Fig. 2B at different surface pressures. From the graph, the most stable monolayer is that which contains 40% CER; this allows us to establish that the most stable ternary monolayer is PC:CHOL:CER (0.36:0.24:0.40, mol/mol/mol).

Based on the results of the monolayer study, we prepared PC:CHOL:CER (0.36:0.24:0.40, mol/mol/mol) liposomes. The diameter and PdI, together with the  $\zeta$ -potential and encapsulation efficiencies of

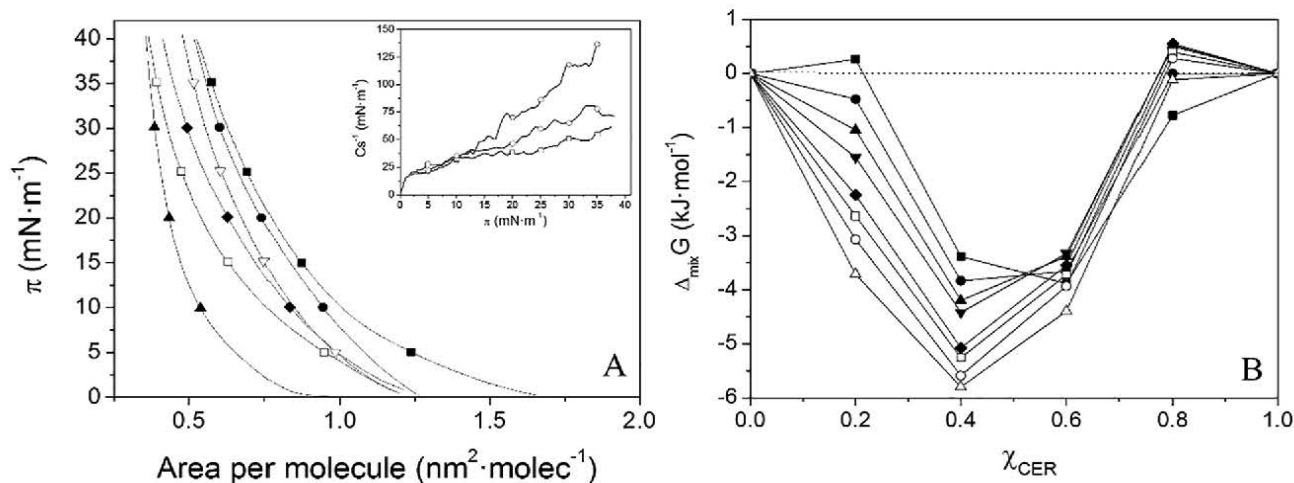


**Fig. 2.** Isotherms of the PC:CHOL:CER mixtures (A) (■)  $\chi_{\text{CER}} = 0$ , (●)  $\chi_{\text{CER}} = 0.20$ , (▽)  $\chi_{\text{CER}} = 0.40$ , (◆)  $\chi_{\text{CER}} = 0.60$ , (□)  $\chi_{\text{CER}} = 0.80$ , (▲)  $\chi_{\text{CER}} = 1$  and corresponding compressibility modulus in the inset; Gibbs energy of mixing of the ternary PC:CHOL:CER system (B) (■)  $\pi = 5$ , (●)  $\pi = 10$ , (▲)  $\pi = 15$ , (▼)  $\pi = 20$ , (◆)  $\pi = 25$ , (□)  $\pi = 30$ , (○)  $\pi = 35$  and (Δ)  $\pi = 40$  mN m<sup>-1</sup>.

**Table 2**

Activity coefficients for PC:CHOL (0.6:0.4, mol/mol) and CER for the different monolayers studied.

$\pi$ (mN m <sup>-1</sup> )	$\chi_{\text{CER}}$							
	0.2		0.4		0.6		0.8	
	$\gamma_{\text{PC:CHOL}}$	$\gamma_{\text{CER}}$	$\gamma_{\text{PC:CHOL}}$	$\gamma_{\text{CER}}$	$\gamma_{\text{PC:CHOL}}$	$\gamma_{\text{CER}}$	$\gamma_{\text{PC:CHOL}}$	$\gamma_{\text{CER}}$
5	1.08	3.36	0.79	0.59	0.51	0.74	1.45	1.02
10	1.04	1.86	0.75	0.52	0.55	0.76	2.71	1.06
15	1.01	1.17	0.71	0.46	0.59	0.79	4.16	1.09
20	0.98	0.78	0.69	0.43	0.60	0.80	4.07	1.09
25	0.95	0.44	0.63	0.36	0.57	0.78	4.25	1.09
30	0.93	0.32	0.62	0.34	0.54	0.76	3.74	1.09
35	0.91	0.23	0.59	0.31	0.50	0.74	3.40	1.08
40	0.88	0.14	0.57	0.29	0.44	0.69	2.48	1.06

**Table 3**

Characterization of the different formulations of PC:CHOL:CER (0.36:0.24:0.40, mol/mol/mol) liposomes with or without ibuprofen (IBP) or hyaluronic acid (HA), and in the presence or absence of Tween® 80 (T80).

Liposomes	Codification	Diameter (nm)	PDI	$\zeta$ potential (mV)	EE (%)
Blank	F1	110 ± 2	0.153	-4.94	-
Blank + IBP	F2	118 ± 1	0.127	-7.6	88 ± 2
Blank + HA	F3	136 ± 3	0.178	-7.6	3.1 ± 0.9
Blank + IBP + T80	F4	108 ± 4	0.143	-3.90	84 ± 2
Blank + HA + T80	F5	134 ± 2	0.187	-2.15	2.81 ± 1.2

the formulations studied, are shown in Table 3. As can be seen, the presence of the drugs induces slight changes in size, with the PDI being similar in all cases, and the values of the  $\zeta$ -potential being negative. These results are in agreement with previous findings where IBP and HA were encapsulated in PC liposomes (Vázquez-González et al., 2014; Vázquez-González et al., 2015). The most noticeable change actually occurs after the addition of T80 to F2 and F3, as this provokes a decrease of  $\zeta$ . This decrease (see  $\zeta$ -potential of F4 and F5) can be expected to play a role in the extending of these formulations over the skin.

Another factor that can be expected to play a role in the extending of the liposomes is fluidity. Previous studies reported that liposomes with higher membrane fluidity delivered large amounts of encapsulated drugs to the skin (Pérez-Cullell et al., 2000). This is in principle understandable as biological membranes are in the fluid phase ( $L_{\alpha}$ ) under natural conditions. The fluidity of liposomes can be monitored taking

advantage of the dipolar relaxation of laurdan. This molecule is a probe that is sensitive to polarity and tends to locate at the glycerol backbone of the bilayer with the lauric acid tail anchored in the phospholipid acyl chain region (Parasassi and Krasnowska, 1998). Upon excitation, the dipole moment of laurdan increases noticeably, and water molecules in the vicinity of the probe reorient themselves around the new dipole. When the membrane is in a fluid phase, the reorientation rate is faster than the emission process; consequently, a red-shift of the emission spectrum of laurdan can be observed. Conversely, when the bilayer packing increases, some of the water molecules are excluded from the bilayer and the dipolar relaxation of the remaining water molecules is slower, leading to a fluorescent spectrum that is significantly less shifted towards the red (Domènech et al., 2009). In the present work, we studied the changes in fluorescence intensity of the probe as a function of excitation wavelength ( $\lambda_{\text{exc}}$ ) in the range of temperatures from 5 °C to 55 °C were studied. As can be seen in Fig. 3, the excitation  $GP_{\text{exc}}$  spectral values, as a function of the  $\lambda_{\text{exc}}$ , decrease as the temperatures used in these experiments increase. The negative value of the slopes in the graph implies that no phase separation occurs in the mixture, but rather a transition to a more fluid phase is occurring. In general, it is known that high  $GP_{\text{exc}}$  values indicate the existence of the gel phase ( $L_{\beta}$ ); while low  $GP_{\text{exc}}$  values show the existence of the  $L_{\alpha}$  phase. Thus, by fitting Eq. (2) to  $GP_{\text{exc}}$  values at 340 nm, we obtain a

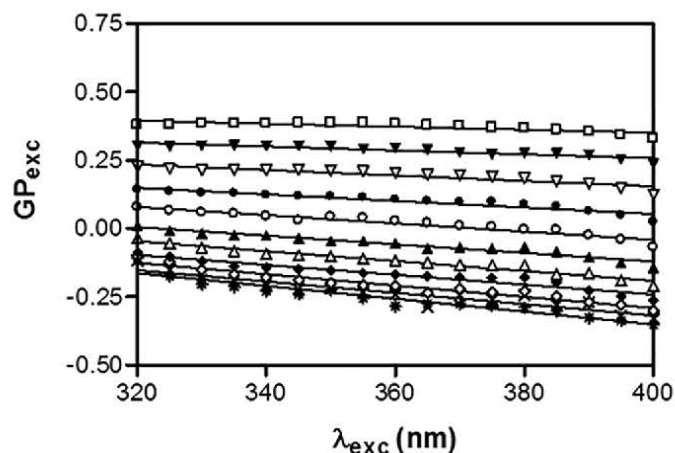


**Fig. 3.**  $GP_{\text{exc}}$  as a function of  $\lambda_{\text{exc}}$  for PC:CHOL:CER, 0.36:0.24:0.40, mol/mol/mol liposomes (□) = 5 °C, (▼) = 10 °C, (▽) = 15 °C, (●) = 20 °C, (○) = 25 °C, (▲) = 30 °C, (Δ) = 35 °C, (◆) = 40 °C, (◇) = 45 °C, (x) = 50 °C, (\*) = 55 °C).



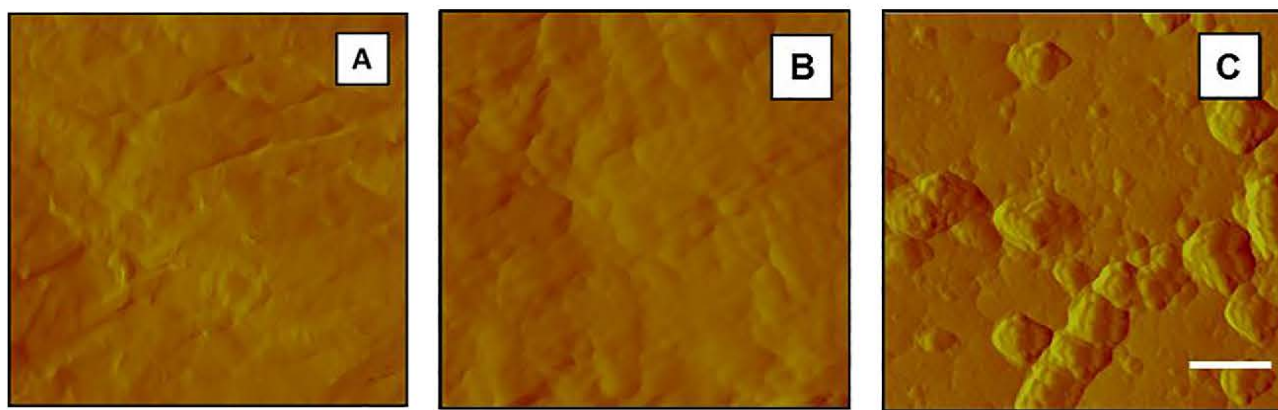


Fig. 4. Deflection images from clean human skin (A), after spreading F1 on it (B), and after spreading the liposomes supplemented with PE extemporaneously (C). Scale bar 1  $\mu\text{m}$ . Z scale 10 nm.

good fit ( $r^2 = 0.9993$ ) with a transition temperature ( $T_m$ ) for the  $L_\beta$ - to  $L_\alpha$  transition of 5.46 °C. This means that, if applied to skin, F1 will be in  $L_\alpha$  phase at room temperature: a condition that can favour the fusion of liposomes with the SC. In accordance with the swiftness of the transition temperature, the  $m$  value was established as 18.06 K, a value which is in agreement with similar observations (Domènech et al., 2009).

When liposomes are spread over hydrophilic surfaces, a three-step mechanism is triggered, adhesion, fusion and extension, which finally yields supported bilayers (SLB) (Richter et al., 2006). Although this result depends on the flatness of the surface to be covered, liposomes have been studied on rough surfaces such as human skin (Vázquez-González et al., 2015).

Using AFM, it can be established that clean human skin presents multiple furrows and terraces; as shown in the deflection image in Fig. 4A. From the corresponding topographic image (data not shown), we can infer a mean roughness value ( $R_a$ ) of 22 nm for the terraces, with furrow depths ranging from 50 to 300 nm. When we extend F1 (in the absence of PE and drugs), the surface of the skin becomes smoother ( $R_a = 8.7$  nm), probably because planar structures are formed on the surface (Fig. 4B). The transformation of liposomes into planar structures occurs over several steps and has been discussed in a previous paper (Vázquez-González et al., 2014). However, depths of 150  $\pm$  50 nm can still be observed when F1 is applied to skin, indicating that the furrows become only partially covered by the formulation. Moreover, the extension process and eventually the final fusion step seem to be favoured by the low transition temperature of the lipid mixture.

When F1 is supplemented extemporaneously with PE (at the same moment as the liposomes are extended over the skin), the AFM images (Fig. 4C) show clear differences from those of the non-supplemented liposomes (Fig. 4B).

As can be seen in Fig. 4C, two regions can be differentiated: one with  $R_a = 4$  nm, with some small flattened round structures and an average diameter of 200  $\pm$  30 nm; and another rougher region ( $R_a = 13.1$  nm) that is formed of larger round structures, with diameters ranging between 520 and 900 nm. Considering that the liposomes in solution showed a 100 nm diameter, at first sight it would seem that the smaller structures could assemble to form the larger ones; as a result, the step height of the high structures is 150  $\pm$  90 nm. These observations allowed us to verify that the addition of PE modifies the transformation of the liposomes into planar structures.

With this knowledge concerning the behaviour of the liposomes, we loaded the PC:CHOL:CER (0.36:0.24:0.40, mol/mol/mol) liposomes with either IBP or HA (F2 and F3, respectively). Then, extending F2 over the skin did not yield round adsorbed structures, but a homogeneous region (Fig. 5A) with  $R_a = 19.7$  nm and step heights of 300  $\pm$  150 nm. Intriguingly, based on the small differences between

the F1 and F2 formulations (Table 2), we expected similar features in the respective AFM images in Fig. 4B and Fig. 5A. Clearly, the differences result from the presence of IBP, which, being amphipathic ( $\log P \sim 3.5$ –3.8), should be mostly encapsulated within the bilayer. With this assumption, the mechanism of adsorption onto the skin would differ between the formulations F1 and F2. To improve the extension of F2, the PE was added to the formulation. Thus, the application of F4 (Fig. 5B) formed large irregular structures with an average width of 340  $\pm$  50 nm, an average  $R_a$  value of 15.8 nm and a mean step height value of 100  $\pm$  40 nm.

The deflection AFM images for the formulations containing HA (Fig. 6) show clear differences between the presence and absence of PE. The formulation without PE (F3) yields two regions (Fig. 6A): a planar region (white stars) with  $R_a = 2.98$  nm, and a second rougher region ( $R_a = 10.3$  nm) where structures ranging from 160 to 285 nm in width can be observed. These structures showed step heights of 300  $\pm$  180 nm. Furthermore, the extension of F5 resulted in a rough surface,  $R_a = 9.5$  nm, displaying poorly defined spherical structures (Fig. 6B) with average widths of 370  $\pm$  210 nm and a mean step height value of 120  $\pm$  30 nm. Again, the incorporation of HA seems to modify the mechanism of deposition of F3 and F5, and the liposomes are transformed into planar structures when HA is incorporated.

Summarising, in the images acquired by means of AFM we observed the deposition and subsequent extending of different liposomal formulations over human skin. Previous work revealed that when liposomal formulations are spread onto clean skin, it becomes smoother; here, the same trend was observed, with the formulations we used, however, the properties of the drug incorporated played an important role as well.

Taking into account the composition of the vesicles used in this study, PC:CHOL:CER (0.36:0.24:0.40, mol/mol/mol), we observed that incorporation of IBP or HA resulted in clear differences, indicating the effect of each molecule on the elasticity of the bilayer membrane, and consequently on the deposition onto the human skin surface.

The liposomes without drugs or PE (F1), exhibited the lowest average values of roughness; however, in the vesicles containing HA (F3), some planar structures were observed beneath the aggregates on top of the human skin. In the case of liposomes containing IBP (F2), homogeneous structures were observed with the highest values of roughness, comparable with F1 and F3. In accordance with this information, we can state that incorporation of HA allows the transformation of liposomes into planar structure more effectively than the incorporation of IBP. This fact is mainly related with the place at which the molecules are incorporated into the vesicles: in accordance with their polarity, IBP is mainly incorporated into the bilayer, while HA is entrapped within the aqueous phase of the liposome. Apparently, the incorporation of the drugs could influence the effect of PEs as



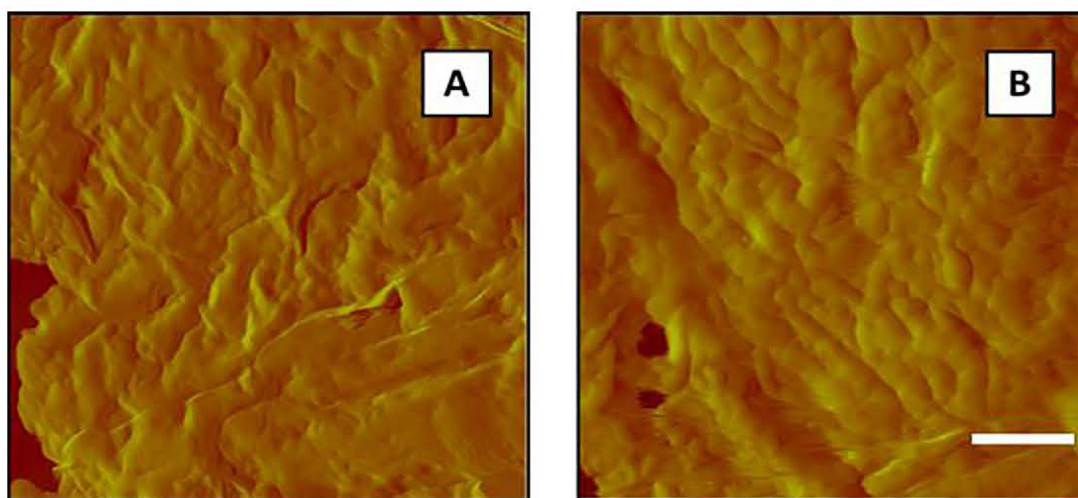


Fig. 5. Deflection images after spreading the F2 (A), and F4 (B) formulations onto the skin. Scale bar 1  $\mu\text{m}$ . Z scale 10 nm.

facilitators of the fusion process.

In comparison with previous papers where we evaluated the extension of liposomes formed only with PC with IBP (Vázquez-González et al., 2014) and HA (Vázquez-González et al., 2015), the presence of CER and CHOL in the composition of liposomes influences indeed their extension onto human skin. On the one hand, liposomes mimicking the SC lipid matrix with drugs formed higher and rougher structures onto human skin than PC liposomes. On the other hand, the extemporaneous addition of PEs to the thermodynamically-optimized formulation enhance the formation of flat structures with minimum change in their roughness values than when PEs were incorporated to PC liposomes containing the same drugs.

Although AFM studies demonstrate the extension of liposomes covering the human skin surface, these studies are focused at the microscale and they need to be taken cautiously in the estimation for a real drug delivery system where samples will be evaluated at the macroscale. Indeed, if liposomes are part of a formulation which has a secondary vehicle, many factors as lipid concentration and drug concentration gradient should be reevaluated. Moreover, it will become imperative to investigate how different components present in more complex formulations can modify planar lipid bilayers formation. In any event, the different extension due to the lipid composition of liposomes and the different effects observed after addition of PEs can be a valuable information to design complete pharmaceutical forms as far as

the permeation of drugs through human skin could be significantly different than the observed in liposomes not supplemented with enhancers.

#### 4. Conclusions

In this paper we have evaluated and optimized the lipid composition mimicking the human SC by means of the thermodynamic behaviour of lipid monolayers. The ternary mixture PC:CHOL:CER (0.36:0.24:0.40, mol/mol/mol) showed the lowest Gibbs energy of mixing, thereby suggesting to us that it would be the more suitable formulation to prepare drug carriers for topical administration. Laurdan fluorescence evidenced non-phase-separated liposomes in the fluid phase at room temperature, improving their extension over surfaces due to the higher fluidity. AFM showed the different behaviour of drugs incorporated into this kind of liposomes: HA improves the extension over and formation of flat structures on human skin, more than IBP does. The incorporation of PEs, while modifying the permeation of the molecule through the SC, does not dramatically enhance the extension of the formulations over human skin, under our experimental conditions. Results presented in this work revealed how thermodynamically-optimized liposomes interact with the human skin surface and evidenced that liposomes tend to form flat layers covering the human skin surface. Although results are encouraging, further studies should be addressed to improve

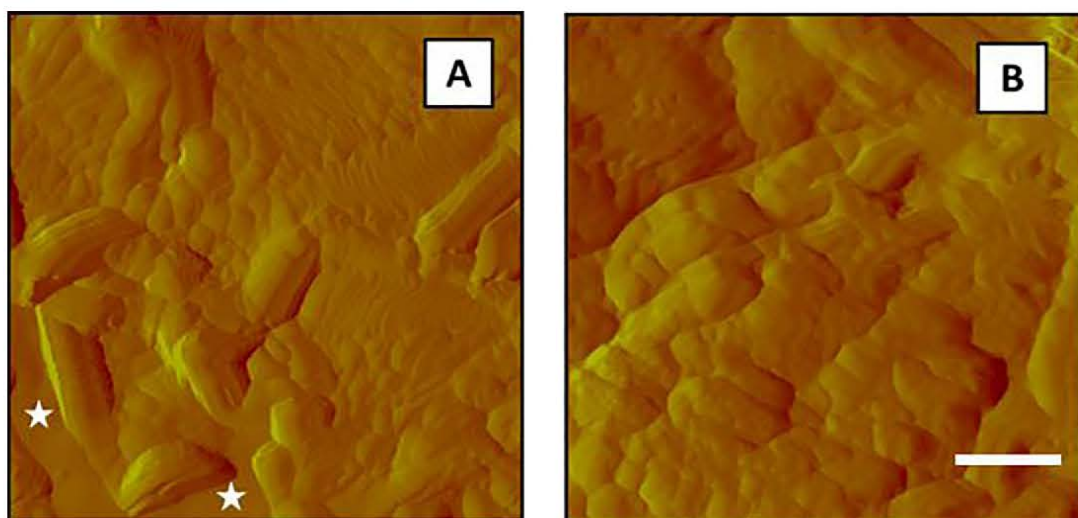


Fig. 6. Deflection images after spreading the F3 (A) and F5 (B) formulations onto the skin. Scale bar 1  $\mu\text{m}$ . Z scale 10 nm.

liposomes extension, may be by replacing PC molecules with free fatty acids or different PEs.

### Acknowledgments

Vázquez-González M.L. acknowledges the fellowship from National Council of Science and Technology (CONACYT), México, to conduct this research. The authors are grateful to the University of Barcelona for financial support.

### Conflict of interest

The authors declare that they have no conflict of interest.

### Appendix A. Supplementary data

Supplementary data to this article can be found online at <https://doi.org/10.1016/j.ijpharm.2019.03.052>.

### References

- Abraham, W., Downing, D.T., 1989. Preparation of model membranes for skin permeability studies using stratum corneum lipids. *J. Invest. Dermatol.* 93 (6), 809–813.
- Bouwstra, J.A., Ponc, M., 2006. The skin barrier in healthy and diseased state. *Biochim. Biophys. Acta Biomembr.* 1758, 2080–2095.
- Davies, J.T., Rideal, E.K., 1963. *Interfacial Phenomena*, first. ed. Academic Press Inc., New York.
- Domènech, Ò., Francius, G., Tulkens, P.M., Van Bambeke, F., Dufrêne, Y., Mingeot-Leclercq, M.P., 2009. Interactions of oritavancin, a new lipoglycopeptide derived from vancomycin, with phospholipid bilayers: effect on membrane permeability and nanoscale lipid membrane organization. *Biochim. Biophys. Acta Biomembr.* 1788 (9), 1832–1840.
- Elsayed, M.M., Abdallah, O.Y., Naggat, V.F., Khalafallah, N.M., 2007. Lipid vesicles for skin delivery of drugs: reviewing three decades of research. *Int. J. Pharm.* 332 (1–2), 1–16.
- Gaur, P.K., Mishra, S., Purohit, S., Kumar, Y., Bhandari, A., 2013. Development of a new nanovesicle formulation as transdermal carrier: formulation, physicochemical characterization, permeation studies and anti-inflammatory activity. *Artif. Cells Nanomed. Biotechnol.* 42 (5), 323–330.
- Kindt, R., Jorge, L., Dumont, E., Couturon, P., David, F., Sandra, P., Sandra, K., 2012. Profiling and characterizing skin ceramides using reversed-phase liquid chromatography-quadrupole time-of-flight mass spectrometry. *Anal. Chem.* 84 (1), 403–411.
- Kodama, M., Shibata, O., Nakamura, S., Lee, S., Sugihara, G., 2004. A monolayer study on three binary mixed systems of dipalmitoyl phosphatidyl choline with cholesterol, cholesterol and stigmaterol. *Colloid Surface B* 33 (3–4), 211–226.
- Man, M.M., Feingold, K.R., Thornfeldt, C.R., Elias, P.M., 1996. Optimization of physiological lipid mixtures for barrier repair. *J. Invest. Dermatol.* 106, 1096–1101.
- Marsh, D., 1996. Lateral pressure in membranes. *Biochim. Biophys. Acta – Rev. Biomembr.* 1286 (3), 183–223.
- Parasassi, T., Krasnowska, E.K., 1998. Laurdan and Prodan as polarity-sensitive fluorescent membrane probes. *J. Fluoresc.* 8 (4), 365–373.
- Pérez-Cullell, N., Coderch, L., de la Maza, A., Parra, J.L., Estelrich, J., 2000. Influence of the fluidity of liposome compositions on percutaneous absorption. *Drug Deliv.* 7 (1), 7–13.
- Picas, L., Suárez-Germà, C., Teresa Montero, M., Hernández-Borrell, J., 2010. Force spectroscopy study of langmuir-blodgett asymmetric bilayers of phosphatidylethanolamine and phosphatidylglycerol. *J. Phys. Chem. B* 114 (10), 3543–3549.
- Richter, R.P., Bérat, R., Brisson, A.R., 2006. Formation of solid-supported lipid bilayers: an integrated view. *Langmuir* 22 (8), 3497–3505.
- Steward, J.C., 1980. Colorimetric determination of phospholipids with ammonium ferri-thiocyanate. *Anal. Biochem.* 10 (4), 10–14.
- Tokudome, Y., Saito, Y., Sato, F., Kikuchi, M., Hinokitani, T., Goto, K., 2009. Preparation and characterization of ceramide-based liposomes with high fusion activity and high membrane fluidity. *Colloid Surface B* 73 (1), 92–96.
- Vázquez-González, M.L., Bernad, R., Calpena, A.C., Domènech, O., Montero, M.T., Hernández-Borrell, J., 2014. Improving ex vivo skin permeation of non-steroidal anti-inflammatory drugs: enhancing extemporaneous transformation of liposomes into planar lipid bilayers. *Int. J. Pharm.* 461 (1–2), 427–436.
- Vázquez-González, M.L., Calpena, A.C., Domènech, Ò., Montero, M.T., Borrell, J.H., 2015. Enhanced topical delivery of hyaluronic acid encapsulated in liposomes: a surface-dependent phenomenon. *Colloid Surface B* 134, 31–39.
- Xu, G., Hao, C., Zhang, L., Sun, R., 2017. Investigation of surface behavior of DPPC and curcumin in Langmuir monolayers at the air-water interface. *Scanning* 2017, 6582019.

## Chapter 5. Results: The model

Characterization of monolayers and liposomes that mimic lipid composition of HeLa cells.

**A. Botet-Carreras**, M. T. Montero, J. Sot, Ò. Domènech, and J. H. Borrell

*Colloids and Surfaces B Biointerfaces*, vol. 196, p. 111288, Dec. 2020

DOI: 10.1016/j.colsurfb.2020.111288

### Techniques introduced

Langmuir-Blodgett trough

#### *Monolayer fusion*

A preliminary fusion test was performed using the Langmuir-Blodgett trough, in which a monolayer of the HeLa-cell-membrane-mimicking (HeLa-mimicking) mixture was obtained and stabilized at  $30 \text{ mN m}^{-1}$  [114–116]. After adding the engineered fusogenic liposomes beneath the interface using an injection port (preventing the disruption of the monolayer), we observed that the surface area between the barriers increased to keep constant at the same nominal surface pressure of the monolayer. This technique (constant lateral surface pressure approach) enables us to detect the fusion of liposomes (or other surface active agents) with a large half-membrane. Although we only had a monolayer, this allowed us to follow the interaction process between the polar heads and, therefore, the firsts steps of the expected fusion event that occurs in a lipid bilayer.



## BAM

A Brewster angle microscope (BAM) coupled to a Langmuir-Blodgett trough was used to determine Brewster's angle, which is a unique angle ( $\sim 53^\circ$  for water), based on a simple formula shown in Figure 16.

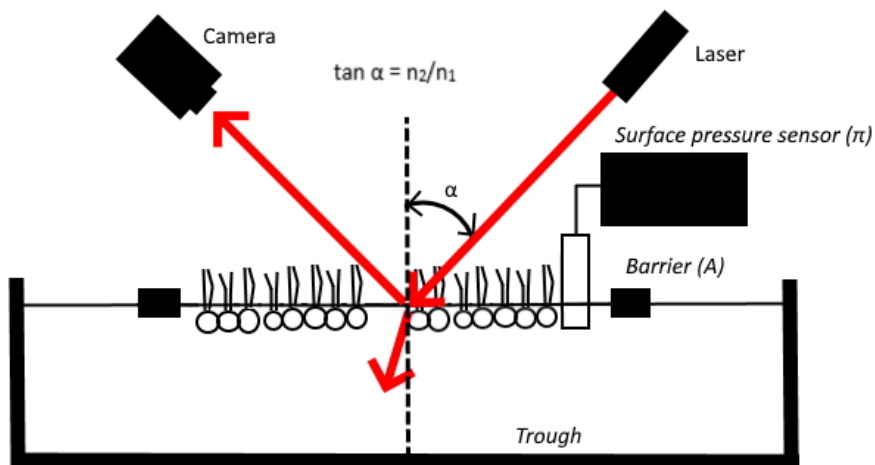


Figure 16. Langmuir-Blodgett trough configured to a Brewster angle microscope. Brewster angle ( $\alpha$ ), refractive index of air and buffer solution ( $n_1$  and  $n_2$ , respectively).

When an incident laser beam strikes the buffer solution at a particular angle (Brewster's angle), all the light directed at the water surface will not reflect on the air-water interface of the pure water surface, making it appear black. Any material added to the interface modifies the reflection, causing a small amount of light to be reflected to the camera and show up on the image. The resulting image is a conjunction of different brightness determined by the molecules at the interface and their packing densities.

## Summary

Once we obtained a suitable composition to develop the engineered liposomes, we needed a model to test it. One of the most studied cell lines is the immortal HeLa cell line, which is commonly used in many biological studies. We developed a novel artificial lipid mixture based on the results of several studies [131–134] that mimicked the outer lipid membrane of HeLa cells. This artificial membrane was used in tests to avoid the hassle of using living cells and to perform faster and cheaper tests with the engineered liposomes before undertaking *in vitro* tests with cell models.

Based on the abovementioned studies evaluating the composition of HeLa cell membranes, we reduced the number of components of our membrane model to four constituents: 1–palmitoyl–2–oleoyl–sn–glycero–3–phosphatidylcholine (POPC), 1–palmitoyl–2–oleoyl–sn–glycero–3–phospho ethanolamine (POPE), 1–palmitoyl–2–oleoyl–sn–glycero–3–phospho–L–serine (POPS) and cholesterol (CHOL) at a molar ratio of 0.29:0.31:0.06:0.34 mol/mol/mol/mol, respectively.

To characterize the membrane model, we performed several tests starting with the compression isotherms. The membrane model presented an isotherm showing a monotonic increase in surface pressure when the molecular area decreased until collapse. Compared to the other single pure components forming the mixture, the isotherm of the HeLa-mimicking membrane mixture showed lower molecular areas at all surface pressures, except for CHOL, which was already anticipated based on the findings of previous studies. Furthermore, none of the specific characteristic features of the pure phospholipids, like the collapse pressures or the transitions of POPS and POPE from the LE to LC phases, was observed.

This confirmed that the different lipids were effectively mixed in the monolayer and that the presence of CHOL was effective in condensing pure phospholipids at the interface, thus playing an important role in the properties of the whole mixture.



In accordance with the findings of other studies [135], evaluation of the  $C_S^{-1}$  values extracted from the isotherms revealed that the mixture remained in the LE phase at the working temperature (24 °C) at all the surface pressures studied. This was expected since biological membranes are in the fluid state under biological conditions.

Studying the vertical component of the dipole moment ( $\mu_{\perp}$ ), we observed that  $\mu_{\perp}$  decreased with increasing  $\pi$ . This was attributed to the strengthening of the depolarized molecular interactions in the monolayer. In addition, as compression progressed, the drop in the  $\mu_{\perp}$  values indicated a decrease in van der Waals forces with rising pressure. The results suggested that the decrease observed was not from the geometric orientation of the lipids in the vertical, but from changes in the position and orientation of the headgroups in the water layer immediately beneath the monolayer. This could be supported by the findings of molecular dynamics experiments that are presently under progress in a collaborating laboratory.

To obtain further information on the structural organization of the lipid monolayer, we explored if the HeLa-mimicking lipid mixture was able to create micro and/or nanostructures. To this end, we performed several tests with BAM.

At low surface pressures, BAM revealed dark lipid regions (a fluid phase) coexisting with brighter lipid domains (a more condensed phase). As surface pressure increased (reaching 30 mN m<sup>-1</sup>), these round bright domains measuring 10 to 50  $\mu$ m started to disaggregate, forming an image of homogeneous small dots. From the compressibility modulus, we know that the lipid monolayer remains in the LE phase. Therefore, these lipid domains could not be composed of pure lipids (as indicated by the lack of collapse at pressures close to the collapse surface pressure of the pure phospholipids in the isotherm experiments). Thus, we can presume that the more condensed domains could be enriched with CHOL, which controls the other phospholipids and forms these regions without modifying the macroscopic behavior of the monolayer.

To analyze the possible nanostructures present in the monolayer, we placed an LB of the HeLa-mimicking mixture at 30 mN m<sup>-1</sup> onto a mica surface. AFM revealed two different

regions: 85% of the surface was covered by a relatively uniform film, and 15% was covered by a series of small domains approximately 400 nm wide that rose 0.6 nm above the base region.

The domains were clearly smaller than the ones observed in the BAM images, showing nanostructures inside the microstructures.

We also obtained a force adhesion map with AFM-FS paired with a topographic image of the same region. The  $F_{adh}$  data obtained showed clear differences between the base area and the small domains. Moreover, according to other studies [136], the low values of  $F_{adh}$  indicated that the lipids were in the LE phase, which is consistent with the earlier results demonstrating the LE phase of the lipid monolayer of the HeLa-mimicking mixture.

After the study of the monolayer model, we switched to the vesicle model as it was more similar to a lipid membrane. We formulated liposomes with the HeLa-mimicking mixture and evaluated the possible existence of lipid domains in the bilayer system. These liposomes were characterized by the DLS technique, which revealed diameters of around  $117.6 \pm 1.1$  nm, a PDI value of 0.122 and a  $\zeta$ -potential value of around  $-8.9 \pm 1.1$  mV. Thus, the liposomes were negatively charged like the HeLa cell membrane. However, mainly due to the size of the liposomes, they were not as negative as a living HeLa cell ( $-19.4 \pm 0.8$  mV) [137].

Laurdan fluorescence assays were performed at temperatures ranging from 0 °C to 50 °C. The  $T_m$  value was  $33.6 \pm 0.6$  °C. We observed that from 0 °C to 15 °C, the  $GP_{ex}$  &  $\lambda_{ex}$  plots showed positive slopes, indicating the presence of domains of different composition and different ordered phases in the lipid bilayer. By contrast, from 20 °C to 40 °C, the plots showed negative slopes, indicating a transition towards a more fluid phase.

After gathering information on the physicochemical properties of the HeLa-mimicking mixture, we performed some preliminary tests with it.

First, we developed two types of engineered liposomes with POPC, which had been determined to be the most suitable candidate [136] (Chapter 3). We then added the cationic phospholipid 1,2-dioleoyl-3-trimethylammonium-propane (DOTAP), which seems to

facilitate the fusion process. The difference between the two formulations was the presence or absence of CHOL. It is well known that CHOL plays a key modulating role in the fusion process [138].

Therefore, we prepared two different liposome compositions: POPC:DOTAP (0.80:0.20, mol/mol) and POPC:CHOL:DOTAP (0.65:0.15:0.20, mol/mol/mol) liposomes that showed similar average sizes of 120 nm, a PDI of 0.194 and 0.168, respectively, and a  $\zeta$ -potential value of  $9.0 \pm 1.2$  mV and  $10.2 \pm 0.6$  mV, respectively. A positive charge seemed to be adequate to investigate their interaction with living cells, which have a native negative charge.

To evaluate the possible fusion of the engineered liposomes with the monolayer of the HeLa-mimicking mixture, we performed an experiment where the monolayer was compressed and stabilized at a surface pressure of  $30 \text{ mN m}^{-1}$ . Once the monolayer was stabilized, the liposomes were injected underneath the surface. The interaction between the liposome and monolayer was followed, varying the area but controlling the pressure of the monolayer and stabilizing it constantly at  $30 \text{ mN m}^{-1}$ .

The experiments were carried out with three types of liposomes: the two engineered ones (POPC:DOTAP and POPC:CHOL:DOTAP liposomes) and pure POPC liposomes (used as a blank).

After the injection of any of the two engineered liposomes, the molecular area of the monolayer increased while maintaining the same surface pressure. This was clear evidence of a fusion process between the monolayer and the liposomes.

The increase in the molecular area reached a maximum value after about two hours. This increase was greater for liposomes containing CHOL than for those without the sterol. Unexpectedly, the fusion process was faster for the liposomes without CHOL than for those with CHOL. Thus, the fusion process was slower in terms of time, but greater in quantitative terms in the liposomes containing CHOL.

The pure POPC liposomes did not produce any change in the molecular area of the monolayer, most probably because of the absence of DOTAP and, consequently, the missing electrostatic charge difference between the HeLa-mimicking monolayer and the POPC liposomes. This highlighted the importance of DOTAP and CHOL in the fusion process, as reported previously [139].

After evaluating the physicochemical characteristics of the HeLa-mimicking monolayer, the last step in this research project was to continue studying the interactions between the HeLa-mimicking membrane model and engineered liposomes.

## Highlights

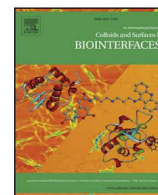
- We created artificial membrane models based on the lipid composition of the plasma membrane of living HeLa cells.
- We engineered two different types of liposomes based on POPC to fuse with the membrane models and, in the future, with living cells.
- BAM and AFM revealed micro- and nanostructure domains in the lipid bilayer model mimicking the HeLa cell membrane.
- The first tests performed suggested that the fusion process had a primary step involving electrostatic and adhesion forces.
- We corroborated that CHOL modulates and enhances the fusion process.





Contents lists available at ScienceDirect

## Colloids and Surfaces B: Biointerfaces

journal homepage: [www.elsevier.com/locate/colsurfb](http://www.elsevier.com/locate/colsurfb)

# Characterization of monolayers and liposomes that mimic lipid composition of HeLa cells

Adrià Botet-Carreras<sup>a,b</sup>, M. Teresa Montero<sup>a,b</sup>, Jesús Sot<sup>c</sup>, Òscar Domènech<sup>a,b</sup>, Jordi H. Borrell<sup>a,b,\*</sup>

<sup>a</sup> Secció de Físicoquímica, Facultat de Farmàcia i Ciències de l'Alimentació, Spain

<sup>b</sup> Institute of Nanoscience and Nanotechnology (IN<sup>2</sup>UB), Universitat de Barcelona (UB), 08028, Barcelona, Catalonia, Spain

<sup>c</sup> Instituto Biofísica (CSIC-UPV/HEU, Campus Universitario, 48940, Leioa, Basque Country, Spain

## ARTICLE INFO

## Keywords:

HeLa cells  
Lipid monolayers  
Fluorescence  
Langmuir-Blodgett films  
BAM  
AFM

## ABSTRACT

In this work, based on several studies, we develop an artificial lipid membrane to mimic the HeLa cell membrane using 1-palmitoyl-2-oleoyl-sn-glycero-3-phosphatidylcholine (POPC), 1-palmitoyl-2-oleoyl-sn-glycero-3-phosphoethanolamine (POPE), 1-palmitoyl-2-oleoyl-sn-glycero-3-phospho-L-serine (POPS) and cholesterol (CHOL). This is then a means to further study the fusion process of specific engineered liposomes. To characterize the mimicked HeLa cell membrane, we determined a series of surface pressure–area ( $\pi$ -A) isotherms and the isothermal compression modulus was calculated together with the dipole moment normal to the plane of the monolayer. The existence of laterally segregated domains was assessed using a fluorescence technique (Laurdan) and two microscopy techniques: Brewster angle microscopy (BAM) and atomic force microscopy (AFM) of Langmuir-Blodgett films (LBs) extracted at  $30 \text{ mN m}^{-1}$ . To examine the nature and composition of the observed domains, force spectroscopy (FS) based on AFM was applied to the LBs. Finally, two engineered liposome formulations were tested in a fusion assay against mimicked HeLa cell membrane LBs, showing good results and thereby opening the door to further assays and uses.

## 1. Introduction

Many diseases are associated with defects in cell membranes, particularly those attributed to malfunction of proteins that are either absent due to a mutation (as happens in hereditary elliptocytosis because of the absence of the *4.1R* protein [1]) or present in a non-functional conformation (as occurs in cystic fibrosis with the *CFTR* protein [2] or in Bartter's syndrome with the *CLCNKB* protein [3]). In principle, the ideal strategy when treating these diseases would be to reintroduce the missing or flawed proteins back into the cell with the hope that they will be operative. Along these lines, transfection of cells using liposomes to introduce/incorporate genetic material [4], or indeed to effect some other treatments [5], has become the subject of intensive research over the years. While some of the problems regarding formulation, administration and biodistribution of the genetic material have been studied in depth, to the point of reaching commercialization of some pharmaceutical forms based on liposomes as drug-carriers, one of the issues that remain open is the mechanism of interaction of the liposome with cell membranes. It is generally accepted that non-functionalized liposomes [6] may interact in different ways with cell membranes: fusion, endocytosis and adsorption. While the endocytotic

process consists of the internalization of liposomes, adsorption may be considered, in physicochemical terms, as a previous step to the fusion and subsequent release of the substance transported in the cell cytoplasm.

The versatility of liposomes, which allows us to define their size and composition, makes them excellent potential carriers of drugs, genetic material or proteins. Hypothetically, by varying the lipid composition of the bilayers of the liposomes, a surface electric charge can be conferred to them and a surface potential that favours adsorption and eventual fusion. The idea of using lipid compositions that are biomimetic of those of the target cells is appealing. However, there are some controversies regarding whether this strategy will work, mostly because the physicochemical properties of the lipid components, some of them not very well known, may play a crucial role in the fusion mechanism [7]. Such properties include the intrinsic curvature of the phospholipids and the transition temperature of the lipid mixtures assayed; but other less thoroughly explored ones are the lateral packing and adhesion forces between lipids in the layer, which may well also affect the fusion process.

Within the framework of our project, we aim to use liposomes carrying different proteins and gens [8,9] to transfect HeLa cells. For

\* Corresponding author at: Secció de Físicoquímica, Facultat de Farmàcia i Ciències de l'Alimentació, Av. Joan XXIII 27-31, 08028, Barcelona, Spain.

E-mail address: [jordiborrell@ub.edu](mailto:jordiborrell@ub.edu) (J.H. Borrell).



this reason, as a first stage of our work, we prepared liposomes with a lipid composition that mimics the cytoplasmic membrane of HeLa cells [10–13]. We then study the properties of the monolayers with the lipid composition of the HeLa cells when extended across the air–water interface; specifically, their compressibility coefficient and the molecular dipole moment behaviour. We also analyse the microstructure and nanostructure of these monolayers using Brewster angle microscopy (BAM) and atomic force microscopy (AFM), thereby probing their mechanical properties further and especially advancing in the determination of the force adhesion measured when the AFM tip is pull out of the lipid layer. We further examined the variation of the anisotropy of liposomes with the same lipid composition using fluorimetry; and finally we tested the potential fusion capacity of these liposomes with monolayers mimicking HeLa cells by performing experiments at constant surface pressure.

## 2. Experimental section

### 2.1. Materials

1-Palmitoyl-2-oleoyl-sn-glycero-3-phosphatidylcholine (POPC), 1-palmitoyl-2-oleoyl-sn-glycero-3-phosphoethanolamine (POPE), 1-palmitoyl-2-oleoyl-sn-glycero-3-phospho-L-serine (POPS), 1,2-dioleoyl-3-trimethylammonium-propane (chloride salt) (DOTAP) and cholesterol (CHOL) were purchased from Avanti Polar Lipids (Alabaster, AL, USA). All the other chemicals were acquired from Sigma-Aldrich (St. Louis, MO, USA) and used as received. The lipids were dissolved in a chloroform:methanol (2:1, v/v) solution to obtain a final concentration of 1 mg ml<sup>-1</sup>. These solutions were used to obtain the mixtures: POPC:POPE:POPS:CHOL (0.29:0.31:0.06:0.34, mol/mol/mol/mol) referred to throughout the text as the HeLa-mimicking mixture, POPC:DOTAP (0.80:0.20, mol/mol) and POPC:CHOL:DOTAP, (0.65:0.15:0.20, mol/mol/mol).

### 2.2. Compression isotherms and deposition of Langmuir-Blodgett monolayers

Monolayers were prepared in a 312 DMC Langmuir-Blodgett trough (NIMA Technology Ltd., Coventry, UK) with a total area of 300 cm<sup>2</sup>. The trough was placed on a vibration-isolated table (Newport, Irvine, CA, USA) enclosed in an environmental chamber. The resolution of surface pressure measurements was 0.1 mN m<sup>-1</sup> and the barrier speed was fixed at 20 cm<sup>2</sup> min<sup>-1</sup>. The entire system was maintained at 24.0 °C ± 0.2 °C with a circulating water bath. The trough was filled with buffer solution (10 mM Tris, 150 mM NaCl, pH 7.40), then aliquots of lipid dissolved in the chloroform:methanol (2:1, v/v) solution were spread carefully, drop by drop, onto the surface with a microsyringe. A period of 15 min was required to allow the solvent to evaporate before the experiment started. No less than three identical replicas were performed for each isotherm analysed. The Langmuir-Blodgett monolayer deposition was performed on square mica surfaces (Ted Pella, Redding, CA, USA) at 30 mN m<sup>-1</sup>, which is considered a biologically relevant surface pressure, and with a dip speed of 1 mm min<sup>-1</sup>. Prior to observation of the surface, the mica squares were attached to steel discs with double-sided tape.

### 2.3. Brewster angle microscopy

Images of the film morphology were obtained by Brewster angle microscopy (BAM) [14] using a KSV NIMA BAM coupled to a large KSV NIMA Langmuir trough. A standard 10 mW He – Ne laser with a Glan-Thomson polarizer was used to provide p-polarized light. A black wedge-shaped plate was placed at the bottom of the trough, where the laser was pointing, to prevent stray light leaving the surface. All the images were acquired using a 1360 × 1024 pixel CCD camera. The spatial resolution of the BAM was 2 μm (horizontal image direction),

according to Rayleigh's criterion.

### 2.4. Elasticity of the monolayer

To evaluate the lateral packing of the monolayer, the inverse of the compression modulus ( $C_s$ ) [15,16] for defined compositions was calculated according to

$$C_s^{-1} = -A \left( \frac{\partial \pi}{\partial A} \right)_{T,n} \quad (1)$$

where  $A$  is the molecular area and  $\left( \frac{\partial \pi}{\partial A} \right)_{T,n}$  is the slope of the monolayer curve, both values determined at the point of interest. The derivative of the experimental data was computed by fitting a straight line to a window of area 0.2 nm<sup>2</sup> molecule<sup>-1</sup> around any given surface pressure value, so that experimental noise was filtered out.

### 2.5. Surface potential measurements

The average molecular dipole moment component normal to the plane of the monolayer ( $\mu_{\perp}$ ) was calculated according to the Helmholtz equation

$$\mu_{\perp} = \Delta V A \epsilon_0 \epsilon_r \quad (2)$$

where  $A$  is the average molecular area,  $\Delta V$  is the experimentally determined surface potential, and  $\epsilon_0$  and  $\epsilon$  are the permittivity values of a vacuum and the monolayer, respectively. Usually,  $\epsilon$  is taken as 1, but some authors [17] have determined that for a DPPC bilayer this value is 3.2. Therefore, in this work we considered a monolayer as half of a lipid bilayer, so we took a value of 1.6 as representative of  $\epsilon$  for the lipid monolayer.

### 2.6. Liposome preparation

The liposomes were prepared according to methods published elsewhere [18]. Briefly, the chloroform:methanol (2:1, v/v) solution containing the appropriate amount of lipids was placed in a glass balloon flask and dried in a rotary evaporator at room temperature protected from light. The resulting thin film was kept under high vacuum overnight to remove any traces of organic solvent. Multi-lamellar liposomes were obtained by redispersion of the thin film in 10 mM TrisHCl, 150 mM NaCl buffer, pH 7.4. The liposomes were extruded through polycarbonate membranes with a pore size of 100 nm using an Avanti®Mini-extruder (Avanti Polar Lipids Inc., Alabaster AL, USA). The mean particle size and polydispersity values of the liposomes were measured by dynamic light scattering with a Zetasizer Nano S (Malvern Instruments, UK). To assess the effective surface electrical charge, electrophoretic mobility was determined with a Zetasizer Nano ZS90 (Malvern Instruments, UK). Each sample was measured at least three times.

### 2.7. AFM imaging and force spectroscopy

AFM images were captured and force spectroscopy measurements were performed with a Nanoscope IV from Digital Instruments (Bruker, AXS Co., Madison, WI, USA) equipped with a 15 μm piezoelectric scanner. As in previous work [19], images and force curves were acquired using V-shaped silicon nitride cantilevers (OMCL TR400PSA, Olympus, Japan) with a nominal spring constant of 80 pN nm<sup>-1</sup>, in air and in intermittent contact mode. During the experiments, the force applied to the samples was kept as low as possible to minimize monolayer damage. All the images were processed using NanoScope® analysis software (Bruker, AXS Co., Madison, WI, USA).

For force spectroscopy experiments, individual spring constants ( $k_c$ ) were calibrated using the thermal noise method, after having correctly determined the photodetector optical sensitivity (V nm<sup>-1</sup>) by



measuring it at high voltages. Applied forces,  $F$ , are given by  $F = k_c \times \Delta$ , where  $\Delta$  stands for the cantilever deflection. Force–volume images of  $32 \times 32$  individual force curves were recorded using a constant approach and retraction speed of  $1 \mu\text{m s}^{-1}$ . Temperature and humidity were maintained at  $24^\circ\text{C}$  and  $60\%$ .

### 2.8. Generalized polarization measurements of bilayers

Bilayer fluidity was monitored using the dipolar relaxation of Laurdan. Briefly, Laurdan is a polarity-sensitive probe that tends to locate at the glycerol backbone of the bilayer with the lauric acid tail anchored in the phospholipid acyl chain region [20,21]. We monitored the bilayer fluidity-dependent fluorescence spectral shift of Laurdan due to dipolar relaxation phenomena. Determinations were carried out using an SLM-Aminco 8100 spectrofluorimeter equipped with a jacketed cuvette holder. Temperature ( $\pm 0.2^\circ\text{C}$ ) was controlled using a circulating bath (Haake K20, Germany). The excitation and emission slits were 4 and 4 nm, and 8 and 8 nm, respectively. The lipid concentration in the liposome suspension was adjusted to  $250 \mu\text{M}$ , and Laurdan was added to give a lipid/probe ratio of 300 to 1. The generalized polarization ( $GP_{ex}$ ) value for the emission spectra was calculated using

$$GP_{ex} = \frac{I_{440} - I_{490}}{I_{440} + I_{490}} \quad (3)$$

where  $I_{440}$  and  $I_{490}$  are the fluorescence intensities at emission wavelengths of 440 nm (gel phase,  $L_\beta$ ) and 490 nm (liquid-crystalline phase,  $L_\alpha$ ), respectively.

$GP_{ex}$  values, as a function of temperature, were fitted to a Boltzmann-like equation

$$GP_{ex} = GP_{ex}^2 + \frac{GP_{ex}^1 - GP_{ex}^2}{1 + \exp\left\{\frac{T_m - T}{m}\right\}} \quad (4)$$

where  $GP_{ex}^1$  and  $GP_{ex}^2$  are the maximum and minimum values of  $GP_{ex}$ , respectively;  $T_m$  is the gel-to-fluid phase transition temperature of the composition studied and  $m$  is related to the slope of the transition that provides information on the cooperativity of the process.

### 2.9. Constant surface pressure experiments

In the constant surface pressure experiments we formed a monolayer of HeLa-mimicking mixture on the subphase, and then compressed the lipid film to the desired surface pressure ( $\pi = 30 \text{ mN m}^{-1}$ ). Volumes of lipids in the chloroform:methanol solution were carefully deposited onto the subphase using a microsyringe (Hamilton, Reno, NV, USA). After 15 min, to allow the solvent to evaporate, the lipids were laterally compressed to the desired surface pressure. After another period of 15 min for monolayer stabilization,  $10 \mu\text{L}$  of either POPC:DOTAP (0.80:0.20, mol/mol) or POPC:CHOL:DOTAP (0.65:0.15:0.20, mol/mol/mol), at a liposome concentration of  $500 \mu\text{M}$ , was injected beneath the monolayer to reach a final concentration of  $0.07 \mu\text{M}$ . Then the change of surface area per molecule ( $\Delta A$ ) over time ( $t$ ) was recorded. To obtain a quantitative interpretation of these experiments, the data were fitted to a Langmuir-like equation [22]

$$\Delta A = \Delta A_{max} \frac{(kt)b}{1 + (kt)b} \quad (5)$$

where  $\Delta A_{max}$  is the maximum increase of the area reached under steady-state conditions by the monolayer;  $k$  is a rate constant determined by the nature of the substances involved and the experimental conditions; and  $b$  is a parameter that is related to the cooperativity of the process.

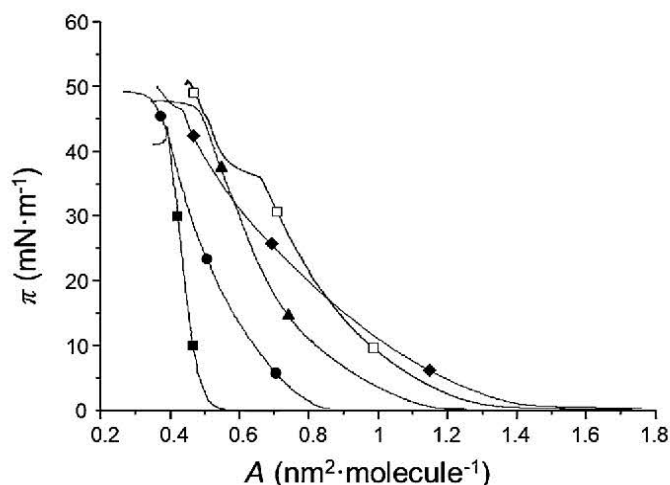
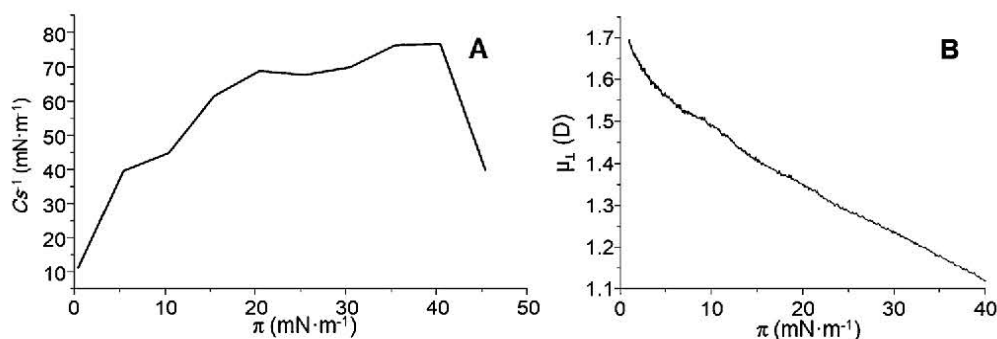


Fig. 1. Surface pressure versus area per molecule isotherms. CHOL (■), pure POPC (▲), pure POPE (□), pure POPS (◆) and HeLa-mimicking mixture (●).

### 3. Results

The compression isotherms ( $\pi$  versus molecular area) of the pure lipids and the HeLa-mimicking mixture recorded at  $24.0^\circ\text{C}$  are presented in Fig. 1. The features of the single component monolayers coincide with those published previously [23,24]. As can be seen, the HeLa-mimicking mixture, lipid mixture mimicking the HeLa plasma membrane, presented a monotonic increase in surface pressure up to  $49 \text{ mN m}^{-1}$ , when it collapsed. Remarkably, the isotherm of the HeLa-mimicking mixture showed lower molecular areas at all surface pressures, except for the case of the pure CHOL isotherm, the –solid-like structure at the interfaces that has been extensively discussed elsewhere [23]. None of the specific features, such as the liquid condensed (LC)-liquid expanded (LE) phase transition of POPE or POPS, were observable in the mixture. These observations confirm two things: i) the different lipids were mixed in the monolayer; ii) CHOL was effective at condensing pure phospholipid monolayers and played a crucial role in the properties of the whole mixture.

Meanwhile, the actual phase of the lipids in a monolayer at a given surface pressure can be inferred by calculation of the inverse of the compressibility modulus ( $C_s^{-1}$ ). Fig. 2A shows  $C_s^{-1}$  values at different surface pressures for the lipid monolayer of the HeLa-mimicking mixture. According to the criterion of Davies and Rideal [15], at the working temperature the mixture remains in the LE phase (below  $100 \text{ mN m}^{-1}$ ) throughout all the ranges of surface pressure studied. This behaviour is expected since biological membranes keep their fluid state under biological conditions. Indeed, it is accepted that there is an equivalence between the liquid-crystalline phase in bilayers ( $L_\alpha$ ) and the LE in monolayers. In contrast, the normal component of the dipolar moment ( $\mu_\perp$ ) is indicative of the different interactions between the lipids in the monolayer, and between the lipids and the solvent. The decrease of  $\mu_\perp$  as  $\pi$  increases (Fig. 2B) has previously been reported for other phospholipids [23] and it has primarily been attributed to strengthening of the depolarized molecular interactions in the monolayers as compression progresses. It is worth recalling that according to the three-layer model, three independent contributions to  $\mu_\perp$  should be considered: one from the hydrophilic head group, a second from the hydrophobic tails and the third from the underlying water subphase [15,16]. A more subtle analysis (data not shown) suggests that the decrease observed in Fig. 2B mainly arises not from the resultant  $\mu_\perp$  originated by the molecular structure of the lipids, but from changes in the orientation and the spatial position of the phospholipid headgroups in the water layer immediately beneath the monolayers. Thus, the resultant  $\mu_\perp$  cannot be interpreted directly as an indication of the verticality of the whole molecule, in fact different molecules could have



**Fig. 2.** Reciprocal of the compression modulus ( $C_s^{-1}$ ) as a function of surface pressure (A); and vertical component of the dipole moment ( $\mu_{\perp}$ ) as a function of surface pressure (B) of HeLa-mimicking mixture.

different interactions with water molecules thereby confounding the interpretation of  $\mu_{\perp}$ . Taking into account all of this, the effective  $\mu_{\perp}$  value in the lipid monolayer of the HeLa-mimicking mixture decreases as the surface pressure increases, suggesting a less important effect of van der Waals forces at higher surface pressures (including the biologically relevant  $\sim 30 \text{ mN m}^{-2}$ ) when the monolayer could interact with molecules or other membranes. Although these data are from monolayer studies, they may be important for understanding how electrical properties are involved in the interaction with the plasma membrane, i.e. in processes of fusion with cell membranes.

To further probe the structural organization of the lipid monolayer of the HeLa-mimicking mixture, we used two microscopy techniques: BAM and AFM. BAM is an optical technique that allows in situ visualization of the microstructures formed at the lipid-water interface [25–27]. Fig. 3 shows representative images of the lipid monolayer of the HeLa-mimicking mixture at a surface pressure of 5, 10, 30 and 40  $\text{mN m}^{-2}$ . Dark lipidic regions (fluid phase) coexist with brighter lipidic

domains (more condensed phase) across the range of surface pressures. The microstructure of these brighter domains is of interest: two different populations of holey round regions coexist (Fig. 3A and B). Smaller domains with an average diameter of 10  $\mu\text{m}$  coexist with larger domains of more than 50  $\mu\text{m}$  in diameter at lower surface pressures. The larger domains seem to disaggregate at surface pressures of 30  $\text{mN m}^{-2}$  (Fig. 3C), where the small domains predominate. As can be seen, further increasing the surface pressure results in a featureless monolayer (Fig. 3D). Although analysis of the compressibility modulus showed that the lipid monolayer of the HeLa-mimicking mixture always remains in the LE phase, the BAM images confirm the presence of more condensed domains whose extension increases when the lipid monolayer is compressed. However, the lipid isotherm of the HeLa-mimicking mixture did not show multiple collapse pressures, indicating the absence of segregated pure lipid domains in the monolayer. All this suggests that these more condensed domains could be formed of CHOL molecules that control the other phospholipids and form these holey

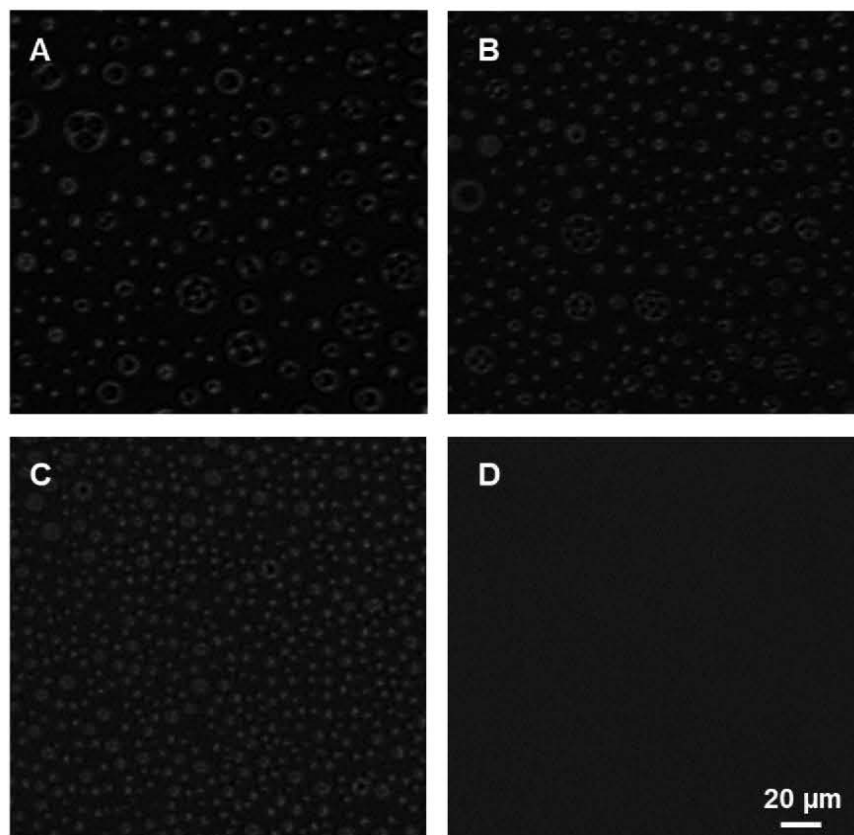


**Fig. 3.** BAM images of HeLa-mimicking mixture at a surface pressure of: 5 (A), 10 (B), 30 (C), and 40 (D)  $\text{mN m}^{-2}$ .



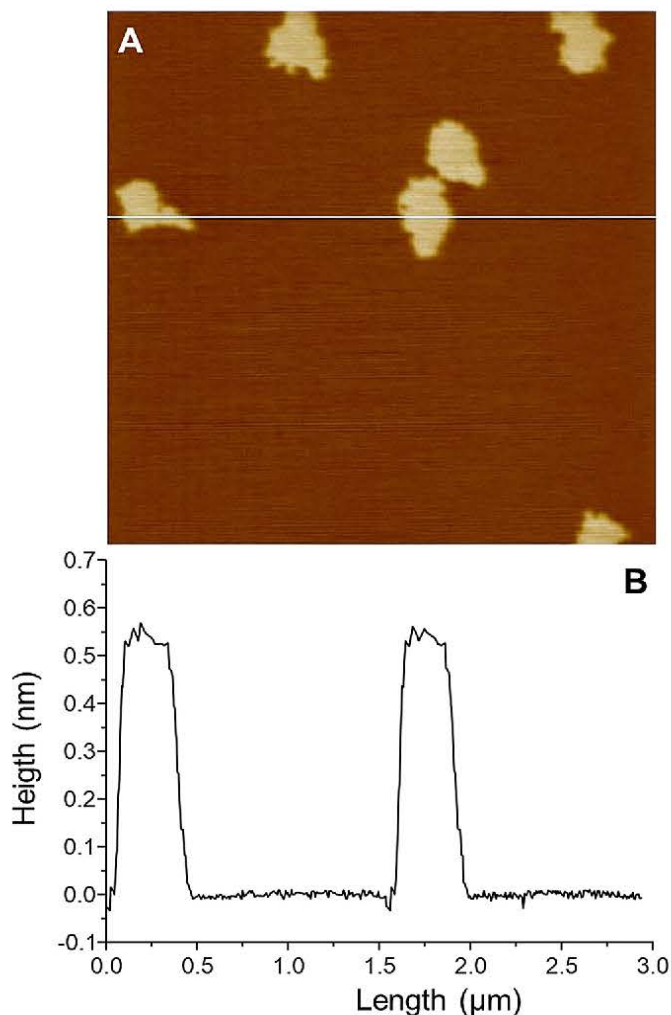


Fig. 4. AFM topography of lipid monolayer of HeLa-mimicking mixture, extracted at  $30 \text{ mN m}^{-1}$  on a mica surface (A); and line profile analysis along the white line in A (B). Z scale bar in image A is 2 nm.

regions without modification of the macroscopic behaviour of the monolayer. The exact characterization of monolayers with complex compositions by BAM is always difficult [14]. However, other authors [24] studying quite a similar monolayer system (POPE:POPS:CHOL, POPS/POPE = 0.44 and (POPE + POPS)/CHOL = 0.88) reported BAM images at similar pressures that show small bright spots apparently similar to ours but smaller in size. Taking into account the different lipid proportions and the presence of CHOL in our system, the resemblances are remarkable. Those authors excluded the formation of crystallites at the interface.

Fig. 4 shows a representative AFM image of a Langmuir-Blodgett film of the HeLa-mimicking mixture monolayer extracted at  $30 \text{ mN m}^{-1}$ . In the image, the whole mica surface is covered by the lipid film showing different regions 85 % of the image is filled with a relatively uniform film,  $1.6 \pm 0.3 \text{ nm}$  thick; while the remaining 15 % consists of a series of small regions that are dotted about the otherwise smooth film, each about  $400 \text{ nm}$  across and raised  $0.6 \text{ nm}$  above it. The small region present a roughness value of  $0.25 \text{ nm}$ . The size of the small domain is clearly different from the bright spots observed in the BAM experiments, apart from the difference in scale, meaning that the AFM image is showing nanostructures inside the microstructures observed in the BAM images. The AFM imaging mode does not provide information on the composition of these domains, which is even more difficult to determine with the lipid monolayer of the HeLa-mimicking mixture formed by four different molecules. It is feasible, however, to obtain some information on the adhesion properties of these lipidic domains by applying AFM in force spectroscopy mode to the domains observed in Fig. 4. Fig. 5A shows a more detailed topographic image of the domains presented in Fig. 4A, together with the corresponding force adhesion map in Fig. 5B, where the edges of the taller lipid domain are highlighted. For completeness, Fig. 5C and D present  $F_{\text{adh}}$  histograms of the taller and shorter domains, respectively. Whilst the taller domains present a mean adhesion force of  $49.70 \pm 0.04 \text{ nN}$ , the shorter domain presents a value of  $52.60 \pm 0.02 \text{ nN}$ . These  $F_{\text{adh}}$  values are in agreement with others determined in binary mixtures of a series of phosphatidylcholines and cholesterol [23], where it was shown that low values of  $F_{\text{adh}}$  represent lipids in the LE phase. That agrees with the LE phase nature of the lipid monolayer of the HeLa-mimicking mixture.

Although the monolayer model is suitable as a first approximation to mimic a lipid membrane, the vesicle model is a step closer to a real system. So, we studied liposomes formed with the HeLa-mimicking mixture and evaluated the possible existence of lipid domains in the bilayer system. Changes in the Laurdan fluorescence intensity as a function of temperature and excitation wavelength ( $\lambda_{\text{ex}}$ ) in the range of temperatures from  $0^\circ \text{C}$  to  $50^\circ \text{C}$  were studied. Laurdan is a fluorescence probe that can be used to distinguish differences in phospholipid order from changes in membrane fluidity by examining the dependence of Laurdan  $GP_{\text{ex}}$  values as a function of the excitation wavelength in liposomes. Liposome characterization, size, polydispersity and surface potential values are summarized in Table 1. As can be seen in Fig. 6A, the excitation  $GP_{\text{ex}}$  values calculated according Eq. 3 as a function of  $\lambda_{\text{ex}}$  show positive slopes from  $0^\circ \text{C}$  until  $15^\circ \text{C}$ , and negative slopes in the range of  $20^\circ \text{C} - 40^\circ \text{C}$ . Positive slopes are interpreted as a result of the presence of domains of different compositions in different ordered phases in the lipid bilayer; whereas negative slopes imply transition towards a more fluid phase. In general, high  $GP_{\text{ex}}$  values indicate the presence of gel phase ( $L_{\beta}$ ), while low  $GP_{\text{ex}}$  values show the presence of a liquid-crystalline phase ( $L_{\alpha}$ ). Fig. 6B shows the variation of  $GP_{\text{ex}}$  values at  $340 \text{ nm}$  as a function of temperature. In the figure, sigmoidal behaviour is observed and fitting the  $GP_{\text{ex}}$  values to Eq. 4, we can evaluate  $T_m$  and the slope of the curve ( $m$ ), which is correlated with the

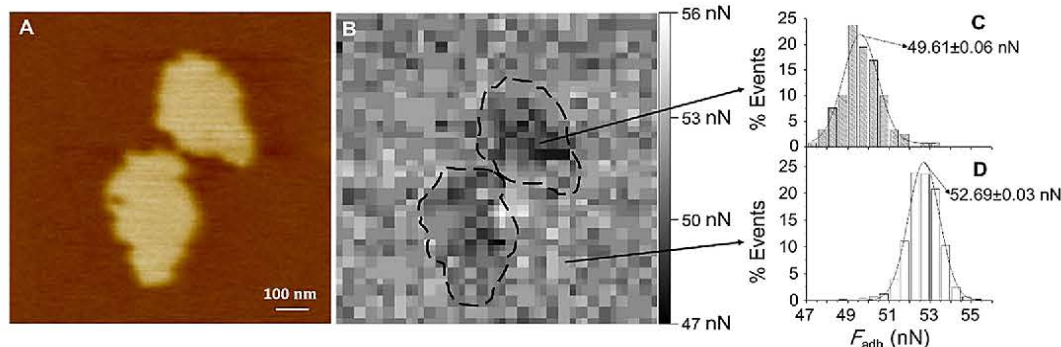


Fig. 5. AFM topography of lipid monolayer of HeLa-mimicking mixture, extracted at  $30 \text{ mN m}^{-1}$  on a mica surface (A); adhesion force map where lipid domains are highlighted (B); and histograms for  $F_{\text{adh}}$  values of the thicker or tall domain of the HeLa-mimicking mixture (C); and the thinner or low domain (D). Continuous lines in C and D are Gaussian distributions fitted to our experimental data. Z scale bar in image A is 2 nm.



**Table 1**  
Diameter, polydispersity index (PDI) and zeta potential values of liposomes.

Mol Composition	Diameter (nm)	PDI	Zeta Potential (mV)
POPC:POPE:POPS:CHOL (0.29:0.31:0.06:0.34)	117.6 ± 1.1	0.122	-8.9 ± 1.1
POPC:DOTAP (0.8:0.2)	120 ± 3	0.194	9.0 ± 1.2
POPC:CHOL:DOTAP (0.65:0.15:0.20)	120.7 ± 0.5	0.168	10.2 ± 0.6

cooperativity of the systems studied. These values were 33.6 °C ± 0.6 °C and 9.0 °C ± 0.7 °C for  $T_m$  and  $m$ , respectively. Because of the high proportion of CHOL the features of Fig. 6B may be compatible with a homogeneous system in liquid-ordered phase ( $L_o$ ) which becomes more fluid/less ordered with temperature. Such hypothesis, however, cannot be inferred by using Laurdan as a fluorescence probe and other methods should be considered.

After gathering the information on the physicochemical properties of the monolayer and bilayers mimicking the lipid composition of HeLa cells, we studied the fusion of two membranes of different compositions. On the one hand, in the transfection processes, the cationic phospholipid DOTAP, which seems to facilitate the fusion process, is usually used; on the other hand, CHOL, which seems to somehow modulate the fusion [28], is also present in liposome formulations. Therefore we engineered two different liposome compositions: POPC:DOTAP (0.80:0.20, mol/mol) and POPC:CHOL:DOTAP, (0.65:0.15:0.20, mol/mol/mol) to evaluate their possible fusion with the lipid monolayer of the HeLa-mimicking mixture studied before. Size, polydispersity and surface potential values of the liposomes used are summarized in Table 1. Fig. 7 shows the time dependence of the molecular area variation of the lipid monolayer of the HeLa-mimicking mixture compressed at 30 mN m<sup>-1</sup> after the injection of liposomes into the subphase. The increase of the molecular area tends to follow a saturation curve that reaches its maximum at ~7000 s. This is, therefore, clear evidence that fusion occurs between the monolayer and liposomes. Remarkably, liposomes containing CHOL provoke a greater increase in the molecular area than liposomes without the sterol. Furthermore, if we fit the experimental data to Eq. 5, the process is faster for the POPC:DOTAP than for the POPC:CHOL:DOTAP liposomes (Table 2). Hence, the fusion process in the monolayer appears to be slower but more extended in quantitative terms in the presence of CHOL. Also, liposomes of pure POPC were studied but showed no variation in molecular area (data not shown); therefore, they can be said to have no fusion properties, which indicates the important role of DOTAP and CHOL in the process.

#### 4. Discussion

Membrane fusion in the absence of proteins has been extensively

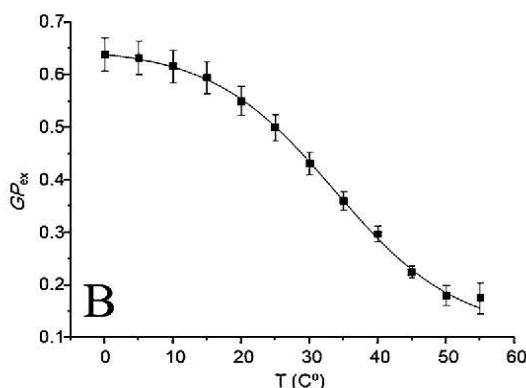
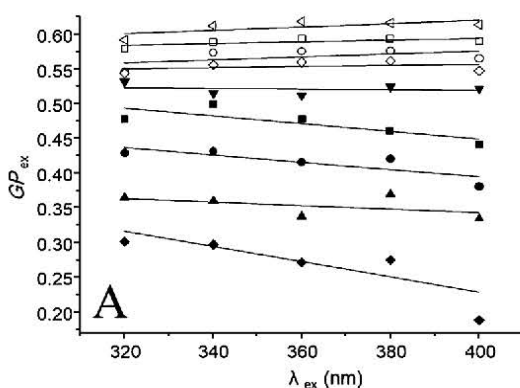


**Fig. 6.** Variation of  $GP_{ex}$  values as a function of the excitation wavelength ( $\lambda_{ex}$ ) at 0 °C ( $\triangleleft$ ), °C ( $\square$ ), °C ( $\circ$ ), °C ( $\diamond$ ), °C ( $\nabla$ ), °C ( $\blacksquare$ ), °C ( $\bullet$ ), °C ( $\blacktriangle$ ), °C ( $\blacklozenge$ ), (A);  $GP_{ex}$  values at 340 nm as a function of temperature (B).

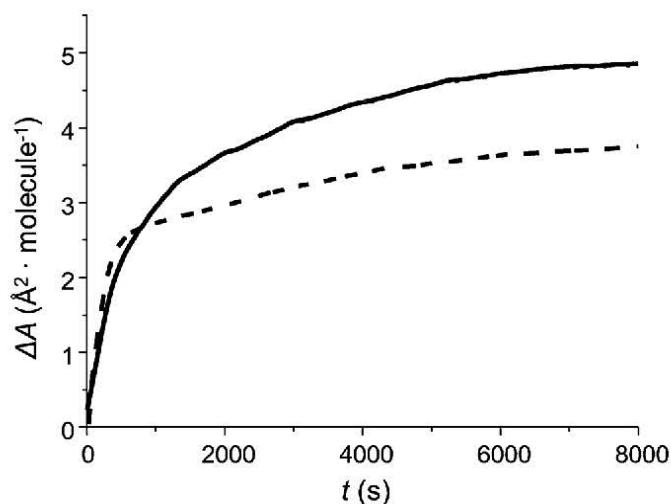


**Fig. 7.** Molecular area variation as a function of time after the addition beneath the lipid monolayer liposomes of POPC:DOTAP (0.8:0.2, mol/mol) (dashed line) and POPC:CHOL:DOTAP (0.65:0.15:0.20, mol/mol/mol) (solid line).

**Table 2**  
Parameters obtained from constant-surface pressure experiments.

	POPC:DOTAP (0.8:0.2, mol/mol)	POPC:CHOL:DOTAP (0.65:0.15:0.20, mol/mol/mol)
$\Delta A_{max}$ ( $\text{\AA}^2 \text{ molecule}^{-1}$ )	4.62 ± 0.02	5.95 ± 0.02
$k$ ( $\times 10^{-5}$ ) s <sup>-1</sup>	168.0 ± 1.6	94.3 ± 0.2
$b$	0.540 ± 0.003	0.760 ± 0.002
$r^2$	0.9683	0.9985

studied, and two intermediate structures have been identified: hemi fusion and fusion pores [29,30]. Whilst in the first case, there is a mixing of the lipids in the outer leaflets but not of those present in the inner layer of the bilayer, in pore formation both leaflets are considered to merge and result in a pore. The experiments we carried out in the present work were not aimed at proving the existence of either of these structures or the fusion mechanism itself, but to investigate whether the HeLa plasma membrane may incorporate liposome content (proteins, genes or drugs) via fusion. The main question that arose addressed the physicochemical properties of a HeLa model membrane mimicking the natural behaviour of the bilayers of HeLa cells. The composition we chose was a mixture of POPC, POPE, POPS and CHOL at molar ratios similar to those in the HeLa bilayer [10–13]. The presence of CHOL, as expected, caused condensation of the phospholipids, as shown by recording compression isotherms at the air–water interface of the single lipids and the mixture of the four. Since the main transition temperature of the individual pure phospholipids is below 24 °C, the lipid monolayer of the HeLa-mimicking mixture showed an LE nature in all



ranges of surface pressures applied, including  $30 \text{ mN m}^{-1}$  which is considered to be that of natural bilayers [31]. Note that the LE phase in monolayers is usually considered as the corresponding  $L_\alpha$  phase in bilayers. To corroborate such a correspondence, we performed experiments to establish the fluidity of the HeLa-mimicking mixture liposomes by calculating generalized polarization magnitudes from fluorescence measurements. Clearly, the HeLa-mimicking mixture liposomes present a transition temperature below  $37^\circ\text{C}$  but higher than the individual transition temperatures of the pure phospholipids, due to the rigidification caused by the presence of CHOL in the membrane. Moreover, Laurdan fluorescence experiments clearly corroborated the existence of domains which match the BAM and AFM observations reasonably well. Hence, the process of fusion should, in principle, be favoured in accordance with the fluid nature of the HeLa membrane. We also report the values of the vertical component of the molecular dipolar moment ( $\mu_\perp$ ), which is positive for the HeLa-mimicking mixture monolayer and reaches a relatively low value at  $30 \text{ mN m}^{-1}$ . Although  $\mu_\perp$  values could not be directly interpreted as an indication of molecular orientation at the interface, it is certain that the HeLa-mimicking mixture as a whole is less polarized at higher than at lower surface pressures [32]. Although this magnitude cannot be directly extrapolated to the real HeLa lipid membrane, since the radius of curvature of the cell is large, it may be indicative of the interaction of the lipid components when liposomes reach the surface of the cell.

Beyond the electrical properties, we studied the microstructure of the monolayer using BAM and AFM; we found that the HeLa-mimicking mixture monolayer is not homogeneous, but presents laterally segregated domains. Moreover, the adhesion force attributed to the different domains is moderate, in the range expected for a fluid membrane, but shows different values. Since the adhesion force data is in fact the force obtained when extracting the AFM tip from the LBs, it is conceivable that this magnitude may play a role in the fusion process after a primary step of adsorption of the liposomes onto the cell membrane. In fact, our constant surface pressure experiments performed with the HeLa-mimicking mixture monolayer exposed to the interaction of liposomes, with and without CHOL, injected beneath the bilayer, clearly demonstrate that the fusion process occurs for the two kinds of liposomes studied. Here, it is important to recall the sign of the zeta potential of HeLa-mimicking mixture liposomes. Considering their negative zeta potential, mainly due to the negative charge of the PS lipid, together with their positive value of the perpendicular component of the molecular dipole moment, it seems correct to assume that the first step of the interaction with liposomes containing DOTAP, with positive zeta potential values, is electrostatic and precedes or promotes the insertion of the lipids from the liposomes into the monolayer. At this point, when the rupture of the liposomes starts, the adhesion forces may contribute with other factors, such as the intrinsic curvature of each phospholipid, to a complex fusion mechanism. The whole process is relatively fast and proceeds until saturation, when all lipids that form the liposomes are fused with the target cell membrane represented by the HeLa-mimicking mixture monolayer. One additional finding of our work is that the presence of CHOL in the liposome formulation provokes a significant increase in the fusion mechanism. It has been reported that phosphatidylserine is intimately related with cholesterol in the endocytosis process [33] and to maintain the transbilayer distribution of cholesterol [34]. Besides, replacing phosphatidylserine by phosphatidylglycerol under the same experimental conditions, the fusion process does not occur. Therefore, with the present results we may only suggest a tentative explanation about the fusion mechanism. The possible steps leading to the fusion are depicted in the cartoon shown in Fig. 8. After the injection of liposomes beneath the lipid monolayer mimicking the HeLa plasma membrane Fig. 8A, liposomes diffuse and reach the monolayer where cholesterol and PS molecules could interact Fig. 8B. Then part of the liposome could be integrated in the monolayer Fig. 8C while part of the liposome could remain unfused Fig. 8D.

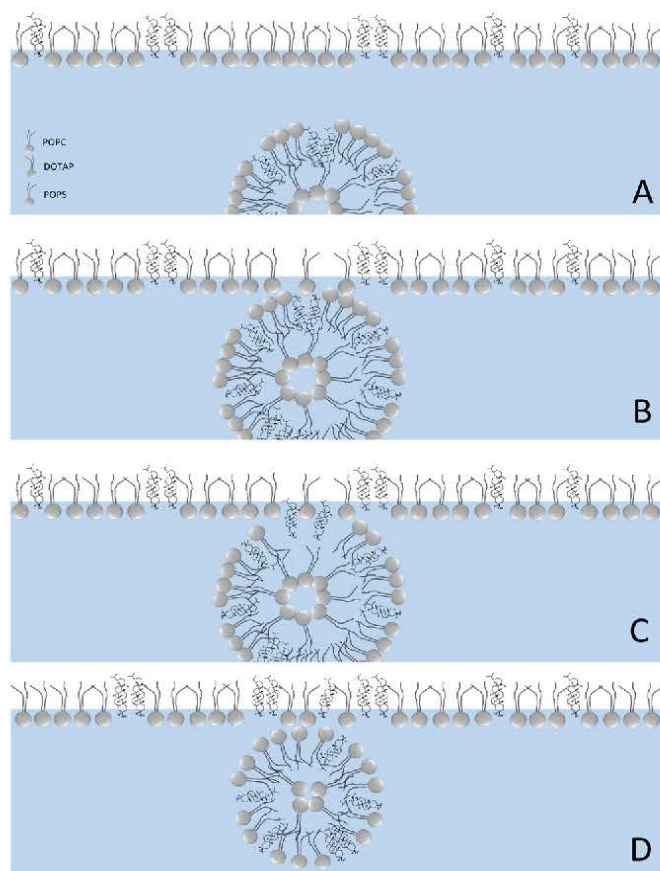


**Fig. 8.** Cartoon depicting a possible fusion process. Liposomes diffuse near the lipid monolayer (A), POPS and cholesterol molecules could interact (B), part of the liposome could be integrated in the monolayer (C) and part of the liposome could remain unfused (D).

## 5. Conclusions

In conclusion, we engineered an artificial membrane model based on the lipid composition of real HeLa cells [10–13]. In addition to the characterization of the monolayer and bilayer models, we provide basic physicochemical data that help to understand the fusion mechanism at the molecular level. Our results suggest that the fusion mechanism may involve, at least in primary steps, electrostatic and adhesion forces. Furthermore, using our bilayer–monolayer approach at constant surface pressure, we demonstrate that CHOL enhances the fusion process. Therefore, this information should be considered when developing liposome formulations aimed at transferring to HeLa cells. Works are ongoing in our laboratory and will be submitted in a later paper.

## Credit author statement

A.B–C, conducted the monolayer and BAM experiments; T.M. and J.S., conducted the fluorescence experiments; O.D., conducted AFM-FS experiments; J.H.B conceptualization and writing. All authors collaborate in the writing process and editing process.

## Declaration of Competing Interest

The authors declare that they have no known competing financial interests or personal relationships that could have appeared to influence the work reported in this paper.



## Acknowledgements

This study was carried out with the support of grants ART2017 from the IN<sup>2</sup>UB, TEC2016-79156-P from the Spanish Ministry of Economy and Competitiveness and 214SGR 1442 from the Catalan authorities (*Generalitat de Catalunya*). J.S. thanks Fundació Biofísica Bizkaia and the Basque Excellence Research Centre (BERC) program of the Basque Government. Special thanks to Dr. Félix M. Goñi for sharing his insight about polarization data. The authors would like to thank Dr. Christopher Evans for correcting the English.

## References

- [1] W. Barcellini, P. Bianchi, E. Fermo, F.G. Imperiali, A.P. Marcello, C. Vercellati, A. Zaninoni, A. Zanella, Hereditary red cell membrane defects: diagnostic and clinical aspects, *Blood Transfus.* 9 (2011) 274–277.
- [2] WHO, The molecular genetic epidemiology of cystic fibrosis Report of a joint meeting of, World Heal. Organ. (2004) 1–24.
- [3] C.A. Hubner, Ion channel diseases, *Hum. Mol. Genet.* 11 (2002) 2435–2445.
- [4] T.K. Kim, J.H. Eberwine, Mammalian cell transfection: the present and the future, *Anal. Bioanal. Chem.* 397 (2010) 3173–3178.
- [5] J.K. Patra, G. Das, L.F. Praceto, E.V.R. Campos, M.D.P. Rodriguez-Torres, L.S. Acosta-Torres, L.A. Diaz-Torres, R. Grillo, M.K. Swamy, S. Sharma, S. Habtemariam, H.S. Shin, Nano based drug delivery systems: recent developments and future prospects, *J. Nanobiotechnology* 16 (2018).
- [6] J. Hernández-Borrell, A new confirmation of selective action of liposomes, *Int. J. Pharm.* 47 (1988) 129–132.
- [7] L.V. Chernomordik, M.M. Kozlov, Mechanics of membrane fusion, *Nat. Struct. Mol. Biol.* 15 (2008) 675–683.
- [8] P. Ciancaglini, A.M.S. Simão, M. Bolean, J.L. Millán, C.F. Rigos, J.S. Yoneda, M.C. Colhane, R.G. Stabeli, Proteoliposomes in nanobiotechnology, *Biophys. Rev.* 4 (2012) 67–81.
- [9] M. Scailse, L. Pochini, N. Giangregorio, A. Tonazzi, C. Indiveri, Proteoliposomes as tool for assaying membrane transporter functions and interactions with xenobiotics, *Pharmaceutics* 5 (2013) 472–497.
- [10] X. Li, Y.-J. Yuan, Lipidomic analysis of apoptotic hela cells induced by paclitaxel, *Omi. A J. Integr. Biol.* 15 (2011) 655–664.
- [11] M.L. Torgersen, T.I. Klokke, S. Kavaliuskienė, C. Klose, K. Simons, T. Skotland, K. Sandvig, The anti-tumor drug 2-hydroxyoleic acid (Minerval) stimulates signaling and retrograde transport, *Oncotarget* 7 (2016) 86871–86888.
- [12] M.J. Gerl, V. Bittl, S. Kirchner, T. Sachsenheimer, H.L. Brunner, C. Lichtenborg, C. Özbalci, H. Wiedemann, S. Wegehangel, W. Nickel, P. Haberkant, C. Schultz, M. Krüger, B. Brügger, Sphingosine-1-phosphate lyase deficient cells as a tool to study protein lipid interactions, *PLoS One* 11 (2016).
- [13] M. Lorizate, T. Sachsenheimer, B. Glass, A. Habermann, M.J. Gerl, H.G. Kräusslich, B. Brügger, Comparative lipidomics analysis of HIV-1 particles and their producer cell membrane in different cell lines, *Cell. Microbiol.* (2013) 292–304.
- [14] W. Daeer, M. Mahadeo, E.J. Prenner, Applications of Brewster angle microscopy from biological materials to biological systems, *Biochim. Biophys. Acta Biomembr.* 1859 (2017) 1749–1766.
- [15] J.T. Davies, E.K. Rideal, *Interfacial Phenomena*, 1st., Academic Press Inc., New York, 1963.
- [16] M.C. Petty, *Langmuir-Blodgett Films: an Introduction*, dge Univ. Press Cambridge, Cambri, 1996.
- [17] G. Gramse, A. Dols-Perez, M.A. Edwards, L. Fumagalli, G. Gomila, Nanoscale measurement of the dielectric constant of supported lipid bilayers in aqueous solutions with electrostatic force microscopy, *Biophys. J.* 104 (2013) 1257–1262.
- [18] C. Suárez-Germà, L.M.S. Loura, M. Prieto, Ò. Domènech, M.T. Montero, A. Rodríguez-Banqueri, J.L. Vázquez-Ibar, J. Hernández-Borrell, Membrane protein-lipid selectivity: enhancing sensitivity for modeling FRET data, *J. Phys. Chem. B* 116 (2012) 2438–2445.
- [19] G. Oncins, G. Oncins, L. Picas, L. Picas, J. Hernandez-Borrell, J. Hernandez-Borrell, S. Garcia-Manyes, S. Garcia-Manyes, F. Sanz, F. Sanz, Thermal response of Langmuir-Blodgett films of dipalmitoylphosphatidylcholine studied by atomic force microscopy and force spectroscopy, *Biophys. J.* 93 (2007) 2713–2725.
- [20] T. Parasassi, E.K. Krasnowska, Laurdan and Prodan as polarity-sensitive fluorescent membrane probes, *J. Fluoresc.* 8 (1998) 365–373.
- [21] O. Domenech, G. Francius, P.M. Tulkens, F. Van Bambeke, Y. Dufrêne, M.P. Mingeot-Leclercq, Interactions of oritavancin, a new lipoglycopeptide derived from vancomycin, with phospholipid bilayers: effect on membrane permeability and nanoscale lipid membrane organization, *Biochim. Biophys. Acta Biomembr.* 1788 (2009) 1832–1840.
- [22] Ò. Domènech, L. Redondo, M.T. Montero, J. Hernández-Borrell, Specific adsorption of cytochrome c on cardiolipin-glycerophospholipid monolayers and bilayers, *Langmuir* 23 (2007) 5651–5656.
- [23] A. Botet-Carreras, M.T. Montero, Ò. Domènech, J.H. Borrell, Effect of cholesterol on monolayer structure of different acyl chained phospholipids, *Colloids Surf. B Biointerfaces* 174 (2019) 374–383.
- [24] K. Hac-Wydro, R. Lenartowicz, P. Dynarowicz-Latka, The influence of plant stanol ( $\beta$ -sitosterol) on inner leaflet of human erythrocytes membrane modeled with the Langmuir monolayer technique, *Colloids Surf. B Biointerfaces* 102 (2013) 178–188.
- [25] D.-L. Patrycja, K. Hac-Wydro, Interactions between phosphatidylcholines and cholesterol in monolayers at the air/water interface, *Colloids Surf. B Biointerfaces* 37 (2004) 21–25.
- [26] K. Hac-Wydro, P. Wydro, The influence of fatty acids on model cholesterol/phospholipid membranes, *Chem. Phys. Lipids* 150 (2007) 66–81.
- [27] P. Wydro, The influence of cholesterol on multicomponent Langmuir monolayers imitating outer and inner leaflet of human erythrocyte membrane, *Colloids Surf. B Biointerfaces* 103 (2013) 67–74.
- [28] L.K. Yang, A.T. Kreutzberger, A.J.B. Lee, J. Kiessling, V. Tamm, The role of cholesterol in membrane fusion, *Chem. Phys. Lipids* 199 (2016) 136–143.
- [29] L.V. Chernomordik, M.M. Kozlov, Protein-lipid interplay in fusion and fission of biological membranes, *Annu. Rev. Biochem.* 72 (2003) 175–207.
- [30] B.R. Lentz, V. Malinin, M.E. Haque, K. Evans, Protein machines and lipid assemblies: current views of cell membrane fusion, *Curr. Opin. Struct. Biol.* 10 (2000) 607–615.
- [31] D. Marsh, Lateral pressure in membranes, *Biochim. Biophys. Acta - Rev. Biomembranes* 1286 (1996) 183–223.
- [32] H.M. Möhwald, Phospholipid monolayers, in: R. Lipowsky, E. Sackman (Eds.), *Handbook of Biological Physics — Structure and Dynamics of Membranes*, Elsevier, Amsterdam, The Netherlands, 1995, pp. 161–211.
- [33] M. Jedynak, R. Worch, M. Podsiadla-Bialoskórska, J. Chroboczek, E. Szolajska, Cholesterol and phosphatidylserine are engaged in adenoviral dodecahedron endocytosis, *Biochim. Biophys. Acta - Biomembranes* 1860 (2018) 2215–2223.
- [34] M. Maekawa, G.D. Fairm, Complementary probes reveal that phosphatidylserine is required for the proper transbilayer distribution of cholesterol, *J. Cell. Sci.* 128 (2015) 1422–1433.



## Chapter 6. Results: Testing

Engineering and development of model lipid membranes mimicking the HeLa cell membrane

**A. Botet-Carreras**, M.T. Montero, J. Sot, Ò. Domènech, J.H. Borrell

*Colloids and Surfaces A: Physicochemical and Engineering Aspects*, vol. 630 pp. 127663, Dec. 2021

DOI: 10.1016/j.colsurfa.2021.127663

### Techniques introduced

Spectrofluorometry

#### *Anisotropic fluorescence emission*

Fluorescence anisotropy and fluorescence polarization, as discussed in the previous chapters, can be used to determine the fluidity of a lipid bilayer. In fluorescence anisotropy, the light emitted by a fluorophore has different intensities depending on the axis of polarization due to rotational movements.

The use of fluorophores enables us to get a deeper insight into the physicochemical parameters of the lipid bilayer and help build the composition of the engineered liposomes.

Using the fluorophores 1,6-diphenylhexatriene (DPH) and 1-(4-trimethylammonium-phenyl)-6-phenyl-1,3,5-hexatriene (TMA-DPH), it is possible to evaluate the membrane fluidity of a liposome bilayer. More accurately, using the anisotropy data, we were able to calculate the microviscosity ( $\eta$ ) of a liposome bilayer [140,141].

The difference between DPH and TMA-DPH is in the location of the fluorophore in the membrane after mixing and incubation with the liposomes of interest at a lipid:probe molar ratio of 300:1. The DPH probe is used to assess the bilayer core, while the TMA-DPH probe is used to visualize the area near the phospholipid headgroup due to its net positive charge. This is important since the different locations can provide information about the two main areas of a lipid bilayer. To proceed with this type of assay, we needed a spectrofluorometer equipped with proper polarizers. The assays were performed using excitation and emission wavelengths of 381 nm and 426 nm, respectively.

To establish a relationship between the  $\eta$  of the medium (the liposome membrane in our case) and anisotropy ( $r$ ), we used the Perrin equation:

$$\frac{r_0}{r} = 1 + C(r) \frac{T \cdot \tau}{\eta}$$

where  $T$  is the absolute temperature,  $\tau$  the excited-state lifetime of the fluorescent probe,  $r_0$  the limiting anisotropy and  $C(r)$  a parameter related to the molecular shape and the location of the transition dipoles of the rotating fluorophore at each  $r$  value. The term  $C(r) \cdot T \cdot \tau$  was experimentally determined to be 0.24 Pa, while the  $r_0$  value for the DPH molecule was 0.362. Hence, we could rearrange the equation as:

$$\eta(\text{Pa} \cdot \text{s}) = \frac{0.24 \cdot r}{0.362 - r}$$

Another interesting information that can be obtained from this technique is the dependence of the viscosity on temperature. More precisely, we were interested in the values of the activation energy ( $\Delta E$ ), which considers the minimum energy value required for a fluid to flow. This can be either understood as an estimation of the minimum energy required to trigger the first events occurring in the fusion of different bilayers or the spread of liposomes on surfaces. Regarding the fusion studies, the higher this energy is, the lower the probability is of fusion between the lipid membranes.

Considering that commonly used solvents and linear hydrocarbon chain liquids show an exponential decay in their viscosity as a function of temperature, we used the following equation to calculate  $\Delta E$ :

$$\eta = \eta_0 e^{\frac{\Delta E}{RT}}$$

where  $\eta_0$  is the lowest viscosity value of the liquid and  $R$  the gas constant.

Using another probe, 1-formyl-6-(N-cyclohexyl) aminopyrene (PA), in liposomes at a lipid:probe molar ratio of 250:1, we were able to analyze the red/blue intensity ratio (RBIR). This technique calculates the integral intensity ratio of red/blue regions of an emission band (573-631 nm/500-530 nm, respectively) to distinguish between the  $L_0$ ,  $L_\alpha$  and  $L_\beta$  phases [142] comparing the experimental values with reference ones.

#### *Fluorescence resonance energy transfer*

Fluorescence resonance energy transfer (FRET) assays were performed with two fluorophores and based on the extent of resonance transfer (RET). The emission spectrum of one fluorophore, the donor, overlaps with the excitation spectrum of the second, the acceptor. When the donor is excited, if the acceptor is at the Förster distance from the donor, the acceptor will emit fluorescence through excitation by the emission of the donor. Two classical FRET fluorophores are 1,2-dioleoyl-sn-glycero-3-phosphoethanolamine-N-(lissamine rhodamine B sulfonyl) (Rh-PE or rhodamine-PE) and 1,2-dioleoyl-sn-glycero-3-phosphoethanolamine-N-(7-nitro-2-1,3-benzoxadiazol-4-yl) (NBD-PE).

In this case, the donor was NBD, which has a maximum excitation wavelength of around 460 nm and an emission wavelength of 547 nm, while the acceptor was Rh, which has a maximum excitation wavelength of around 553 nm and an emission wavelength of 590 nm. If NBD and Rh are close to one another, Rh fluorescence emission should occur.

FRET is highly dependent on the distance between the donor and the acceptor. This distance in nanometers is characterized by the Förster radius ( $R_0$ ), which is the donor/acceptor distance at which energy transfer is 50% efficient.  $R_0$  values are specific for each donor/acceptor pair, but are usually between 1.5 and 6 nm. The  $R_0$  of the NBD/Rh fluorophore pair is approximately 5 nm [143], making FRET a nanometric technique unlike conventional optical microscopy.

There are two different ways to perform a FRET assay to assess fusion between liposomes. One consists of adding 0.6% mol of each fluorophore to the different liposomes that are going to be tested against one another. When fusion occurs, the maximum fluorescence value of NBD diminishes, while Rh fluorescence increases as the molecules get closer and NBD emission excites the Rh molecules. This behavior occurs only if the fusion process happens.

This approach has one significant drawback. If one of the two different models being studied is mimicking a cell membrane, adding one of the fluorophores to the cell will be hard to control and might cause some modifications to the cell prior to the assay. Hence, the second way, which involves adding the two fluorophores to the same type of liposome (in this study, the engineered POPC:DOTAP or POPC:CHOL:DOTAP liposomes), can help in future experiments with living cells or other models that cannot be modified. This means that if fusion occurs and the FRET decreases, we should see the NBD signal grow and the Rh signal drop, as can be seen in Figure 17.

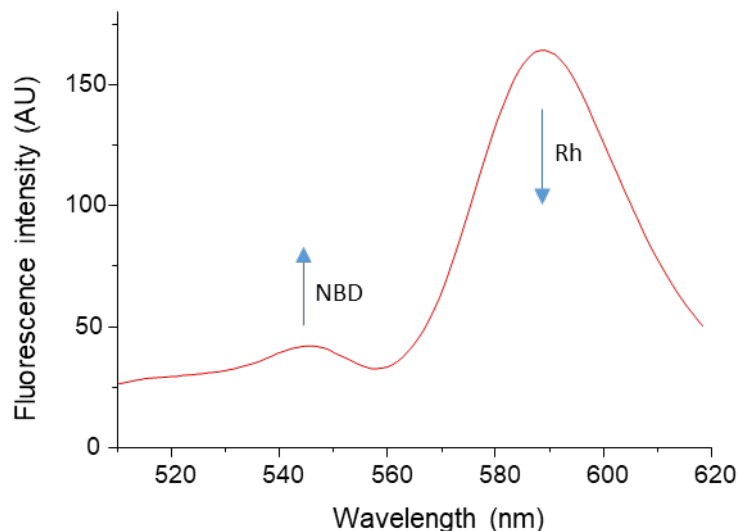


Figure 17. FRET curves, as the fusion process advances, with the NBD signal rising and the Rh signal drops as RET breaks.

By adding the two fluorophores to the same liposome (both at 0.6% mol) before the fusion process begins, low NBD and high Rh fluorescence signals should be detected, with the NBD fluorescence signal growing and the Rh one decreasing as the fusion process progresses. This will occur because the unlabeled liposomes (in this work, the HeLa-mimicking liposomes) will dilute the NBD and Rh concentrations present in the original liposome, making them spatially distant and impeding the RET process.

The percentage of fusion was calculated using the growth signal of NBD fluorescence, as follows:

$$\%Fusion = \left( \frac{F_t - F_0}{F_\infty} \right) \times 100$$

where  $F_t$  is the NBD fluorescence intensity at each given time,  $F_0$  the initial NBD fluorescence intensity and  $F_\infty$  the fluorescence intensity at an infinite dilution of the fluorescent probe in liposomes.

$F_\infty$  requires evaluation. The classical approach for obtaining this value is by breaking the liposomes down with a detergent (e.g., Triton X-100). This brings the lipids down to an



infinite dilution state. It has been reported that NBD in detergent micelles presents less fluorescence than the NBD molecules that are infinitely diluted in lipid bilayers [144]. To correct for this error produced by the detergent,  $F_{\infty}$  can be estimated as:

$$F_{\infty} = \alpha \cdot F_{\text{det}}$$

where  $F_{\text{det}}$  is the fluorescence of NBD in micelles and  $\alpha$  is a ratio of the real fluorescence at an infinite dilution to that with detergent. Experimentally, we obtained  $F_{\text{det}}$  values after the addition of Triton X-100 at a final concentration of 1%. The  $\alpha$  value used, 1.79, was determined at 37 °C [144].

The abovementioned method to obtain the percentage of fusion considers that both fluorescent probes are infinitely diluted in the liposomes at the end of the fusion process. This could be achieved easily if the number of unlabeled liposomes is much greater than that of the labeled ones.

In the assays, the molar ratio of labeled to unlabeled liposomes was 1. It is known that due to the speed and possible collision events between the liposomes during a typical fusion experiment (1 h – 2 h), the maximum number of fusion events for a liposome will be only one [144]. Therefore, the model where we reach an infinite dilution could be considered not valid for obtaining the percentage of fusion, as infinite dilution will never be reached. To obtain  $F_{\infty}$  values, we created a special batch of liposomes combining the HeLa-mimicking liposomes and the engineered liposomes (with or without CHOL) supplemented with the two fluorophores. By creating these liposomes, we artificially created a system where all the possible fusions between the HeLa-mimicking liposomes and the engineered liposomes (at a ratio of one to one) had already happened and maximum dilution had been achieved.

We evaluated the percentage of fusion achieved by considering the two methods mentioned above. We added 1% Triton X-100 to break down the liposomes and obtained the value for infinite dilution using the classical method. We also considered maximum dilution as if there were only one-to-one fusion events. In this way, the fluorescence value of the mixed preparation could be adjusted and corrected to the value of the FRET assay.

Using the second method to obtain  $F_{\infty}$ , the percentage of fusion obtained was almost quadruple that obtained with the classical method involving infinite dilution.

Finally, the fusion data were fitted to a modified Langmuir saturation curve to evaluate the physicochemical parameters of the process:

$$\%Fusion = A_{max} \frac{(kt)^b}{(1 + kt)^b}$$

where  $A_{max}$  is the maximum value of fusion achieved,  $k$  the rate constant of the process and  $b$  a parameter related to the cooperativity of the process.

#### *Fluorescence lifetime decay*

Fluorescence lifetime decay is an intrinsic property of a fluorophore and it is the time that a molecule remains in the excited state before returning to its ground state. The lifetimes of fluorophores can range from picoseconds to hundreds of nanoseconds. During this lifetime, the fluorophores can interact with other molecules, rotate and diffuse through the local environment as well as undergo conformational changes [145,146].

Intensity decay curves ( $F(t)$ ) need to be corrected to avoid the instrument response factor (IRF), which is the consequence of scattered photons arriving at the detector (Figure 18). This correction is usually achieved by measuring a reference colloidal silica solution, but can be also obtained with other substances as long as they are colloidal systems.

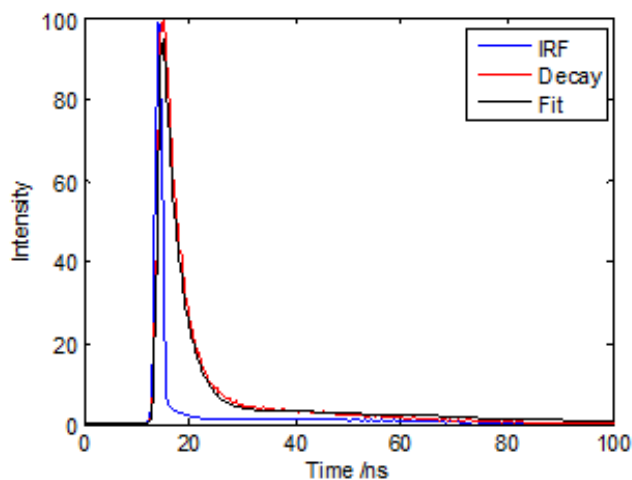


Figure 18. Lifetime fluorescence decay curves. Fluorophore decay (red); IRF (blue); curve fitting (black).

Once the IRF is subtracted from the  $F(t)$  curves, these curves can be fitted to one or multiple exponential decay curves depending on the fluorophores studied. In this work, the engineered liposomes containing NBD and Rh were fitted to a multiple exponential decay curve expressed as:

$$F(t) = \sum_i \alpha_i \cdot e^{-t/\tau_i}$$

where  $\alpha_i$  is the preexponential factor (fraction contribution to the time-resolved decay) and  $\tau_i$  the corresponding lifetime value. Mean lifetime values can be calculated as [147]:

$$\langle \tau \rangle = \frac{\sum_i^n \alpha_i \tau_i^2}{\sum_i^n \alpha_i \tau_i}$$

## AFM

### *Young's modulus for SLBs*

As mentioned previously, calculating the stiffness of a membrane by AFM-FS [148] is really helpful in studying the changes in the mechanical properties of samples. To evaluate the stiffness of a sample, we used Young's modulus to provide information on how difficult it is to deform a sample in the direction of the force applied, i.e., between the lipids forming the lipid bilayer [149]. To calculate the Young's modulus of the different samples, a mathematical approximation was needed. Although there is debate on the nanomechanical model to be applied, the Hertz model is widely accepted to be the most reliable [150].

This model introduces three considerations or restrains:

1. The surface of the sample is a homogeneous and linear elastic solid.
2. The indenter is not deformable.
3. The interaction between the sample and the indenter is through elastic forces only.

Considering the shape of the tip (the indenter), we can apply different formulas. If we consider the indenter to be a parabolic tip, Young's modulus can be calculated through force indentation curves ( $F$  vs  $\delta$ ) using the following equation:

$$F = \frac{4\sqrt{r_{tip}}}{3} \cdot \frac{E}{1-\nu^2} \cdot \delta^{3/2}$$

where  $r_{tip}$  is the tip radius (in our case, 2 nm),  $\nu$  the Poisson's ratio (0.5 for most biological samples),  $E$  the Young's modulus and  $\delta$  the indentation.

For a better sample distribution and to obtain more force curves to study, we used the force-volume mode to gather the highest number of individual force curves.

## Summary

After investigating and selecting the lipids we could use for the engineered liposomes, together with the creation of a membrane model mimicking the HeLa cell membrane, we were ready to study the fusion process between the engineered liposomes and the HeLa-mimicking models.

We made liposomes of different compositions: POPC:CHOL:DOTAP liposomes, POPC:DOTAP liposomes and HeLa-mimicking liposomes. As mentioned before, the average diameter of all the liposomes was approximately 120 nm. The two engineered POPC liposomes had a positive  $\zeta$ -potential due to the presence of the cationic lipid DOTAP, while the HeLa-mimicking liposomes had a negative  $\zeta$ -potential due to the presence of POPS, an anionic lipid.

Only for the experiments measuring the RBIR, HeLa-mimicking MLVs were created, showing an average diameter of 506 nm.

Evaluation of the lipid phase of the HeLa-mimicking liposomes with the RBIR revealed that liposomes at temperatures from 0 °C to 13 °C were in the  $L_o$  phase, while those at temperatures between 34 °C and 55 °C showed values similar to those of mixtures in the  $L_\alpha$  phase that contain CHOL [142]. Finally, liposomes at the intermediate temperature range of 13 °C to 34 °C showed an intermediate state between  $L_o$  and  $L_\alpha$  and also intermediate properties between those of the  $L_o$  and  $L_\alpha$  phases.

For a better understanding of what was happening at the membrane level in terms of fluidity, we measured the anisotropic fluorescence emission. The assays were performed using DPH and TMA-DPH incorporated into the HeLa-mimicking liposomes as well as two types of special liposomes obtained by fusing HeLa-mimicking liposomes with the engineered POPC:DOTAP or POPC:CHOL:DOTAP liposomes at a ratio of 1:1. These formulations allowed us to calculate the microviscosity ( $\eta$ ) of the resulting fused liposomes.

In general,  $\eta$  values decreased as the temperature increased for both fluorophores. The  $\eta$  values of the HeLa-mimicking liposomes were higher at all the temperatures studied compared to the other two types of liposomes. The  $\eta$  values of the other two types of liposomes decreased when the temperature increased, being lower for the POPC:DOTAP liposomes.

DPH provides information on the core of the bilayers. The results showed that CHOL did not modify the  $\Delta E$  values, probably due to its anchored position within the lipid bilayer. On the contrary, TMA-DPH, being placed near the phospholipid headgroup, showed decreased  $\Delta E$  values for the HeLa-mimicking liposomes fused with the POPC:CHOL:DOTAP liposomes, but not for the HeLa-mimicking liposomes fused with the POPC:DOTAP liposomes.

To investigate the abilities of the engineered liposomes to fuse with the HeLa-mimicking liposomes at a ratio of 1:1, we added both NBD-PE and Rh-PE to the engineered vesicles to carry out FRET assays and followed the kinetics of the NBD-PE fluorescence signal. We observed that both types of engineered liposomes effectively fused with the HeLa-mimicking liposomes. Furthermore, the POPC:CHOL:DOTAP liposomes showed a higher dilution of the NBD-Rh FRET, greater NBD fluorescence, a higher rate of fusion and a large cooperativity of the transition compared to the POPC:DOTAP liposomes, indicating a higher overall fusion rate.

Depending on what we consider as the maximum dilution of the fluorescent probes, the value of the overall fusion rate can have a different value. This observation will be discussed later in the Discussion.

We also evaluated the changes in the NBD-PE lifetime in the two types of engineered liposomes when fused with the HeLa-mimicking liposomes. The average lifetime of NBD-PE was quite similar for both formulations, but decreased in both cases, with this being greater for the POPC:CHOL:DOTAP formulation.

Finally, we used AFM-FS to study the SLBs created by fusing HeLa-mimicking liposomes onto mica surfaces. These SLBs were featureless and the covering of the mica surface was incomplete on purpose to create some holes in the SLB in order to assess the possible effect



of the engineered liposomes on the line tension of the SLBs. Indeed, after the addition of the engineered liposomes, these holes became smaller over time until they had almost disappeared as the liposomes had fused with the HeLa-mimicking SLB and integrated into it. No unfused liposomes were observed close to the holes, neither in the edges nor in the center of the hole, suggesting that the liposomes had been adsorbed onto the SLB and subsequently absorbed into the mica surface, laterally displacing the SLB components to cover the defects. In accordance with the findings of the FRET assays, POPC:CHOL:DOTAP liposomes were faster in fusing, therefore closing the holes in the SLB more quickly.

In the FS mode, we calculated the Young's modulus of the SLBs. The adjustment of the distribution to a normal distribution gave a maximum value of  $29.6 \pm 0.8$  MPa for the Young's modulus of the HeLa-mimicking SLB. After the addition of the engineered liposomes, this value changed. We observed two maximal  $E$  values after the addition of POPC:DOTAP liposomes, one centered at  $26 \pm 5$  MPa, similar to that of the HeLa-mimicking SLB, and the other at  $70.2 \pm 1.6$  MPa. After the addition of POPC:CHOL:DOTAP liposomes, we could observe only one maximum value of  $E$  centered at  $63.3 \pm 0.8$  MPa. These values were a clear indication of the changes in the composition of the HeLa-mimicking SLBs after the engineered liposomes had fused with them.

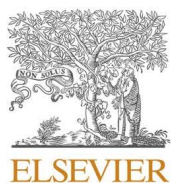
The force maps for the SLBs after the addition of POPC:DOTAP or POPC:CHOL:DOTAP liposomes were obtained 40 minutes after the addition of the engineered liposomes. Since the measurements were taken approximately at the same time, we suggest that the bimodal distribution obtained after the addition of the POPC:DOTAP liposomes was most probably due to an intermediate state where not all the liposomes had completely fused. Thus, some areas of the SLB remained as the original, without any integrated POPC:DOTAP liposomes. On the contrary, since the POPC:CHOL:DOTAP liposomes fused more quickly, the entire SLB had been altered. In other words, the results demonstrated the speed of the fusion process, being faster for the POPC:CHOL:DOTAP liposomes than for the POPC:DOTAP liposomes.

After evaluating the results provided by these experiments, we pursued our final objective of using biophysical approaches to prove that the fusion process between engineered liposomes and living HeLa cells can be modulated by selecting specific components that enhance fusion.

## Highlights

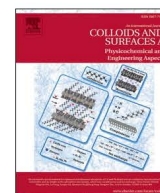
- The HeLa-mimicking lipid composition can form SLBs and stable liposomes.
- Due to its high proportion of CHOL, the HeLa-mimicking lipid membrane presented an equilibrium between the  $L_o$  and  $L_\alpha$  phases.
- The changes in microviscosity confirmed the integration of the lipids from the engineered liposomes into the HeLa-mimicking liposomes.
- DPH and TMA-DPH experiments suggested that the presence of CHOL decreased the activation energy.
- Fusion of any of the two types of engineered liposomes with the HeLa-mimicking models was positively confirmed by the FRET assays.
- The mean NBD lifetime was affected by changes in the composition after the fusion process.
- HeLa-mimicking SLBs did not show evidence of a surface lateral segregation of lipids.
- Engineered POPC:DOTAP and POPC:CHOL:DOTAP liposomes were capable of integrating into the HeLa-mimicking SLBs, confirming the fusion process.
- Changes in Young's modulus, which indicates membrane stiffness, demonstrated the integration of the POPC:DOTAP and POPC:CHOL:DOTAP liposomes into the HeLa-mimicking SLBs.
- We confirmed that CHOL enhances fusion, using different techniques.





Contents lists available at ScienceDirect

# Colloids and Surfaces A: Physicochemical and Engineering Aspects

journal homepage: [www.elsevier.com/locate/colsurfa](http://www.elsevier.com/locate/colsurfa)

## Engineering and development of model lipid membranes mimicking the HeLa cell membrane

Adrià Botet-Carreras<sup>a,b</sup>, M. Teresa Montero<sup>a,b</sup>, Jesús Sot<sup>c</sup>, Òscar Domènech<sup>a,b,\*</sup>,  
Jordi H. Borrell<sup>a,b</sup>

<sup>a</sup> Secció de Físicoquímica, Facultat de Farmàcia i Ciències de l'Alimentació, Spain

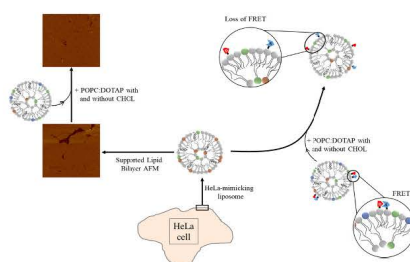
<sup>b</sup> Institute of Nanoscience and Nanotechnology (IN2UB), Universitat de Barcelona (UB), 08028 Barcelona, Catalonia, Spain

<sup>c</sup> Instituto Biofísica (CSIC-UPV/EHU) Campus Universitario, 48940 Leioa, Basque Country, Spain

### HIGHLIGHTS

- A lipid bilayer mimicking the HeLa membrane cell is characterised.
- HeLa-mimicking liposomes show phase coexistence at room temperature.
- Laterally segregated domains are not observed by AFM in Supported Lipid Bilayers.
- Fusion of liposomes changes Young's modulus of HeLa-mimicking bilayers.
- POPC:DOTAP and POPC:CHOL:DOTAP liposomes fusing process with HeLa-mimicking bilayers is characterised by FRET fluorescence.
- Changes in liposomes microviscosity and fluorescence lifetime corroborate the fusion process.

### GRAPHICAL ABSTRACT



### ARTICLE INFO

#### Keywords:

HeLa lipid bilayer models  
Atomic force microscopy (AFM)  
Förster resonance energy transfer (FRET)  
Microviscosity

### ABSTRACT

Cells are complex systems whose interaction with nanocarriers, i.e., liposomes, are continuously under investigation to improve drug uptake. Model membranes can facilitate the understanding of the processes involved in fusion or endocytosis. In this work, we engineered two different lipid model membranes, vesicles and supported lipid bilayers (SLBs), mimicking the lipid composition of the HeLa cell plasma membrane. We characterized the model using atomic force microscopy (AFM) and fluorescence. We found that liposomes formed with four lipid components mimicking the HeLa cell bilayer show a liquid ordered fluid nature between 13 °C and 34 °C and yield featureless SLBs onto mica. We evaluated the fusion between the model and liposomes positively charged with and without cholesterol by AFM-based force spectroscopy and fluorescence techniques, such as Förster resonance energy transfer, fluorescence lifetime decay and fluorescence anisotropy. The results indicated a primary electrostatic interaction between the HeLa bilayer model and the liposomes. It was also confirmed the well-known fact that cholesterol enhances the fusion process with the engineered HeLa bilayer. All results support the usefulness of the engineered model in the rationale design of liposomes for drug delivery.

\* Corresponding author at: Secció de Físicoquímica, Facultat de Farmàcia i Ciències de l'Alimentació, Av. Joan XXIII 27-31, 08028 Barcelona, Spain.  
E-mail address: [odomenech@ub.edu](mailto:odomenech@ub.edu) (Ò. Domènech).

<https://doi.org/10.1016/j.colsurfa.2021.127663>

Received 23 August 2021; Received in revised form 28 September 2021; Accepted 29 September 2021

Available online 2 October 2021

0927-7757/© 2021 The Author(s).

Published by Elsevier B.V. This is an open access article under the CC BY-NC-ND license

(<http://creativecommons.org/licenses/by-nc-nd/4.0/>).



## 1. Introduction

One of the most widely researched phenomena in biophysics is to understand the interaction of macromolecules with cells as it is the first step in several biophysical/biochemical processes, such as DNA transfection and drug delivery [1–3]. The complexity of cell membranes, i.e., lipid heterogeneity as well as the adsorbed or embedded membrane proteins, is a barrier for the interpretation of the physicochemical properties governing these processes. To overcome this, simplified model membrane systems are mandatory to unveil the nature of the interaction with cell membranes. The most common and well-known model membrane systems are monolayers, liposomes and membranes formed onto solid substrates. All these systems mimic the properties of cell membranes such as the lipid composition, lipid curvature, domains and rafts, depending on the system and the combination of compounds chosen as well as on the physicochemical properties of interest.

Transfecting material into cells has been a wide field of study, with liposomes playing a significant role. Liposomes, referred to as drug delivery systems, are an excellent model for mimicking cell membranes and experimentally testing the conditions that favour the internalisation of the encapsulated drug or carrying molecules by eukaryotic cells or bacteria. The extensive literature on liposome-based drug-delivery systems has been enriched by the development of surface functionalisation and modifications designed to achieve selectivity as well as to overcome removal by the reticuloendothelial system and circumvent the immune response system among other challenges [4]. However, it is not fully understood if liposomes fuse with the cell membrane or if they are endocytosed and subsequently degraded liberating their content into the cytoplasm. Despite the many years of extensive research into these processes (fusion and fission) at the molecular level, research in this field continues to expand and is of paramount importance for understanding the various biological processes in which fusion plays a leading role.

The fusion of two membranes, e.g., a cell membrane with a vesicle, is a complex process that involves many factors, but can be improved by engineering appropriate vesicles. For example, the addition of SNARE (Soluble NSF Attachment Protein Receptor) proteins promotes fusion and leads to pore opening in the cell membrane to release the liposome content [5]. The presence of lipids promoting the negative curvature of the vesicle, such as phosphatidylethanolamine (PE)[6,7], also facilitates the fusion process after adsorption of the two bilayers possibly through the emergence of hexagonal phases ( $H_{II}$ ) at the intermediate stages of the fusion process. It is also well known that cholesterol plays a key role in the fusion process as well as the cationic lipid 1,2-dioleoyl-3-trimethylammonium-propane (DOTAP), particularly in DNA transfection.

One of our current research projects is the engineering of liposomes for transporting proteins and genes into HeLa cell membranes [8]. Our ultimate goal is to test the ability of a liposome-based nanocarrier that can transfect proteins or genes to repair defects in cell membranes caused by the malfunction of proteins that are either absent due to DNA mutation or not well folded and presenting a non-functional conformation. Such defects are the main cause of many unrelated diseases that have severe consequences [9–11]. In a previous work [12], we developed and characterised an artificial monolayer lipid membrane that mimicked the HeLa lipid membrane. This lipid model had four components: 1-palmitoyl-2-oleoyl-*sn*-glycero-3-phosphatidylcholine (POPC), 1-palmitoyl-2-oleoyl-*sn*-glycero-3-phosphoethanolamine (POPE), 1-palmitoyl-2-oleoyl-*sn*-glycero-3-phospho-L-serine (POPS) and cholesterol (CHOL).

In the present work, we present data extending the characterisation of HeLa lipid vesicles and supported lipid bilayers (SLBs). The physicochemical characterisation of both models and how they behave when investigating the fusion with engineered liposomes may be relevant to interpret the events occurring in the interaction between these liposomes and living cells. Thus, in the present paper we have evaluated these two HeLa lipid models in their fusion with liposomes containing the cationic lipid DOTAP with or without cholesterol. For the phase

characterisation of the vesicle HeLa lipid bilayer model we used fluorescence spectroscopy applying a ratiometric parameter, the red/blue intensity ratio (RBIR), of the 1-formyl-6-(*N*-cyclohexyl) aminopyrene (PA) probe [13] alongside conventional fluorescence anisotropy. These information provided by the latter measurements indicated the changes in viscosity of the HeLa lipid membrane model after fusion with POPC:DOTAP or POPC:CHOL:DOTAP liposomes. Furthermore, exploiting the Förster resonance energy transfer (FRET) technique, we examined the fusion process between liposomes mimicking the HeLa lipid membrane and liposomes containing two fluorescent probes, nitrobenzoxadiazole (NBD) and rhodamine (Rh). Finally, fluorescence lifetime decay measurements were used to corroborate the interaction between the engineered liposomes and the engineered model. We also investigated the topographic characteristics and viscoelastic properties (Young's modulus) of SLBs through atomic force microscopy (AFM)-based force spectroscopy analysis in the presence and absence of POPC:DOTAP or POPC:CHOL:DOTAP liposomes.

## 2. Experimental section

### 2.1. Materials

1-palmitoyl-2-oleoyl-*sn*-glycero-3-phosphatidylcholine (POPC), 1-palmitoyl-2-oleoyl-*sn*-glycero-3-phosphoethanolamine (POPE), 1-palmitoyl-2-oleoyl-*sn*-glycero-3-phospho-L-serine (POPS), 1,2-dioleoyl-3-trimethylammonium-propane (chloride salt) (DOTAP), cholesterol (CHOL), 1,2-dioleoyl-*sn*-glycero-3-phosphoethanolamine-*N*-(lissamine rhodamine B sulfonyl)(ammonium salt) (Rh-PE) and 1,2-dioleoyl-*sn*-glycero-3-phosphoethanolamine-*N*-(7-nitro-2-*l*,3-benzoxadiazol-4-yl) (ammonium salt) (NBD-PE) were purchased from Avanti Polar Lipids (Alabaster, AL, USA). The lipophilic fluorescent probe 1-formyl-6-(*N*-cyclohexyl) aminopyrene (PA) was synthesized as previously described [14] and was a kind gift from Andrey Klymchenko (CNRS, Illkirch, France). 1,6-diphenylhexatriene (DPH) and 1-(4-trimethylammonium-phenyl)-6-phenyl-1,3,5-hexatriene (TMA-DPH) were purchased from Invitrogen (Life Technologies Ltd., Paisley, UK). All the other chemicals were acquired from Sigma-Aldrich (St. Louis, MO, USA) and used as received. Round muscovite mica discs, 9.5 mm diameter and 0.15–0.21 mm thickness, were purchased from Electron Microscopy Sciences (Hatfield, PA, USA). The lipids were dissolved in a chloroform:methanol (2:1, v/v) solution to obtain a final concentration of 1 mg mL<sup>-1</sup>. These solutions were used to obtain the mixtures POPC:POPE:POPS:CHOL (0.29:0.31:0.06:0.34, mol/mol/mol/mol) [15–18], and is referred through the text as HeLa-mimicking mixture (either HeLa liposomes or HeLa SLBs), POPC:DOTAP (0.80:0.20, mol/mol) and POPC:CHOL:DOTAP (0.65:0.15:0.20, mol/mol/mol).

### 2.2. Liposome preparation

Chloroform:methanol (2:1, v/v) solution containing the appropriate amount of lipids was placed in a glass balloon flask and dried in a rotary evaporator at room temperature, protected from light. The resulting thin film was kept under high vacuum overnight to remove any traces of organic solvent. Multilamellar liposomes (MLVs) were obtained by redispersion of the thin film in 10 mM Tris-HCl, 150 mM NaCl buffer, pH 7.4. Large unilamellar vesicles (LUVs) were obtained by extrusion through polycarbonate membranes with a pore size of 100 nm, using an Avanti®Mini-extruder (Avanti Polar Lipids Inc., Alabaster, AL, USA). The mean particle size and polydispersity values of the liposomes were measured by dynamic light scattering with a Zetasizer Nano S (Malvern Instruments, UK). To assess the effective surface electrical charge, electrophoretic mobility was determined with a Zetasizer Nano ZS90 (Malvern Instruments, UK). Each sample was measured at least three times.



### 2.3. Supported lipid bilayers

Supported lipid bilayers (SLBs) were obtained through the vesicle fusion method, as previously described in detail [19]. Briefly, a round Teflon disc was glued to a steel disc and a mica disc was mounted on top of the Teflon disc. 50  $\mu\text{L}$  of 250  $\mu\text{M}$  HeLa-mimicking liposomes were deposited onto freshly cleaved mica surface. Liposome suspension was incubated for 2 h at 40  $^{\circ}\text{C}$ , temperature over the transition temperature of any individual pure phospholipid used in the study. To prevent sample evaporation, the sample was enclosed in a small petri dish inside a bigger petri dish with some water at the bottom used as a reservoir. The big petri dish was then sealed with Teflon ribbon and placed inside an oven (Termaks AS, Bergen, Norway) with temperature control of  $\pm 0.2$   $^{\circ}\text{C}$ . After incubation, non-adsorbed liposomes were removed by gently rinsing samples with buffer and letting them stabilize overnight at room temperature.

### 2.4. AFM imaging and force spectroscopy

AFM images and force spectroscopy measurements were performed with a Nanoscope IV from Digital Instruments (Bruker, AXS Co., Madison, WI, USA), equipped with a 15  $\mu\text{m}$  piezoelectric scanner. Samples were directly mounted on the top of the AFM scanner and let to stabilize for no less than 30 min before beginning the scan. Temperature and humidity were maintained at 24  $^{\circ}\text{C}$  and 60%, respectively. SLB images were obtained using V-shaped silicon nitride cantilevers (MSNL-10, Bruker, USA) with a nominal spring constant of 30  $\text{pN nm}^{-1}$ , in liquid and in intermittent contact mode. During the experiments, the force applied to the samples was kept as low as possible to minimize sample damage. All the images were processed using NanoScope<sup>®</sup> analysis software (Bruker, AXS Co., Madison, WI, USA).

When performing force spectroscopy experiments in liquid, individual spring constants ( $k_c$ ) were calibrated using the thermal noise method, after the photodetector optical sensitivity ( $\text{V nm}^{-1}$ ) had been correctly determined by measuring it at high voltages. Applied forces,  $F$ , are given by  $F = k_c \times \delta$ , where  $\delta$  stands for the cantilever deflection. Mechanical properties were measured by recording arrays of  $32 \times 32$  force curves, using a maximum force of 0.5–1 nN to avoid sample damage, and approach and retract speeds of 1.0  $\mu\text{m/s}$ .

### 2.5. Young's modulus

Young's modulus is a physicochemical parameter that evaluates the stiffness of a sample, providing information on how difficult is to deform the sample in the direction of the force applied. In the present study, we have calculated the Young's modulus by means of AFM [20] as a physicochemical parameter that informs on the cohesive force between the lipids forming the lipid bilayer [21]. The Young's modulus of the different samples was determined as a first approximation and with the aim of observing relative differences in its value after liposome fusion using the Hertz model. This model considers that: (i) the surface of the sample is a homogeneous, isotropic and linear elastic solid, (ii) the indenter is not deformable, and (iii) the interaction between sample and indenter is through elastic forces only. If we consider the indenter as a parabolic tip, the Young's modulus can be calculated from force-indentation curve data thus,

$$F = \frac{4\sqrt{r_{\text{tip}}}}{3} \cdot \frac{E}{1-\nu^2} \cdot \delta^{3/2} \quad (1)$$

where  $r_{\text{tip}}$  is the tip radius,  $\nu$  the Poisson's ratio (0.5 for most biological samples) and  $E$  the Young's modulus. Tip radius values were evaluated using a reference pattern and show satisfactory matches with the values supplied by the manufacturer (2 nm).

### 2.6. Fluorescence experiments

#### 2.6.1. Red/blue intensity ratio (RBIR) measurements

MLV for the RBIR measurements at 1 mM with PA were prepared, as described above, by mixing the desired lipids and PA at a molar ratio of 250:1 (lipid:PA). Samples were sonicated in a bath sonicator FB-15049 (Fisher Scientific, Waltham, MA, USA) at a temperature above the transition temperature for 10 min and finally diluted to a 0.3 mM final lipid concentration. The fluorescence spectra of the PA probe were measured at different temperatures in a QuantaMaster 40 Spectrofluorometer (Photon Technology International, Lawrenceville, N.J., USA). Emission spectra were collected between 450 and 700 nm, exciting at 430 nm for PA using a 430 nm bandpass filter to minimize detection of dispersed light. A thermal TC125 controller (Quantum Northwest, Liberty Lake, WA, USA) was used to stabilize the sample temperature. Data analysis was performed in a similar way to that used by Niko et al. [14], using the ratiometric response of the dye, i.e., calculating the integral intensity ratio of red/blue regions of the emission band (573–613 nm/500–530 nm). In order to calculate the RBIR values, the areas of the blue (500–530 nm) and red (573–613 nm) regions of the emission spectra were subtracted with PTI Felix-GT software (Photon Technology International, Lawrenceville, N.J., USA). This methodology allows distinguishing between  $L_o$ ,  $L_\alpha$  and  $L_\beta$  phases [13].

#### 2.6.2. Förster resonance energy transfer (FRET) assays

Typically, FRET assays are performed on the extent of resonance energy transfer (RET) between two labelled lipids, in our case between NBD-PE and Rh-PE, as described in other publications [22]. In our experiments both probes are in the same engineered liposome and, under the fusion process with non-labelled liposomes of the HeLa-mimicking mixture, the fluorescent probes will be more diluted. Therefore, the RET signal, more precisely Rh-PE fluorescence, will not be detected while the NBD-PE signal will increase.

Liposomes for FRET assays were labelled adding 0.6% of each probe (NBD-PE and Rh-PE) to the desired liposome composition during liposome formation. Fluorescence measurements were performed in 1 mL of 10 mM Tris-HCl, 150 mM NaCl buffer, pH 7.4 containing 20  $\mu\text{M}$  of fluorescent labelled liposomes. The sample was left to stabilize for 30 min at 37  $^{\circ}\text{C}$  in a dark environment before the fusion experiments started. After that period, 20  $\mu\text{M}$  of unlabelled HeLa-mimicking liposomes were added to the cuvette and fluorescence of NBD at 547 nm was monitored as a function of time.

The percentage of fusion was calculated using the following equation,

$$\%Fusion = \left( \frac{F_t - F_0}{F_\infty} \right) \times 100 \quad (2)$$

where  $F_t$  is the NBD fluorescence intensity at each given time,  $F_0$  the initial NBD fluorescence intensity and  $F_\infty$  the fluorescence intensity at infinite dilution of the fluorescent probe in liposomes. It is commonly used the addition of detergents to obtain the  $F_\infty$  value, but NBD fluorescence is affected by the local environment of the dye. It is reported that NBD fluorescence in micelles presents less fluorescence than when NBD molecules are infinite diluted [23]. More precisely  $F_\infty = \alpha \cdot F_{\text{det}}$  where  $F_{\text{det}}$  is the fluorescence of NBD in micelles and  $\alpha$  is a ratio of the real fluorescence at infinite dilution to that with detergent. In our experiments,  $F_{\text{det}}$  was experimentally determined after the rupture of the sample by TritonX-100 at a final concentration of 1% (checked by quasi-elastic light spectroscopy), and  $\alpha$  value used was 1.79 at 37  $^{\circ}\text{C}$  [23]. Under our experimental conditions, and considering that aggregation number of TritonX-100 is between 150 and 200, after the solubilization of liposomes by the detergent we had less than 0.3 lipid molecules in each micelle, so FRET signal should be almost suppressed. All experimental data were corrected from inner filter and reabsorption effects.



Fusion data can be fitted to a modified Langmuir saturation curve to evaluate the physicochemical parameters of the process as:

$$\%Fusion = A_{max} \frac{kt^b}{1 + kt^b} \quad (3)$$

where  $A_{max}$  is the maximum value of fusion achieved,  $k$  the rate constant of the process and  $b$  a parameter related with the cooperativity of the process.

### 2.6.3. Measurement of viscosity using DPH and TMA-DPH fluorescence anisotropy

Liposome membrane fluidity can be investigated by using the decrease in fluorescence polarization of DPH or TMA-DPH. Briefly, as described elsewhere [24] liposomes were labelled using a lipid to probe molar ratio of 300. The desired DPH or TMA-DPH volume was added to a 500  $\mu$ M liposome solution and incubated, protected from light, for 30 min at a temperature above the transition temperature of the lipidic mixture. Afterwards, the degree of polarization of the sample was determined measuring the fluorescence intensity parallel and perpendicular with respect to the plane of linearly polarized excitation light at 381 nm.

To calculate the microviscosity of liposomes from polarization data we follow the method previously established by Shinitzky and Barenholz [25] and recently applied by Kure and Sakai [26]. A relationship between the microviscosity ( $\eta$ ) of the medium (the liposome membrane) and the anisotropy ( $r$ ) in the steady state of a fluorescent probe dissolved in that medium can be evaluated by using the Perrin equation,

$$\frac{r_0}{r} = 1 + C(r) \frac{T \cdot \tau}{\eta} \quad (4)$$

where  $T$  is the absolute temperature,  $\tau$  the excited-state lifetime of the fluorescent probe,  $r_0$  the limiting anisotropy and  $C(r)$  a parameter related to the molecular shape and the location of the transition dipoles of the rotating fluorophore at each  $r$  value. The term  $C(r) \cdot T \cdot \tau$  in Eq. 4 has been experimentally determined as 0.24 Pa·s while the  $r_0$  value for the DPH molecule is 0.362. Eq. 4 can be rearranged, as a first approximation thus,

$$\eta(\text{Pa}\cdot\text{s}) = \frac{0.24 \cdot r}{0.362 - r} \quad (5)$$

To further the analysis of the physicochemical properties of liposomes used in this study, we evaluate the dependence of the viscosity on temperature. The common solvents and linear hydrocarbon chain liquids follow an exponential decay of their viscosity as a function of temperature, as described by the empirical correlation,

$$\eta = \eta_0 e^{\frac{AE}{RT}} \quad (6)$$

where  $\eta_0$  is lowest viscosity value of the liquid,  $R$  the gas constant and  $\Delta E$  the activation energy that accounts for the minimum energy value required for the fluid to flow. In our case, where the liquid is confined in the form of a liposome membrane this energy could be considered as the minimum energy to diffuse or flow. This magnitude can be either understood as an estimation of the minimum energy required to trigger the first events occurring in fusion between different bilayers or extension of liposomes onto surfaces. Therefore, the higher this energy is the lower would be the probability of fusion between lipid membranes.

FRET assays, DPH and TMA-DPH anisotropy measurements were performed using an SLM-Aminco 8100 spectrofluorometer equipped with a jacketed cuvette holder. Temperature ( $\pm 0.2$  °C) was controlled using a circulating bath (Haake K20, Germany). The excitation and emission slit widths were 4 and 4 nm, and 8 and 8 nm, respectively.

### 2.6.4. Lifetime fluorescence decay

NBD-PE and Rh-PE fluorescence lifetime decay in liposomes were determined with a PTI EasyLife LED fluorescence lifetime instrument

(Horiba Ltd., UK) using 460 nm excitation pulses while monitoring the emission through a band pass filter of 530 nm. Samples of 1 mL at 20  $\mu$ M of lipid were analysed with an integration time of 0.3 s and with an average of 3 runs. Ludox® solution was used to correct the instrument response factor (IRF). All data were processed with the PTI software. Intensity decay curves,  $F(t)$ , were fitted to multiple exponential decays as:

$$F(t) = \sum_i \alpha_i \cdot e^{-t/\tau_i} \quad (7)$$

where  $\alpha_i$  is the preexponential factor (fraction contribution to the time-resolved decay) and  $\tau_i$  the corresponding lifetime value. Lifetime mean values can be calculated as [27]:

$$\langle \tau \rangle = \frac{\sum_i \alpha_i \tau_i^2}{\sum_i \alpha_i \tau_i} \quad (8)$$

## 3. Results

The characteristics of the liposomes are shown in Table 1. The liposomes mimicking the lipid composition of the HeLa bilayer used for the RBIR experiments were multilamellar vesicles (MLVs) and had an average size of  $\sim 506$  nm after sonication. The large unilamellar vesicles (LUVs) used in the other experiments were similar in diameter ( $\sim 120$  nm) after extrusion through the nominal cut-off filter. Polydispersity indices (PDIs) were lower for the LUVs than for the MLVs. On the other hand, the  $\zeta$ -potentials were quite different in sign. Thus, while HeLa liposomes had a negative charge due to the anionic lipid POPS, the POPC:DOTAP and POPC:CHOL:DOTAP liposomes presented positive values due to the presence of the cationic lipid DOTAP.

HeLa liposome model consisted of three different phospholipids and cholesterol, with the lipid phase of the mixture evaluated by the RBIR methodology. Fig. 1 shows the RBIR values at different temperatures. Linear regression was applied to several portions of the RBIR data. The best fits delimited three regions. After comparing the values obtained in Fig. 1 with those from the study of Sot et al. [13], we assigned the phases for each of the regions. The values of the first region (between 0 and 13 °C), ranging from 0.4 to 0.52, were close to the RBIR values of the membranes in the  $L_o$  phase ( $\approx 0.32$ ), which indicated that the membrane would be in the  $L_o$  phase within this region. The values of the last region (between 34 and 55 °C), ranging from 1 to 1.45, were close to those of mixtures in the  $L_\alpha$  phase containing cholesterol, such as POPC:CHOL (7:3, mol/mol) and 1,2-dioleoyl-*sn*-glycero-3-phosphocholine DOPC:CHOL (7:3, mol/mol). Thus, above 34 °C, the HeLa-mimicking lipid bilayer would be in the  $L_\alpha$  phase. Finally, in the region between 13 and 34 °C, the membrane would be in an intermediate state between those of the  $L_o$  and  $L_\alpha$  phases. This intermediate state would have intermediate properties between the  $L_o$  and  $L_\alpha$  phases whose proportions would depend on the specific temperature. That is, it would be closer to the  $L_o$  phase at lower temperatures and to the  $L_\alpha$  phase at higher temperatures.

We also evaluated the fluidity of the HeLa liposomes by measuring the anisotropic emission of fluorescence, using the DPH or TMA-DPH fluorescent probes. While DPH reports on fluidity at the bilayer core, TMA-DPH, with a net positive charge, reports on the changes near the phospholipid head groups. In these experiments, to compare how the

**Table 1**  
Size, PDI and  $\zeta$ -potential average values for the liposome formulations.

Liposome composition	Diameter (nm)	PDI	$\zeta$ (mV)
HeLa-mimicking LUVs	117.6 $\pm$ 1.1	0.122	-8.9 $\pm$ 1.1
POPC: DOTAP	120 $\pm$ 3	0.194	9.0 $\pm$ 1.1
POPC: CHOL: DOTAP	120.7 $\pm$ 0.5	0.168	10.1 $\pm$ 0.6
HeLa mimicking MLVs (for RBIR)	506 $\pm$ 50	0.29	-15.3 $\pm$ 0.7



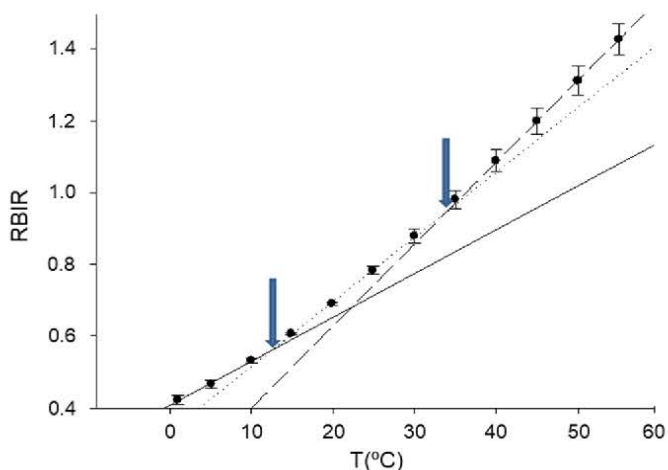


**Fig. 1.** Red/blue intensity ratio (RBIR) values as a function of temperature of HeLa-mimicking mixture. Linear regression analysis of three groups of experimental data (solid, points and dashed lines), with three delimited regions indicated by the two arrows.

fusion of two vesicle populations influences the microviscosity of the resulting vesicle, we engineered a system with the HeLa-mimicking mixture and the intended fusogenic liposomes at a ratio of 1:1. Fig. 2 shows microviscosity ( $\eta$ ), calculated using Eq. 5, as a function of temperature for the three types of liposomes studied. As expected, the  $\eta$  values decreased when the temperature increased for all the lipid compositions studied and for both fluorophores. The microviscosity values of the HeLa liposomes were higher than those of the other two compositions at all the temperatures studied in both regions, showing lower  $\eta$  values in the more hydrophobic region with DPH (Fig. 2A) than in the more hydrophilic region close to the phospholipid head-groups using TMA-DPH (Fig. 2B). When HeLa liposomes were fused with POPC:DOTAP liposomes (dashed lines in Fig. 2), the  $\eta$  values of the sample decreased, especially at lower temperatures. A similar effect was found when POPC:CHOL:DOTAP liposomes were tested for fusion (continuous lines in Fig. 2), although this decrease in the  $\eta$  values was lower than that for the POPC:DOTAP liposomes. Fitting the data from Fig. 2 to Eq. 6 enabled us to obtain  $\Delta E$  (Table 2). The analysis of the liposome core (DPH) revealed that CHOL in liposomes did not modify the  $\Delta E$  values, possibly due to its position in the lipid bilayer. On the contrary, the  $\Delta E$  values obtained with the TMA-DPH probe were of particular interest. While the fusion of the HeLa liposomes with POPC:DOTAP liposomes did not modify the  $\Delta E$  value, the  $\Delta E$  value decreased

**Table 2**

$\Delta E$  energy required for flow of DPH and TMA-DPH, and Young's modulus values for HeLa-mimicking liposomes, HeLa-mimicking liposomes with POPC:DOTAP liposomes and HeLa-mimicking liposomes with POPC:CHOL:DOTAP liposomes.

	HeLa-mimicking liposomes		
		+POPC: DOTAP	+POPC: CHOL: DOTAP
$\Delta E_{DPH}$ (kJ)	$30.8 \pm 0.9$	$34.0 \pm 0.7$	$34.1 \pm 0.5$
$\Delta E_{TMA-DPH}$ (kJ)	$23.9 \pm 0.7$	$23.6 \pm 0.9$	$22.3 \pm 0.7$
Young's modulus (MPa)	$29.6 \pm 0.8$	$26 \pm 5$	$63.3 \pm 0.8$
		$70.2 \pm 1.6$	

when incubated with POPC:CHOL:DOTAP liposomes.

Fig. 3 A shows the kinetics of the NBD-PE fluorescence signal in POPC:DOTAP or POPC:CHOL:DOTAP liposomes after the addition of the HeLa liposomes at a ratio of 1:1 ( $t = 0$ ). These results indicated that POPC:CHOL:DOTAP shows higher fluorescence values than POPC:DOTAP, most likely due to the higher dilution of the NBD-PE molecules in the resultant liposome after the fusion process occurred. After one hour of incubation, we used Eq. 2 to calculate the percentage of fusion (Fig. 3B). The fitting of data parameters to Eq. 3 are summarised in Table 3. These values indicated that POPC:CHOL:DOTAP liposomes experienced a more extended degree of fusion ( $A_{max}$ ), a higher rate of fusion ( $k$ ) and a large cooperativity value ( $b$ ) than the POPC:DOTAP liposomes when incubated with the HeLa liposomes.

Furthermore, we evaluated the changes in NBD-PE lifetime according to the lipid composition where it was embedded. Fluorescence lifetime data fitting to Eq. 7 is shown in Table S1 (Supplementary Information), while the experimental data are provided in Fig. 4. The average lifetime of NBD-PE was quite similar in the POPC:DOTAP and POPC:CHOL:DOTAP samples, but this decreased when incubated with the HeLa liposomes, notably in the case of POPC:CHOL:DOTAP liposomes.

Fig. 5 shows two AFM images (A and D) of the SLBs obtained by the deposition of HeLa liposomes onto the surface of mica with its corresponding line profiles along the white line (G and J). In both images one can observe that SLBs surfaces are featureless, showing an average height of  $4.6 \text{ nm} \pm 0.5 \text{ nm}$  with respect to the mica (darker areas) and with roughness values ( $Ra$ ) of  $0.45 \text{ nm}$  and  $0.32 \text{ nm}$ , respectively. Fig. 5B was acquired 14 min after the addition of POPC:DOTAP liposomes to the SLB shown in Fig. 5A while Fig. 5C was obtained 30 min after the addition. Both images with  $Ra$  values of  $0.42$  and  $0.32 \text{ nm}$ , respectively showed similar line profiles (5H and I) where the uncovered mica surface became smaller after the addition of liposomes, indicating

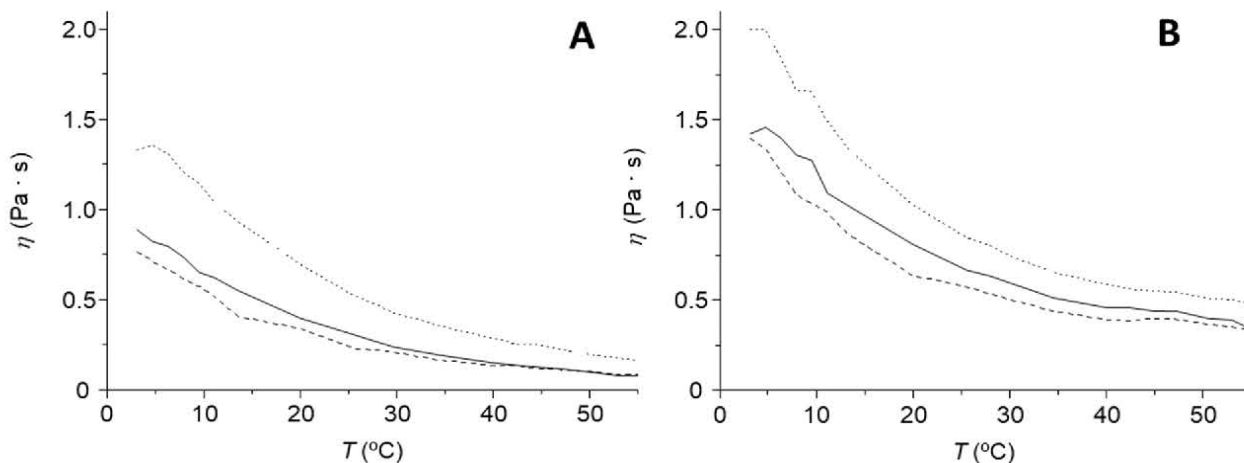


**Fig. 2.** Microviscosity values ( $\eta$ ) and temperature profiles for DPH (A) and TMA-DPH (B) for HeLa-mimicking liposomes before (dotted line) and after the addition of POPC:DOTAP liposomes (dashed line) and POPC:CHOL:DOTAP liposomes (solid line).

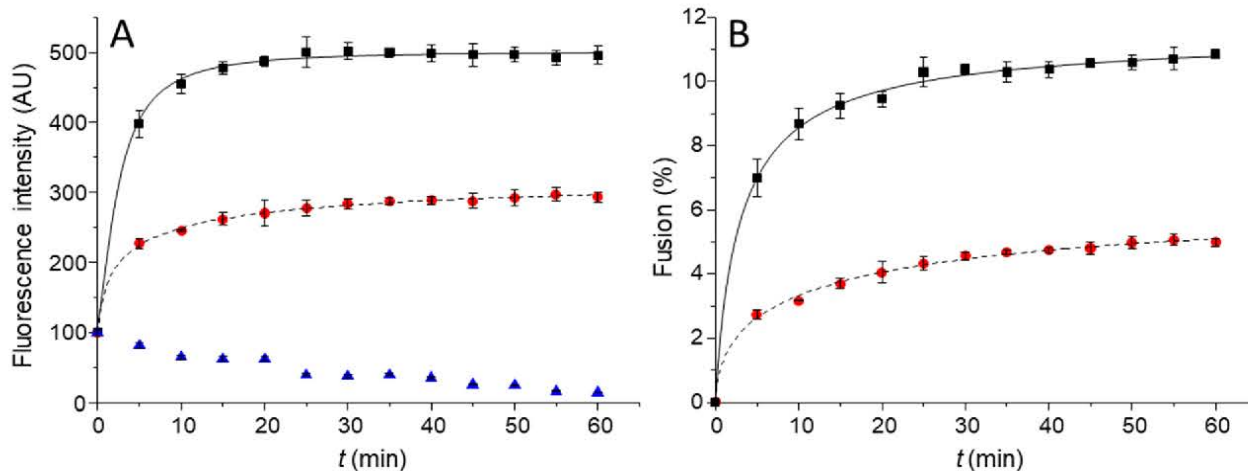


**Fig. 3.** NBD-PE fluorescence intensity A) and fusion percentage B) as a function of time for HeLa-mimicking liposomes incubated with POPC:DOTAP liposomes (dashed line, circles) and POPC:CHOL:DOTAP liposomes (solid line, squares). Triangles are liposomes without incubation with HeLa-mimicking liposomes (blank).

**Table 3**

Fitting parameters,  $A_{max}$ ,  $k$  and  $b$ , of the fusion ratio as a function of time using Eq. 3.

HeLa-mimicking liposomes	$A_{max}$	$k$ (min <sup>-b</sup> )	$b$	$r^2$
+				
POPC: DOTAP	$7.2 \pm 0.9$	$0.23 \pm 0.02$	$0.60 \pm 0.10$	0.996
POPC: CHOL: DOTAP	$11.4 \pm 0.3$	$0.36 \pm 0.06$	$0.90 \pm 0.12$	0.997

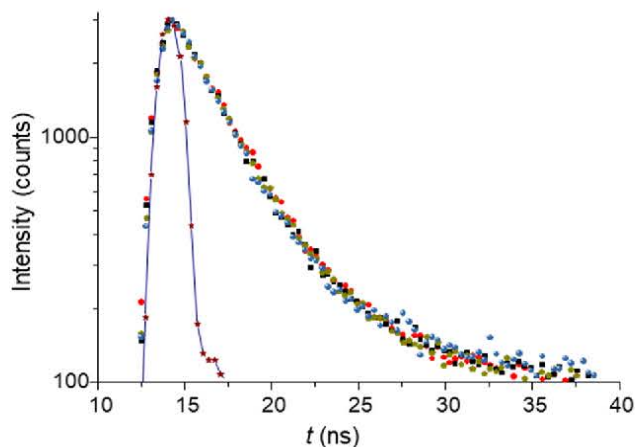


**Fig. 4.** Fluorescence decay of POPC:DOTAP (Red circles); POPC:CHOL:DOTAP (Black squares); POPC:DOTAP after the addition of HeLa-mimicking liposomes in a ratio of 1:1 ( $t = 60$  min) (Gold pentagons); POPC:CHOL:DOTAP after the addition of HeLa-mimicking liposomes in a ratio of 1:1 ( $t = 60$  min) (Blue spheres) and IRF (Ludox®) (Blue line with brown stars).

that POPC and DOTAP had been integrated into the SLBs. Similarly, 9 min after the addition of POPC:CHOL:DOTAP liposomes to the SLBs previously formed the HeLa-mimicking mixture (Fig. 5D), we observed that defects showing bare mica (three small areas) became significantly smaller (Fig. 5E with a  $R_a$  value of 0.40 nm), to the point that the SLBs covered almost the entire mica surface, as observed after 15 min (Fig. 5F with a  $R_a$  value of 0.51 nm).

The application of AFM-based force spectroscopy enabled us to calculate the Young's modulus of the SLBs. Fig. 6 shows the histogram-like distribution of the Young's modulus calculated according to Eq. 1 and representative force-curve plots can be found as Supplementary Information (Fig. S1). The adjustment of the distribution to a normal

distribution gave a maximum value of  $29.6 \pm 0.8$  MPa for the Young's modulus (Fig. 6A), corresponding to the HeLa-mimicking SLB. The most interesting effect is shown in Fig. 6B, corresponding to the SLB obtained after the addition of POPC:DOTAP liposomes, where two maxima are observed, one centered at  $26 \pm 5$  MPa and the other at  $70.2 \pm 1.6$  MPa. Similar to Fig. 6A, Fig. 6C shows the distribution of the Young's modulus of the SLB resulting from the addition of POPC:CHOL:DOTAP liposomes centered in this case at  $63.3 \pm 0.8$  MPa (Fig. 6C). For clarity, the average Young's modulus values for each system are listed in Table 2.

#### 4. Discussion

The aims of the present work were twofold: (i) to engineer simplified membranes mimicking the lipid composition of the plasma membrane of HeLa cells; and (ii) to assess how they respond to fusion when incubated with liposomes with a defined lipid composition. Such information can be of interest in future works delineated to select lipid liposome composition able to enhance drugs delivery into target cells. Natural membranes, i.e., HeLa cell membrane, present a negative charge due to the presence of phosphatidylglycerol, phosphatidic acid or phosphatidyl inositol groups. Hence, liposomes bearing a positive charge should be electrostatically attracted by the cells. Furthermore, CHOL has been used extensively to promote fusion between lipid vesicles. Thus, we evaluated the fusion of the HeLa-mimicking mixture with liposomes bearing a positive charge, i.e., containing DOTAP lipids, with or without CHOL. In this paper and to this extent, it is worth recalling the value of the zeta potentials of the liposomes investigated. With these effective charges in the bilayers, the primary event occurring in the interaction between the HeLa-mimicking model and the liposomes should be governed by electrostatic forces. Such a mechanism has already been suggested by previous biophysical experiments and also in *in vitro* experiments using liposomes applied to solid tumours [28]. Remarkably, it has been elsewhere reported that the electrostatic surface event might be the primary step in transfection [29] and viral infection [30]. Moreover, DOTAP appears to cause some structural destabilisation of the bilayer that would precede the fusion process [31].

To evaluate how the HeLa-mimicking bilayer simulated the actual cell lipid bilayer, we analyzed its physicochemical properties by using a planar model (SLBs). In fact, when two vesicles of different sizes come into contact, i.e., eventually HeLa cell and liposomes, the first event would be the adsorption of the smaller system (higher lipid curvature) onto the larger one (low lipid curvature). Therefore, the properties of our flat HeLa SLBs are of interest, especially when a liposome adsorption onto the cell membrane surface or undergoes endocytosis by the cell.

A flat/planar model of the HeLa lipid membrane for AFM



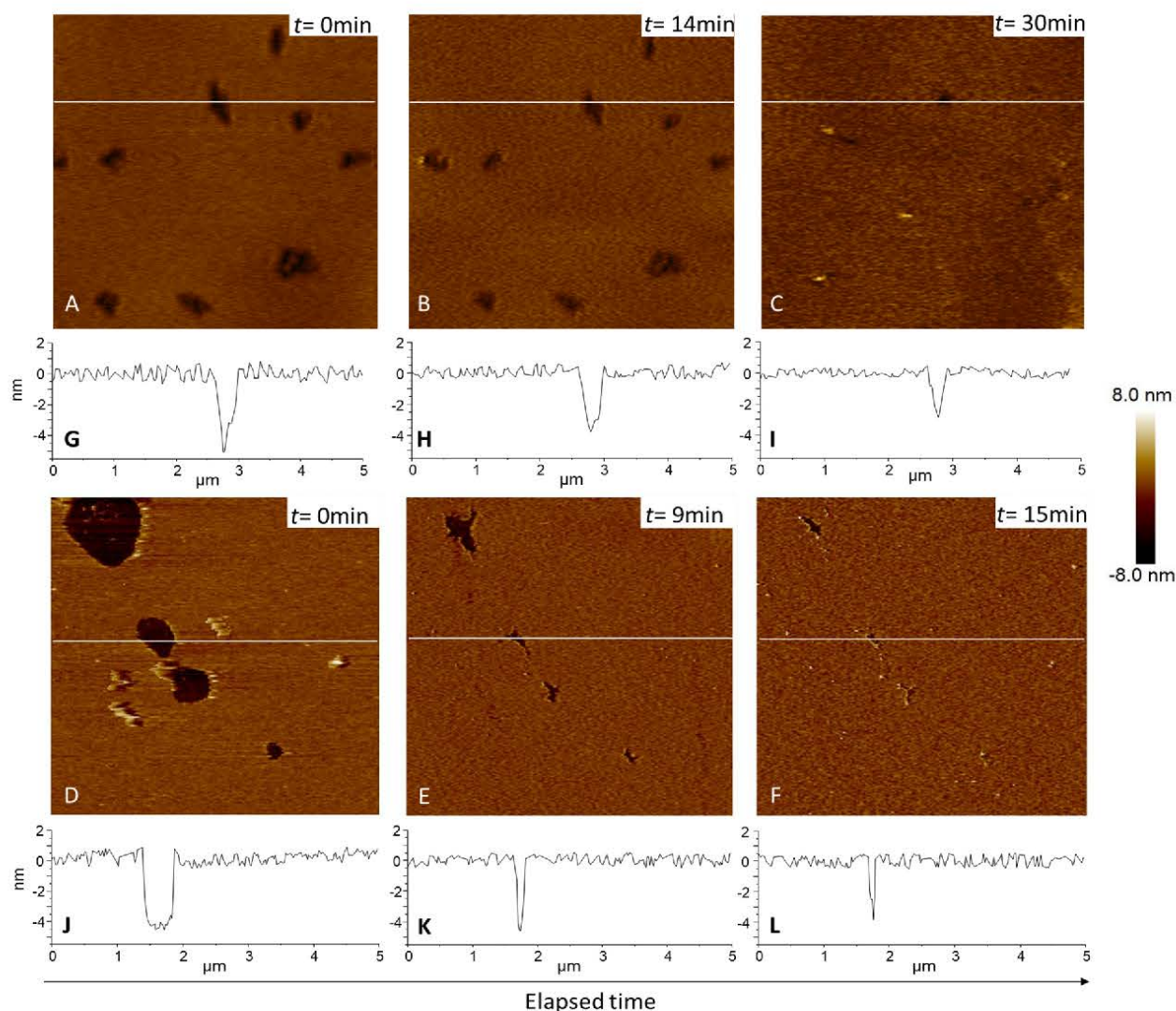


**Fig. 5.** AFM topographic images of supported lipid bilayers of the HeLa-mimicking mixture before (A, D) and after the addition of POPC:DOTAP liposomes (B and C) and POPC:CHOL:DOTAP liposomes (E and F). Images G-L show the line profiles along the white line in the corresponding upper AFM image.

observations can be obtained by depositing a Langmuir-Blodgett monolayer or by forming a SLBs through the deposition of liposomes onto a mica surface [32]. In a previous study, we observed lipid domains in a HeLa-mimicking monolayer model that seemed to be corroborated the findings of previous Laurdan polarisation and Brewster angle microscopy (BAM) experiments where lipid domains were also observed [12]. Interestingly, in the present work, no laterally segregated domains were observed in the SLBs, suggesting a rearrangement of the lipid components when the liposomes spontaneously adsorbed onto the mica surface. To get a deeper insight into the state of the HeLa-mimicking model we investigated the thermotropic nature of the HeLa liposomes, taking advantage of the PA fluorescent probe [14]. Thus, according to the RBIR values, the liposomes mimicking the HeLa cell lipid membrane, presented an intermediate state between the  $L_o$  and  $L_\alpha$  phases across the full range of temperatures studied [33]. Fluid states are believed to be preponderant in natural membranes [34], but lateral phase separation, or domains with distinct compositions may exist [35]. However, these domains were not observed by the AFM imaging of the SLBs. Although the RBIR results indicated that the  $L_o$  and  $L_\alpha$  domains might coexist, we have already reported for POPE and POPE:POPG SLBs that the domains observed in monolayers can disappear when bilayers are formed [36]. If we assume, according to previous BAM observations, that the size of these domains is  $\sim 10 \mu\text{m}$  at  $30 \text{ mN m}^{-1}$  (which is the estimated surface

pressure of a bilayer), they fall beyond the scale of the SLB images acquired by AFM in this study. The relationship between coexistence of micro- and nanodomains has been discussed elsewhere [37]. Otherwise, the featureless nature of the HeLa-mimicking SLBs can probably be attributed to the high amount of CHOL (33%) they contain. This observation compares well with other SLB models containing a high proportion of this sterol [38,39].

When POPC:DOTAP liposomes were added to the HeLa SLBs, we observed that they became integrated. Topographic AFM images taken at specific times points did not provide evidence of either vesicular entities adsorbed onto the SLB or reminiscent morphologies of the liposomes. Therefore, the apparent process should probably be attributed to the fusion of the liposomes with preformed SLBs. A similar phenomenon occurred with POPC:CHOL:DOTAP liposomes. Interestingly, when comparing the AFM images acquired for both systems at a similar time point, the results confirmed that the presence of CHOL enhanced the fusion rate. This is in agreement with the results obtained using other techniques investigating the role of CHOL in the fusion process with SLBs of different compositions [40]. The role of CHOL in enhancing membrane fusion has been extensively investigated, but its contribution to the regulation of the process, at least in the presence of other lipids and proteins, remains unknown [41]. We have previously reported that the presence of CHOL increased the fusion of liposomes with monolayers



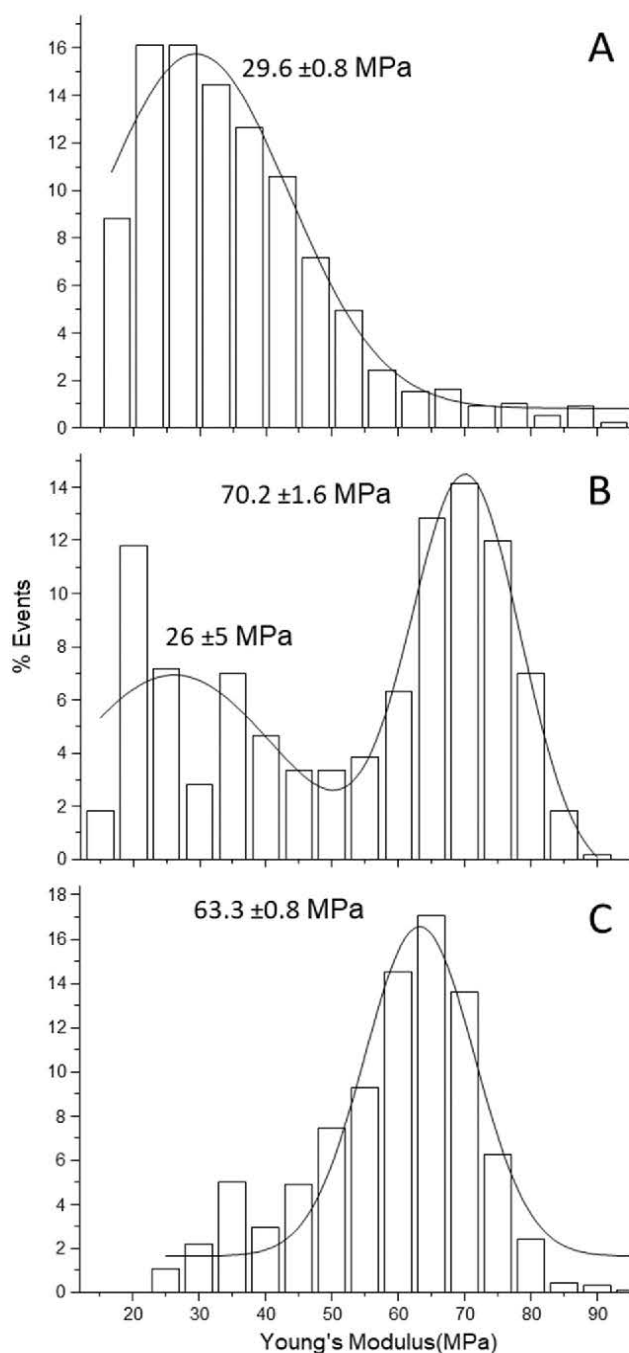


**Fig. 6.** Young's modulus ( $E$ ) histograms of HeLa-mimicking bilayer before (A) and after the addition of POPC:DOTAP liposomes (B) and POPC:CHOL:DOTAP liposomes (C). Representational curves are plotted assuming the  $E$  distribution fits normal distributions centered in the inset values.

presenting the same composition of that HeLa liposomes used in this work, which agrees with the present AFM observations with liposomes and SLBs.

Analysis of the Young's modulus ( $E$ ) provided further information on the compactness of the SLBs observed with AFM. While high values of  $E$  correspond to gel or ordered states, low values are typical for fluid or disordered states. For instance, in a well-defined binary phase separated system of 1,2-dioleoyl-*sn*-glycero-3-phosphocholine (DOPC) and 1,2-dipalmitoyl-*sn*-glycero-3-phosphocholine (DPPC), 19.3 MPa and 28.1 MPa have been assigned to the fluid and gel phases, respectively [21]. Even higher values for the same system have been reported when

using different AFM probes [42]. From these reference  $E$  values, our HeLa-mimicking SLB presented an average  $E$  value of  $\sim 30$  MPa. Therefore, we tentatively propose that the coexistence of the  $L_o$  and  $L_\alpha$  domains, as predicted by the RBIR measurements, could be displaced towards the  $L_o$  phase. However, it is worth noting that for multicomponent SLBs, higher values of up to 80 MPa have been reported for fluid disordered phases [43]. In any case, the increase in the  $E$  values after incubation with POPC:DOTAP or POPC:CHOL:DOTAP liposomes demonstrates that the flat/planar HeLa-mimicking model is useful for monitoring the fusion of liposomes (high lipid curvature) with a cell membrane (low lipid curvature).

Remarkably, the fusion of liposomes with the HeLa-mimicking flat/planar lipid model membrane resulted in substantial changes in the values and distribution of the Young's modulus. Thus, by fitting the Gaussian model to the experimental results, the unimodal distribution for the HeLa-mimicking SLB becomes bimodal when liposomes of POPC:DOTAP were fused, but unimodal and shifting to higher values when POPC:CHOL:DOTAP liposomes were added. Since both types of liposomes contain the same proportion of DOTAP, the positive charge borne by this phospholipid provoked the same repulsion against the AFM tip. Hence, the AFM tip perceived greater repulsion when approaching the lipid and consequently more force was required to deform the surface. The bimodal behaviour observed when adding POPC:DOTAP liposomes could be due to the fact that these components are difficult to integrate or dilute into the SLBs. Therefore, the result would be one region enriched in POPC:DOTAP (which we did not observe in the topographic images by AFM) and with a high Young's modulus value because of the repulsion exerted by DOTAP [44] and another region retaining the elastic properties of the SLB mimicking the HeLa cell lipid membrane. Alternatively, the second peak observed could be due to the DOTAP and the CHOL present in the SLBs interacting in a specific way. In any event, with the addition of the POPC:CHOL:DOTAP liposomes, the unimodal distribution shifted towards values slightly lower than that of the second peak observed in the absence of CHOL. These observations are consistent with the reported increase in the bending modulus of liposomes upon the addition of CHOL to different lipid compositions [45] and with seminal works on the nanomechanical properties of SLBs using AFM-based force spectroscopy [46]. As discussed elsewhere, the presence of CHOL in the membrane results in a higher degree of compactness or less elastic deformation of the bilayer [43].

The HeLa-mimicking lipid bilayer model interacted differently with liposomes containing CHOL and those that did not. The results presented in this work, such as the shift towards shorter lifetimes of the NBD-PE fluorescent probe, support the fusion between the bilayers of both types of the liposome formulations studied and the bilayer of the liposomes formed by the HeLa-mimicking composition. As expected, these findings confirmed previous results observed with the monolayer-liposome system, which showed that fusion becomes more extensive in the presence of CHOL [12]. Notice, however, that although the topographic observations made with AFM could call into question the temporal resolution of the technique, the FRET results confirmed that the fusion process was faster in the presence of CHOL, as depicted by the kinetic constant values (Table 3), being  $\sim 40\%$  higher in the presence of the sterol. Although the fusion percentage did not reach high values (11.4% and 7.2% for the POPC:CHOL:DOTAP and POPC:DOTAP liposomes, respectively), it is worth mentioning here that the maximum fusion values were calculated by considering that all the liposomes bearing the fluorescent dyes were infinitely diluted, i.e., disrupting liposomes with detergents. Instead, by considering that all the liposomes bearing fluorescent probes fused with all the liposomes of the HeLa-mimicking mixture, the maximum percentage of fusion was calculated to be 42.1% and 18.1% for the POPC:CHOL:DOTAP and POPC:DOTAP liposomes, respectively. (Fig. S2 and Table S2 in the Supplementary Information).

HeLa liposomes showed more viscosity before than after fusion with the different liposomes studied. The decrease in viscosity was greater



after fusion with the POPC:DOTAP liposomes than after fusion with the POPC:CHOL:DOTAP liposomes. Since both liposomes contain the same molar proportion of DOTAP (20%), the structural destabilisation caused by the positive phospholipid [47] results in lower values of microviscosity. However, the presence of CHOL in the liposomes increases viscosity by causing an ordering effect in the membrane [48]. The changes in viscosity of the HeLa-mimicking liposomes during fusion with liposomes demonstrate that the composition of the bilayer changes due to the fusion and consequent insertion of the molecules from the engineered liposomes. Furthermore, the  $\Delta E$  values extracted from the microviscosity measurements could be interpreted, in a comparative manner, as an indicator of the ease with which liposomes extend onto a surface. However, no major differences were observed when using either DPH or TMA-DPH, indicating that both types of liposomes require a similar amount of energy to promote the fusion mechanisms.

## 5. Conclusions

The HeLa bilayer lipid model formed by four phospholipids (POPC:POPE:POPS:CHOL) is able to form liposomes and SLBs after deposition onto mica. Because of the high proportion of CHOL, HeLa liposomes present an equilibrium between  $L_o$  and  $L_\alpha$  phases, according to RBIR measurements. AFM observations have shown flat and featureless SLBs with no evidence of lateral segregation in either phase. POPC:DOTAP and POPC:CHOL:DOTAP liposomes are able to integrate into the preformed HeLa SLBs, suggesting the existence of a fusion process as the SLBs expand covering the empty areas of the substrate. From AFM force spectroscopy assays, it is observed that the stiffness of the membrane varies because of the integration in the SLBs of the lipids supplied by the liposomes. We also observed by means of fluorescence lifetime experiments, that the mean decay lifetime is also affected in the resultant liposome. We have positively confirmed the fusion mechanism by incubating HeLa liposomes with POPC:DOTAP or POPC:CHOL:DOTAP liposomes using FRET assays. While the presence of CHOL increases the Young's modulus of the resultant SLBs, FRET experiments confirm that CHOL enhances the fusion mechanism. The changes in microviscosity confirm the integration of the lipids from the liposomes within the HeLa-mimicking lipid model. It is important to emphasise here that stiffness and viscosity values obtained from Young's modulus (AFM) and from fluorescence (DPH and TMA-DPH probes) are not contradictory but complementary. While from the Young's modulus data we obtain information on the compactness between phospholipids, the amount of force applied in the Z axis needed to separate them, and the increase of the Young's modulus value demonstrates the changes in the composition of the resultant SLBs. Finally, viscosity data obtained from anisotropy of TMA-DPH probe provide information on the mobility of the lipids in the XY plane suggesting that the presence of CHOL decreases the activation energy.

By assessing two simplified HeLa-mimicking lipid model membranes in the fusion process with two types of liposomes bearing CHOL and/or a positive charge we have undertaken a new research project aiming to use these lipid compositions to evaluate how the lipid composition of the HeLa plasma membrane could be the responsible of the delivery and internalization of encapsulated substances into the intracellular liquid medium. We are presently undertaking a project that is directed to bring light, from a biophysical point of view, on how genes and/or proteins can be delivered into living HeLa cell membranes. One of the strategies contemplates the use of fusion peptides integrated into the liposome bilayer with the goal of facilitating liposome-cell recognition.

Outcoming results outcoming from this new project will be present in a following paper.

## CRedit authorship contribution statement

A. Botet-Carreras: Investigation, Formal analysis, Writing – original draft; M.T. Montero: Conceptualization, Visualization, Writing –

reviewing & editing; J. Sot: Investigation, Formal analysis, Writing – reviewing & editing; Ò. Domènech: Formal analysis, Supervision, Writing – reviewing & editing; J.H. Borrell: Conceptualization, Supervision, Writing – reviewing & editing.

## Declaration of Competing Interest

The authors declare the following financial interests/personal relationships which may be considered as potential competing interests: Jordi H. Borrell reports equipment, drugs, or supplies was provided by Spanish Ministry of Economy and Competitiveness (PID2019-110210GB-I00) and the Catalan Government (Generalitat de Catalunya) (214SGR 1442). Oscar Domenech reports equipment, drugs, or supplies was provided by Spanish Ministry of Economy and Competitiveness (PID2019-110210GB-I00) and the Catalan Government (Generalitat de Catalunya) (214SGR 1442). M. Teresa Montero reports equipment, drugs, or supplies was provided by Spanish Ministry of Economy and Competitiveness (PID2019-110210GB-I00) and the Catalan Government (Generalitat de Catalunya) (214SGR 1442). Jesus Sot reports equipment, drugs, or supplies was provided by Basque Government (IT1264-19 and IT1270-19).

## Acknowledgements

This study was supported by the Spanish Ministry of Economy and Competitiveness (PID2019-110210GB-I00), the Catalan Government (*Generalitat de Catalunya*) (214SGR 1442), the Basque Government (grants No. IT1264-19 and IT1270-19), the Fundación Biofísica Bizkaia and the Basque Excellence Research Centre (BERC). We thank Andrey Klymchenko (Laboratoire de Bioimagerie et Pathologies, UMR 7021 CNRS, Faculté de Pharmacie, Université de Strasbourg, 67401 Illkirch, France) for the generous gift of PA. Special thanks to Dr Felix M. Goñi and Dr Manuel Prieto for their comments and suggestions. The authors want to thank Dr Pawel Wydro for hosting A. B-C. in his lab during a short stay and Dr Christopher Evans for English language revision.

## Appendix A. Supporting information

Supplementary data associated with this article can be found in the online version at [doi:10.1016/j.colsurfa.2021.127663](https://doi.org/10.1016/j.colsurfa.2021.127663).

## References

- [1] Q. Guo, C. Jiang, Delivery strategies for macromolecular drugs in cancer therapy, *Acta Pharm. Sin.* B 10 (2020) 979–986.
- [2] N. Azad, Y. Rojanasakul, Macromolecular drug delivery, *Biopharm. Drug Des. Dev., Humana Press, Totowa, NJ*, 2008, pp. 293–323.
- [3] R. Zhang, X. Qin, F. Kong, P. Chen, G. Pan, Improving cellular uptake of therapeutic entities through interaction with components of cell membrane, *Drug Deliv.* 26 (2019) 328–342.
- [4] M. Riaz, M. Riaz, X. Zhang, C. Lin, K. Wong, X. Chen, G. Zhang, A. Lu, Z. Yang, Surface functionalization and targeting strategies of liposomes in solid tumor therapy: a review, *Int. J. Mol. Sci.* 19 (2018) 195.
- [5] J.E. Rothman, The principle of membrane fusion in the cell (Nobel Lecture), in: *Angew. Chemie Int. Ed.*, 53, 2014, pp. 12676–12694.
- [6] C. Hamai, T. Yang, S. Kataoka, P.S. Cremer, S.M. Musser, Effect of average phospholipid curvature on supported bilayer formation on glass by vesicle fusion, *Biophys. J.* 90 (2006) 1241–1248.
- [7] R. Kolašinac, S. Jaksch, G. Dreissen, A. Braeutigam, R. Merkle, A. Csizsár, Influence of environmental conditions on the fusion of cationic liposomes with living mammalian cells, *Nanomaterials* 9 (2019) 1025.
- [8] R. Rahbari, T. Sheahan, V. Modes, P. Collier, C. Macfarlane, R.M. Badge, A novel LI retrotransposon marker for HeLa cell line identification, *Biotechniques* 46 (2009) 277–284.
- [9] W. Barcellini, P. Bianchi, E. Fermo, F.G. Imperiali, A.P. Marcello, C. Vercellati, A. Zaninoni, A. Zanella, Hereditary red cell membrane defects: diagnostic and clinical aspects, *Blood Transfus.* 9 (2011) 274–277.
- [10] WHO Human Genetics Programme, The molecular genetic epidemiology of cystic fibrosis: report of a joint meeting of WHO/IECF/N/ICF(PM)A/ECFS, *World Heal. Organ.* (2004) 1–24.
- [11] C.A. Hubner, Ion channel diseases, *Hum. Mol. Genet.* 11 (2002) 2435–2445.

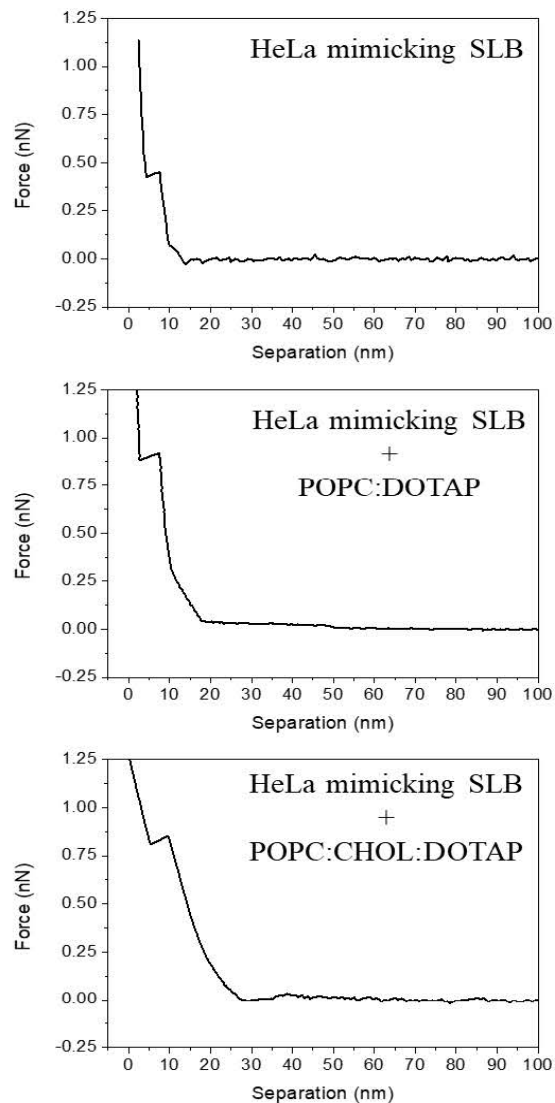


- [12] A. Botet-Carreras, M.T. Montero, J. Sot, Ò. Domènech, J.H. Borrell, Characterization of monolayers and liposomes that mimic lipid composition of HeLa cells, *Colloids Surf. B* 196 (2020), 111288.
- [13] J. Sot, I. Esnal, B.G. Monasterio, R. León-Irra, Y. Niko, F.M. Goñi, A. Klymchenko, A. Alonso, Phase-selective staining of model and cell membranes, lipid droplets and lipoproteins with fluorescent solvatochromic pyrene probes, *BBA-Biomembr.* 2021 (1863), 183470.
- [14] Y. Niko, S. Kawachi, G. Konishi, Solvatochromic pyrene analogues of prodan exhibiting extremely high fluorescence quantum yields in apolar and polar solvents, *Chem. -Eur. J.* 19 (2013) 9760–9765.
- [15] X. Li, Y.-J. Yuan, Lipidomic analysis of apoptotic HeLa cells induced by paclitaxel, *Omi. A J. Integr. Biol.* 15 (2011) 655–664.
- [16] M.L. Torgersen, T.I. Klokke, S. Kavaliauskiene, C. Klose, K. Simons, T. Skotland, K. Sandvig, The anti-tumor drug 2-hydroxyoleic acid (Minerval) stimulates signaling and retrograde transport, *Oncotarget* 7 (2016) 86871–86888.
- [17] M.J. Gerl, V. Bittl, S. Kirchner, T. Sachsenheimer, H.L. Brunner, C. Lichtenborg, C. Özbalci, H. Wiedemann, S. Wegehinged, W. Nickel, P. Haberkant, C. Schultz, M. Krüger, B. Brügger, Sphingosine-1-phosphate lyase deficient cells as a tool to study protein lipid interactions, *PLoS One* 11 (2016), e0153009.
- [18] M. Lorizate, T. Sachsenheimer, B. Glass, A. Habermann, M.J. Gerl, H.-G. Kräusslich, B. Brügger, Comparative lipidomics analysis of HIV-1 particles and their producer cell membrane in different cell lines, *Cell. Microbiol.* 15 (2013) 292–304.
- [19] C. Suárez-Germà, M.T. Montero, J. Ignés-Mullol, J. Hernández-Borrell, Ò. Domènech, Acyl chain differences in phosphatidylethanolamine determine domain formation and LacY distribution in biomimetic model membranes, *J. Phys. Chem. B* 115 (2011) 12778–12784.
- [20] J.J. Roa, G. Oncins, J. Diaz, F. Sanz, M. Segarra, Calculation of Young's modulus value by means of AFM, *Recent Pat. Nanotechnol.* 5 (2011) 27–36.
- [21] L. Picas, F. Rico, S. Scheuring, Direct measurement of the mechanical properties of lipid phases in supported bilayers, *Biophys. J.* 102 (2012) L01–L03.
- [22] D.K. Struck, D. Hoekstra, R.E. Pagano, Use of resonance energy transfer to monitor membrane fusion, *Biochemistry* 20 (1981) 4093–4099.
- [23] C. François-Martin, F. Pincet, Actual fusion efficiency in the lipid mixing assay - comparison between nanodisks and liposomes, *Sci. Rep.* 7 (2017) 43860.
- [24] S. Merino-Montero, M.T. Montero, J. Hernández-Borrell, Effects of lactose permease of *Escherichia coli* on the anisotropy and electrostatic surface potential of liposomes, *Biophys. Chem.* 119 (2006) 101–105.
- [25] M. Shinitzky, Y. Barenholz, Fluidity parameters of lipid regions determined by fluorescence polarization, *BBA-Biomembr.* 515 (1978) 367–394.
- [26] T. Kure, H. Sakai, Transmembrane difference in colloid osmotic pressure affects the lipid membrane fluidity of liposomes encapsulating a concentrated protein solution, *Langmuir* 33 (2017) 1533–1540.
- [27] J.R. Lakowicz, Measurement of fluorescence lifetimes, in: *Princ. Fluoresc. Spectrosc.*, Springer US, Boston, MA, 1983, pp. 51–93.
- [28] S. Krasnici, A. Werner, M.E. Eichhorn, M. Schmitt-Sody, S.A. Pahernik, B. Sauer, B. Schulze, M. Teifed, U. Michaelis, K. Naujoks, M. Dellian, Effect of the surface charge of liposomes on their uptake by angiogenic tumor vessels, *Int. J. Cancer* 105 (2003) 561–567.
- [29] D. Simberg, S. Weisman, Y. Talmon, Y. Barenholz, DOTAP (and other cationic lipids): chemistry, biophysics, and transfection, *Crit. Rev. Ther. Drug* 21 (2004) 257–317.
- [30] S.C. Harrison, Viral membrane fusion, *Virology* 479–480 (2015) 498–507.
- [31] R. Guo, Y. Liu, K. Li, B. Tian, W. Li, S. Niu, W. Hong, Direct interactions between cationic liposomes and bacterial cells ameliorate the systemic treatment of invasive multidrug-resistant *Staphylococcus aureus* infections, *Nanomed. Nanotechnol.* 34 (2021), 102382.
- [32] L. Picas, P.-E. Milhiet, J. Hernández-Borrell, Atomic force microscopy: a versatile tool to probe the physical and chemical properties of supported membranes at the nanoscale, *Chem. Phys. Lipids* 165 (2012) 845–860.
- [33] G. van Meer, D.R. Vodker, G.W. Feigenson, Membrane lipids: where they are and how they behave, *Nat. Rev. Mol. Cell Biol.* 9 (2008) 112–124.
- [34] M.D. Houslay, K.K. Stanley, *Dynamics of Biological Membranes*, John & Wiley Sons, Chichester, 1983.
- [35] T. Baumgart, S.T. Hess, W.W. Webb, Imaging coexisting fluid domains in biomembrane models coupling curvature and line tension, *Nature* 425 (2003) 821–824.
- [36] L. Picas, C. Suárez-Germà, M. Teresa Montero, J. Hernández-Borrell, Force spectroscopy study of Langmuir–Blodgett asymmetric bilayers of phosphatidylethanolamine and phosphatidylglycerol, *J. Phys. Chem. B* 114 (2010) 3543–3549.
- [37] Ò. Domènech, J. Ignés-Mullol, M.T. Montero, J. Hernández-Borrell, Unveiling a complex phase transition in monolayers of a phospholipid from the annular region of transmembrane proteins, *J. Phys. Chem. B* 111 (2007) 10946–10951.
- [38] L. Redondo-Morata, M.I. Giannotti, F. Sanz, Influence of cholesterol on the phase transition of lipid bilayers: a temperature-controlled force spectroscopy study, *Langmuir* 28 (2012) 12851–12860.
- [39] Z. Al-Rekabi, S. Contera, Multifrequency AFM reveals lipid membrane mechanical properties and the effect of cholesterol in modulating viscoelasticity, *Proc. Natl. Acad. Sci.* 115 (2018) 2658–2663.
- [40] D.E. Lee, M.G. Lew, D.J. Woodbury, Vesicle fusion to planar membranes is enhanced by cholesterol and low temperature, *Chem. Phys. Lipids* 166 (2013) 45–54.
- [41] S.-T. Yang, A.J.B. Kreutzberger, J. Lee, V. Kiessling, L.K. Tamm, The role of cholesterol in membrane fusion, *Chem. Phys. Lipids* 199 (2016) 136–143.
- [42] O. Saavedra V, T.F.D. Fernandes, P.-E. Milhiet, L. Costa, Compression, rupture, and puncture of model membranes at the molecular scale, *Langmuir* 36 (2020) 5709–5716.
- [43] R.M. a Sullan, J.K. Li, S. Zou, Direct correlation of structures and nanomechanical properties of multicomponent lipid bilayers, *Langmuir* 25 (2009) 7471–7477.
- [44] M. N'Diaye, J.-P. Michel, V. Rosilio, Relevance of charges and polymer mechanical stiffness in the mechanism and kinetics of formation of liponanoparticles probed by the supported bilayer model approach, *Phys. Chem. Chem. Phys.* 21 (2019) 4306–4319.
- [45] Y. Takechi-Haraya, K. Sakai-Kato, Y. Abe, T. Kawanishi, H. Okuda, Y. Goda, Atomic force microscopic analysis of the effect of lipid composition on liposome membrane rigidity, *Langmuir* 32 (2016) 6074–6082.
- [46] S. Garcia-Manyes, L. Redondo-Morata, G. Oncins, F. Sanz, Nanomechanics of lipid bilayers: heads or tails? *J. Am. Chem. Soc.* 132 (2010) 12874–12886.
- [47] N. Benne, R.J.T. Lebourg, M. Glandrup, J. van Duijn, F. Lozano Vigario, M. A. Neustrup, S. Romeijn, F. Galli, J. Kuiper, W. Jiskoot, B. Slütter, Atomic force microscopy measurements of anionic liposomes reveal the effect of liposomal rigidity on antigen-specific regulatory T cell responses, *J. Control. Release* 318 (2020) 246–255.
- [48] T. Róg, M. Pasenkiewicz-Gierula, I. Vattulainen, M. Karttunen, Ordering effects of cholesterol and its analogues, *BBA-Biomembr.* 2009 (1788) 97–121.

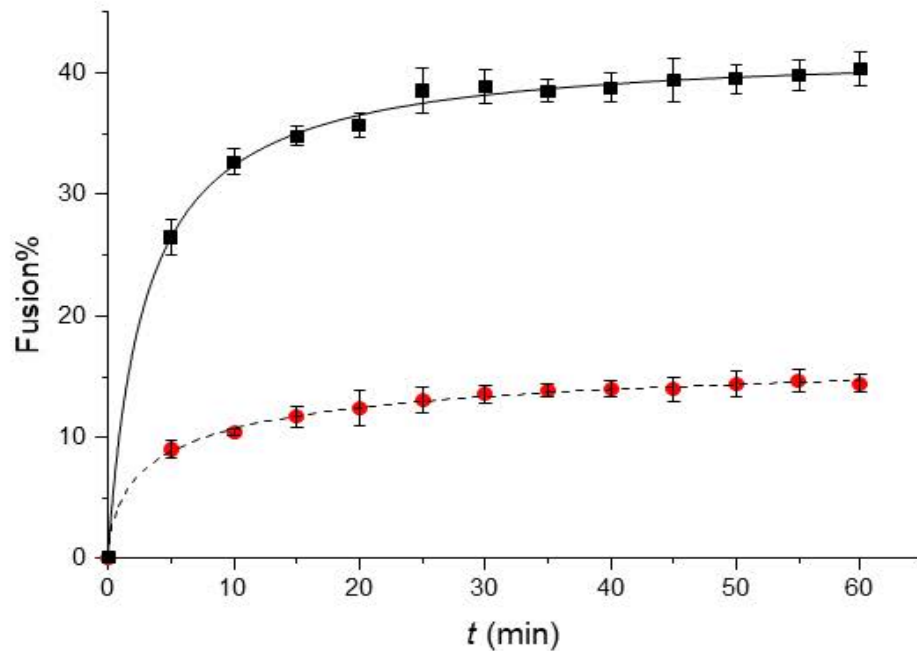
## Supplementary material

### Engineering and development of model lipid membranes mimicking the HeLa cell membranes

*Adrià Botet-Carreras, M. Teresa Montero, Jesús Sot, Òscar Domènech and Jordi H. Borrell*



**Supplementary Figure S1.** AFM representative force-separation curves used to determine Young's modulus. All fittings were performed before the SLB break-through point.



**Supplementary Figure S2.** Fusion percentage as a function of time for the HeLa-mimicking liposomes incubated with POPC:DOTAP liposomes (squares, dashed line) and POPC:CHOL:DOTAP liposomes (circles, solid line). Maximum dilution was evaluated preparing liposomes of the resultant composition after the fusion of HeLa-mimicking liposomes with POPC:DOTAP or POPC:CHOL:DOTAP considering that i) incubation time is too short for a significant number of liposomes to undergo more than one round of fusion and ii) the ratio between liposomes of the HeLa-mimicking composition and the ones bearing the fluorescent dyes is 1:1.

**Supplementary Table S1.** Parameters  $\alpha_i$  and  $\tau_i$ , describing fluorescence intensity decays, Eq. 7 and Eq. 8 in the manuscript text, of NBD-PE in different liposome compositions at 37 °C.

Sample	$\alpha_1$	$\tau_1$ (ns)	$\alpha_2$	$\tau_2$ (ns)	$\langle\tau\rangle$ (ns)	$\chi^2$
POPC:DOTAP	0.89	3.03	0.11	1.57	2.94	0.24
POPC:CHOL:DOTAP	0.66	3.31	0.34	2.24	3.03	0.28
HeLa + POPC:DOTAP	0.54	3.31	0.46	2.13	2.89	0.20
HeLa + POPC:CHOL:DOTAP	0.29	3.42	0.71	1.95	2.56	0.20

**Supplementary Table S2.** Fitting parameters,  $A_{\max}$ ,  $k$  and  $b$ , from data in Supplementary Figure S1 (fusion ratio as a function of time) using Eq. 3 in section 2.6.2 *Förster resonance energy transfer (FRET) assays* in the manuscript text.

HeLa-mimicking liposomes +	$A$	$k$ (min <sup>-b</sup> )	$b$	$r^2$
POPC: DOTAP	$18.1 \pm 1.3$	$0.36 \pm 0.02$	$0.60 \pm 0.09$	0.997
POPC: CHOL: DOTAP	$42.1 \pm 0.3$	$0.35 \pm 0.06$	$0.90 \pm 0.10$	0.998





## Chapter 7. Results: The cell

On the uptake of cationic liposomes by HeLa cells: from changes in elasticity to internalization

**A. Botet-Carreras**, M. Bosch Marimón, R. Millan-Solsonad, E. Aubets, C. J. Ciudad, V. Noé, M. T. Montero, Ò. Domènech, and J.H. Borrell

*Nanomedicine: Nanotechnology, Biology and Medicine. Submitted*

### Techniques introduced

#### Flow cytometry

A flow cytometer is used to study single cells or particles in solution as they flow past one or more lasers while suspended in buffer. Each particle or cell is analyzed for visible light scattering and/or multiple fluorescent probes. The technique to analyze visible light scattering is quite similar to the DLS technique. Samples can be evaluated in the forward direction, which can indicate the relative size of the cell. Moreover, at 90°, side scattering analysis is used to obtain information on the internal complexity or granularity of the cell.

This technique allows us to study tens of thousands of cells in a quick way. Ideally, the flow diameter of the capillary tube through which the sample flows is small enough for the cells to pass one by one in front of the laser beam so that they can be analyzed individually.

Fluorescence analysis is relevant for analyzing cells labeled with a fluorescent dye. In this study, it was used to determine if the engineered liposomes labeled with Rh-PE had integrated into HeLa cells. This technique does not allow us to determine where this fluorophore is located, which is instead measured by other techniques.

## Confocal microscopy

Confocal microscopy is an optical imaging technique that uses a spatial pinhole to obtain better optical resolution and contrast compared to conventional widefield optical microscopy. The key point of confocal microscopy is the use of spatial filtering to eliminate out-of-focus light or glare in specimens whose thickness exceeds the immediate plane of focus. Capturing multiple images at different depths in a sample allows the associated software to build a three-dimensional image known as optical sectioning (Figure 19).

The first confocal microscopes were slow in providing a full image since the scanning process took a long time. These instruments evolved into the confocal laser scanning microscope (CLSM), which uses a laser that is diffracted into a three-dimensional pattern so that it shines on different planes. In addition, these microscopes incorporate a series of fluorescence barrier filters so that different fluorescent probes can be visualized in the same sample.

Usually, for biological observations involving living cells, CLSM are inverted and use an immersion lens.

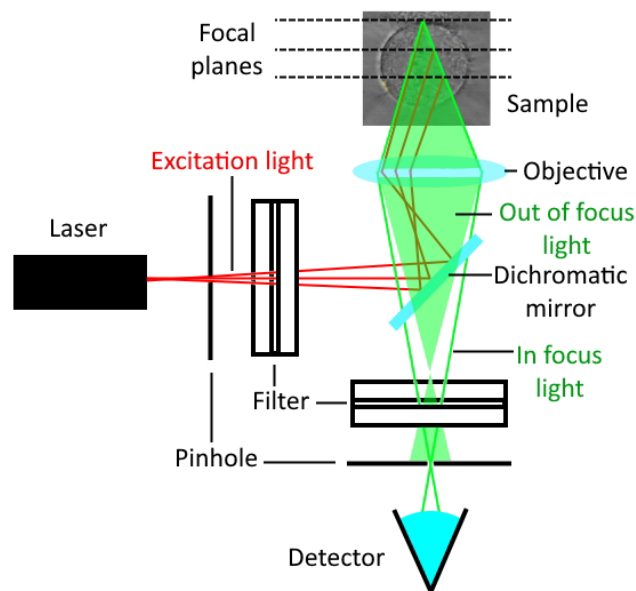


Figure 19. Basic configuration of a confocal laser scanning microscope (CLSM). A laser is focused through an excitation pinhole, then reflected into the sample by a dichromic mirror. Out-of-focus light emitted from the sample is rejected by the pinhole, generating an optical section.

## Viability assays

Viability assays are required to assess cell proliferation, cytotoxicity and cell mortality. These assays consist of adding a concentration of the substance under study to a culture of a specific cell line, HeLa cells in our case. After incubating the cells with the substance, we can visually assess the effect of the substance or quantitatively evaluate the survival rate of the cells by counting the number of remaining living cells in a culture compared to a blank.

3-[4,5-dimethylthiazol-2-yl]-2,5-diphenyltetrazolium bromide (MTT) is used in many studies to assess cell death. When added to a cell culture containing living cells, mitochondrial dehydrogenases of the viable cells cleave the tetrazolium ring of the MTT, changing the yellowish MTT into purple formazan crystals that are insoluble in aqueous solution. The addition of MTT to a cell culture allows the evaluation of the number of living cells in a colorimetric way by measuring absorbance at 570 nm. The absorbance values can be compared with, for example, those of a negative control where no active agents have been added to the cell culture and therefore have the highest possible absorbance values.

## Phospholipid quantification with the Marshall dye

Quantifying the number of phospholipids in a formulation after liposome production and encapsulation (probably also including a last filtering step to separate the unloaded drugs from the encapsulated ones) is essential to understand and quantify the lipidic loss occurring during the process of production.

The technique to quantify this is based on the hydrophobic nature of the phospholipids and involves a dye [151]. The liposomes are first dissolved in chloroform. This disassembles the liposomes, causing the phospholipids to dissolve in the liquid organic phase. The Marshall dye, which contains ferric chloride and thiocyanate and has a dark red color, is then added. This mixture is water based. Therefore, when added to the chloroform in the tube, the two

liquids separate into two phases. The key point of this dye-based technique is that ferric thiocyanate binds to the phospholipids even if it is water-soluble. For proper binding, the two phases need to be vigorously shaken. After the agitation process, the two phases separate. The chloroform phase is then recovered to measure the amount of stained phospholipids using a conventional spectrophotometer and a calibration curve built under the same experimental conditions.

This technique can be used irrespectively of the amount of drug or other substances encapsulated in the liposomes, providing a lipid/drug ratio that is helpful in understanding the yield of the encapsulation process.

## Summary

Earlier, we showed positive fusion results with the HeLa-mimicking monolayers and bilayers (liposomes and SLBs, respectively). Here, we extended the experiments to living HeLa cells to evaluate if the engineered liposomes can effectively fuse with HeLa cells.

We previously observed that the POPC:CHOL:DOTAP liposomes showed higher fusion rates. Therefore, we selected these liposomes to investigate the efficacy of fusion with living HeLa cells.

To evaluate if the engineered liposomes were effectively able to reach the cells, we added Rh-PE to the engineered liposomes and followed their fluorescence signals. After incubating them at different concentrations for 24 h with HeLa cells, we evaluated the fluorescence signal using a flow cytometer. This revealed that the liposomes were indeed associated with the cells. Thus, the fluorescence intensity increased when the liposome concentration increased too, showing a concentration-dependent behavior. As more liposomes were added to the cell culture, there were more possibilities for fusion events.

To get a deeper insight into the membrane topography or mechanics after the addition of the POPC:CHOL:DOTAP liposomes, we examined the HeLa cells with AFM.

There were no substantial changes in the topographic images of the HeLa cells before or 40 minutes after the addition of the engineered liposomes, but we could observe some changes in the adhesion and deformation channels.

Interestingly, in the adhesion images, we observed that the difference in the adhesion force values between the substrate and HeLa cells was high before the addition of the liposomes and clearly distinguishable in the images. After incubation with the liposomes, this difference between the two regions was almost equalized. This was probably due to the homogeneous deposition of the liposomes across the surfaces on the cells and substrate alike. To quantify the effect of the incorporation of liposomes into the sample, we evaluated the adhesion force distributions from the images before and after the incorporation of the



POPC:CHOL:DOTAP liposomes. While the histograms of  $F_{adh}$  before the incubation with liposomes showed a bimodal distribution (one peak for the values of the HeLa cell and the other for the substrate), those after the incubation showed only one peak.

From the slope images, we could see differences related to changes in the membrane after incubation with the liposomes. We also observed rigidification of the cells (higher slope values) after the incubation, which can be understood as an increase in the stiffness of the sample.

To get a deeper insight into the possible rigidification of the sample after the incorporation of liposomes, we obtained elasticity maps of the center of a cell to calculate Young's modulus before and after the incubation with the engineered liposomes. We obtained force maps from the center of the cell in order to avoid the edges where the substrate could have interfered with the results.

The histogram of Young's modulus values showed a clear shift in the mean peak value to higher  $E$  values after incubation with the engineered liposomes. This was similar to the findings obtained previously [152] (Chapter 6), where incubating the same engineered liposomes with HeLa-mimicking SLBs resulted in a peak shift to higher  $E$  values.

To see what was happening exactly with the liposomes when they were incorporated into a cell, we performed several incubation assays under a confocal microscope.

To distinguish between the cell membrane and the liposomes, we had to label them all. Cell membranes were dyed with the CellMask™ Deep Red plasma membrane stain, while the liposomes were tagged with Rh-PE. In addition, to see if the liposomes could work effectively as drug carriers, we encapsulated calcein at a self-quenching concentration. This means that calcein fluorescence at high concentrations is shifted towards longer emission wavelengths (red light), but when calcein concentration is diluted, the self-quenching effect disappears, emitting fluorescence at shorter wavelengths (bright green). Therefore, this was used to unveil if the engineered liposomes were able to release an encapsulated drug into the cells or, oppositely, if they were unable to release their content and were acting as a hermetic box.

After adding the engineered liposomes to the media containing HeLa cells, we observed that the liposomes quickly reached the cells, probably due to the electrostatic interactions between the positively-charged liposomes and the negatively-charged HeLa cell membrane.

Besides the primary electrostatic interaction, the filopodia of the HeLa cells were also involved, capturing the liposomes that were close by or still in the medium. This was probably also helped by the charge differences between the liposomes (positive) and the filopodia (negative), like for the rest of the HeLa cell membrane. The activity of the filopodia was really intense, producing different movements that have been reported before [153] and can be described as: (i) *surfing*, when a liposome slides down a filopodium to the plasma membrane; (ii) *contractile actions*, where a filopodium captures one liposome on its tip and then bends and actively pulls the liposome towards the cell surface; and (iii) *laterally moving*, when a filopodium catches one liposome from the medium, swings it from side to side to finally bring it to the cell body.

After 40 min, most of the liposomes were adsorbed onto the surface of the HeLa cells and a few had already been internalized inside the cell and had started to release their calcein content, showing bright green fluorescence around them. After 24 h, most of the liposomes had been internalized, with some located in the cell membrane. The liposomes inside the HeLa cells had released their calcein load, even leaving a trace of calcein behind as they moved inside the cell.

All these observations confirmed that the engineered liposomes acted as effective drug carriers. For extra proof of concept, we encapsulated the cytotoxic drug methotrexate (MTX) inside the engineered liposomes. We filtered them to eliminate the non-encapsulated MTX from the media and incubated the liposomes with HeLa cells at different MTX concentrations. The results from 24 h to 72 h were clear. The cells incubated with the MTX-loaded liposomes were almost completely killed, while the negative control or the cells incubated with the unloaded liposomes thrived and duplicated with no problem. Incubation with the unloaded liposomes was of special interest since it demonstrated that the liposomes by themselves were not toxic to the cells.

Finally, to determine the amount of encapsulated MTX and using the Marshall dye to quantify the number of phospholipids in our formulation, we obtained an MTX-to-lipid ratio of 0.20.

## Highlights

- Engineered POPC:CHOL:DOTAP liposomes interacted with HeLa cells immediately after they were added to the media.
- Cytometry assays showed a concentration-dependent effect.
- Changes in the HeLa cell membrane were observed with AFM after incubation with the engineered liposomes.
- The interaction of liposomes with the HeLa cell membrane increased its rigidity.
- Filopodia clearly played an important role, capturing liposomes and bringing them to the cell body. They increased the number of liposomes that reached the cell in addition to normal liposome deposition.
- During the first 40 min, the engineered POPC:CHOL:DOTAP liposomes adsorbed onto the cell membranes and started to internalize. At 24 h, most of the liposomes had been internalized and had liberated their content.
- The engineered POPC:CHOL:DOTAP liposomes were able to encapsulate and deliver drugs. Therefore, they could be used as drug carriers.

## **On the uptake of cationic liposomes by HeLa cells: from changes in elasticity to internalization**

Adrià Botet-Carreras<sup>a,b</sup>, Manel Bosch Marimón<sup>c</sup>, Ruben Millan-Solsona<sup>d,e</sup>, Eva Aubets<sup>f</sup>, Carlos J. Ciudad<sup>f,b</sup>, Véronique Noé<sup>f,b</sup>, M. Teresa Montero<sup>a,b</sup>, Òscar Domènech<sup>a,b\*</sup> and Jordi H. Borrell<sup>a</sup>

<sup>a</sup>Secció de Físicoquímica, Facultat de Farmàcia i Ciències de l'Alimentació,

<sup>b</sup>Institute of Nanoscience and Nanotechnology (IN<sup>2</sup>UB).

<sup>c</sup>Departament de Bioquímica i Biomedicina Molecular, Facultat de Biologia.

<sup>d</sup>Nanoscale Bioelectrical Characterization, Institute for Bioengineering of Catalonia (IBEC),  
The Barcelona Institute of Science and Technology (BIST).

<sup>e</sup>Departament d'Enginyeria Electrònica i Biomèdica, Facultat de Física.

<sup>f</sup>Departament de Bioquímica i Fisiologia, Facultat de Farmàcia i Ciències de l'Alimentació.

Universitat de Barcelona (UB). 08028-Barcelona, Catalonia, Spain.

### **Abstract**

In this work, we evaluated the capabilities of an engineered liposomal formulation, studied in previous works and tested in HeLa model membranes, to fuse and work as nanocarriers in cells using live HeLa cells as a model. This study focuses on the physicochemical changes suffered on the surface of the cells as seen by Atomic Force Microscopy (AFM), and how the liposomes enter inside the cells and liberate their load by means of Confocal Microscopy (CM). As well as viability assays with real drugs (MTX) as a prove of concept of the capabilities of the formulation to work as delivery-systems. All results support the capabilities of the proposed engineered liposomal formulation to work as nanocarriers.

### **Introduction**

Since the first observation back to 60's of the last century, liposomes have been considered either as model membranes or drug delivery systems [1]. Regarding the last, several

engineered formulations based on liposomes have emerged in the market as successful anticancer agents [2]. Additionally, to the phospholipids as basic matrix, most of the available liposomes formulations include polyethylene glycol (PEG-glycated liposomes). PEG was earlier recognized as a fusogenic agent [3] that also extend blood circulation and enhancing target efficiency and activity as well [4,5]. This is a crucial point because liposomes activity on cancer and other therapeutical uses may be efficient when applied to cell cultures but may fail dramatically many times when administrated to animal models. Even immunoliposomes can be specific against cells in culture but unsuccessful for specific targeting when injected into the blood stream [6-8]. Although all drawbacks encountered through the years several liposomes formulations have reached the market [9]. Presently, decorated liposomes and surface engineered liposomes emerged as one promising strategy in drug delivery systems [10].

Apart of the formulation strategies, one of the still unsolved problems is how row lipid-based liposomes interact with cell membranes and which of the basic mechanisms such, adsorption, fusion, endocytosis, or may be a combination of them, become involved in liposomes internalization by the cells. Liposome-cell membrane cell interactions can be extremely different depending on the cell membrane nature (lipid composition and structure), and liposome lipid composition. All these aspects have been elderly reviewed [11]. In principle, liposomes, internalization may be promoted by including specific lipids that enhance the recognition with the bilayer membrane of the cell targeted. In this regard it is known that cholesterol (CHOL) and cationic liposomes containing positively charged lipids enhance fusion with the cell membrane promoting subsequent internalization [12]. Liposome-cell interactions are dependent on each membrane cell composition, structure, and dynamics. Concisness, a variety of biophysical methods have been applied along the years to investigate the fusion mechanism or/and effectiveness of drug delivery by using membrane models with specific lipid composition [13].

In precedent papers we have investigate the fusion mechanism of liposomes with a simplified model of the HeLa membrane mimicking the cell lipid membrane [14]. We have shown that liposomes formed with 1-palmitoyl-2-oleoyl-phosphatidylcholine (POPC), 1,2-



dioleoyl-3-trimethylammonium-propane (DOTAP) and CHOL (0.80:0.20, mol/mol), at a molar ratio POPC:CHOL:DOTAP (0.65:0.15:0.20, mol/mol/mol) liposomes, both, fuse with lipid monolayers and liposomes mimicking the HeLa cell lipid membrane. In that paper, we hypothesize on a possible mechanism, which would involve adsorption and insertion of the phospholipids within the lipid model HeLa monolayer. Actually, we confirmed the fusion mechanism by using Förster resonance energy transfer (FRET) tools by incubating double labeled (NBD-PE and Rh-PE pair) of the liposomes [15] and following the increase of NBD fluorescence once incubated with HeLa liposomes model. One of the interesting findings arise from atomic force spectroscopy (AFM) in force mode (FS) that show that there were variations of the viscosity of HeLa supported lipid bilayers when incubated with liposomes. These studies suggested the involvement of adhesion forces in the whole fusion process [16]. This physicochemical magnitude emerges was involved not only in the membrane-membrane fusion but also in the uptake mechanism of liposomes into cells. However, the membrane of living HeLa cells is much more complex than the model earlier investigated. For this reason, in this paper we take a step forward to get a better insight on the mechanism of interaction of the engineered liposomes that positively fuse with the lipid HeLa model, with HeLa living cells. To this end we have investigated by means of AFM, and confocal microscopy (CM) how the incubation of POPC:DOTAP:CHOL liposomes with HeLa cells affect the nanomechanics of the membrane and the eventual internalization of liposomes. Since flow cytometry does not discriminate between adsorption, fusion or association of liposomes on the cells, we have further investigated the incorporation of liposomes into HeLa cytoplasm by means of CM. To that end we engineered liposomes marked with Rh-PE encapsulating calcein at self-quenching concentration and, after incubation with HeLa cells, observe the release of calcein into the cytoplasm of the HeLa cell. Finally, we have investigated how nanomechanical properties may be correlated with the pharmacological action of engineered liposomes loaded with methotrexate (MTX).

## Materials

1-palmitoyl-2-oleoyl-*sn*-glycero-3-phosphatidylcholine (POPC), 1,2-dioleoyl-3-trimethylammonium-propane (chloride salt) (DOTAP) and cholesterol (CHOL) were purchased from Avanti Polar Lipids (Alabaster, AL, USA). 1,2-dioleoyl-*sn*-glycero-3-phosphoethanolamine-N-(lissamine rhodamine B sulfonyl) (Rh-PE) and Cell Mask Deep Red Plasma membrane stain were purchased from ThermoFisher Scientific. Calcein was purchased to Sigma-Aldrich, Madrid, Spain.

## Methods

### Preparation of cationic liposomes

Liposomes were prepared as described elsewhere [17]. Briefly Chloroform:methanol (2:1, v/v) solutions containing the appropriate amount of lipids of POPC:CHOL:DOTAP (0.65:0.15:0.20, mol/mol/mol) were placed in a glass balloon flask and dried in a rotary evaporator at room temperature, protected from light. The resulting thin film was kept under high vacuum overnight to remove any traces of organic solvent. Multilamellar liposomes (MLVs) were obtained by redispersion of the thin film in 10 mM Tris·HCl, 150 mM NaCl buffer, pH 7.4. Large unilamellar vesicles (LUVs) were obtained by extrusion through polycarbonate membranes with a pore size of 100 nm, using an Avanti<sup>®</sup> Mini-extruder (Avanti Polar Lipids Inc., Alabaster, AL, USA). The mean particle size and polydispersity values of the liposomes were measured by dynamic light scattering with a Zetasizer Nano S (Malvern Instruments, UK). To assess the effective surface electrical charge, electrophoretic mobility was determined with a Zetasizer Nano ZS90 (Malvern Instruments, UK). Each sample was measured at least three times.

To mark the liposomes with Rh-PE, 0,6% mol of Rh-PE was added at the initial Chloroform:methanol solution of lipids.

To encapsulate calcein for CM experiments a procedure earlier described was used to get the molecule self-quenched into the aqueous space of the liposomes [18]. To this end MLVs, were formed in buffer containing 103 mM of calcein, which after the extrusion process and the formation of LUVa we eluted through a Sephadex G-50 column to separate the free calcein from the encapsulated one. The critical point of this process was to keep always the same osmolarity in the intra- and extra- liposomal solutions (240 mOsm/kg).

### **Force volume microscopy AFM and force curves analysis**

Force Volume Microscopy is based in acquiring deflection curves at all points of sample. Later, the post-processing and quantification of the acquired curves enables obtaining topographic, slope, adherence images and Young's module maps. Experiments were performed with a Nanowizard 4 Bio-Atomic Force Microscope, integrated with an inverted optical microscope (Zeiss). The Zeiss microscope was used to visually position the AFM cantilever with respect to the sample. The nanoindentation AFM probes used in this work had 4  $\mu\text{m}$  diameter and nominal  $k = 0.2 \text{ N/m}$  (Nanotools). Before each experiment, the cantilever spring constant was calibrated using the thermal noise method and the photodetector optical sensitivity was determined using a clean Petri dish area as an infinitely rigid substrate. The rate of a single approach-retract cycle was set to 13 Hz and with a resolution of 128 x 128 pixels. Under these conditions, the mapping of one area took 20 min. During the experiments, the force applied to the samples was kept as low as possible to minimize sample damage. A force threshold was chosen to ensure sample penetration of 0.5–1 micron for all experiments (force threshold = 5 nN). Force curves in each map were fitted according to the Hertz model using the routine implemented in the JPK Data processing to obtain elastic modulus maps. Used parameters ( $k_{\text{thermal}}=0.109 \text{ N/m}$ ,  $E_{\text{tip}} = \infty \text{ Pa}$ ,  $\nu= 0.5$ ).

### Young's modulus determination

We have calculated the Young's modulus as described elsewhere [19]. The values of this parameter informs on the cohesive force between the lipids forming the lipid bilayer providing means to unveil changes on a cell membrane [20,21]. In order to study cellular process by AFM, the Young's modulus are usually determined as a first approximation by using the Hertz model [22]. This model considers that: (i) the surface of the sample is a homogeneous and linear elastic solid, (ii) the indenter is not deformable, and (iii) the interaction between sample and indenter occurs through elastic forces only. If we consider the indenter as a parabolic tip, the Young's modulus can be calculated from force-indentation curve data by using

$$F = \frac{4\sqrt{r_{tip}}}{3} \cdot \frac{E}{1-\nu^2} \cdot \delta^{3/2} \quad (1)$$

where  $F$  is the force from the force curve,  $r_{tip}$  is the radius of the spherical punch,  $\delta$  the indentation,  $\nu$  the Poisson's ratio (0.5 for most biological samples) and  $E$  the Young's modulus.

### Cell culture

HeLa cells were maintained in high glucose DMEM (Dulbecco's Modified Eagle Medium) supplemented with 10% FCS (Fetal Calf Serum) and incubated at 37 °C in a humidified 5% CO<sub>2</sub> atmosphere. Subculture was performed using 0.05% Trypsin (Merck, Madrid, Spain).

In the experiments involving the incubation with Methotrexate (MTX, Pfizer, Madrid, Spain), cells were incubated in RPMI medium lacking the final products of DHFR activity, hypoxanthine and thymidine (-HT), and supplemented with 7% v/v dialyzed fetal bovine serum (Life Technologies, Madrid, Spain).

### **Flow cytometry**

HeLa cells (50,000) were plated in 6-well dishes the day before adding liposomes marked with Rh-PE. After 24 h of incubation with liposomes (5, 10 or 20  $\mu$ M), cells were trypsinized and collected, centrifuged at 800 x g at 4 °C for 5 min and washed once in PBS. The pellet was resuspended in 500  $\mu$ L of PBS and Propidium Iodide was added to a final concentration of 5  $\mu$ g/mL (Merck, Madrid, Spain). Flow cytometry analyses were performed in a FACSAria Fusion System cell sorter (Becton Dickinson, Spain).

### **Fluorescence staining**

For confocal microscopy observation cells were seeded on glass-bottom dishes. The incubation of cells with liposomes (40  $\mu$ M) for the initial observation of membrane-liposomes interaction was done directly under the microscope in low glucose DMEM without phenol red with Hepes (10 mM). Incubation with liposomes (20  $\mu$ M) for 24h and 48h was done inside a CO<sub>2</sub> incubator in supplemented DMEM.

Cell membranes were stained using Cell Mask Deep Red Plasma membrane stain. Cells were incubated for 5 min at 37 °C with Cell Mask (3  $\mu$ g/ml) diluted in supplemented DMEM. Then cells were washed with prewarmed DPBS (Dulbecco's Phosphate Buffered Saline, pH 7.0–7.3) and kept in low glucose DMEM without phenol red with Hepes (10 mM) for fluorescence imaging.

### **Confocal microscopy and image analyses**

Confocal microscopy images were acquired using a Zeiss LSM 880 confocal microscope equipped with a Heating Insert P S (Pecon) and a 5% CO<sub>2</sub> providing system. Cells were observed at 37°C using a 63X 1.4 NA oil immersion objective. Images were acquired with a pixel size of 0.09x0.09x0.37  $\mu$ m (xyz). Calcein, Rhodamine and Cell Mask Deep Red stains were excited with the 488 nm, 561 nm and 633 nm laser lines, respectively.



CM images were analyzed using the Fiji software [23]. Intensity analysis plots were generated with the Multichannel Plot Profile analysis tool of the BAR plugin [24].

### **Cell assay viability**

Cells (10,000) were plated in 6-well dishes in RPMI medium. Fifteen hours later, liposomes loaded with MTX were added to the culture media. Five days after treatment, 0.63 mM of 3-(4,5-dimethylthiazol-2-yl)-2,5-dipheniltetrazolium bromide and 100  $\mu$ M sodium succinate (both from Sigma-Aldrich, Madrid, Spain) were added to the culture medium and incubated for 2,5h at 37 °C. After incubation, culture medium was removed and the lysis solution (0.57% of acetic acid and 10% of sodium dodecyl sulfate in dimethyl sulfoxide) (Sigma-Aldrich, Madrid, Spain) was added. Absorbance was measured at 570 nm in a Modulus Microplate spectrophotometer (Turner BioSystems). The results were expressed as the percentage of cell survival relative to the controls.

In addition, cell images for each condition were taken using a ZOE Fluorescent Cell Imager (Bio-Rad Laboratories, Inc, Spain) before the MTT assays.

### **Results**

We have evaluated the primary interaction between liposomes and HeLa cells by flow cytometry. Figure 1 shows the results when HeLa cells are incubated for 24h with different concentration of liposomes containing a fluorescent label. From Figure 1A it has been possible to verify that liposomes are on or into the cells. Noticeable also seen Figure 1B shows that fluorescence intensity increases when liposomes concentration increases.

AFM has evolved as a technique from visualizing samples at high resolution to modes that allow to obtain physicochemical properties, such as Young's modulus, adhesion forces or deformation at the nanoscopic level. In the present work AFM has been used to analyse

adhesion forces and Young's modulus of HeLa cells, before and after the addition of liposomes, to investigate if these liposomes become adsorbed, integrated or embedded into the cell membrane. With this purpose, a spherical punch particle (2  $\mu\text{m}$ ) was attached to the sharp tip of the cantilever (Figure S1A) to minimize the puncturing of the lipid membrane of the cell and maximizing the surface interaction in the *sphere-plane geometry* (Figure S1B). Topographic, adhesion and slope images of a HeLa cells are shown in Figure 2: before (images A, B and C) and 40 min after the addition of the engineered liposomes (images D, E and F). HeLa cells deposited onto the surface substrate (Figure 2A) were elliptical structures with main diameters values ranging from 38 to 45  $\mu\text{m}$  and with average height values of 4-5  $\mu\text{m}$ . The adhesion force values between the tip and the HeLa surface (Figure 2B) were smaller (darker) than the adhesion with the substrate (Figure 2E). Interestingly, after the incorporation of the engineered liposomes to the sample the adhesion force difference between the cell and the substrate was almost reduced. The adhesion force distribution histograms from Figures 2B and 2E (Figure S2A) showed a bimodal distribution of the sample before the incorporation of the engineered liposomes with a peak centered at 2.91 nN corresponding to the HeLa cell surface and a second peak centered at 4.33 nN. After the incorporation of the engineered liposomes the distribution became unimodal with a mean adhesion force value of 3.12 nN indicating that the second peak could not be detected because the liposomes have been most likely adsorbed onto the modified surface of the substrate. The mean value of the adhesion force after the incorporation of the engineered liposomes was a slightly higher than the peak attributed to the HeLa cell before its incorporation. This supports that the liposomes indeed reached the surface of HeLa cells.

From the slope images C and F in Figure 2 we can get information about the rigidity of the regions observed. Thus, the higher (brighter) the slope value is, greater will be the stiffness of the sample (Figure S1C). We can appreciate image C in figure 2 that the substrate region was much more rigid than the HeLa cell surface, and that after the incorporation of the

liposomes image F in Figure 2 no significant changes were observed neither in the HeLa surface nor in the substrate.

To get deeper insight in the interaction between the liposomes and the HeLa cells the Young's modulus was determined before and 40 min after the addition of the engineered liposomes. Figures 3A and 3B show the elasticity maps of the central region of the HeLa cell observed in Figure 2A and 2D respectively. Higher values (brighter regions) are observed after the incorporation of the liposomes. In Figure 3C histograms of individual Young's modulus values from Figures 3A and 3B are shown. Fitting the Gaussian distribution model to the experimental data the mean Young's modulus values could be established, before and after incorporation of liposomes, in  $1.45 \pm 0.01$  kPa and  $2.13 \pm 0.02$  kPa, respectively.

Although AFM is a suitable technique to visualise and determine physicochemical parameters of biological samples it is very limited for the identification of the nature of structures analysed. Therefore, we investigate the effect of the engineered liposomes on HeLa cells by means of CM. Thus, we incubated HeLa cells for 40 min with liposomes labelled Rh-PE (red in the images) encapsulating calcein in this aqueous inner volume at its self-quenching concentration. Whether liposomes release their content, calcein concentration decreases, and the quenching process vanishes (green in the images). Besides, as described in the *Material and Methods* section in the *Supplementary Information*, HeLa membranes were stained with Cell Mask Deep Red showing grey contrast in the images to distinguish the limits of the cells. In Figure 4 representative lapse time images from the early distribution of the engineered liposomes just after their addition on the HeLa cells culture are shown. Liposomes were quickly adsorbed to the extracellular membranes and also to filopodia becoming the latter an active structure in liposomes capture (see video of the kinetic process of interaction of engineered liposomes with HeLa cells SV1 in *Supplementary Information*). In Figure 4A we can observe the initial stages of the interaction where few liposomes are adsorbed onto the HeLa plasmatic membrane. Remarkably, one can see filopodia, slender cytoplasmic projections (white arrows) which are characteristics in motile cells. Of interest, when liposomes were captured by filopodia they changed their

fluorescence emission from red (PE-Rho fluorescence) to orange light indicating the release of entrapped calcein from the liposome. Increasing the incubation time (Figures 4B and 4C) liposomes began to reach the cell membrane (white arrow heads) either because filopodia transport them to the membrane or by simple sedimentation from the solution.

Images of HeLa cells after 40 min and 24 h incubation with the engineered liposomes are shown in Figure 5. At 40 min (Figure 5A) few liposomes have been internalized into the cell (cyan arrow heads) and they become accumulated in the membrane (white arrow heads) or still adhered to filopodia (white arrows). Intensity profile along yellow line in Figure 5A evidenced that liposomes presented both, the red and green fluorescence suggesting that part of the entrapped calcein was released close to the liposome (Figure 5B). After 24h of incubation (Figure 5C) few filopodia presented liposomes capture and most of them can be observed at the membrane level and inside the cell. Some liposomes could be found inside the cells showing high calcein intensity. Of interest, in Figure 5C two liposomes inside the cell (white arrows) display an orange colour (coexistence of green and red fluorescence signals) with a greenly wake, probably due to the release of calcein during their internalization. Figure 5D shows the intensity profiles along yellow line in Figure 5C where the fluorescence signal after 24h of incubation is inherent to the Rh-PE fluorescence. Most of the liposomes were observed inside the cells and only some of them were still detected at the membrane level. In some cells the internalized liposomes showed almost no signal of calcein. Unexpectedly, in other cells, liposomes present high calcein intensity and clear evidences of being released (compare intensity profiles in Figure 5D and 5E). The lack of calcein fluorescence signal in some cells could be due to different reasons: i) calcein was released and due to the incubation time distributed in the whole cell; or ii) liposomes were endocytosed and calcein remain self-quenched. Besides, in presence of calcein, fluorescence signal is concentrated close to the PE-Rho fluorescence signal (Figure 5E) indicating that calcein is close to the lipid membrane of the liposome.

A proof of concept was required to demonstrate that the engineered liposomes could be useful as drug delivery systems. To this end, methotrexate (MTX) was encapsulated into the liposomes, the free drug removed, and viability assays performed by incubating them with HeLa cells. Image A in Figure 6 shows a representative image of HeLa cells growth in RPMI medium with liposomes without MTX. In Figure 6B engineered liposomes containing MTX were added to the cells to reach a final concentration of  $3 \times 10^{-7}$  M in the culture medium and incubated for 5 days. That results in a 80% suppression of cell viability as compared with the negative control in (image C in Figure 6) which corresponded to the cells growth without liposomes or any agent. As an additional control, a MTX solution at the same concentration as the one used in the preparation of liposomes was subjected to gel-filtration (G-50) and the eluate added to the cells. As shown in image D in Figure 6 cell viability was 75% of the control, which proved that free MTX was mostly retained by the column and thus the effects observed in Figure 6B can be positively attributed to the encapsulated MTX.

## **Discussion**

In this study we have investigated the interaction between engineered liposomes with a specific lipid composition and HeLa cells. Flow cytometry evidenced that the liposomes which lipid composition was established in a former study: POPC:CHOL:DOTAP (0.65:0.15:0.20, mol/mol/mol) [14] interact with HeLa cells. Notice that the amount of CHOL present is enough to prevent the gel to liquid-crystalline phase transition of the three components mixture since DOTAP presents a transition temperature of  $<5$  °C [25], close to the one shown by POPC [26]. On one hand this means that liposomes bilayer will not present any cooperativity against external stimuli becoming resilient to external changes of temperature, pH or ionic strength. On the other hand, the predominant fluidity of this mixture [27] becomes a key parameter for membrane fusion [28].



Besides, the presence of positively charged lipids as DOTAP enhances the fusion process with the cytoplasmatic membrane thanks to the electrostatic interaction between the positive charge brought by the DOTAP and the negative charges exposed by the plasma membrane because of the presence of several phospholipids (i.e. phosphatidylglycerol, phosphatidylserine or phosphatidylinositol lipids [29]). All these properties suggest that the lipid composition of the liposomes previously characterized should be considered as candidates with fusogenic and drug delivery capabilities into HeLa cells.

Flow cytometry indicated that liposomes were somehow within the cells. However, to get insights on the interaction and internalization mechanisms of liposomes by HeLa cells we took advantage of the complementarity of AFM and CM [30,31]. The features and nanomechanical properties of the HeLa cells presented in this paper AFM compares well with works previously published [32-34]. However here we were interested on the effect exerted by the liposomes on Young's modulus and adhesion forces and how these magnitudes may be relating with the interaction and internalization into the HeLa cells.

We analyzed the Young's modulus values at the central part of the HeLa cell before and after the interaction with the engineered liposomes. A clear rigidification (greater mean Young's modulus value) was detected after the incorporation of the liposomes most likely due to their partial or total integration in the lipid membrane of the cell. This rigidification was somehow expected due to the relatively high CHOL proportions presented in the engineered liposomes. This is a well-known behavior [35] and as we have confirmed it in liposomes mimicking the HeLa lipid bilayer by using the RBIR method [14]. However, AFM has evolved as a conventional technique to obtain physicochemical properties at the nanoscopic level, but it presents a lack of information to discriminate the nature of the structures, i.e. lateral segregated lipid domains, studied. At this point, we exploited visualization by CM, with the objective of inspecting the mechanisms underlying the interaction between the liposomes and the HeLa cells.

Confocal observations evidenced the quick interaction of liposomes with cells after their incorporation in the media. Whilst we were focused on conventional membrane structure

CM showed that liposomes quickly reached the membrane thanks to the filopodia. Related with such observation it has been reported that some virus infection depends on filopodia, where the underlying mechanism consists of virus surfing on the filopodia reaching the lipid membrane [36]. This surfing effect was also observed in the present study (see video in Supplementing Material SV1) where liposomes were captured from the media with other already reported capture movements of the filopodia. Remarkably, since liposomes were marked with two fluorescent dyes, PE-Rh at the lipid membrane and calcein at a self-quenching concentration inside the inner aqueous space of liposome, we observed how the red fluorescence of liposomes before their interaction with filopodia evolved in an orange fluorescence signal when captured. This orange color was the superposition of the red fluorescence of the Rh-PE and the green fluorescence of the calcein when released from the liposome into a wider region.

After 40 min most of liposomes were near the membrane layer of the cells and they showed orange fluorescence emission indicating that calcein release was quite fast when interacting with the cell membrane and/or with the filopodia. After 24 h, most of the liposomes were observed inside the cells confirming the internalization of the liposomes into the HeLa's cell cytoplasm. Most of these internalized liposomes emitted a red fluorescence signal, Rh-PE, almost no green fluorescence (calcein signal) suggesting the molecule was released, and that after 24 h of incubation it was diluted or metabolized by the cellular machinery. Of interest, we could observe few regions where liposomes were present at the membrane level and emitting orange fluorescence signal (coexistence of Rh-PE and calcein). Strikingly, we observed HeLa cells where liposomes, internalized and at the membrane level, emit green fluorescence signal, although some red signal from Rh-PE was present but masked (see cyan line intensity in Figure 5E). This cell presenting green fluorescence signal from calcein at 24 h seemed to experience the same phenomena that the others but time elapsed. This could be due to a delayed interaction with liposomes. It is reported that some viral infections are almost suppressed when filopodia number are reduced (less filopodia activity) [37].

This effect could appear in the cells showing emitting of calcein green fluorescence. Filopodia number in this cell were reduced, because of other cells where close to it i.e., less filopodia were motile and able to capture liposomes in suspension and delaying the internalization of liposomes at their encapsulated content into the cytoplasm. Another possibility for the delayed interaction of liposomes with the cell showing green calcein fluorescence could be due to the possibility that this cell experienced mitosis and the new cell had adhered to the extracellular matrix where liposomes could be deposited non-specifically onto the substrate surface. Because on the first minutes of incubation with the liposomes, CM evidenced that liposomes were firstly adhered or absorbed at the membrane level of the cell but also, some liposomes were present at the extracellular matrix between cells. This suggests that although many liposomes interacted with the cell there was a reservoir of liposomes close to them that could enter in contact lately or whilst cells grow.

Finally, we tested the viability of the engineered liposomes carrying MTX as a drug-delivery system showing the efficiency of liberation of the loaded MTX after 5 days demonstrating the usefulness of the liposomes as drug-delivery systems. Conversely, unloaded liposomes or the eluded solvent containing possible traces of the drug showed similar results as the control not affecting the viability of the HeLa cells.

All data evidenced that the POPC:CHOL:DOTAP (0.65:0.15:0.20, mol/mol/mol) liposomes represent a suitable composition to be used as a drug nanocarriers against HeLa cells. On one hand, the fact that the interaction between the liposomes and the cell is enhanced by the filopodia capture, open news perspectives considering the release of the liposome content but through the filopodia actin enriched membranes. On the other hand, a part of filopodia activity, at the membrane level we have confirmed the fusion mechanism between the engineered liposomes and the HeLa cells previously observed in model. Hence that determinations of changes in the nanomechanical properties as Young's modulus or

adhesion forces of HeLa cells turns into a practical tool to test lipid liposomes composition adequacy for drug delivery.

## **Conclusion**

POPC:CHOL:DOTAP (0.65:0.15:0.20, mol/mol/mol) engineered liposomes interact with HeLa cells immediately after they are added into the media. The Cytometry assays showed a concentration dependent effect which was further studied by other means like AFM, which showed changes on HeLa cell membranes after the incubation with the engineered liposomes, revealing an increase in its rigidity.

By means of CM we could observe how filopodia clearly plays an important role capturing liposomes and bringing them into the cell's membrane body. They increased the number of liposomes that reached the cell besides normal liposome deposition. During the first 40 minutes, POPC:CHOL:DOTAP engineered liposomes adsorb on the cell membranes and start their internalization. At 24h most of the liposomes have been internalized and have liberate their content.

POPC:CHOL:DOTAP engineered liposomes are able to encapsulate and later liberate drugs, therefore could be used as drug carriers.

## **References**

- [1] D.J.A. Crommelin, P. van Hoogevest, G. Storm, The role of liposomes in clinical nanomedicine development. What now? Now what?, *J. Control. Release.* 318 (2020) 256–263.

- [2] M. Rahman, S. Beg, A. Verma, I. Kazmi, F.J. Ahmed, V. Kumar, F. Anwar, S. Akhter, Liposomes as Anticancer Therapeutic Drug Carrier's Systems: More than a Tour de Force, *Curr. Nanomedicine*. 10 (2020) 178–185.
- [3] Y. Okumura, M. Yamauchi, M. Yamamoto, J. Sunamoto, Interaction of a Fusogenic Liposome with HeLa Cell., *Proc. Japan Acad. Ser. B*. 69 (1993) 45–50.
- [4] M.L. Immordino, F. Dosio, L. Cattel, Stealth liposomes: review of the basic science, rationale, and clinical applications, existing and potential., *Int. J. Nanomedicine*. 1 (2006) 297–315.
- [5] D.J. a Crommelin, G.W. Bos, G. Storm, Liposomes : Successful carrier systems, *Drug Deliv.* (2002).
- [6] C. Noé, J. Hernandez-Borrell, S.C. Kinsky, E. Matsuura, L. Leserman, Inhibition of cell proliferation with antibody-targeted liposomes containing methotrexate- $\gamma$ -dimyristoylphosphatidylethanolamine, *Biochim. Biophys. Acta - Biomembr.* 946 (1988) 253–260.
- [7] J. Hernández-Borrell, A new confirmation of selective action of liposomes, *Int. J. Pharm.* (1988).
- [8] M. Li, C. Du, N. Guo, Y. Teng, X. Meng, H. Sun, S. Li, P. Yu, H. Galons, Composition design and medical application of liposomes, *Eur. J. Med. Chem.* 164 (2019) 640–653.
- [9] S. Singh, P. Chaturvedi, A. Singh, S.K. Jain, Clinical approved liposomal formulations: an over view, *J. Emerg. Technol. Innov. Res.* 8 (2021) 856–868.

- [10] M.A. Busquets, J. Estelrich, Prussian blue nanoparticles: synthesis, surface modification, and biomedical applications, *Drug Discov. Today*. 25 (2020) 1431–1443.
- [11] N. Düzgüneş, S. Nir, Mechanisms and kinetics of liposome–cell interactions, *Adv. Drug Deliv. Rev.* 40 (1999) 3–18.
- [12] S.-T. Yang, A.J.B. Kreutzberger, J. Lee, V. Kiessling, L.K. Tamm, The role of cholesterol in membrane fusion, *Chem. Phys. Lipids*. 199 (2016) 136–143.
- [13] T.L. Andresen, J.B. Larsen, Compositional inhomogeneity of drug delivery liposomes quantified at the single liposome level, *Acta Biomater.* 118 (2020) 207–214.
- [14] A. Botet-Carreras, M.T. Montero, J. Sot, Ò. Domènech, J.H. Borrell, Characterization of monolayers and liposomes that mimic lipid composition of HeLa cells, *Colloids Surfaces B Biointerfaces*. 196 (2020) 111288.
- [15] D.K. Struck, D. Hoekstra, R.E. Pagano, Use of resonance energy transfer to monitor membrane fusion, *Biochemistry*. 20 (1981) 4093–4099.
- [16] R. Blumenthal, M.J. Clague, S.R. Durell, R.M. Epand, Membrane fusion, *Chem. Rev.* 103 (2003) 53–69.
- [17] C. Suárez-Germà, L.M.S. Loura, M. Prieto, Ò. Domènech, M.T. Montero, A. Rodríguez-Banqueri, J.L. Vázquez-Ibar, J. Hernández-Borrell, Membrane Protein–Lipid Selectivity: Enhancing Sensitivity for Modeling FRET Data, *J. Phys. Chem. B*. 116 (2012) 2438–2445.
- [18] S. Dutta, B. Watson, S. Mattoo, J. Rochet, Calcein Release Assay to Measure Membrane Permeabilization by Recombinant Alpha-Synuclein, *Bio-Protocol*. 10 (2020).



- [19] J. J. Roa, G. Oncins, J. Diaz, F. Sanz, M. Segarra, Calculation of Young's Modulus Value by Means of AFM, *Recent Pat. Nanotechnol.* 5 (2011) 27–36.
- [20] S.E. Cross, Y.-S. Jin, J. Rao, J.K. Gimzewski, Nanomechanical analysis of cells from cancer patients, *Nat. Nanotechnol.* 2 (2007) 780–783.
- [21] K. Pogoda, J. Jaczewska, J. Wiltowska-Zuber, O. Klymenko, K. Zuber, M. Fornal, M. Lekka, Depth-sensing analysis of cytoskeleton organization based on AFM data, *Eur. Biophys. J.* 41 (2012) 79–87.
- [22] M. Radmacher, Studying the Mechanics of Cellular Processes by Atomic Force Microscopy, in: *Methods Cell Biol.*, 2007: pp. 347–372.
- [23] J. Schindelin, I. Arganda-Carreras, E. Frise, V. Kaynig, M. Longair, T. Pietzsch, S. Preibisch, C. Rueden, S. Saalfeld, B. Schmid, J.-Y. Tinevez, D.J. White, V. Hartenstein, K. Eliceiri, P. Tomancak, A. Cardona, Fiji: an open-source platform for biological-image analysis, *Nat. Methods.* 9 (2012) 676–682.
- [24] T. Ferreira, K. Miura, B. Chef, J. Eglinger, *Scripts: BAR 1.1.6*, (2015).
- [25] A.E. Regelin, S. Fankhaenel, L. Gürtesch, C. Prinz, G. von Kiedrowski, U. Massing, Biophysical and lipofection studies of DOTAP analogs, *Biochim. Biophys. Acta - Biomembr.* 1464 (2000) 151–164.
- [26] J. Hernandez-Borrell, K.M.W. Keough, Heteroacid phosphatidylcholines with different amounts of unsaturation respond differently to cholesterol, *Biochim. Biophys. Acta - Biomembr.* 1153 (1993) 277–282.

- [27] A. Botet-Carreras, M.T. Montero, J. Sot, Ò. Domènech, J.H. Borrell, Engineering and development of model lipid membranes mimicking the HeLa cell membrane, *Colloids Surfaces A Physicochem. Eng. Asp.* 630 (2021) 127663.
- [28] J. Bompard, A. Rosso, L. Brizuela, S. Mebarek, L.J. Blum, A.-M. Trunfio-Sfarghiu, G. Lollo, T. Granjon, A. Girard-Egrot, O. Maniti, Membrane Fluidity as a New Means to Selectively Target Cancer Cells with Fusogenic Lipid Carriers, *Langmuir.* 36 (2020) 5134–5144.
- [29] K. Stebelska, P. Wyrozumska, J. Gubernator, A. Sikorski, Highly fusogenic cationic liposomes transiently permeabilize the plasma membrane of HeLa cells, *Cell. Mol. Biol. Lett.* 12 (2007).
- [30] C.A.J. Putman, A.M. van Leeuwen, B.G. de Grooth, K. Radošević, K.O. van der Werf, N.F. Van Hulst, J. Greve, Atomic force microscopy combined with confocal laser scanning microscopy: A new look at cells, *Bioimaging.* 1 (1993) 63–70.
- [31] T.F.D. Fernandes, O. Saavedra-Villanueva, E. Margeat, P. Milhiet, L. Costa, Synchronous, Crosstalk-free Correlative AFM and Confocal Microscopies/Spectroscopies, *Sci. Rep.* 10 (2020) 7098.
- [32] A. Gigler, M. Holzwarth, O. Marti, Local nanomechanical properties of HeLa-cell surfaces, *J. Phys. Conf. Ser.* 61 (2007) 780–784.
- [33] M. Checa, R. Millan-Solsona, A. Glinkowska Mares, S. Pujals, G. Gomila, Dielectric Imaging of Fixed HeLa Cells by In-Liquid Scanning Dielectric Force Volume Microscopy, *Nanomaterials.* 11 (2021) 1402.

[34] K. Hayashi, M. Iwata, Stiffness of cancer cells measured with an AFM indentation method, *J. Mech. Behav. Biomed. Mater.* 49 (2015) 105–111.

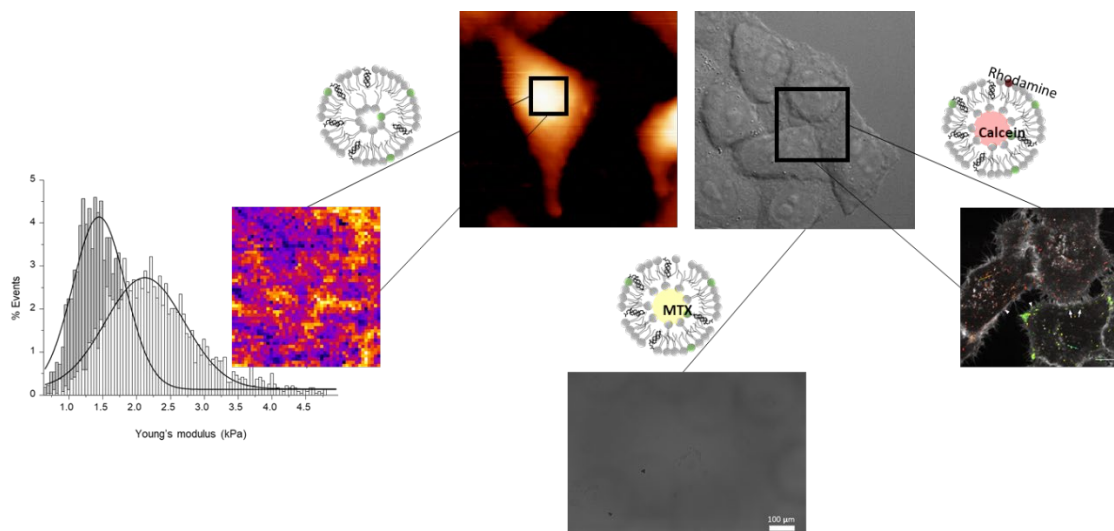
[35] M.D. Houslay, K.K. Stanley, Dynamics of Biological Membranes, *Biochem. Educ.* 11 (1983) 157.

[36] K. Chang, J. Baginski, S.F. Hassan, M. Volin, D. Shukla, V. Tiwari, Filopodia and Viruses: An Analysis of Membrane Processes in Entry Mechanisms, *Front. Microbiol.* 7 (2016) 300.

[37] M.J. Lehmann, N.M. Sherer, C.B. Marks, M. Pypaert, W. Mothes, Actin- and myosin-driven movement of viruses along filopodia precedes their entry into cells, *J. Cell Biol.* 170 (2005) 317–325.

## Acknowledgments

This study was supported by the Spanish Ministry of Economy and Competitiveness (PID2019-110210GB-I00), the Catalan Government (Generalitat de Catalunya) (214SGR 1442).



TOC image

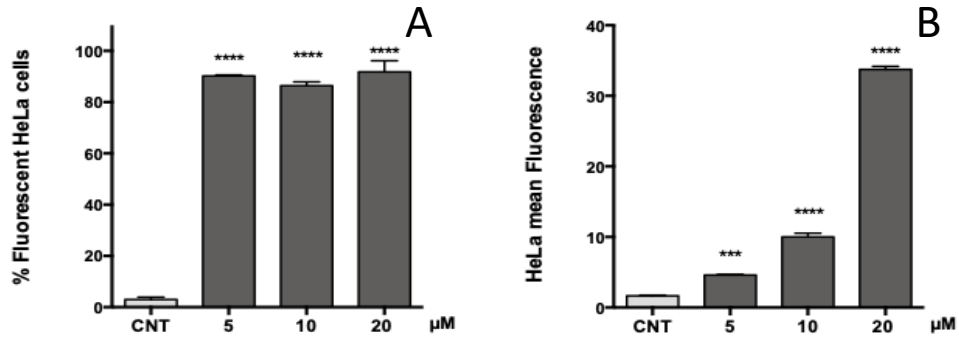


Figure 1. Flow cytometry assay after 24h incubation of HeLa cells with engineered liposomes. Percentage of fluorescence (A) and total fluorescence signal as a function of liposome concentration (B). Data are represented as the mean  $\pm$  SEM of at least three independent experiments. GraphPad Prism version 6.0 software (GraphPad Software, CA, USA) was used to analyze and represent the data. Statistical significance was calculated using one-way ANOVA with Dunnett's multiple comparisons test. The levels of statistical significance were denoted as follows:  $p < 0.001$  (\*\*\*) or  $p < 0.0001$  (\*\*\*\*).

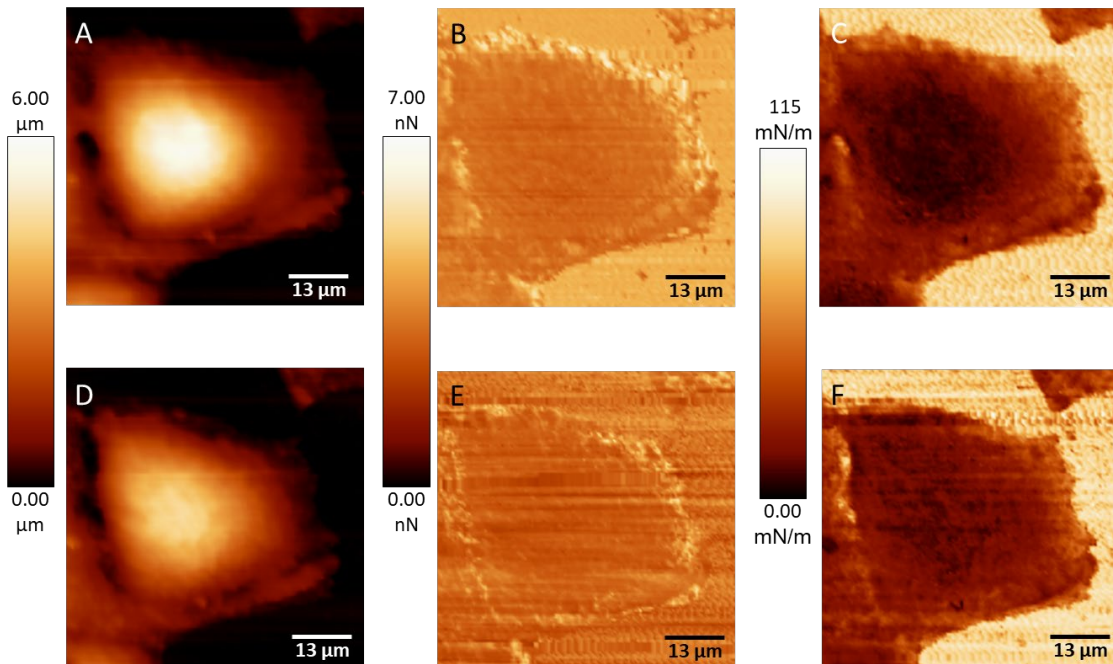


Figure 2. AFM images of HeLa cells providing different information; Topography (A) and (D); Adhesion (B) and (E); Slope (C) and (F) and comparing them without the addition of liposomes (A, B, C) or after a 40 min. after the liposomes were added (D, E, F).

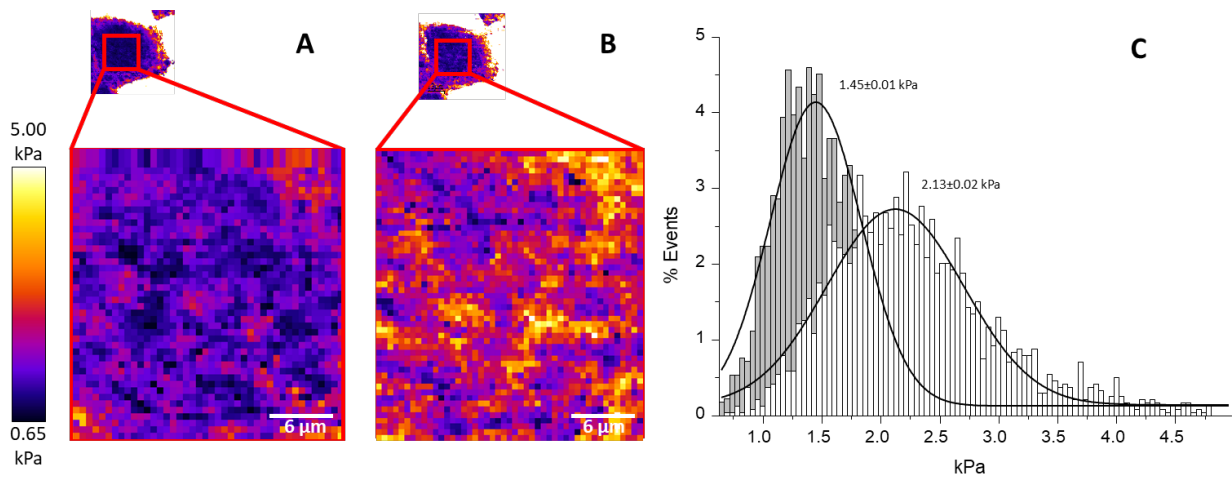


Figure 3. Force volume of the HeLa cell before incubation (A) and after incubation with engineered liposomes (B). Histogram plot of the force curves on each section A (1.45 kPa) and B (2.13 kPa) (C).

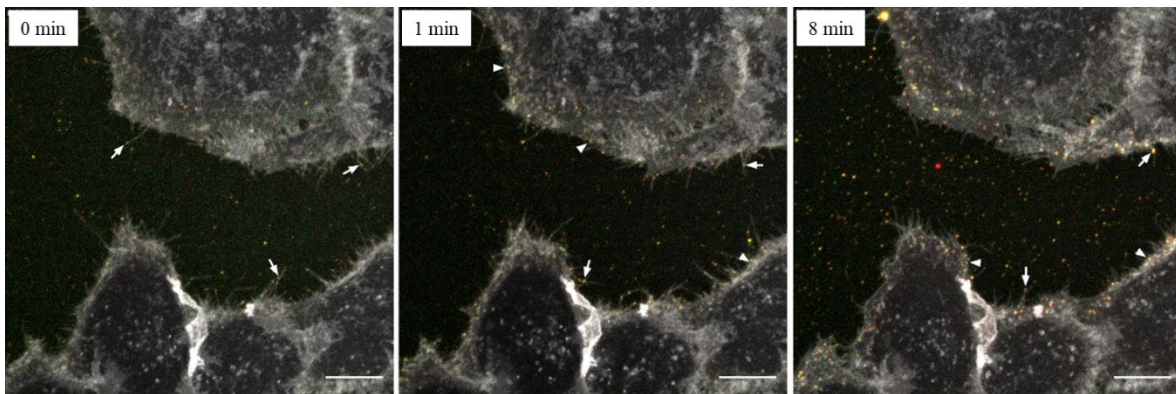


Figure 4. Liposome-membrane interaction in HeLa cells. Maximum intensity projection of 9 confocal planes (0.369 step size) from the basal side of the cell and at different time points showing calcein staining (green), rhodamine (red) and membranes (gray). Arrows point out liposomes attached to the filopodia and arrowheads point out liposomes at the cell membrane. Scale bar: 10  $\mu$ m. Images extracted from supplementary video.

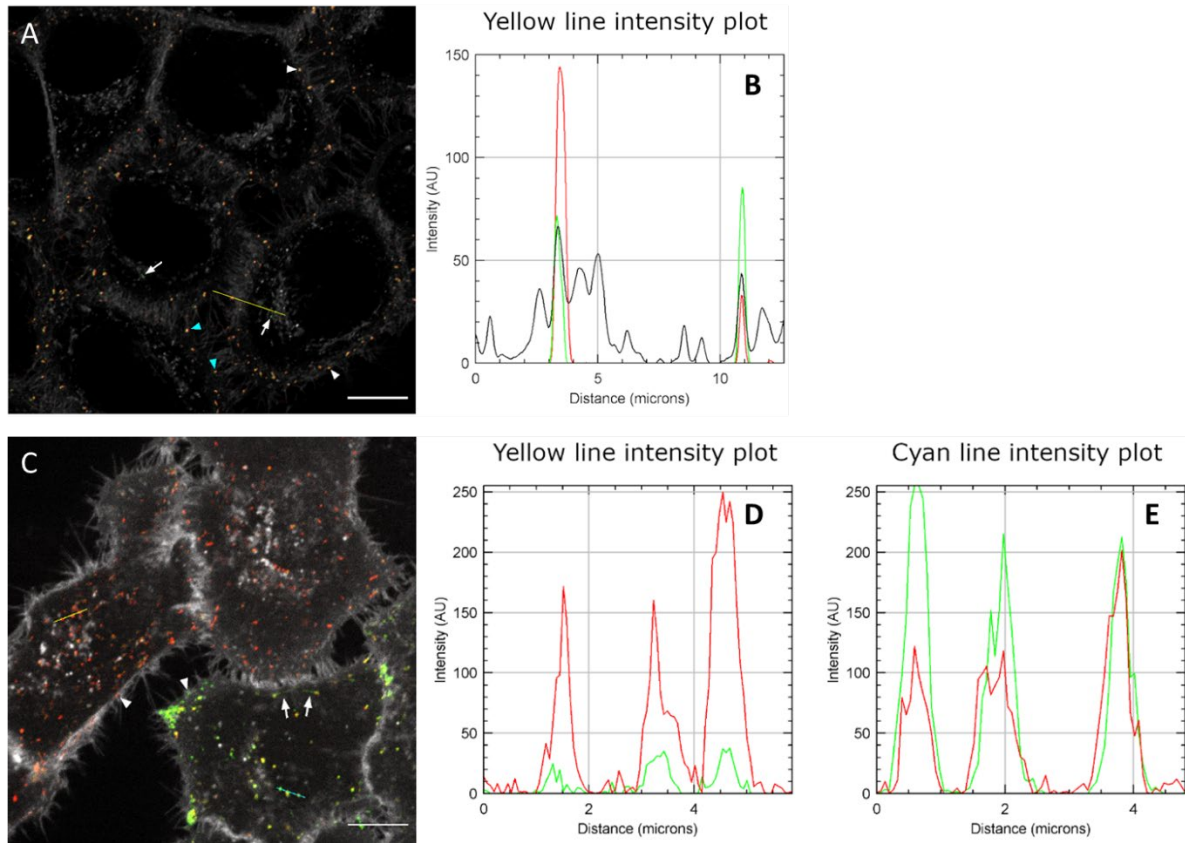


Figure 5. Liposome localization after 40 min (A, B) and 24 h (C,D,E) of incubation on HeLa cells. calcein staining is shown in green, rhodamine in red and membranes in grey. Scale bars: 10  $\mu$ m. A, Single confocal plane. Arrows point out internalized liposomes, white arrowheads point out liposomes at the cell membrane and cyan arrowheads point out liposomes attached to the filopodia. B, Intensity plot of yellow line in A. C, Single confocal plane. Arrows point out calcein release from internalized liposomes and arrowheads point out liposomes at the cell membrane. D and E, Intensity plots of yellow (D) and cyan (E) lines in C, respectively.



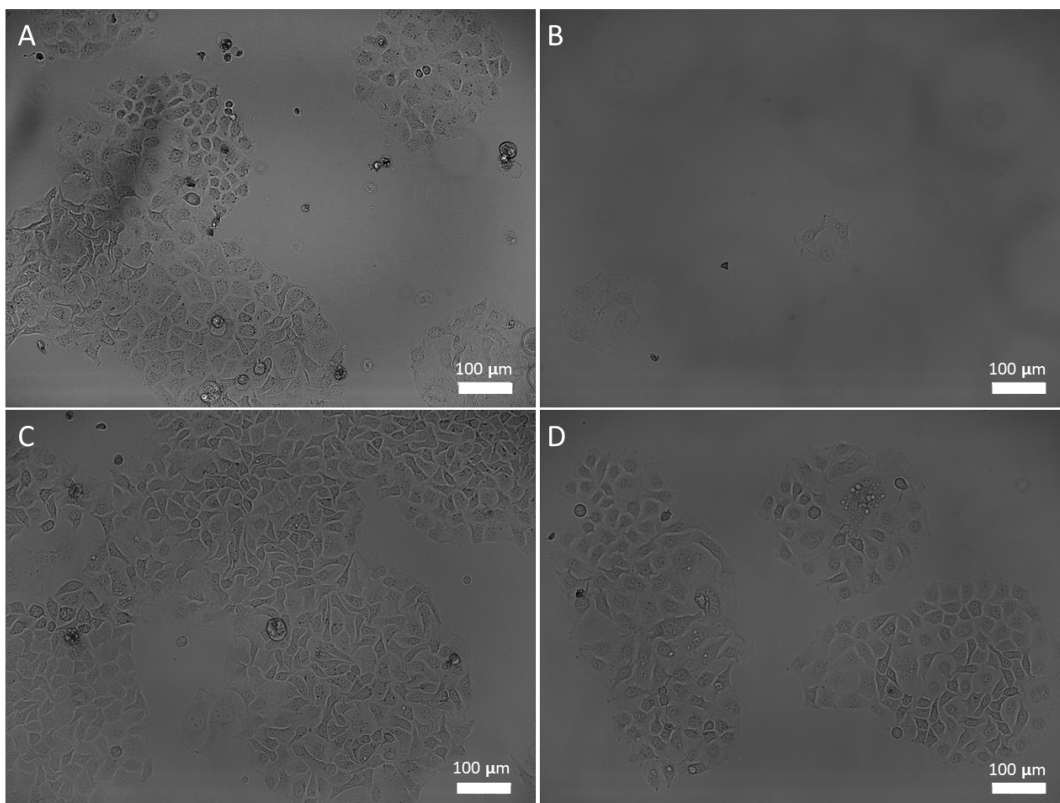


Figure 6. Growth of HeLa cells under different treatments. Representative pictures of HeLa cells after 72 hour of incubation in the following conditions: A) HeLa cells incubated with blank engineered liposomes; B) HeLa cells incubated with MTX loaded engineered liposomes; C) HeLa cells incubated without any liposomes or other agents (control); D) HeLa cells incubated with MTX upon filtering through a Sephadex G50 column.

Supporting information

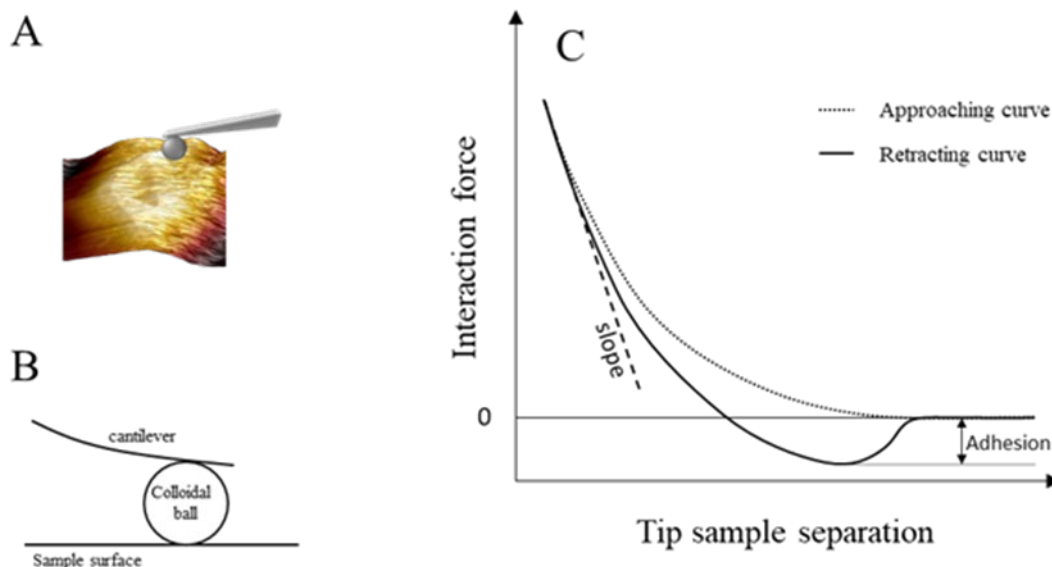


Figure S1: Cantilever with a spherical punch particle (2  $\mu\text{m}$ ) (A); *sphere-plane geometry* diagram (B). Force curves showing the approaching and retracting curves to calculate slope (C).

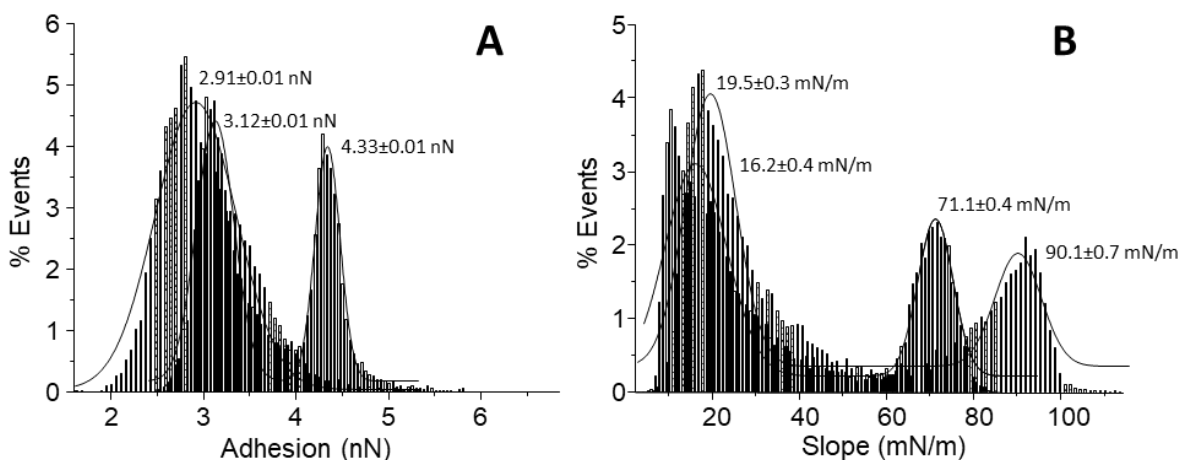


Figure S2: Histograms from Figure 2; A, adhesion forces from (Figure 2B&E) before (white bars with a double peak at 3.12 and 4.33 nN) and after 40 min. of incubation with POPC:CHOL:DOTAP liposomes (dashed bars with a single peak at 2.91 nN); B, slope curves from (Figure 2C&F) before (white bars with a double peak at 16.2 and 71.1 nN) and after 40 min. of incubation with POPC:CHOL:DOTAP liposomes (dashed bars with a double peak at 19.5 and 90.1 nN).



Video SV1: Video showing the liposome-membrane interaction in HeLa cells. Maximum intensity projection of 9 confocal planes (0.369 step size) from the basal side of the cell and at different time points showing calcein staining (green), rhodamine (red) and membranes (gray).



## Chapter 8. Discussion

### Detailed discussion

The objective of the present thesis was to create a simple liposomal delivery system using a bottom-up approach that took advantage of the physicochemical properties of phospholipids to modulate the passage through a cell membrane.

We started by selecting several phospholipids, taking into account that cells contain an incredibly wide variety of phospholipids at different concentrations as well as varying CHOL percentages in their membranes. We selected phosphocholine headgroups (PCs), as they are the most abundant lipids present in eukaryotic cells. We selected: (i) two heteroacid unsaturated phospholipids, POPC (with one double bond) and PLPC (with two double bonds); (ii) two homoacid saturated phospholipids, DPPC and DSPC, differing by two methylene groups in length; and (iii) one heteroacid saturated phospholipid, PSPC. All of them were mixed with CHOL at the minimal concentration of the sterol that was enough to abolish the transition from  $L_{\beta}$  to  $L_{\alpha}$  in the bilayers. These proportions were based on seminal studies carried out using differential scanning calorimetry [124].

Evaluation of the compression isotherms at 24 °C revealed that each pure phospholipid showed particular features and specific collapse surface pressures that matched the values reported before in other publications for POPC and PLPC [154], POPC and DSPC [155,156], PSPC [157,158] and DSPC [159–161].

We observed that CHOL showed its characteristic condensed-like state until it collapsed at 44.1 mN m<sup>-1</sup>, as seen before [162]. When CHOL was mixed with the different pure phospholipids, it induced a shift to lower molecular areas, thus showing a condensation effect. Since the percentage of CHOL was different for each phospholipid, we observed a different degree of the condensation effect of the resulting isotherm. DPPC was useful since it has been widely studied and is often used as a reference phospholipid in biomembrane

research [161,163]. The typical features of an isothermally compressed DPPC monolayer are well known: it presents a characteristic plateau with a change of phase at around  $10 \text{ mN m}^{-1}$ , which makes it a convenient candidate to validate the results of the study. The binary mixture of DPPC and CHOL, besides the shift of the isotherm to lower molecular areas that is also observed with other phospholipids, did not show the plateau region, indicating that the DPPC and CHOL had mixed to some extent. In general, binary monolayers showed a condensation effect in the presence of CHOL. Mixtures with a higher percentage of CHOL showed greater shifts than those with a lower percentage of CHOL. Furthermore, the characteristic features of pure phospholipids were abolished, the collapse surface pressure depended on the amount of CHOL and there were no double collapse surface pressures. All these findings suggested that all the phospholipids studied had mixed with CHOL and there was no phase separation.

Using the data from the binary monolayers at a surface pressure of  $30 \text{ mN m}^{-1}$ , which is accepted to be equivalent to the lateral surface pressure in a lipid bilayer, and with the phospholipids being in the LE phase (POPC and PLPC) and LC phase (DPPC, DSPC and PSPC), we evaluated their compressibility modulus ( $C_s$ ). We calculated the  $C_s^{-1}$  values for pure and mixed monolayers. The highest values were obtained for the pure CHOL monolayer, as expected considering its solid state all along the isotherm. It was also relevant that the combination of CHOL and pure saturated phospholipids increased  $C_s^{-1}$  values, except for PSPC:CHOL. In the case of unsaturated phospholipids, CHOL did not significantly modify the  $C_s^{-1}$  values. This implies that CHOL was able to rearrange the lateral organization of phospholipids, increasing the packing density in the monolayers.

Surface thermodynamic analysis with the isotherm data was used to obtain the Gibbs energy of mixing ( $\Delta_{\text{mix}}G$ ) for the mixtures to estimate their stability at the air-water interface.

In general, binary systems showed negative  $\Delta_{\text{mix}}G$  values, indicating that the mixed monolayers were stable. POPC and PLPC showed the lowest absolute  $\Delta_{\text{mix}}G$  values, being the least stable binary systems. Although this part of the project aimed to select the most



convenient mixture for engineering a liposome, it is worth mentioning here that heteroacid unsaturated phospholipids are the most abundant in eukaryotic cell membranes. Hence, the relatively lower stability of POPC and PLPC mixed with CHOL raises an interesting question on how to correlate surface thermodynamic data with the biological properties of ubiquitous phospholipids in living membranes.

These results were enough to compare the overall stability of the possible future candidate mixture, considering that we were comparing the stability of the monolayers at a CHOL molar concentration that abolished the transition from  $L_{\beta}$  to  $L_{\alpha}$  and not by their CHOL proportion since they did not have the same molar ratio.

Other results, like cohesive forces ( $\zeta$ ) and  $G^E$  values, were negative, indicating attractive interactions between the two components of the systems, reinforcing the fact that the mixtures were stable. Another interesting factor, the activity coefficient of CHOL ( $\gamma_{\text{CHOL}}$ ) in the mixtures, was higher for homoacid phospholipid systems than for the heteroacid ones, indicating that monolayers formed with homoacid phospholipids presented less deviation from the ideal mixing.

To discuss the decrease observed in the vertical component of the dipole moment ( $\mu_{\perp}$ ), we need to take into account four considerations: (i) the umbrella model suggests that CHOL preferentially interacts with the hydrophobic tails of the phospholipids, leaving the hydroxyl group near the phospholipid headgroup [164,165]; (ii)  $\mu_{\perp}$  is complex and composed of at least three components that include contributions from the dipole moment of the polar headgroup, the hydrocarbon chain, and the surface water molecules beneath the monolayer close to the headgroup; (iii) the systems only differ in the different hydrocarbon chains of the phospholipids and the presence or not of CHOL; and (iv) CHOL modifies the  $\mu_{\perp}$  component associated with the verticality of the hydrocarbon chains of the phospholipids [166]. For the monolayers in the LE phase (POPC and PLPC) mixed with CHOL, we observed an increase in the  $\mu_{\perp}$  values at all  $\pi$  values with respect to the pure phospholipid, which could be attributed to a more vertical orientation of the acyl chains of the phospholipids. CHOL molecules can be located close to the phospholipid chains, constraining rotational

movements and forcing the phospholipids to be closely packed and, thus, more vertical with respect to the water interface. By contrast, the interaction of saturated phospholipids in the LC phase (DPPC, DSPC and PSPC) with CHOL prevented the acyl chains from adopting the all-*trans* configuration, leading to a tilt in the monolayer chains.

For all the systems studied (both pure and mixed monolayers), the  $\mu_{\perp}$  value decreased as  $\pi$  increased. This is somehow surprising as  $\mu_{\perp}$  is usually understood to reflect a vertical orientation of the hydrocarbon chains of the phospholipids in the monolayer with respect to the water interface. To understand this behavior, it is important to consider that when  $\pi$  increases and the molecules in the monolayer begin to reduce their molecular area, they begin to be more perpendicular with respect to the water interface, with the wetting of the polar head changing too. It seems that this different water content in close contact with the polar head is as important as the verticality of the hydrocarbon chains for the  $\mu_{\perp}$  value.

Thus, the  $\mu_{\perp}$  results reinforced the first conclusions obtained from the  $C_s^{-1}$  analysis that CHOL was able to rearrange the lateral organization of the phospholipids, increasing the packing density in the monolayers.

Using AFM to monitor the lipid monolayers deposited on mica surfaces, we observed the same two distinct domains in all the lipid mixtures. Other studies used water as the subphase and an extraction pressure of  $15 \text{ mN m}^{-1}$ , whereas we used a Tris buffer with NaCl (pH 7.4 and ionic strength 150 mM) to produce a more biomimetic environment and a surface pressure of  $30 \text{ mN m}^{-1}$  as an approximation of the surface pressure in a lipid bilayer.

From the topographic images, all the smaller brighter (higher) domains found in the mixtures were initially attributed to CHOL-enriched domains, as seen in other publications [167] reporting the appearance of these domains even at low CHOL molar percentages [168]. The authors of those publications stated that the CHOL domains appeared in mixtures where the CHOL molar percentage was higher than 5%, leading to the formation of segregated micrometric domains highly enriched in CHOL. The molar percentage of CHOL in each of the binary monolayers exceeded the 5% stated above. Therefore, these CHOL-enriched domains were anticipated. That is, we corroborate this observation for several

other phospholipids with putative applications in liposome formulations and with biological relevance.

Even if the domains were expected, some differences were detected between the mixtures. The smallest domains were observed in the PSPC:CHOL monolayer, which, at the same time, was the most stable binary system according to the  $\Delta_{\text{mix}}G$  data. In general, the size of the domains seemed to be related to the concentration of CHOL in the monolayer, the saturated or unsaturated nature of the phospholipids, the thermodynamic stability of the monolayers and the verticality of the molecules at the interface. For instance, the step height difference between the domains in the mixed monolayer was higher for the mixtures in the LE phase (POPC:CHOL and PLPC:CHOL) than for the monolayers in the LC phase. It is interesting to note that the AFM tip could slightly push down the unsaturated lipids since they were less rigid than the saturated ones, but not the brighter domains that were probably highly enriched with CHOL, since CHOL was in the  $L_o$  phase. As the monolayer-tip interaction could increase the step height difference between the domains, we considered this a drawback in the application of AFM for more precise measurements. A similar criticism has been made for other lipid systems [169].

However, comparison of the images of the pure phospholipids showing no evidence of domains with those of mixtures showing domains appearing after the addition of CHOL suggested, like previously reported [167,168], that the smaller bright regions observed by AFM in the binary mixtures could be attributed to the segregation of CHOL-enriched domains.

BAM observations agreed with this conclusion as phase separation was observed in PSPC:CHOL [155]. Based on the structural nature of PSPC, this effect might also occur for DPPC and DSPC. In the case of POPC and PLPC with CHOL, the most probable interaction reported in the literature was based on an epifluorescence microscopy assay involving POPC:CHOL [170], where hydrogen bonding and van der Waals forces acted as stabilizing forces, resulting in the formation of larger domains. In all these examples, as well as in the

mixtures, we observed the existence of domains that were most probably produced by the addition of CHOL.

In general, the results agreed with the general assumption that CHOL has a weaker effect on unsaturated phospholipids than on saturated ones.

Another interesting factor that we could extract from the AFM images was the roughness of the surfaces. The higher domains showed a rougher surface than the lower domains, reinforcing again the different nature of the two areas.

Unfortunately, the basic operational modes of AFM imaging are not meant to provide direct information about the composition of the domains. Without coupling AFM to other techniques (i.e., surface-enhanced Raman spectroscopy), the single measurement of the physical properties of the domains only provides a window into their composition. The nominal molar percentage of CHOL did not match with the percentage of area displayed by the higher domains. This hinted at the possibility that CHOL was probably mixed in the base area and occurring at higher proportions in the brighter domains. Another way of corroborating this was by comparing the adhesion forces of the monolayers formed with pure phospholipids to those of the base area (lower region) of their homonymous mixtures and see if they had similar  $F_{adh}$  values. We were certain that CHOL had to be present in the base area because the  $F_{adh}$  values of the base area of the binary mixtures were different to those of the pure phospholipid monolayers. Similar experiments discriminating between regions have been performed before with positive results, being used to discriminate between phase-separated lipid domains [171] or lipid-protein segregated domains [172].

The  $F_{adh}$  values provided another interesting piece of information. The histograms revealed lower adhesion values for unsaturated phospholipids than for saturated ones, being the lowest for the POPC monolayer and the highest for the DSPC and PSPC monolayers. In this case, since the tip was retracting instead of pushing, we did not consider the varying softness of the phospholipids like we did before when discussing the possible differences in the measurements of the step height of the lipid domains.

In this case, the determining factor was probably the packing of the phospholipids. The ones in the LE phase had a larger area per molecule. Therefore, their LBs were less dense compared to those with fewer molecules that could interact with the AFM tip. This, in terms of  $F_{adh}$  forces, would mean lower values because having fewer tails in the same area would mean a lower overall strength in adhering to the tip.

Analysis of the  $F_{adh}$  values for the binary mixtures revealed that the base area showed the same behavior as their respectively pure phospholipid LBs. Even if they contained CHOL, they behaved as we have already discussed. Interestingly, knowing that there were no purely CHOL domains, the CHOL-enriched domains (high) showed different behaviors like those observed with the  $\mu_L$  values. On the one hand, the mean  $F_{adh}$  values for the POPC:CHOL and PLPC:CHOL monolayers showed higher values for the high domains than the background domains. On the other hand, the DPPC:CHOL, DSPC:CHOL and PSPC:CHOL monolayers showed lower  $F_{adh}$  values for the high domains than the background domains.

It should be noted again the difference between the saturated and unsaturated phospholipids. Therefore, their shape, tail length, and lateral packing in a monolayer all play important roles.

Considering that the monolayers were extracted at  $30 \text{ mN m}^{-1}$  and assuming that the different high domains in the extracted mixed monolayers were also at this surface pressure, the different  $F_{adh}$  values obtained suggested that they were not domains containing only CHOL, but a mixture of CHOL and the corresponding phospholipid. This may be similar to what happens when mixing two components in solution, which displays regions of partial mixing at certain proportions and complete phase separation at other proportions.

After the analysis of the different compositions studied, the POPC:CHOL composition was chosen as the best option to formulate liposomes for use as nanocarriers and for interactions with lipid membranes. Although being a stable composition, POPC:CHOL presented one of the lowest absolute  $\Delta_{mix}G$  values, suggesting that interactions with other membranes could easily destabilize it. Furthermore, since we were looking for a biomimetic

composition, phospholipids in natural extracts usually present one saturated hydrocarbon chain and one hydrocarbon chain with one unsaturation. Therefore, POPC was the best option.

After selecting the composition of the engineered liposomes, we needed to test them by performing *in vitro* tests in cells.

Since working *in vitro* with living cells to test several formulations is time-consuming and expensive, a simplified model replacing the cells was first used to identify the physicochemical properties involved in the interaction between the lipid layers. Thus, we decided to form liposomes containing lipid mixtures that mimicked the lipid composition of a HeLa plasma membrane. We developed a composition using published sources [131–134] that detailed the components and percentages of HeLa cell membranes, focusing on the four main lipids: PC, PE, PS and CHOL. Like many bacterial and cell membranes, the HeLa cell membrane bilayer contains heteroacid phospholipids. With the information gathered, we used POPC, POPE, POPS and CHOL at a molar composition of 0.29:0.31:0.06:0.34, respectively. Before using it in experiments with the engineered liposomes, we needed to obtain more physicochemical data to characterize the model membrane and verify that it mimicked the lipid composition of a HeLa cell membrane. To this end, we took advantage of the experience gained with the experiments on the monolayers and complemented it with other techniques.

The comparison of the HeLa-mimicking monolayer with those of the pure phospholipids demonstrated, as expected, that CHOL caused a condensation in the molecular area of the pure phospholipid monolayers and no phase transition was observed along the isotherm of the mixture. The same behavior had been seen before with the engineered liposome compositions. In addition, since the main melting transition temperature of the pure phospholipids is below the working temperature, the HeLa-mimicking monolayer was in the LE state at room temperature at all the surface pressures studied. No phase transitions were observed in the isotherm and, more importantly, at  $30 \text{ mN m}^{-1}$ , which is considered to be equivalent to the surface pressure found in a natural bilayer.



Usually, the LE phase in monolayers is considered to correspond to the  $L_{\alpha}$  phase in bilayers. Calculating generalized polarization magnitudes with fluorescence experiments, we wanted to corroborate the LE- $L_{\alpha}$  correlation by measuring the fluidity of the HeLa-mimicking liposomes. These liposomes presented a melting transition temperature below 37 °C that was higher than the individual transition temperatures of the pure phospholipids, as expected, due to the stiffness caused by the presence of CHOL.

Another assay that provided results along the same direction was the RBIR experiments performed on the liposomes. Taking advantage of the PA fluorescent probe [173] across the full range of temperatures studied, HeLa-mimicking liposomes presented an intermediate state between the  $L_o$  and  $L_{\alpha}$  phases [174]. The fluid states are believed to be preponderant in natural membranes [175], but lateral phase separation, or domains with distinct compositions may occur [176].

Laurdan fluorescence experiments, BAM and AFM demonstrated the existence of domains in the monolayers. Furthermore,  $\mu_{\perp}$  values reached a relatively low value at 30 mN m<sup>-1</sup>, showing that the HeLa-mimicking mixture was less polarized at higher than at lower surface pressures [27]. All these results indicated favorable conditions for the fusion process, given the fluid nature of the HeLa cell membrane.

Going back to the BAM and AFM observations, the microstructures found on the monolayers demonstrated that the HeLa-mimicking mixture was not homogenous, but laterally segregated into domains. In addition, we observed two different levels of organization. In the monolayers at 30 mN m<sup>-1</sup>, 10  $\mu$ m domains could be observed in the BAM images, while bright domains measuring about 500 nm could be discerned in the AFM images. This demonstrated two levels of organization, one at the micrometric level and the other at the nanometric scale. The relationship between microdomains and nanodomains has been already reported [177]. Briefly, biological membrane models follow a hierarchical arrangement from top to bottom that include macrodomains observed by conventional microscopies, microdomains observed by BAM, and nanodomains observed by AFM.

Investigations of the bright domains by AFM-FS and pixel analysis with the force volume images revealed differences in the adhesion forces between the domains and the base area, with values in the range expected for a fluid membrane. In this case, the higher domains had a lower  $F_{adh}$  value than the base area. Interestingly, although the HeLa-mimicking mixture was formed with heteroacid phospholipids, the higher lipid domains showed lower values compared to the base area, as observed previously for saturated phospholipids and in contrast to what would be expected. In this case, the different headgroup nature and especially the charge of the PS molecule might have played important roles.

After studying the newly developed HeLa-mimicking mixture, it was used in experiments with engineered liposomes. Several studies have clearly established that for liposomes to fuse with a cell lipid membrane, which is negatively charged at physiological pH, the liposomes should present a positively-charged membrane for an electrostatic attraction between the membranes. In these assays, engineered liposomes containing POPC as the PC matrix were supplemented with the cationic lipid DOTAP [178,179]. Both liposome formulations, with and without CHOL, contained 20% mol of DOTAP. The incorporation of DOTAP into the engineered liposomes conferred a positive  $\zeta$ -potential value, which would promote an electrostatic attraction and help the adsorption of the engineered liposomes onto the HeLa cell membrane as well as HeLa-mimicking membrane models, which have a negative  $\zeta$ -potential value due to the presence of PS. It is worth remembering here that natural cell membranes, like the HeLa cell membrane, present negative charges due to the presence of phosphatidylglycerol, phosphatidic acid, phosphatidylserine or phosphatidylinositol groups.

Firstly, we incubated a HeLa-mimicking monolayer with the engineered liposomes, maintaining the surface pressure of the monolayer at  $30 \text{ mN m}^{-1}$  and following the increase in the molecular area of the multicomponent monolayer. The injection of the engineered liposomes beneath the lipid monolayer demonstrated that both formulations of the engineered liposomes could fuse with the monolayer, since the molecular area of the HeLa-mimicking monolayer increased with time, which can only occur if the liposomes have fused with the monolayer.

Considering the difference in the  $\zeta$ -potential values and the results of the perpendicular component of the molecular dipole moment of the HeLa-mimicking bilayer model, the first step in the interaction with liposomes containing DOTAP should be electrostatic, promoting the insertion of the lipids from the liposomes into the HeLa-mimicking outer lipid monolayer. As the fusion process continues, the lipid bilayer structure of the liposome is disrupted. This primary step may lead to the occurrence of adhesion forces between the molecules of the liposome and the molecules of the monolayer and among probable hexagonal structural intermediates [180], promoting the fusion process. We observed that the fusion process was relatively fast, probably due to this first electrostatic step and how it proceeded until saturation.

Another interesting observation was the effect of CHOL on the engineered liposomes. The liposomes containing CHOL provoked a significant increase in the molecular area of the monolayer, i.e., the fusion process. This effect could be due to the phosphatidylserine molecule being intimately involved with CHOL in the endocytosis process [181].

We expected electrostatic forces to govern the primary event occurring in the interaction between the outer monolayer of the liposomes and the HeLa-mimicking membrane model. This mechanism has been already suggested in *in vitro* experiments involving liposomes applied to solid tumors [182]. Moreover, the first electrostatic event might be the primary step in the transfection mechanism [183] and in viral infections [184]. The initial electrostatic interaction is most likely to be due to the structural destabilization of the bilayer caused by DOTAP, which would precede the fusion process.

Membrane fusion has been extensively studied, and usually, two intermediate structures have been identified [185,186]: hemifusion, where there is a mixing of the lipids in the outer leaflets, but not of those present in the inner layer of the bilayer, and fusion pores, where both leaflets merge, resulting in the formation of a pore.

To simulate the actual HeLa cell membrane bilayer, we analyzed its physicochemical properties by using a planar bilayer model. When two vesicles of different sizes make

contact, such as a cell and a liposome, the first event would be the adsorption of the smaller system with a higher lipid curvature onto the larger one with a low lipid curvature. Therefore, the use of a flat model like SLBs can represent the difference in sizes between a cell (micron scale) and a liposome (nanometric scale). This is of particular interest when liposomes adsorb onto a cell membrane or undergo endocytosis by a cell.

When the SLBs were formed by depositing liposomes onto a mica surface, no laterally segregated domains were observed, suggesting a rearrangement of the lipid components [187]. This was interesting when considering that we observed two different types of domains in the monolayers at the nanoscale (through AFM) and a larger organization of domains at the micrometric scale (as observed by BAM). Moreover, RBIR assays with liposomes indicated that  $L_o$  and  $L_\alpha$  domains might coexist. Clearly, the domains previously observed in the monolayers vanished when the bilayers were formed [188]. Other SLBs models rich in CHOL show a similar behavior [189,190], which would explain the featureless nature of the HeLa-mimicking SLBs due to the high amount of CHOL (33%) in the composition.

After the addition of POPC:DOTAP or POPC:CHOL:DOTAP liposomes to the HeLa-mimicking SLBs, the liposomes integrated into the SLBs, as could be seen in the topographic images. The small holes in the SLBs that were purposely created began to close as the engineered liposomes fused into the SLBs. From the images, we can infer that the liposomes fused with the SLBs because we could not observe any adsorbed liposomes on the surface or inside the holes. In addition, the defects on the surface closed from the edges to the center as if the SLBs were growing in the XY plane, closing the gaps.

Another interesting observation from the fusion of the engineered liposomes with the SLBs was that the CHOL-containing liposomes were faster in closing the gaps than the liposomes without CHOL. These results confirmed that the presence of CHOL enhanced the fusion rate, as observed with other SLBs of different compositions [191]. These findings were consistent with the results we obtained from the fusion process of the engineered liposomes injected beneath the HeLa-mimicking monolayer at a surface pressure of  $30 \text{ mN m}^{-1}$ .

The AFM studies were also used to obtain Young's modulus ( $E$ ) of the SLBs. The HeLa-mimicking SLBs had  $E$  values of around 30 MPa. Usually, high values of  $E$  correspond to a gel or ordered states, while low values are typical for fluid or disordered states. In the binary phase-separated system composed of 1,2-dioleoyl-sn-glycero-3-phosphocholine (DOPC) and DPPC,  $E$  values were 19.3 MPa and 28.1 MPa, respectively, corresponding to the fluid and gel phases, respectively. Even higher values for the same system have been reported by other research groups using different AFM probes and experimental conditions [192]. This suggests, as indicated by the RBIR results, a coexistence of the  $L_o$  and  $L_\alpha$  domains, with a more  $L_o$  behavior expected. It is worth noting that the mixture was not binary, but quaternary. For multicomponent SLBs, higher  $E$  values of up to 80 MPa have been reported for fluid disordered phases [193].

After the addition of the engineered liposomes to the HeLa-mimicking SLBs, the increase in the  $E$  values demonstrated the fusion of the engineered liposomes with the SLBs. Only the fusion and integration of a different membrane into an SLB can change its  $E$  values. Therefore, this demonstrates that flat/planar HeLa-mimicking models are useful in monitoring the fusion of liposomes (with high lipid curvature) with a cell membrane (with low lipid curvature).

The fusion of the engineered liposomes with the SLBs resulted in substantial changes in the mean value and distribution of the Young's modulus values. HeLa-mimicking SLBs showed a unimodal distribution that shifted to higher values when POPC:CHOL:DOTAP liposomes were added. Interestingly, when POPC:DOTAP liposomes were added, the distribution of the  $E$  values was bimodal. One of the peaks was centered at values similar to those of the HeLa-mimicking SLBs, while the other was at higher  $E$  values. This suggested that the fusion process was incomplete during the incubation time and that some areas of the HeLa-mimicking SLBs remained unchanged since the liposomes had not fused yet. These results are consistent with the reported increase in the bending modulus of liposomes upon the addition of CHOL to different lipid compositions [194], which has been confirmed by force spectroscopy studies on the nanomechanical properties of SLBs and by the fact that the

presence of CHOL causes a higher degree of compactness or less elastic deformation of the bilayer [193].

It was clear that the two types of engineered liposomes interacted differently with the HeLa-mimicking SLBs. When analyzing the lifetime of the NBD-PE fluorescent probe added to the engineered liposomes, a shift towards shorter lifetime values was detected after the fusion of the HeLa-mimicking liposomes with either of the two types of engineered liposomes. This shift demonstrated a change in the lipid properties of the bilayer in which the fluorophores were inserted. This could only be due to the mixing, putative mixing, of the different bilayers from the engineered liposomes and the HeLa-mimicking liposomes.

AFM topographic and force spectroscopy measurements were valuable in demonstrating that the fusion process was indeed happening, but, unfortunately, they were not enough to quantify the process.

Importantly, FRET results confirmed that the fusion process was faster in the presence of CHOL, as can be seen by the kinetic constants being 40% higher for the engineered liposomes containing CHOL.

Since both fluorophores (NBD and Rh) were together in the engineered liposomes, a reduction in the FRET signal due to the fusion of the engineered liposomes with the HeLa-mimicking liposomes would increase the NBD fluorescence signal, enabling us to quantify the fusion rate. However, the fusion percentages did not achieve large values, being 11.4% and 7.2% for the POPC:CHOL:DOTAP and POPC:DOTAP liposomes, respectively. The maximum fusion values were calculated as if the fluorescent probes were infinitely diluted in the liposomes, like when liposomes are disrupted with a detergent that dissolves Rh and transforms liposomes into micelles, leading to the spatial separation of the NBD and Rh probes. This raises the problem of knowing whether the fusion events between liposomes of different compositions are not going to be infinite [144]. Therefore, under our experimental conditions (e.g., time, liposome concentration and temperature), we expected a one-to-one fusion event where one engineered liposome fused with one HeLa-mimicking liposome. Therefore, when using the FRET data, if we consider that the value of



100% fusion indicates that all the engineered liposomes bearing fluorescent probes are fused with all the HeLa-mimicking liposomes at a one-to-one ratio instead of indicating that the liposomes are infinitely diluted, we can obtain a better approximation of the *in vitro* and *in vivo* behavior. Different values of fusion percentages were obtained using this consideration: 42.1% and 18.1% for the POPC:CHOL:DOTAP and POPC:DOTAP liposomes, respectively. The fusion percentage for the POPC:CHOL:DOTAP liposomes might be the closest to reality as we will discuss later with the confocal microscopy assays.

The differences in the fusion percentages were clearly due to the presence of CHOL, which increased the likelihood of fusion and its speed. This could be seen in the differences between the two types of engineered liposomes when closing the holes in the SLBs and the differences in the values of Young's modulus.

DPH and TMA-DPH fluorescence studies were also undertaken to analyze the physicochemical changes in the HeLa-mimicking liposomes after fusion with the engineered liposomes. The microviscosity values of the different liposomes were calculated using conventional equations. Interestingly, the microviscosity value decreased after the fusion of the HeLa-mimicking liposomes with the engineered liposomes, with this decrease being greater for the engineered POPC:DOTAP liposomes than the POPC:CHOL:DOTAP liposomes. Both types of engineered liposomes had the same molar proportion of DOTAP (20%), which has been suggested to cause structural destabilization that results in lower values of microviscosity. The presence of CHOL in the liposomes had the effect of increasing microviscosity by exerting an ordering effect in the membrane [195,196]. The changes in microviscosity of the HeLa-mimicking liposomes, when fused with the engineered liposomes, were direct evidence that the composition of the HeLa-mimicking liposome bilayer had changed due to the fusion and consequent mixing of the molecules from the engineered liposomes. This is consistent with the Young's modulus values and distributions obtained in this thesis.

The  $\Delta E$  values extracted from the microviscosity measurements were used to calculate the energy needed for the engineered liposomes to fuse with the HeLa-mimicking liposomes in

a comparative manner as an indicator of how easily the liposomes could spread onto a surface. However, the values showed no significant differences when using either the DPH or TMA-DPH data, indicating that both types of engineered liposomes required a similar amount of energy for fusion.

Young's modulus values obtained from the AFM studies and microviscosity measurements acquired with the DPH and TMA-DPH fluorescence data were analyzed. We could see that after the fusion process, the engineered liposomes showed greater values of  $E$  and smaller microviscosity values than the HeLa-mimicking liposomes. It is important to note that both techniques are not contradictory, but complementary. Young's modulus data give information on the compactness between the phospholipids in the Z axis, while the viscosity values obtained from the anisotropy of the DPH and TMA-DPH probes provide information on the mobility of the lipids in the X-Y axis.

The comparison of the results from both techniques (Young's modulus values obtained from the AFM-FS data and the TMA-DPH studies) suggested that the presence of CHOL in the engineered liposomes enhanced spreading on the mica surface (lower Young's modulus and  $\Delta E$  values) compared to the engineered liposomes without CHOL. The  $\Delta E$  values from the DPH studies did not seem to be affected, probably because DPH locates itself close to the lipid hydrocarbon groups in the core of the bilayer, which has small or no effect on the spreading process.

We then assessed whether the engineered liposomes could fuse with living HeLa cells and/or be used as drug carriers. These experiments were also used to validate the different models of the HeLa-mimicking lipid mixture.

Between the two engineered liposome formulations, we decided to exploit POPC:CHOL:DOTAP liposomes because they showed greater rates of fusion.

Different concentrations of the engineered liposomes tagged with Rh-PE were incubated with HeLa cells and examined by flow cytometry. The results showed that all the cells exposed to the engineered liposomes were tagged; therefore, the liposomes were indeed interacting with the cells. As seen in other publications [197], the cells would only be able

to give a fluorescence signal if the tagged liposomes were interacting with the cells, had adsorbed onto the membrane or had been internalized. The fact that the signal was concentration-dependent demonstrated that the number of interactions between the liposomes and cells increased with the liposome concentration, which would be helpful for treatments involving engineered liposomes.

AFM observations of the HeLa cells showed changes after incubation with the engineered liposomes. In 40 minutes, the liposomes had covered all the surfaces, including the glass surface, as also seen in the adhesion images. Furthermore, the physical properties of the cell surface had changed, increasing their stiffness due to the interaction with the liposomes.

A force map of the central areas of the cell revealed a change in the Young's modulus value of the membranes, showing higher values after incubation with the liposomes. This is consistent with the findings obtained previously in this thesis [152] (Chapter 6), where HeLa-mimicking SLBs showed a similar behavior after incubation with the engineered liposomes, with the Young's modulus value of the SLBs increasing. Therefore, this confirmed changes in the cell membrane.

The values obtained for the HeLa cells without liposome treatment were similar to those reported in other studies, with some deviation due to the use of different cantilevers with different tips and stiffness [198,199].

These results also validated the HeLa-mimicking models as they behaved like HeLa cells.

After tagging liposomes with Rh-PE and encapsulating calcein at a self-quenching concentration [200], we observed the cell culture under a confocal microscope. This gave us interesting images showing the cells automatically starting to capture the liposomes from the first seconds they were added to the media by using their filopodia in addition to the fusion of the liposomes that had directly fallen onto the cells. The activity of the filopodia has been reported before and was intense from the first minutes until most of the liposomes had been captured [153]. Among the different movements of filopodia, that described as surfing has been reported to help viruses reach the lipid membrane easily

[201]. Therefore, we suggest that the capturing movements of filopodia increased the number of interactions between the engineered liposomes and the cells.

The first step in the interaction between the liposomes and the HeLa cells was adsorption onto the membrane, where they stayed attached. After 40 minutes, some liposomes had already entered the cell and started to liberate their calcein content, while some liposomes had been internalized into the membrane. Around this time frame, we were able to compare the observed results with the ones obtained from the FRET analysis in Chapter 6. Since almost all the liposomes were interacting with the cells, we concluded that the fusion percentage of 42.1% obtained with the FRET data, considering a one-to-one fusion event for the liposomes, was closer to what we could see occurring in the living cells when compared to the percentage calculated with the infinite dilution method.

After 24 h, most of the liposomes already internalized into the cell had liberated their calcein load. Again, at this time point, we could observe some liposomes inserted into the outer cell membrane. Cell uptake of liposomes is well documented since DOTAP has been used for cell transfection for a long time and some cells avidly take up cationic liposomes [202].

The engineered liposomes liberated their calcein load inside the cells. We assessed if the liposomes could work as nanocarriers and checked whether they were toxic to cells. Therefore, we performed viability assays where we tested blank liposomes to evaluate their toxicity. We also used a batch of engineered liposomes encapsulating MTX, which is toxic to cells. Since the encapsulated MTX is located in the aqueous core of the liposome, we needed to filter the liposomes to eliminate any non-encapsulated MTX. Therefore, a batch of only MTX in buffer was also filtered to corroborate that the filtration process was successful and no free MTX remained in the media.

The results showed that the engineered liposomes encapsulating MTX killed the cells, demonstrating their use as drug nanocarriers. The unloaded or blank liposomes showed no toxicity at all compared to the negative control, demonstrating that the liposomes were not

toxic. This is important since this could allow the engineered liposome formulation to be used for developing treatments in humans.

Finally, the filtered MTX sample produced no cell death, even with doses far higher than the ones used with the encapsulated MTX into the engineered liposomes. To corroborate these results, the buffer solution after liposome precipitation by centrifugation was quantified by spectrophotometry and no traces of MTX were found.

Using a spectrophotometer to quantify the amount of encapsulated MTX and staining with the Marshall dye to quantify the number of phospholipids in the liposomes, we obtained an MTX-to-lipid ratio of 0.20, which consolidated the fact that the engineered liposomes were able to encapsulate MTX.

Therefore, we corroborated the use of the engineered liposomes as drug carriers. Summing up all the previous results, using a bottom-up approach, we developed functional and biomimetic liposomes that were able to fuse with and be internalized into cells and work as nanocarriers.

## General discussion

This thesis had two complementary research lines: (i) to establish a rational design based on the physicochemical properties of lipids to create engineered POPC:CHOL:DOTAP (0.65:0.15:0.20, mol/mol/mol) liposomes that can work as effective nanocarriers; and (ii) to develop a membrane model that reproduces the lipid membrane of HeLa cells with the composition POPC:POPE:POPS:CHOL (0.29:0.31:0.06:0.34, mol/mol/mol/mol). The HeLa-mimicking mixture provides a simple scenario to test the fusion of engineered liposomes and the release of their encapsulated content prior to investigations with living cells.

We exploited a bottom-up approach by evaluating the thermodynamic properties of the lipid components of the systems, before optimizing their composition and finally creating liposomes and SLBs.

For the POPC:CHOL:DOTAP liposomes, we first started by evaluating several PC candidates with different hydrocarbon chain lengths and degree of unsaturation to study their interaction with CHOL at different concentrations that abolished their  $L_{\beta}$  to  $L_{\alpha}$  phase transition in binary bilayers. We observed negative  $\Delta_{\text{mix}}G$  values for mixtures of POPC and CHOL, in which CHOL had a condensation effect on POPC. These results, together with the observation that there were no double collapses in the mixed monolayer, suggested that CHOL was dissolved to some extent in the mixed monolayer. Interestingly, AFM revealed the formation of small high domains in the monolayers of POPC with CHOL, while pure POPC did not show domains, but homogeneous LBs. Although no phase separation was detected in the monolayers, the visualization of the domains by AFM suggested segregation. The presence of these domains in the monolayer could be due to the formation of CHOL-enriched domains, which would make sense according to the BAM observations. To promote the electrostatic interaction between membranes, we added the cationic lipid DOTAP, which could help mediate the fusion events between liposomes and negatively-charged cell membranes such as the HeLa cell lipid membrane.



Before testing the liposomes with living cells, i.e., complex systems with many different lipids and proteins, we created and evaluated a simple membrane model to perform physicochemical studies with the engineered liposomes. Moreover, we needed to verify if this membrane model was able to mimic the natural behavior of the HeLa cell membrane.

We created a mixture based on the composition of the HeLa cell membrane, which was composed of POPC, POPE, POPS and CHOL.

CHOL also had a condensation effect in the HeLa-mimicking monolayer. The LBs observed with AFM showed domains probably due to the presence of CHOL, like in the POPC:CHOL mixture. The deposition of HeLa-mimicking liposomes onto a mica substrate created SLBs that, when visualized with AFM, showed a homogeneous bilayer like the other mixtures rich in CHOL. Interestingly, the domains observed in the monolayer system disappeared in the bilayer system, probably due to an internal reorganization between CHOL and POPC as well as the fact that we observed polar heads instead of hydrophobic tails in the SLBs.

BAM images of the HeLa-mimicking monolayer showed the existence of domains, which were at the micrometric scale compared to the nanometric scale of the AFM images. These results showed that the HeLa-mimicking monolayer was indeed not homogeneous and showed two different levels of organization at the temperature studied.

AFM characterization of the SLBs formed with the HeLa-mimicking lipid mixture showed flat featureless surfaces where some defects were intentionally left through an incomplete SLB formation. After the addition of the engineered liposomes, the holes started to close as the engineered liposomes fused with the SLB surface. The holes closed in the direction from the outer edges to the center and no liposome deposition was observed inside the holes. This indicated that the engineered liposomes were fusing with the HeLa-mimicking bilayer and laterally pushing the membrane, making it close the holes as it grew.

In addition, the  $E$  values obtained with AFM-FS for the HeLa-mimicking SLBs before and after incubation with the engineered liposomes demonstrated the occurrence of fusion, as reflected by the increase in the  $E$  value of the HeLa-mimicking bilayer after the incorporation of the liposomes.

FRET assays corroborated the fusion process between HeLa-mimicking liposomes and the engineered liposomes. The fusion rate was quantified at around 42% during an hour.

The final step was to study the interaction of the engineered liposomes with HeLa cells.

AFM observations in the force mode allowed us to calculate the  $E$  mean value of a HeLa cell before and after incubation with the engineered liposomes. The results showed an increase in the  $E$  values, illustrating a similar trend to that observed with the HeLa-mimicking SLBs [152] (Chapter 6). This confirmed that the modification of the cell membrane by liposomes was similar to that observed with the HeLa-mimicking SLBs, proving that the membrane model could mimic a HeLa cell membrane.

Observing the interactions of cells with the engineered liposomes through confocal microscopy, we observed that at the beginning, some liposomes were captured by the filopodia of the cells, while others were simply deposited directly onto the cell surface. As time passed, the liposomes were adsorbed onto the membrane. Finally, some liposomes remained integrated within the membrane, while the majority had already entered the cell, releasing their calcein load.

As a proof of concept, we encapsulated MTX to test the liposomes as drug carriers. The evaluation of the encapsulation showed an MTX-to-lipid ratio of 0.20 (weight/weight). After incubating HeLa cells with the engineered liposomes carrying MTX, the cells did not survive, demonstrating the effectiveness of the engineered liposomes as drug carriers.

In addition, the toxicity of the engineered liposomes was evaluated with unloaded liposomes, which were incubated in the same experimental conditions. Incubation of cells with these liposomes produced viability results similar to those of the negative control, demonstrating that the engineered liposomes were not toxic.

These assays demonstrated that the engineered liposomes were indeed able to work as nanocarriers. Furthermore, the changes in the HeLa cells observed with AFM-FS were similar to those of the HeLa-mimicking model membrane, validating the usefulness of this new testing tool.

## Chapter 9. Conclusions and perspectives

### Conclusions

- The mixture of POPC and cholesterol was demonstrated to be the most appropriate for the development of engineered liposomes, showing low absolute values of  $\Delta_{\text{mix}}G$ . Furthermore, there is one saturated hydrocarbon chain and one hydrocarbon chain with one unsaturation in POPC, which are the most common structures of phospholipids in natural extracts. DOTAP was also included in the formulation because of its well-known fusogenic properties. POPC:CHOL:DOTAP (0.65:0.15:0.20, mol/mol/mol) liposomes were not toxic to cells and they showed great capacity in encapsulating calcein at a self-quenching concentration and methotrexate at a drug-to-lipid ratio of 0.20.
- We developed an artificial membrane model with the composition POPC:POPE:POPS:CHOL (0.29:0.31:0.06:0.34, mol/mol/mol/mol) that mimicked the properties of HeLa cell lipid membranes.
- POPC:CHOL:DOTAP liposomes positively interacted with monolayers, supported lipid bilayers and liposomes formed with the HeLa-mimicking composition, as demonstrated by Langmuir isotherms, Brewster angle microscopy, atomic force microscopy and fluorescence techniques.
- All the results supported a fusion process occurring between the engineered liposomes and the target HeLa-mimicking model.

- Lipids from the POPC:CHOL:DOTAP liposomes were integrated into the HeLa-mimicking model. In addition, fluorescence resonance energy transfer assays allowed us to quantify this fusion process, which demonstrated that 42% of the liposomes had fused with cell membranes in 60 minutes.
- The plasma membrane of HeLa cells showed different Young's modulus values before and after incubation with the POPC:CHOL:DOTAP liposomes, as determined with the AFM-FS studies.
- Confocal microscopy was used to image the interaction between the liposomes and HeLa cells. The liposomes reached the cell cytoplasm by either deposition or capture by the filopodia of the cells. After 40 minutes, most of the liposomes were in the cell membrane. After 24 h, almost all of these liposomes had been internalized and had liberated their calcein load inside the cell.
- Viability experiments showed that MTX was encapsulated by the engineered liposomes, later killing all the HeLa cells after being liberated from the liposomes.

## Perspectives

The findings from this work can be built on in future projects. This work opens up a wide variety of possibilities for both the engineered POPC:CHOL:DOTAP liposomes and the HeLa-mimicking membrane models.

To reach the final goal of the presented work, *in vivo* assays should be undertaken to determine the biodistribution and bioavailability of the liposomes. Further efforts should be made to develop physicochemically stable liposomes, which include additional components that can overcome the reticuloendothelial system.

Furthermore, it will be interesting to work on the addition of antibodies or other components like the spike (S) protein of SARS-CoV-2 to modify the fusogenic capabilities of liposomes. With this modification, we will be able to direct liposomes to specific target membrane receptors.

Another option will be to implement liposomes with different compositions, using their lipid nature to create delivery systems that can cross the blood-brain barrier.

As the HeLa-mimicking mixture was able to mimic some aspects of the HeLa cell membrane, it could be used as a model to test other formulations. In addition, the creation of similar systems mimicking other cell membranes could increase the knowledge on how membrane fusion processes work in different cells and tissues.





## Chapter 10. References

- [1] H.J. Morowitz, *Beginning of Cellular Life. Metabolism Recapitulates Biogenesis*, 2004.
- [2] S.J. Singer, G. Nicolson, *The Fluid Mosaic Model of the Structure of Cell Membranes*, *Science*. 175 (1972) 720–731.
- [3] J. Yu, D.A. Fischman, T.L. Steck, *Selective solubilization of proteins and phospholipids from red blood cell membranes by nonionic detergents*, *J. Supramol. Struct.* 1 (1973) 233–248.
- [4] K. Simons, W.L.C. Vaz, *Model systems, lipid rafts, and cell membranes*, *Annu. Rev. Biophys. Biomol. Struct.* 33 (2004) 269–295.
- [5] D.A. Brown, E. London, *Structure and function of sphingolipid- and cholesterol-rich membrane rafts*, *J. Biol. Chem.* 275 (2000) 17221–17224.
- [6] S. Rauch, O.T. Fackler, *Viruses, lipid rafts and signal transduction*, *Signal Transduct.* 7 (2007) 53–63.
- [7] W. Dowhan, H. Vitrac, M. Bogdanov, *Lipid-Assisted Membrane Protein Folding and Topogenesis*, *Protein J.* 38 (2019) 274–288.
- [8] H. Sandermann, *Regulation of membrane enzymes by lipids*, *BBA - Rev. Biomembr.* 515 (1978) 209–237.
- [9] R.N. McElhaney, *Membrane Lipid Fluidity, Phase State, and Membrane Function in Prokaryotic Microorganisms*, in: *Membr. Fluidity Biol.*, Elsevier, 1985: pp. 147–208.
- [10] L.J. Pike, *Rafts defined: A report on the Keystone symposium on lipid rafts and cell function*, *J. Lipid Res.* 47 (2006) 1597–1598.
- [11] R. Raghupathy, A. Anupama Ambika Anilkumar Polley, P.P. Singh, M. Yadav, C. Johnson, S. Suryawanshi, V. Saikam, A.P. Sanghapal D. Sawant, Z. Guo, V.R. A., M. Rao, S. Mayor, *Transbilayer Lipid Interactions Mediate Nanoclustering of Lipid-Anchored Proteins*, *Cell*. 161 (2016) 581–594.

- [12] G. Nicolson, Update of the 1972 Singer-Nicolson Fluid-Mosaic Model of Membrane Structure, *Discoveries*. 1 (2013) e3.
- [13] E. Sezgin, I. Levental, S. Mayor, C. Eggeling, The mystery of membrane organization: composition, regulation and roles of lipid rafts, *Nat. Rev. Mol. Cell Biol.* 18 (2017) 361–374.
- [14] H. Barelli, B. Antonny, Lipid unsaturation and organelle dynamics, *Curr. Opin. Cell Biol.* 41 (2016) 25–32.
- [15] J.C.M. Holthuis, A.K. Menon, Lipid landscapes and pipelines in membrane homeostasis, *Nature*. 510 (2014) 48–57.
- [16] K. Zarringhalam, L. Zhang, M.A. Kiebish, K. Yang, X. Han, R.W. Gross, J. Chuang, Statistical analysis of the processes controlling choline and ethanolamine glycerophospholipid molecular species composition, *PLoS One*. 7 (2012) 1–13.
- [17] B. Alberts, A. Johnson, J. Lewis, M. Raff, K. Roberts, P. Walter, *Molecular Biology of the Cell*. 4th edition, Garland Science, New York, 2002.
- [18] F.M. Goñi, The basic structure and dynamics of cell membranes: An update of the Singer-Nicolson model, *Biochim. Biophys. Acta - Biomembr.* 1838 (2014) 1467–1476.
- [19] P.R. Bergethon, *The Physical Basis of Biochemistry*, Springer New York, New York, NY, 2010.
- [20] C. Tanford, *The hydrophobic effect: formation of micelles and biological membranes*, J. Wiley, New York, NY, 1973.
- [21] J.N. Israelachvili, D.J. Mitchell, B.W. Ninham, Theory of self-assembly of lipid bilayers and vesicles, *Biochim. Biophys. Acta - Biomembr.* 470 (1977) 185–201.
- [22] R.N.A.H. Lewis, D.A. Mannock, R.N. Mcelhaney, Membrane Lipid Molecular Structure and Polymorphism, in: R.M. Epand (Ed.), *Curr. Top. Membr.*, 1997: pp. 25–102.

- [23] R. Koynova, M. Caffrey, An index of lipid phase diagrams, *Chem. Phys. Lipids.* 115 (2002) 107–219.
- [24] H.J. Kaiser, D. Lingwood, I. Levental, J.L. Sampaio, L. Kalvodova, L. Rajendran, K. Simons, Order of lipid phases in model and plasma membranes, *Proc. Natl. Acad. Sci. U. S. A.* 106 (2009) 16645–16650.
- [25] T.P. Begley, R. Koynova, B. Tenchov, *Lipids: Phase Transitions*, Wiley Encycl. Chem. Biol. (2008).
- [26] J. Wilschut, D. Hoekstra, *Membrane fusion*, CRC Press, New York, NY, 1991.
- [27] H. Möhwald, Phospholipid Monolayers, in: *Handb. Biol. Phys.*, 1995: pp. 161–211.
- [28] P.L. Yeagle, Chapter 10 – Membrane Proteins, Academic Press Inc., University of Connecticut, Storrs, CT, USA, 2016.
- [29] M.F. Brown, Curvature Forces in Membrane Lipid–Protein Interactions, *Biochemistry.* 51 (2012) 9782–9795.
- [30] D. Marsh, Elastic curvature constants of lipid monolayers and bilayers, *Chem. Phys. Lipids.* 144 (2006) 146–159.
- [31] M.M. Elmer-Dixon, Z. Xie, J.B. Alverson, N.D. Priestley, B.E. Bowler, Curvature-Dependent Binding of Cytochrome c to Cardiolipin, *J. Am. Chem. Soc.* 142 (2020) 19532–19539.
- [32] H. Li, G. Lykotrafitis, Erythrocyte Membrane Model with Explicit Description of the Lipid Bilayer and the Spectrin Network, *Biophys. J.* 107 (2014) 642–653.
- [33] K.R. Vinothkumar, R. Henderson, *Structures of membrane proteins*, 2010.
- [34] H.R. Kaback, A chemiosmotic mechanism of symport, *Proc. Natl. Acad. Sci.* 112 (2015) 1259–1264.
- [35] T.K.M. Nyholm, S. Özdirekcan, J. Antoinette Killian, How protein transmembrane segments sense the lipid environment, *Biochemistry.* 46 (2007) 1457–1465.

- [36] E.J. Denning, O. Beckstein, Influence of lipids on protein-mediated transmembrane transport, *Chem. Phys. Lipids*. 169 (2013) 57–71.
- [37] O.S. Andersen, R.E. Koeppe, Bilayer Thickness and Membrane Protein Function: An Energetic Perspective, *Annu. Rev. Biophys. Biomol. Struct.* 36 (2007) 107–130.
- [38] V. Corradi, E. Mendez-Villuendas, H.I. Ingólfsson, R.X. Gu, I. Siuda, M.N. Melo, A. Moussatova, L.J. Degagné, B.I. Sejdiu, G. Singh, T.A. Wassenaar, K. Delgado Magnero, S.J. Marrink, D.P. Tieleman, Lipid-Protein Interactions Are Unique Fingerprints for Membrane Proteins, *ACS Cent. Sci.* 4 (2018) 709–717.
- [39] A.G. Lee, *Lipid-protein interactions in biological membranes: A structural perspective*, 2003.
- [40] D. Marsh, L.I. Horváth, Structure, dynamics and composition of the lipid-protein interface. Perspectives from spin-labelling, *Biochim. Biophys. Acta - Rev. Biomembr.* 1376 (1998) 267–296.
- [41] A.G. Lee, How lipids affect the activities of integral membrane proteins, *1666* (2004) 62–87.
- [42] H. Palsdottir, C. Hunte, Lipids in membrane protein structures, *1666* (2004) 2–18.
- [43] B. De Foresta, N. Legros, D. Plusquellec, M. Le Maire, P. Champeil, Brominated detergents as tools to study protein-detergent interactions, *Eur. J. Biochem.* 241 (1996) 343–354.
- [44] J. Corbin, H.H. Wang, M.P. Blanton, Identifying the cholesterol binding domain in the nicotinic acetylcholine receptor with [<sup>125</sup>I]azido-cholesterol, *Biochim. Biophys. Acta - Biomembr.* 1414 (1998) 65–74.
- [45] G.H. Addona, H. Sandermann, M.A. Kloczewiak, S.S. Husain, K.W. Miller, Where does cholesterol act during activation of the nicotinic acetylcholine receptor?, *Biochim. Biophys. Acta - Biomembr.* 1370 (1998) 299–309.

- [46] S.E. Rankin, G.H. Addona, M.A. Kloczewiak, B. Bugge, K.W. Miller, The Cholesterol Dependence of Activation and Fast Desensitization of the Nicotinic Acetylcholine Receptor, *73* (1997) 2446–2455.
- [47] W. Kleemann, H.M. McConnell, Interactions of proteins and cholesterol with lipids in bilayer membranes, *Biochim. Biophys. Acta - Biomembr.* 419 (1976) 206–222.
- [48] M. Jaworsky, R. Mendelsohn, Fourier-Transform Infrared Studies of CaATPase Partitioning in Phospholipid Mixtures of 1,2-Dipalmitoylphosphatidylcholine-d62 with 1-Palmitoyl-2-oleoylphosphatidylethanolamine and 1-Stearoyl-2-oleoylphosphatidylcholine, *Biochemistry.* 24 (1985) 3422–3428.
- [49] J.M. East, A.G. Lee, Lipid Selectivity of the Calcium and Magnesium Ion Dependent Adenosinetriphosphatase, Studied with Fluorescence Quenching by a Brominated Phospholipid, *Biochemistry.* 21 (1982) 4144–4151.
- [50] N.C. Robinson, L.H. Talbert, J. Zborowski, Cardiolipin-Depleted Bovine Heart Cytochrome c Oxidase: Binding Stoichiometry and Affinity for Cardiolipin Derivatives, *Biochemistry.* 29 (1990) 8962–8969.
- [51] S. Mall, R. Broadbridge, R.P. Sharma, A.G. Lee, J.M. East, Effects of aromatic residues at the ends of transmembrane  $\alpha$ -helices on helix interactions with lipid bilayers, *Biochemistry.* 39 (2000) 2071–2078.
- [52] R.J. Webb, J.M. East, R.P. Sharma, A.G. Lee, Hydrophobic mismatch and the incorporation of peptides into lipid bilayers: A possible mechanism for retention in the Golgi, *Biochemistry.* 37 (1998) 673–679.
- [53] J.A. Killian, Hydrophobic mismatch between proteins and lipids in membranes, *Biochim. Biophys. Acta - Rev. Biomembr.* 1376 (1998) 401–416.
- [54] A.H. O’Keeffe, J.M. East, A.G. Lee, Selectivity in lipid binding to the bacterial outer membrane protein OmpF, *Biophys. J.* 79 (2000) 2066–2074.

- [55] E. London, G.W. Feigenson, Fluorescence Quenching in Model Membranes. 2. Determination of the Local Lipid Environment of the Calcium Adenosinetriphosphatase from Sarcoplasmic Reticulum, *Biochemistry*. 20 (1981) 1939–1948.
- [56] I.M. Williamson, S.J. Alvis, J. Malcolm East, A.G. Lee, Interactions of phospholipids with the potassium channel KcsA, *Biophys. J.* 83 (2002) 2026–2038.
- [57] K. Scannell, The Immortal Life of Henrietta Lacks, *J. Leg. Med.* 31 (2010) 493–498.
- [58] J.P. Álvarez A., Henrietta Lacks. El nombre detrás de las células HeLa, primera línea celular inmortal humana, *Rev. Médica Clínica Las Condes*. 24 (2013) 726–729.
- [59] B.P. Lucey, W.A. Nelson-Rees, G.M. Hutchins, Henrietta Lacks, HeLa Cells, and Cell Culture Contamination, *Arch. Pathol. Lab. Med.* 133 (2009) 1463–1467.
- [60] K. Morigaki, Y. Tanimoto, Evolution and development of model membranes for physicochemical and functional studies of the membrane lateral heterogeneity, *Biochim. Biophys. Acta - Biomembr.* 1860 (2018) 2012–2017.
- [61] C. Suárez-Germà, L.M.S. Loura, M. Prieto, Ò. Domènech, M.T. Montero, A. Rodríguez-Banqueri, J.L. Vázquez-Ibar, J. Hernández-Borrell, Membrane protein-lipid selectivity: Enhancing sensitivity for modeling FRET data, *J. Phys. Chem. B.* 116 (2012) 2438–2445.
- [62] J.-B. Perez, K.L. Martinez, J.-M. Segura, H. Vogel, Supported Cell-Membrane Sheets for Functional Fluorescence Imaging of Membrane Proteins, *Adv. Funct. Mater.* 16 (2006) 306–312.
- [63] C. Danelon, J.-B. Perez, C. Santschi, J. Brugger, H. Vogel, Cell membranes suspended across nanoaperture arrays, *Langmuir*. 22 (2006) 22–5.
- [64] C. Yoshina-Ishii, S.G. Boxer, Arrays of mobile tethered vesicles on supported lipid bilayers, *J. Am. Chem. Soc.* 125 (2003) 3696–7.

- [65] C. Yoshina-Ishii, G.P. Miller, M.L. Kraft, E.T. Kool, S.G. Boxer, General method for modification of liposomes for encoded assembly on supported bilayers., *J. Am. Chem. Soc.* 127 (2005) 1356–7.
- [66] I. Pfeiffer, F. Höök, Bivalent cholesterol-based coupling of oligonucleotides to lipid membrane assemblies, *J. Am. Chem. Soc.* 126 (2004) 10224–5.
- [67] T.-Y. Yoon, B. Okumus, F. Zhang, Y.-K. Shin, T. Ha, Multiple intermediates in SNARE-induced membrane fusion, *Proc. Natl. Acad. Sci. U. S. A.* 103 (2006) 19731–6.
- [68] E. Rhoades, E. Gussakovsky, G. Haran, Watching proteins fold one molecule at a time, *Proc. Natl. Acad. Sci. U. S. A.* 100 (2003) 3197–202.
- [69] P.-Y. Bolinger, D. Stamou, H. Vogel, Integrated nanoreactor systems: triggering the release and mixing of compounds inside single vesicles., *J. Am. Chem. Soc.* 126 (2004) 8594–5.
- [70] A. Nath, W.M. Atkins, S.G. Sligar, Applications of phospholipid bilayer nanodiscs in the study of membranes and membrane proteins, *Biochemistry.* 46 (2007) 2059–69.
- [71] S. Bhat, M.G. Sorci-Thomas, R. Tuladhar, M.P. Samuel, M.J. Thomas, Conformational adaptation of apolipoprotein A-I to discretely sized phospholipid complexes, *Biochemistry.* 46 (2007) 7811–21.
- [72] G.S. Ayton, G.A. Voth, Multiscale simulation of transmembrane proteins, *J. Struct. Biol.* 157 (2007) 570–8.
- [73] Q. Shi, S. Izvekov, G.A. Voth, Mixed atomistic and coarse-grained molecular dynamics: simulation of a membrane-bound ion channel, *J. Phys. Chem. B.* 110 (2006) 15045–8.
- [74] V. Knecht, S.-J. Marrink, Molecular dynamics simulations of lipid vesicle fusion in atomic detail, *Biophys. J.* 92 (2007) 4254–61.
- [75] I.A. Chen, K. Salehi-Ashtiani, J.W. Szostak, RNA catalysis in model protocell vesicles., *J. Am. Chem. Soc.* 127 (2005) 13213–9.



- [76] A. Astefanei, O. Núñez, M.T. Galceran, Characterization and determination of fullerenes: A critical review, *Anal. Chim. Acta.* 882 (2015) 1–21.
- [77] S. Jain, D.G. Hirst, J.M. O’Sullivan, Gold nanoparticles as novel agents for cancer therapy, *Br. J. Radiol.* 85 (2012) 101–113.
- [78] T. Neuberger, B. Schöpf, H. Hofmann, M. Hofmann, B. von Rechenberg, Superparamagnetic nanoparticles for biomedical applications: Possibilities and limitations of a new drug delivery system, *J. Magn. Magn. Mater.* 293 (2005) 483–496.
- [79] J.A. O’Brien, S.C. Lummis, Nano-biostics: a method of biolistic transfection of cells and tissues using a gene gun with novel nanometer-sized projectiles, *BMC Biotechnol.* 11 (2011) 66.
- [80] W. Sigmund, J. Yuh, H. Park, V. Maneeratana, G. Pyrgiotakis, A. Daga, J. Taylor, J.C. Nino, Processing and Structure Relationships in Electrospinning of Ceramic Fiber Systems, *J. Am. Ceram. Soc.* 89 (2006) 395–407.
- [81] T. Hisatomi, J. Kubota, K. Domen, Recent advances in semiconductors for photocatalytic and photoelectrochemical water splitting, *Chem. Soc. Rev.* 43 (2014) 7520–7535.
- [82] Q. Sun, Y.A. Wang, L.S. Li, D. Wang, T. Zhu, J. Xu, C. Yang, Y. Li, Bright, multicoloured light-emitting diodes based on quantum dots, *Nat. Photonics.* 1 (2007) 717–722.
- [83] A. Botet-Carreras, C. Tamames-Tabar, F. Salles, S. Rojas, E. Imbuluzqueta, H. Lana, M.J. Blanco-Prieto, P. Horcajada, Improving the genistein oral bioavailability via its formulation into the metal–organic framework MIL-100(Fe), *J. Mater. Chem. B.* (2021).
- [84] H.C. Zhou, J.R. Long, O.M. Yaghi, Introduction to metal-organic frameworks, *Chem. Rev.* 112 (2012) 673–674.

- [85] J.R. Long, O.M. Yaghi, The pervasive chemistry of metal-organic frameworks, *Chem. Soc. Rev.* 38 (2009) 1213–1214.
- [86] Y. Dahman, N. Ashfaq, A. Ganesalingam, G. Kobalasingham, Nanoshells, in: *Nanotechnol. Funct. Mater. Eng.*, Elsevier, 2017: pp. 175–190.
- [87] S. Mukherjee, S. Ray, R.S. Thakur, Solid lipid nanoparticles: a modern formulation approach in drug delivery system, *Indian J. Pharm. Sci.* 71 (2009) 349–58.
- [88] R. Nisini, N. Poerio, S. Mariotti, F. De Santis, M. Fraziano, The Multirole of Liposomes in Therapy and Prevention of Infectious Diseases, *Front. Immunol.* 9 (2018) 155.
- [89] A.D. Bangham, M.M. Standish, J.C. Watkins, Diffusion of univalent ions across the lamellae of swollen phospholipids, *J. Mol. Biol.* 13 (1965) 238-IN27.
- [90] M.L. Vázquez-González, A. Botet-Carreras, Ò. Domènech, M. Teresa Montero, J.H. Borrell, Planar lipid bilayers formed from thermodynamically-optimized liposomes as new featured carriers for drug delivery systems through human skin, *Int. J. Pharm.* 563 (2019) 1–8.
- [91] M.R. Mozafari, Liposomes: an overview of manufacturing techniques, *Cell. Mol. Biol. Lett.* 10 (2005) 711–9.
- [92] H. Zhang, Thin-Film Hydration Followed by Extrusion Method for Liposome Preparation, in: *Lipidomics* by S. Bhattacharya, Sanjoy K, 2017: pp. 17–22.
- [93] R. Mendez, S. Banerjee, Sonication-Based Basic Protocol for Liposome Synthesis, in: *Lipidomics* by S. Bhattacharya, Sanjoy K, 2017: pp. 255–260.
- [94] J.. Treat, C. Huang, N. Damjanov, S. Walker, P. Drobins, P. Gokhale, M. Kopeski, G. Massimini, A. Rahman, Phase I trial in advanced malignancies with Liposome Encapsulated Paclitaxel (LEP), *Lung Cancer.* 29 (2000) 64.
- [95] D. Deamer, A.D. Bangham, Large volume liposomes by an ether vaporization method, *Biochim. Biophys. Acta - Biomembr.* 443 (1976) 629–634.

- [96] O. Zumbuehl, H.G. Weder, Liposomes of controllable size in the range of 40 to 180 nm by defined dialysis of lipid/detergent mixed micelles, *Biochim. Biophys. Acta.* 640 (1981) 252–62.
- [97] J.D. Castile, K.M. Taylor, Factors affecting the size distribution of liposomes produced by freeze–thaw extrusion, *Int. J. Pharm.* 188 (1999) 87–95.
- [98] C. Kirby, G. Gregoriadis, Dehydration-Rehydration Vesicles: A Simple Method for High Yield Drug Entrapment in Liposomes, *Nat. Biotechnol.* 2 (1984) 979–984.
- [99] N. Skalko-Basnet, Z. Pavelic, M. Becirevic-Lacan, Liposomes Containing Drug and Cyclodextrin Prepared by the One-Step Spray-Drying Method, *Drug Dev. Ind. Pharm.* 26 (2000) 1279–1284.
- [100] C. Li, Y. Deng, A novel method for the preparation of liposomes: Freeze drying of monophasic solutions, *J. Pharm. Sci.* 93 (2004) 1403–1414.
- [101] A. Wagner, K. Vorauer-Uhl, G. Kreismayr, H. Katinger, The crossflow injection technique: an improvement of the ethanol injection method, *J. Liposome Res.* 12 (2002) 259–70.
- [102] A. Jahn, W.N. Vreeland, D.L. DeVoe, L.E. Locascio, M. Gaitan, Microfluidic Directed Formation of Liposomes of Controlled Size, *Langmuir.* 23 (2007) 6289–6293.
- [103] C. Jaafar-Maalej, C. Charcosset, H. Fessi, A new method for liposome preparation using a membrane contactor, *J. Liposome Res.* 21 (2011) 213–220.
- [104] S. Mourdikoudis, R.M. Pallares, N.T.K. Thanh, Characterization techniques for nanoparticles: Comparison and complementarity upon studying nanoparticle properties, *Nanoscale.* 10 (2018) 12871–12934.
- [105] W. Barcellini, P. Bianchi, E. Fermo, F.G. Imperiali, A.P. Marcello, C. Vercellati, A. Zaninoni, A. Zanella, Hereditary red cell membrane defects: diagnostic and clinical aspects, *Blood Transfus.* 9 (2011) 274–7.

- [106] L. Da Costa, J. Galimand, O. Fenneteau, N. Mohandas, Hereditary spherocytosis, elliptocytosis, and other red cell membrane disorders, *Blood Rev.* 27 (2013) 167–178.
- [107] WHO, The molecular genetic epidemiology of cystic fibrosis Report of a joint meeting of, *World Heal. Organ.* (2004) 1–24.
- [108] C. Bombieri, M. Claustres, K. De Boeck, N. Derichs, J. Dodge, E. Girodon, I. Sermet, M. Schwarz, M. Tzetis, M. Wilschanski, C. Bareil, D. Bilton, C. Castellani, H. Cuppens, G.R. Cutting, P. Drevínek, P. Farrell, J.S. Elborn, K. Jarvi, B. Kerem, E. Kerem, M. Knowles, M. Macek, A. Munck, D. Radojkovic, M. Seia, D.N. Sheppard, K.W. Southern, M. Stuhmann, E. Tullis, J. Zielenski, P.F. Pignatti, C. Ferec, Recommendations for the classification of diseases as CFTR-related disorders, *J. Cyst. Fibros.* 10 (2011) S86–S102.
- [109] J. Rodríguez-Soriano, Bartter and related syndromes: the puzzle is almost solved, *Pediatr. Nephrol.* 12 (1998) 315–327.
- [110] M. Zaffanello, A. Taranta, A. Palma, A. Bettinelli, G.L. Marseglia, F. Emma, Type IV Bartter syndrome: report of two new cases, *Pediatr. Nephrol.* 21 (2006) 766–770.
- [111] G. Sesti, M. Federici, D. Lauro, P. Sbraccia, R. Lauro, Molecular mechanism of insulin resistance in type 2 diabetes mellitus: role of the insulin receptor variant forms, *Diabetes. Metab. Res. Rev.* 17 (2001) 363–373.
- [112] C. Brännmark, E. Nyman, S. Fagerholm, L. Bergenholm, E.-M. Ekstrand, G. Cedersund, P. Strålfors, Insulin Signaling in Type 2 Diabetes, *J. Biol. Chem.* 288 (2013) 9867–9880.
- [113] S. Fröjdö, H. Vidal, L. Pirola, Alterations of insulin signaling in type 2 diabetes: A review of the current evidence from humans, *Biochim. Biophys. Acta - Mol. Basis Dis.* 1792 (2009) 83–92.
- [114] D. Marsh, Lateral pressure in membranes, *Biochim. Biophys. Acta - Rev. Biomembr.* 1286 (1996) 183–223.

- [115] A. Blume, A comparative study of the phase transitions of phospholipid bilayers and monolayers, *Biochim. Biophys. Acta - Biomembr.* 557 (1979) 32–44.
- [116] K. Przykaza, K. Woźniak, M. Jurak, A.E. Wiącek, R. Mroczka, Properties of the Langmuir and Langmuir–Blodgett monolayers of cholesterol-cyclosporine A on water and polymer support, *Adsorption.* 25 (2019) 923–936.
- [117] G. Binnig, H. Rohrer, Scanning tunneling microscopy, *Surf. Sci.* 126 (1983) 236–244.
- [118] C. Gerber, H.P. Lang, How the doors to the nanoworld were opened, *Nat. Nanotechnol.* 1 (2006) 3–5.
- [119] C. Pimenta-Lopes, C. Suay-Corredera, D. Velázquez-Carreras, D. Sánchez-Ortiz, J. Alegre-Cebollada, Concurrent atomic force spectroscopy, *Commun. Phys.* 2 (2019) 91.
- [120] H.-J. Butt, Measuring electrostatic, van der Waals, and hydration forces in electrolyte solutions with an atomic force microscope, *Biophys. J.* 60 (1991) 1438–1444.
- [121] S. Garcia-Manyes, L. Redondo-Morata, G. Oncins, F. Sanz, Nanomechanics of Lipid Bilayers: Heads or Tails?, *J. Am. Chem. Soc.* 132 (2010) 12874–12886.
- [122] M.D. Houslay, K.K. Stanley, Dynamics of Biological Membranes, *Biochem. Educ.* 11 (1983) 157.
- [123] J. Peters, J. Marion, F.J. Becher, M. Trapp, T. Gutberlet, D.J. Bicout, T. Heimburg, Thermodynamics of lipid multi-lamellar vesicles in presence of sterols at high hydrostatic pressure, *Sci. Rep.* 7 (2017) 15339.
- [124] J. Hernández-Borrell, K.M.W. Keough, Heteroacid phosphatidylcholines with different amounts of unsaturation respond differently to cholesterol, *Biochim. Biophys. Acta - Biomembr.* 1153 (1993) 277–282.
- [125] F. He, Y. Lin, R. Li, G. Tang, D. Wu, Effects of lipid chain length on the surface properties of alkylaminomethyl rutin and of its mixture with model lecithin membrane, *Colloids Surfaces B Biointerfaces.* 87 (2011) 164–172.

- [126] Y. Ikeda, M. Inagaki, K. Yamada, T. Miyamoto, R. Higuchi, O. Shibata, Langmuir monolayers of cerebroside with different head groups originated from sea cucumber: Binary systems with dipalmitoylphosphatidylcholine (DPPC), *Colloids Surfaces B Biointerfaces*. 72 (2009) 272–283.
- [127] K. Hoda, H. Nakahara, S. Nakamura, S. Nagadome, G. Sugihara, N. Yoshino, O. Shibata, Langmuir monolayer properties of the fluorinated-hydrogenated hybrid amphiphiles with dipalmitoylphosphatidylcholine (DPPC), *Colloids Surfaces B Biointerfaces*. 47 (2006) 165–175.
- [128] H. Nakahara, S. Nakamura, K. Nakamura, M. Inagaki, M. Aso, R. Higuchi, O. Shibata, Cerebroside Langmuir monolayers originated from the echinoderms, *Colloids Surfaces B Biointerfaces*. 42 (2005) 157–174.
- [129] T. Hiranita, S. Nakamura, M. Kawachi, H.M. Courrier, T.F. Vandamme, M.P. Krafft, O. Shibata, Miscibility behavior of dipalmitoylphosphatidylcholine with a single-chain partially fluorinated amphiphile in Langmuir monolayers, *J. Colloid Interface Sci.* 265 (2003) 83–92.
- [130] J. Stetefeld, S.A. McKenna, T.R. Patel, Dynamic light scattering: a practical guide and applications in biomedical sciences, *Biophys. Rev.* 8 (2016) 409–427.
- [131] X. Li, Y.-J. Yuan, Lipidomic Analysis of Apoptotic Hela Cells Induced by Paclitaxel, *Omi. A J. Integr. Biol.* 15 (2011) 655–664.
- [132] M.L. Torgersen, T.I. Klock, S. Kavaliauskiene, C. Klose, K. Simons, T. Skotland, K. Sandvig, The anti-tumor drug 2-hydroxyoleic acid (Minerval) stimulates signaling and retrograde transport, *Oncotarget*. 7 (2016).
- [133] M.J. Gerl, V. Bittl, S. Kirchner, T. Sachsenheimer, H.L. Brunner, C. Luchtenborg, C. Özbalci, H. Wiedemann, S. Wegehangel, W. Nickel, P. Haberkant, C. Schultz, M. Krüger, B. Brügger, Sphingosine-1-phosphate lyase deficient cells as a tool to study protein lipid interactions, *PLoS One*. 11 (2016).

- [134] M. Lorizate, T. Sachsenheimer, B. Glass, A. Habermann, M.J. Gerl, H.G. Kräusslich, B. Brügger, Comparative lipidomics analysis of HIV-1 particles and their producer cell membrane in different cell lines, *Cell. Microbiol.* (2013).
- [135] J.T. Davies, *Interfacial phenomena*, 1st ed., Academic Press Inc., New York, 1963.
- [136] A. Botet-Carreras, M.T. Montero, Ò. Domènech, J.H. Borrell, Effect of cholesterol on monolayer structure of different acyl chained phospholipids, *Colloids Surfaces B Biointerfaces*. 174 (2019) 374–383.
- [137] O. V Bondar, D. V Saifullina, I.I. Shakhmaeva, I.I. Mavlyutova, T.I. Abdullin, Monitoring of the Zeta Potential of Human Cells upon Reduction in Their Viability and Interaction with Polymers., *Acta Naturae*. 4 (2012) 78–81.
- [138] Y. Yang, F. Shi, J. Zhou, X. Shi, Y. Sha, H. Wu, Short-Term Dynamic Observation of the Color Change and Enhancement Effect of Polyethylenimine-Entrapped Gold Nanoparticles Used for Indirect Lymphography, *ORL*. 78 (2016) 136–143.
- [139] O. Biner, T. Schick, Y. Müller, C. von Ballmoos, Delivery of membrane proteins into small and giant unilamellar vesicles by charge-mediated fusion, *FEBS Lett.* (2016).
- [140] M. Shinitzky, Y. Barenholz, Fluidity parameters of lipid regions determined by fluorescence polarization, *BBA-Biomembranes*. 515 (1978) 367–394.
- [141] T. Kure, H. Sakai, Transmembrane Difference in Colloid Osmotic Pressure Affects the Lipid Membrane Fluidity of Liposomes Encapsulating a Concentrated Protein Solution, *Langmuir*. 33 (2017) 1533–1540.
- [142] J. Sot, I. Esnal, B.G. Monasterio, R. León-Irra, Y. Niko, F.M. Goñi, A. Klymchenko, A. Alonso, Phase-selective staining of model and cell membranes, lipid droplets and lipoproteins with fluorescent solvatochromic pyrene probes, *BBA-Biomembranes*. 1863 (2021) 183470.
- [143] P. Pathak, E. London, The Effect of Membrane Lipid Composition on the Formation of Lipid Ultrananodomains, *Biophys. J.* 109 (2015) 1630–1638.



- [144] C. François-Martin, F. Pincet, Actual fusion efficiency in the lipid mixing assay - Comparison between nanodiscs and liposomes, *Sci. Rep.* 7 (2017) 43860.
- [145] G.E. Tranter, Fluorescence Polarization and Anisotropy, in: *Encycl. Spectrosc. Spectrom.*, Elsevier, 1999: pp. 571–573.
- [146] A. Jain, C. Blum, V. Subramaniam, Fluorescence Lifetime Spectroscopy and Imaging of Visible Fluorescent Proteins, in: *Adv. Biomed. Eng.*, First Edit, Elsevier, 2009: pp. 147–176.
- [147] J.R. Lakowicz, Measurement of Fluorescence Lifetimes, in: *Princ. Fluoresc. Spectrosc.*, Springer US, Boston, MA, 1983: pp. 51–93.
- [148] J. J. Roa, G. Oncins, J. Diaz, F. Sanz, M. Segarra, Calculation of Young's Modulus Value by Means of AFM, *Recent Pat Nanotech.* 5 (2011) 27–36.
- [149] L. Picas, F. Rico, S. Scheuring, Direct Measurement of the Mechanical Properties of Lipid Phases in Supported Bilayers, *Biophys. J.* 102 (2012) L01–L03.
- [150] M. Radmacher, Studying the Mechanics of Cellular Processes by Atomic Force Microscopy, in: *Methods Cell Biol.*, 2007: pp. 347–372.
- [151] J.C.M. Stewart, Colorimetric determination of phospholipids with ammonium ferrothiocyanate, *Anal. Biochem.* 104 (1980) 10–14.
- [152] A. Botet-Carreras, M.T. Montero, J. Sot, Ò. Domènech, J.H. Borrell, Engineering and development of model lipid membranes mimicking the HeLa cell membrane, *Colloids Surfaces A Physicochem. Eng. Asp.* 630 (2021) 127663.
- [153] W. Heusermann, J. Hean, D. Trojer, E. Steib, S. von Bueren, A. Graff-Meyer, C. Genoud, K. Martin, N. Pizzato, J. Voshol, D. V. Morrissey, S.E.L. Andaloussi, M.J. Wood, N.C. Meisner-Kober, Exosomes surf on filopodia to enter cells at endocytic hot spots, traffic within endosomes, and are targeted to the ER, *J. Cell Biol.* 213 (2016) 173–184.

- [154] J.M. Smaby, M.M. Momsen, H.L. Brockman, R.E. Brown, Phosphatidylcholine acyl unsaturation modulates the decrease in interfacial elasticity induced by cholesterol, *Biophys. J.* 73 (1997) 1492–1505.
- [155] P. Wydro, S. Knapczyk, M. Łapczyńska, Variations in the Condensing Effect of Cholesterol on Saturated versus Unsaturated Phosphatidylcholines at Low and High Sterol Concentration, *Langmuir.* 27 (2011) 5433–5444.
- [156] P. Dynarowicz-Łątka, K. Hąc-Wydro, Interactions between phosphatidylcholines and cholesterol in monolayers at the air/water interface, *Colloids Surfaces B Biointerfaces.* 37 (2004) 21–25.
- [157] S. Ali, J.M. Smaby, M.M. Momsen, H.L. Brockman, R.E. Brown, Acyl Chain-Length Asymmetry Alters the Interfacial Elastic Interactions of Phosphatidylcholines, *Biophys. J.* 74 (1998) 338–348.
- [158] O. Bouffieux, A. Berquand, M. Eeman, M. Paquot, Y.F. Dufrêne, R. Brasseur, M. Deleu, Molecular organization of surfactin–phospholipid monolayers: Effect of phospholipid chain length and polar head, *Biochim. Biophys. Acta - Biomembr.* 1768 (2007) 1758–1768.
- [159] T.-H. Chou, C.-H. Chang, Thermodynamic behavior and relaxation processes of mixed DPPC/cholesterol monolayers at the air/water interface, *Colloids Surfaces B Biointerfaces.* 17 (2000) 71–79.
- [160] K. Kim, C. Kim, Y. Byun, Preparation of a Dipalmitoylphosphatidylcholine/Cholesterol Langmuir–Blodgett Monolayer That Suppresses Protein Adsorption, *Langmuir.* 17 (2001) 5066–5070.
- [161] M.C. Phillips, D. Chapman, Monolayer characteristics of saturated 1,2-diacyl phosphatidylcholines (lecithins) and phosphatidylethanolamines at the air-water interface, *Biochim. Biophys. Acta - Biomembr.* 163 (1968) 301–313.

- [162] K. Gong, S.-S. Feng, M.L. Go, P.H. Soew, Effects of pH on the stability and compressibility of DPPC/cholesterol monolayers at the air–water interface, *Colloids Surfaces A Physicochem. Eng. Asp.* 207 (2002) 113–125.
- [163] M. Jurak, Thermodynamic Aspects of Cholesterol Effect on Properties of Phospholipid Monolayers: Langmuir and Langmuir–Blodgett Monolayer Study, *J. Phys. Chem. B.* 117 (2013) 3496–3502.
- [164] J. Huang, G.W. Feigenson, A Microscopic Interaction Model of Maximum Solubility of Cholesterol in Lipid Bilayers, *Biophys. J.* 76 (1999) 2142–2157.
- [165] P.R. Adhyapak, S. V. Panchal, A.V.R. Murthy, Cholesterol induced asymmetry in DOPC bilayers probed by AFM force spectroscopy, *Biochim. Biophys. Acta - Biomembr.* 1860 (2018) 953–959.
- [166] T. Starke-Peterkovic, N. Turner, M.F. Vitha, M.P. Waller, D.E. Hibbs, R.J. Clarke, Cholesterol Effect on the Dipole Potential of Lipid Membranes, *Biophys. J.* 90 (2006) 4060–4070.
- [167] L. Zhao, S.-S. Feng, Effects of cholesterol component on molecular interactions between paclitaxel and phospholipid within the lipid monolayer at the air–water interface, *J. Colloid Interface Sci.* 300 (2006) 314–326.
- [168] K. Kim, S.Q. Choi, Z.A. Zell, T.M. Squires, J.A. Zasadzinski, Effect of cholesterol nanodomains on monolayer morphology and dynamics, *Proc. Natl. Acad. Sci.* 110 (2013) E3054–E3060.
- [169] L. Picas, M.T. Montero, A. Morros, M.E. Cabañas, B. Seantier, P.-E. Milhiet, J. Hernández-Borrell, Calcium-Induced Formation of Subdomains in Phosphatidylethanolamine–Phosphatidylglycerol Bilayers: A Combined DSC, <sup>31</sup>P NMR, and AFM Study, *J. Phys. Chem. B.* 113 (2009) 4648–4655.
- [170] L.A. Worthman, K. Nag, P.J. Davis, K.M. Keough, Cholesterol in condensed and fluid phosphatidylcholine monolayers studied by epifluorescence microscopy, *Biophys. J.* 72 (1997) 2569–2580.

- [171] C.E.H. Berger, K.O. van der Werf, R.P.H. Kooyman, B.G. de Groot, J. Greve, Functional Group Imaging by Adhesion AFM Applied to Lipid Monolayers, *Langmuir*. 11 (1995) 4188–4192.
- [172] C. Suárez-Germà, Ò. Domènech, M.T. Montero, J. Hernández-Borrell, Effect of lactose permease presence on the structure and nanomechanics of two-component supported lipid bilayers, *Biochim. Biophys. Acta - Biomembr.* 1838 (2014) 842–852.
- [173] Y. Niko, S. Kawauchi, G. Konishi, Solvatochromic Pyrene Analogues of Prodan Exhibiting Extremely High Fluorescence Quantum Yields in Apolar and Polar Solvents, *Chem-Eur J.* 19 (2013) 9760–9765.
- [174] G. van Meer, D.R. Voelker, G.W. Feigenson, Membrane lipids: where they are and how they behave, *Nat. Rev. Mol. Cell Biol.* 9 (2008) 112–124.
- [175] M.D. Houslay, K.K. Stanley, *Dynamics of Biological Membranes*, John & Wiley Sons, Chichester, 1983.
- [176] T. Baumgart, S.T. Hess, W.W. Webb, Imaging coexisting fluid domains in biomembrane models coupling curvature and line tension, *Nature*. 425 (2003) 821–824.
- [177] Ò. Domènech, J. Ignés-Mullol, M.T. Montero, J. Hernández-Borrell, Unveiling a Complex Phase Transition in Monolayers of a Phospholipid from the Annular Region of Transmembrane Proteins, *J. Phys. Chem. B.* 111 (2007) 10946–10951.
- [178] P.L. Felgner, T.R. Gadek, M. Holm, R. Roman, H.W. Chan, M. Wenz, J.P. Northrop, G.M. Ringold, M. Danielsen, Lipofection: a highly efficient, lipid-mediated DNA-transfection procedure, *Proc. Natl. Acad. Sci.* 84 (1987) 7413–7417.
- [179] P.L. Felgner, G.M. Ringold, Cationic liposome-mediated transfection, *Nature*. 337 (1989) 387–388.

- [180] Ò. Domènech, A. Morros, M.E. Cabañas, M. Teresa Montero, J. Hernández-Borrell, Supported planar bilayers from hexagonal phases, *Biochim. Biophys. Acta - Biomembr.* 1768 (2007) 100–106.
- [181] M. Jedynak, R. Worch, M. Podsiadła-Białoskórska, J. Chroboczek, E. Szotajska, Cholesterol and phosphatidylserine are engaged in adenoviral dodecahedron endocytosis, *Biochim. Biophys. Acta - Biomembr.* 1860 (2018) 2215–2223.
- [182] S. Krasnici, A. Werner, M.E. Eichhorn, M. Schmitt-Sody, S.A. Pahernik, B. Sauer, B. Schulze, M. Teifel, U. Michaelis, K. Naujoks, M. Dellian, Effect of the surface charge of liposomes on their uptake by angiogenic tumor vessels, *Int. J. Cancer.* 105 (2003) 561–567.
- [183] D. Simberg, S. Weisman, Y. Talmon, Y. Barenholz, DOTAP (and Other Cationic Lipids): Chemistry, Biophysics, and Transfection, *Crit Rev Ther Drug.* 21 (2004) 257–317.
- [184] S.C. Harrison, Viral membrane fusion, *Virology.* 479–480 (2015) 498–507.
- [185] B.R. Lentz, V. Malinin, M.E. Haque, K. Evans, Protein machines and lipid assemblies: current views of cell membrane fusion, *Curr. Opin. Struct. Biol.* 10 (2000) 607–615.
- [186] L. V. Chernomordik, M.M. Kozlov, Protein-Lipid Interplay in Fusion and Fission of Biological Membranes, *Annu. Rev. Biochem.* 72 (2003) 175–207.
- [187] L. Picas, P.-E. Milhiet, J. Hernández-Borrell, Atomic force microscopy: A versatile tool to probe the physical and chemical properties of supported membranes at the nanoscale, *Chem. Phys. Lipids.* 165 (2012) 845–860.
- [188] L. Picas, C. Suárez-Germà, M. Teresa Montero, J. Hernández-Borrell, Force Spectroscopy Study of Langmuir–Blodgett Asymmetric Bilayers of Phosphatidylethanolamine and Phosphatidylglycerol, *J. Phys. Chem. B.* 114 (2010) 3543–3549.

- [189] L. Redondo-Morata, M.I. Giannotti, F. Sanz, Influence of Cholesterol on the Phase Transition of Lipid Bilayers: A Temperature-Controlled Force Spectroscopy Study, *Langmuir*. 28 (2012) 12851–12860.
- [190] Z. Al-Rekabi, S. Contera, Multifrequency AFM reveals lipid membrane mechanical properties and the effect of cholesterol in modulating viscoelasticity, *Proc. Natl. Acad. Sci.* 115 (2018) 2658–2663.
- [191] D.E. Lee, M.G. Lew, D.J. Woodbury, Vesicle fusion to planar membranes is enhanced by cholesterol and low temperature, *Chem. Phys. Lipids*. 166 (2013) 45–54.
- [192] O. Saavedra V., T.F.D. Fernandes, P.-E. Milhiet, L. Costa, Compression, Rupture, and Puncture of Model Membranes at the Molecular Scale, *Langmuir*. 36 (2020) 5709–5716.
- [193] R.M. a Sullan, J.K. Li, S. Zou, Direct Correlation of Structures and Nanomechanical Properties of Multicomponent Lipid Bilayers, *Langmuir*. 25 (2009) 7471–7477.
- [194] Y. Takechi-Haraya, K. Sakai-Kato, Y. Abe, T. Kawanishi, H. Okuda, Y. Goda, Atomic Force Microscopic Analysis of the Effect of Lipid Composition on Liposome Membrane Rigidity, *Langmuir*. 32 (2016) 6074–6082.
- [195] N. Benne, R.J.T. Leboux, M. Glandrup, J. van Duijn, F. Lozano Vigario, M.A. Neustrup, S. Romeijn, F. Galli, J. Kuiper, W. Jiskoot, B. Slütter, Atomic force microscopy measurements of anionic liposomes reveal the effect of liposomal rigidity on antigen-specific regulatory T cell responses, *J. Control. Release*. 318 (2020) 246–255.
- [196] T. Róg, M. Pasenkiewicz-Gierula, I. Vattulainen, M. Karttunen, Ordering effects of cholesterol and its analogues, *BBA-Biomembranes*. 1788 (2009) 97–121.
- [197] E. Ducat, B. Evrard, O. Peulen, G. Piel, Cellular uptake of liposomes monitored by confocal microscopy and flow cytometry, *J. Drug Deliv. Sci. Technol.* 21 (2011) 469–477.

- [198] K. Hayashi, M. Iwata, Stiffness of cancer cells measured with an AFM indentation method, *J. Mech. Behav. Biomed. Mater.* 49 (2015) 105–111.
- [199] M. Li, L. Liu, N. Xi, Y. Wang, X. Xiao, W. Zhang, Effects of temperature and cellular interactions on the mechanics and morphology of human cancer cells investigated by atomic force microscopy, *Sci. China Life Sci.* 58 (2015) 889–901.
- [200] S. Dutta, B. Watson, S. Mattoo, J. Rochet, Calcein Release Assay to Measure Membrane Permeabilization by Recombinant Alpha-Synuclein, *BIO-PROTOCOL.* 10 (2020).
- [201] K. Chang, J. Baginski, S.F. Hassan, M. Volin, D. Shukla, V. Tiwari, Filopodia and Viruses: An Analysis of Membrane Processes in Entry Mechanisms, *Front. Microbiol.* 7 (2016) 300.
- [202] C.R. Miller, B. Bondurant, S.D. McLean, K.A. McGovern, D.F. O'Brien, Liposome–Cell Interactions in Vitro: Effect of Liposome Surface Charge on the Binding and Endocytosis of Conventional and Sterically Stabilized Liposomes, *Biochemistry.* 37 (1998) 12875–12883.





## Appendix

### List of publications

During the doctoral studies, the author has published the following articles:

[1] **A. Botet-Carreras**, M. T. Montero, Ò. Domènech, J. H. Borrell, Effect of cholesterol on monolayer structure of different acyl chained phospholipids, *Colloids Surf B Biointerfaces*. 174 (2019) 374–383. DOI: 10.1016/j.colsurfb.2018.11.040

Impact index: 4.389, Quartile: 1, Category: BIOPHYSICS -- SCIE

[2] M. L. Vázquez-González, **A. Botet-Carreras**, Ò. Domènech, M. Teresa Montero, J. H. Borrell, Planar lipid bilayers formed from thermodynamically-optimized liposomes as new featured carriers for drug delivery systems through human skin, *Int J Pharm*. 563 (2019) 1–8. DOI: 10.1016/j.ijpharm.2019.03.052

Impact index: 4.845, Quartile: 1, Category: PHARMACOLOGY & PHARMACY -- SCIE

[3] **A. Botet-Carreras**, M. T. Montero, J. Sot, Ò. Domènech, J. H. Borrell, Characterization of monolayers and liposomes that mimic lipid composition of HeLa cells, *Colloids Surf B Biointerfaces*. 196 (2020) 111288. DOI: 10.1016/j.colsurfb.2020.111288

Impact index: 5.268, Quartile: 1, Category: BIOPHYSICS -- SCIE

## **Appendix**

[4] **A. Botet-Carreras**, C. Tamames-Tabar, F. Salles, S. Rojas, E. Imbuluzqueta, H. Lana, M. J. Blanco-Prieto, P. Horcajada, Improving the genistein oral bioavailability via its formulation into the metal–organic framework MIL-100(Fe), *J Mater Chem B*. 9 (2021) 2233–2239. DOI: 10.1039/D0TB02804E

Impact index: 6.331, Quartile: 2, Category: MATERIALS SCIENCE, BIOMATERIALS -- SCIE

[5] **A. Botet-Carreras**, M. T. Montero, J. Sot, Ò. Domènech, J. H. Borrell, Engineering and development of model lipid membranes mimicking the HeLa cell membrane, *Colloids Surf A Physicochem Eng Asp*. 630 (2021) 127663. DOI: 10.1016/j.colsurfa.2021.127663

Impact index: 4.539, Quartile: 2, Category: CHEMISTRY, PHYSICAL – SCIE (based on data from 2020)

## Conference participations and other events

Institute of Nanoscience and Nanotechnology of the University of Barcelona (IN<sup>2</sup>UB) annual meeting in 2016, 2017, 2018, and 2019.

X Research Day at the Faculty of Pharmacy and Food Sciences, 2017, at the University of Barcelona.

XI Research Day at the Faculty of Pharmacy and Food Sciences, 2018, at the University of Barcelona.

XII Research Day at the Faculty of Pharmacy and Food Sciences, 2019, at the University of Barcelona.

Training course in polarography at the Faculty of Pharmacy and Food Sciences at the University of Barcelona, 27/02/2019.

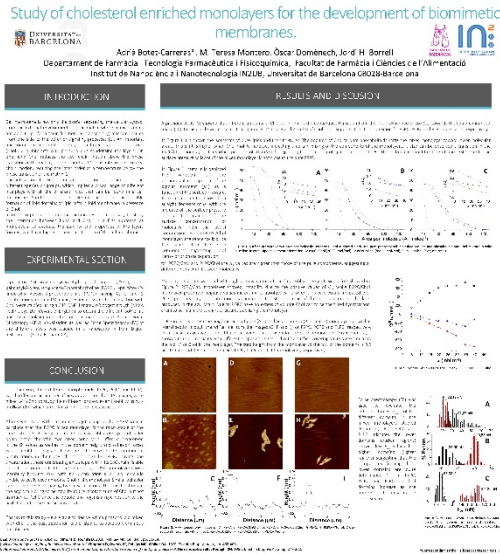
Scholarship at the Department of Physical Chemistry and Electrochemistry, Faculty of Chemistry, Jagiellonian University, Poland, for training on a BAM microscope connected to a Langmuir-Blodgett trough, from 18/06/2019 to 28/06/2019.

7th European Joint Theoretical/Experimental Meeting on Membranes (EJTEMM) 2021 in Graz, Austria.



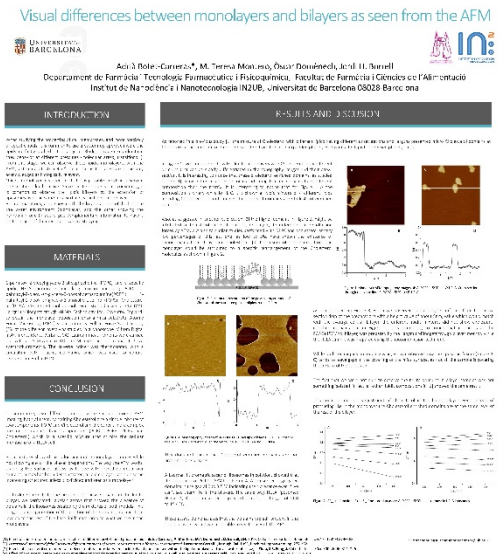
## Contributions to scientific events

### Study of cholesterol enriched monolayers for the development of biomimetic membranes.



In this poster presented at the IN<sup>2</sup>UB annual meeting in 2017 in Barcelona, we discussed three of the lipids presented in the first article published from this work (POPC, PSPC and PLPC). We evaluated their relationship with CHOL and compared their stability.

### Visual differences between monolayers and bilayers as seen from the AFM.



In this poster presented at the XII Research Day at the Faculty of Pharmacy and Food Sciences, 2019, in Barcelona, we discussed the characteristics of the HeLa-mimicking mixture compared to the POPC:CHOL mixture. We compared monolayers, bilayers and the presence of domains.

## HeLa model lipid membrane used as evidence of liposome fusion.

**HELA MODEL LIPID MEMBRANE USED AS EVIDENCE OF LIPOSOME FUSION**  
Adrià Betes-Caracas, M. Teresa Montero, **Óscar Doménech** and Jordi H. Borrell  
Department of Pharmacy, Pharmacology of Technology and Physical Pharmacy, Faculty of Pharmacy and Food Sciences and Institute of Biotechnology (IBT) University of Lleida, Lleida, Catalonia, Spain

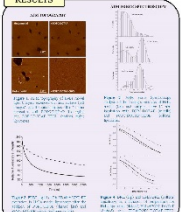
PP22 - 2-B | Thursday, April 8, 2021 20:50 - 22:00  
<https://www.sciencedirect.com/journal/EJEMM/issue/S0927324421000222>

**ABSTRACT**  
The aim of this work was to study the fusion of liposomes with a HeLa model lipid membrane. For this purpose, liposomes were prepared with different lipid compositions and sizes. The fusion of liposomes with the HeLa model lipid membrane was studied by fluorescence resonance energy transfer (FRET) and fluorescence correlation spectroscopy (FCS). The results showed that the fusion of liposomes with the HeLa model lipid membrane was dependent on the lipid composition and size of the liposomes. The fusion of liposomes with the HeLa model lipid membrane was more efficient when the liposomes had a lipid composition similar to the HeLa model lipid membrane and a size of 100-200 nm.

**RESULTS**  
The results of the FRET and FCS experiments are shown in Figure 1. The FRET efficiency was higher for liposomes with a lipid composition similar to the HeLa model lipid membrane and a size of 100-200 nm. The FCS results showed that the fusion of liposomes with the HeLa model lipid membrane was dependent on the lipid composition and size of the liposomes.

**DISCUSSION**  
The results of this work demonstrate that the fusion of liposomes with a HeLa model lipid membrane is dependent on the lipid composition and size of the liposomes. This is in agreement with previous studies that have shown that the fusion of liposomes with biological membranes is dependent on the lipid composition and size of the liposomes.

**CONCLUSION**  
The results of this work demonstrate that the fusion of liposomes with a HeLa model lipid membrane is dependent on the lipid composition and size of the liposomes. This is in agreement with previous studies that have shown that the fusion of liposomes with biological membranes is dependent on the lipid composition and size of the liposomes.



In this poster presented at the EJTEMM 2021 in Graz, we discussed the fusion process between the engineered liposomes and the HeLa-mimicking mixture, which is the core information provided in the fourth article published from this work.



## Acknowledgments

I would like to thank all people involved and supportive during the time of this thesis.

Specially to my directors Dr. Domènech and Dr. Borrell, and the rest of the group with Dr. Montero.

I also would like to thank all the good friends I made in the department of phisicochemistry and the many lunches we have shared.

Also a special thanks to all the friends I made in Krakow, it was a wonderful time.

To all, thanks.



## Symbols and acronyms

$\Delta E$ : Activation energy

$\Delta_{\text{mix}}G$ : Gibbs energy of mixing

$\gamma_{\text{CHOL}}$ : Ideal molar fraction of cholesterol

$\eta$ : Microviscosity

$\mu_{\perp}$ : Vertical component of the dipole moment

$\xi$ : Cohesive forces

$\pi$ : Surface pressure

$\zeta$ -potential: Zeta potential

AChR: Nicotinic acetylcholine receptors

AFM: Atomic force microscope

AFM-FS: Atomic force microscope-force spectroscopy

BAM: Brewster angle microscope

BET: Brunauer–Emmett–Teller (Surface Area Analysis)

CER: Ceramides

CFTR: Cystic fibrosis transmembrane conductance regulator

CHOL: Cholesterol

CLSM: Confocal laser scanning microscope

Cryo-TEM: Cryogenic transmission electron microscopy

Cs: Compressibility modulus

*Symbols and acronyms*

DCS: Differential scanning calorimetry

DLS: Dynamic light scattering

DOPC: 1,2-dioleoyl-sn-glycero-3-phosphocholine

DOTAP: 1,2-dioleoyl-3-trimethylammonium-propane

DPH: 1,6-diphenylhexatriene

DPPC: 1,2-palmitoyl-sn-glycerol-3-phosphocholine

DSPC: 1,2-distearoyl-sn-glycerol-3-phosphocholine

DTA: Differential thermal analysis

E: Young's modulus

EBSD: Electron backscatter diffraction

EELS: Electron energy loss spectroscopy

EELS-STEM: Electron energy loss spectroscopy combined with scanning transmission electron microscopy

EPLS: Elliptically polarized light scattering

EPM: Electrophoretic mobility

EXAFS: X-ray absorption fine structure

F(t): Fluorescence intensity decay curves

F $\infty$ : Infinite dilution factor

Fadh: Adhesion forces

FMR: Ferromagnetic resonance

FRET: Fluorescence resonance energy transfer

FTIR: Fourier transform infrared spectroscopy

GE: Gibbs excess energy

GPex: Generalized polarization

GUVs: Giant unilamellar vesicles

HPLC: High-performance liquid chromatography

HRTEM: High-resolution TEM

ICP-MS: Inductively coupled plasma-Mass spectrometry

ICP-OES: Inductively coupled plasma optical emission spectrometry

IRF: Instrument response factor

L0: Liquid ordered

LB: Langmuir-Blodgett

LC: Liquid condensed

LE: Liquid expanded

LEIS: Low-energy ion scattering

Liquid-NMR: Liquid nuclear magnetic resonance

Liquid-TEM: Liquid transmission electron microscopy

LUVs: Unilamellar vesicles

L $\alpha$ : Liquid-crystalline

L $\beta$ : Gel

MALDI: Matrix-assisted laser desorption/ionisation

MFM: Magnetic force microscopy

MHF: Microfluidic hydrodynamic focusing platform

MLVs: Multilamellar vesicles

*Symbols and acronyms*

MOFs: Metal-organic frameworks

MTT: 3-[4,5- dimethylthiazol-2-yl]-2,5-diphenyl tetrazolium bromide

MTX: Methotrexate

NBD-PE: 1,2-dioleoyl-sn-glycero-3-phosphoethanolamine-N-(7-nitro-2-1,3-benzoxadiazol-4-yl)

NMR: Nuclear magnetic resonance

NTA: Nanoparticle tracking analysis

PA: 1-formyl-6-(N-cyclohexyl) aminopyrene

PC: Phosphatidylcholine

PCs: Phosphocholine head groups

PDI: Polydispersity index

PE: Phosphatidylethanolamine

PL: Photoluminescence

PLPC: 1-palmitoyl-2-linoleoyl-sn-glycero-3-phosphatidylcholine

POPC: 1-palmitoyl-2-oleoyl-sn-glycero-3-phosphatidylcholine

POPE: 1-palmitoyl-2-oleoyl-sn-glycero-3-phospho ethanolamine

POPS: 1-palmitoyl-2-oleoyl-sn-glycero-3-phospho-L-serine

PS: Phosphatidylserine

PSPC: 1-palmitoyl-2-stearoyl-sn-glycerol-3-phosphatidylcholine

PTA: Particle tracking analysis

RBIR: Red/blue Intensity ratio

RET: Extent of resonance transfer

REV: Reverse-phase evaporation vesicles

Rh-PE or Rhodamine-PE: 1,2-dioleoyl-sn-glycero-3-phosphoethanolamine-N-(lissamine rhodamine B sulfonyl)

RMM-MEMS: Resonant mass measurement microelectro-mechanical system

SANS: Small angle neutron scattering

SAXS: Small-angle X-ray scattering

SC: Stratum corneum

SEM: Scanning electron microscopy

SEM-EDX: Scanning electron microscopy-dispersive X-ray

SIMS: Secondary ion mass spectrometry

SLB: Supported lipid bilayers

Sp-ICP-MS: Single particle operation mode-inductively coupled plasma-mass spectrometry

SPMs: Scanning probes microscopes

SQUID: Superconducting quantum interference device magnetometry

STEM: Scanning transmission electron microscopy

SUVs: Small unilamellar vesicles

TEM: Transmission electron microscopy

TGA: Thermal gravimetric analysis

T<sub>m</sub>: Melting transition temperature

TMA-DPH: 1-(4-trimethylammonium-phenyl)-6-phenyl-1,3,5-hexatriene

TRPS: Tunable resistive pulse sensing

UV-Vis: Ultraviolet-visible spectroscopy



***Symbols and acronyms***

UV-Vis-NIR: Near-infrared ultraviolet-visible spectroscopy

VSM: Vibrating sample magnetometry

XAS: X-ray absorption spectroscopy

XMCD: X-ray magnetic circular dichroism

XPS: X-ray photoelectron spectroscopy

XRD: X-ray diffraction